INFORMATION TO USERS

This manuscript has been reproduced from the microfilm master. UMI films the text directly from the original or copy submitted. Thus, some thesis and dissertation copies are in typewriter face, while others may be from any type of computer printer.

The quality of this reproduction is dependent upon the quality of the copy submitted. Broken or indistinct print, colored or poor quality illustrations and photographs, print bleedthrough, substandard margins, and improper alignment can adversely affect reproduction.

In the unlikely event that the author did not send UMI a complete manuscript and there are missing pages, these will be noted. Also, if unauthorized copyright material had to be removed, a note will indicate the deletion.

Oversize materials (e.g., maps, drawings, charts) are reproduced by sectioning the original, beginning at the upper left-hand corner and continuing from left to right in equal sections with small overlaps.

Photographs included in the original manuscript have been reproduced xerographically in this copy. Higher quality 6" x 9" black and white photographic prints are available for any photographs or illustrations appearing in this copy for an additional charge. Contact UMI directly to order.

Bell & Howell Information and Learning
300 North Zeeb Road, Ann Arbor, MI 48106-1346 USA
800-521-0600

UMI®

Reproduced with permission of the copyright owner. Further reproduction prohibited without permission.

DISSERTATION

SOIL CARBON AND WATER DYNAMICS: ^{13}C AND ^{18}O AS SYSTEM TRACERS

Submitted by

Elizabeth W. Sulzman

Graduate Degree Program in Ecology

In partial fulfillment of the requirements

for the Degree of Doctor of Philosophy

Colorado State University

Fort Collins, Colorado

Fall 2000

Reproduced with permission of the copyright owner. Further reproduction prohibited without permission.

UMI Number: 3002103

UMI®

UMI Microform 3002103
Copyright 2001 by Bell & Howell Information and Learning Company.
All rights reserved. This microform edition is protected against
unauthorized copying under Title 17, United States Code.

Bell & Howell Information and Learning Company
300 North Zeeb Road
P.O. Box 1346
Ann Arbor, MI 48106-1346

Reproduced with permission of the copyright owner. Further reproduction prohibited without permission.

COLORADO STATE UNIVERSITY

JULY 19, 2000

WE HEREBY RECOMMEND THAT THE DISSERTATION PREPARED UNDER OUR SUPERVISION BY ELIZABETH SULZMAN ENTITLED SOIL CARBON AND WATER DYNAMICS: ^{13}C AND ^{18}O AS SYSTEM TRACERS BE ACCEPTED AS FULFILLING IN PART REQUIREMENTS FOR THE DEGREE OF DOCTOR OF PHILOSOPHY.

Committee on Graduate Work

Advisor

Co-Advisor

Department Head

Reproduced with permission of the copyright owner. Further reproduction prohibited without permission.

ABSTRACT OF DISSERTATION

SOIL CARBON AND WATER DYNAMICS: ^{13}C AND ^{18}O AS SYSTEM TRACERS

The goal of this research was to determine whether measurements of the stable isotopic composition of soil CO_2 could be used to separate the net terrestrial CO_2 flux to the atmosphere into the component fluxes of photosynthesis and respiration. Knowledge of these gross fluxes is needed to quantify terrestrial carbon storage. I measured the isotopic composition of soil CO_2 along two bioclimatic gradients in the Rocky Mountains of Colorado. Sites were selected based on the state factor approach such that variability in results could be attributed primarily to differences in climate, vegetation type, and soil texture. Sites were sampled weekly (one site) or every three weeks over the growing season, with additional sampling before bud-break and after plant senescence. Soil organic matter and soil gas were analyzed for $\delta^{13}C$, and soil gas and soil water for $\delta^{18}O$, via continuous-flow mass spectrometry. One-dimensional, linear regression, and full equilibration-diffusion models were employed to calculate the isotopic composition of the soil CO_2 flux. Through my study I identified serious flaws in the "equilibrium-only" approach to calculation of the $\delta^{18}O$ value of soil-respired CO_2. Data suggest that under some field conditions CO_2 and water are not in isotopic equilibrium. Diffusion is central to the correct calculation of the $\delta^{18}O$ value of soil-respired CO_2, as shown by comparison of linear regression model output with that from a full diffusion-equilibration model. In addition, the isotopic composition of soil-respired CO_2 depends on soil physical

Reproduced with permission of the copyright owner. Further reproduction prohibited without permission.

conditions. For example, some of the variability in expressed kinetic fractionation was explained by soil moisture. When moisture content was high, kinetic fractionation was as great as 7.5‰, but it was as low as 3.4‰ under drier conditions. Third, simpler models were shown to be incapable of reproducing the observed temporal variability in the isotopic composition of the soil CO_2 flux, which was as large as 8‰ over the course of the growing season at a single location. Finally, the $\delta^{13}C$ value of the soil CO_2 efflux was controlled primarily by the proportion of C_4 vegetation at a site, with no significant differences in $\delta^{13}CO_2$ across pure C_3 sites.

Elizabeth Waterous Sulzman
Graduate Degree Program in Ecology
Colorado State University
Fort Collins, CO 80523
Fall 2000

Reproduced with permission of the copyright owner. Further reproduction prohibited without permission.

ACKNOWLEDGEMENTS

I am very thankful for funding from NASA (Earth System Science Fellowship 1996-1998). The LTER Shortgrass Steppe provided funds for my first year, and provided beautiful scenery and facilities throughout my project. The Max-Planck-Institut für Biogeochemie, Jena, Germany, supported me for the final grueling stretch, including a stipend, use of facilities, and most of all, a tremendously positive "oversea" experience. There are many individuals to whom I owe thanks. I thank Steve Blecker for sharing his wealth of knowledge on soils and lab work as well as patience and good talks during the many miles and hours during the site selection process. Thanks to Caroline Yonker for help in the field and for being there through the worst of it. Thanks also to Elise Pendall for many helpful conversations and good company, and to Pieter Tans for the use of his model and help improving it. Thanks to John Miller for help in interpreting initial model runs, and to Dan Yakir for helpful discussions. Thanks also to the lab-master, Dan Reuss. Willi Brand was instrumental in getting the soil water samples analyzed (thanks also to Beate Rothe). Craig Cook went way beyond the call of duty when he not only let me take over the SIRFER lab for a very long weekend, but also provided a bed! Thanks to many friends for help throughout, especially Robin Kelly, Galina Churkina, Angela Plaia, Rob Braswell, and Antje Weitz. Thanks also to my committee for hanging in there with me. Last, and most important, many hugs and thanks to Serita and James for unending patience as well as programming lessons (James) and company in the field (both).

Reproduced with permission of the copyright owner. Further reproduction prohibited without permission.

TABLE OF CONTENTS

Reproduced with permission of the copyright owner. Further reproduction prohibited without permission.

Reproduced with permission of the copyright owner. Further reproduction prohibited without permission.

Reproduced with permission of the copyright owner. Further reproduction prohibited without permission.

LIST OF TABLES

Reproduced with permission of the copyright owner. Further reproduction prohibited without permission.

LIST OF FIGURES

Reproduced with permission of the copyright owner. Further reproduction prohibited without permission.

Reproduced with permission of the copyright owner. Further reproduction prohibited without permission.

Reproduced with permission of the copyright owner. Further reproduction prohibited without permission.

CHAPTER 1

INTRODUCTION

The carbon cycle is a key link between human activities and our environment. When the carbon cycle is altered through fossil fuel use, the climate system responds with implications for plant and animal well-being. Figure 1.1 shows the relative sizes of the global stocks of carbon that interact on annual to decadal time scales.

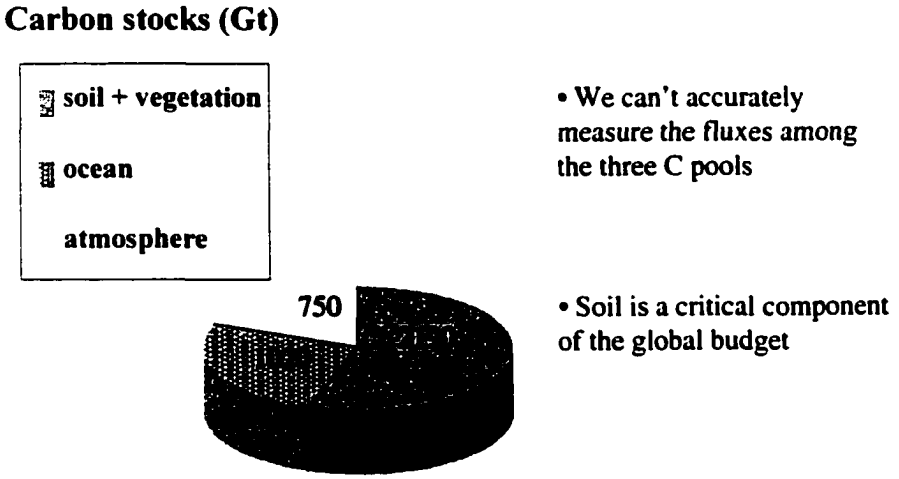

Figure 1.1. The three components of the short-term carbon cycle. Pie wedges indicate size of pools in Gt (10^{15} g) carbon.

The deep ocean is not included in this figure because it interacts with the atmosphere only on time scales of hundreds to thousands of years. The amount of carbon stored in terrestrial systems, 72% of which is in soils, is over twice that stored in the mixed-layer

Reproduced with permission of the copyright owner. Further reproduction prohibited without permission.

of the world's oceans, and is nearly three-times more than the amount of carbon in the atmosphere. The fluxes, or transfers, among these three pools cannot yet be accurately measured, but only about half of the carbon emitted every year as a result of fossil fuel consumption and cement manufacture ends up in the atmosphere. The other portion of the emitted carbon (roughly 3.5 Gt, or 10^9 metric tons) enters either the terrestrial or oceanic system. Recently, the use of the ratio of oxygen to nitrogen and $\delta^{13}C$ composition of the atmosphere have allowed quantification of the proportion of emitted carbon entering land versus the ocean. Data suggest that the proportion going to each of these systems changes as a result of changing environmental conditions. The response of soils in particular is critical, because not only do soils store large amounts of carbon, but they are sensitive to changes in temperature and moisture conditions.

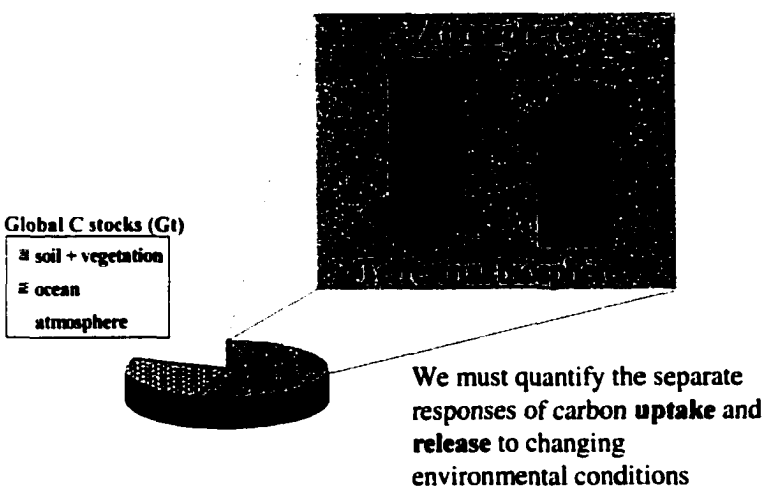

Figure 1.2. The exchange of carbon between the terrestrial biosphere and the atmosphere. The imbalance between the gross fluxes of photosynthesis and respiration influences the amount of carbon in the atmosphere.

Reproduced with permission of the copyright owner. Further reproduction prohibited without permission.

Figure 1.2 magnifies the terrestrial portion of the global carbon cycle. The gross fluxes of uptake (photosynthesis) and release (respiration) are very large and are not perfectly balanced. Under any given set of environmental conditions in a particular region, the difference can mean a net flux to the atmosphere or net uptake from the atmosphere. It is this net difference between uptake and release that affects the amount of carbon stored in the atmosphere. In order to understand the net exchange of carbon between the terrestrial system and the atmosphere, and in order to make accurate projections about the future size of the atmospheric carbon pool, we must separate the effects of changing environmental conditions on carbon uptake and release by terrestrial systems. It is only quite recently that we have developed the technology to do this. In a study in *Science*, Goulden et al. [1996] used eddy covariance to measure uptake and release at the stand scale. Another new tool to address this challenge is the use of ^{18}O, which required some methods development, but now is very promising in the study of the carbon cycle, as well as for other applications.

The oxygen isotopic composition of atmospheric CO_2 is determined by the $\delta^{18}O$ of the water in soil and that in plant leaves according to the following reaction [*Bottinga and Craig*, 1969; *Farquhar et al.*, 1993]:

$$H_2{}^{18}O + C^{16}O^{16}O \rightleftharpoons H^+ + [HC^{16}O^{16}O^{18}O] \rightleftharpoons H_2{}^{16}O + C^{16}O^{18}O$$

Because the average $\delta^{18}O$ of soil water is quite distinct from that of leaf water (Figure 1.3), measurements of $\delta^{18}O$ in atmospheric CO_2 and soil water can be used to partition plant and soil contributions to the terrestrial-to-atmosphere CO_2 flux.

Reproduced with permission of the copyright owner. Further reproduction prohibited without permission.

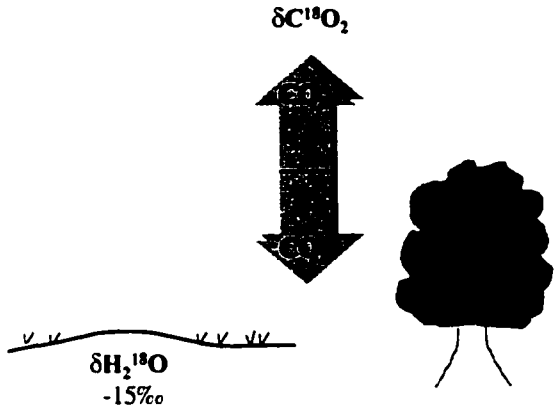

Figure 1.3. The distinct oxygen isotopic values of soil water and plant chloroplast water. Values shown are average values for illustrative purposes only. The isotopic equilibrium reaction that occurs between CO_2 and water controls the $\delta^{18}O$ of atmospheric CO_2.

Previous methods to estimate the oxygen isotopic composition of the soil CO_2 flux have produced widely different results for the same ecosystem (Figure 1.4).

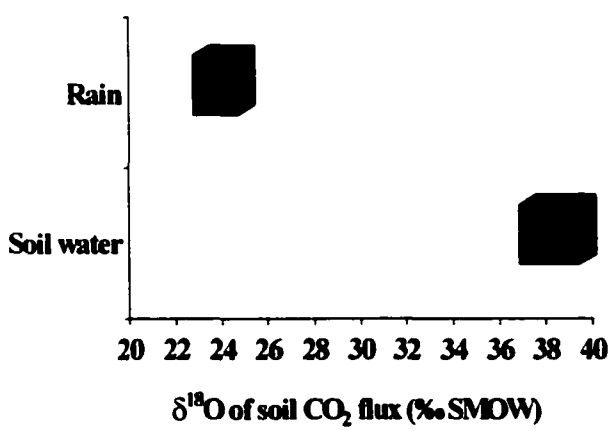

Figure 1.4. The isotopic composition of the flux of CO_2 from soil to atmosphere as calculated for a central US grassland using two different approaches. The approach labeled "rain" assumes that the ^{18}O of respired CO_2 arises from the ^{18}O of precipitation plus a fractionation factor to account for diffusion (published values for the fractionation factor range from 5‰ to 8.8‰). The approach labeled "soil water" assumes that the ^{18}O of respired CO_2 arises from the ^{18}O measured in soil water at 10 cm depth plus a fractionation factor to account for diffusion. Both approaches assume full isotopic equilibrium between soil water and soil CO_2.

Reproduced with permission of the copyright owner. Further reproduction prohibited without permission.

The large discrepancy between the two methods suggests the need for a process-level approach. As the physical process of diffusion can alter the $\delta^{18}O$ of soil-respired CO_2 by up to 8.8‰, addition of soil properties and soil physics was seen as the means to answer the following questions:

- Is isotopic equilibrium between CO_2 and H_2O always faster than diffusion (a competing process)?
- Can we identify the isotopic composition of water that exchanges isotopically with CO_2?
- How do soil physical conditions control soil-respired CO_2?

The work presented in this dissertation was designed to answer those questions, and to assess whether $\delta^{18}O$ is a useful tool for the separation of the net terrestrial CO_2 flux into its separate uptake and release components.

Literature Cited

Bottinga, Y., and H. Craig, Oxygen isotope fractionation between CO_2 and water, and the isotopic composition of marine atmospheric air, *Earth and Planetary Science Letters*, *5*, 285-295, 1969.

Farquhar, G.D., J. Lloyd, J.A. Taylor, L.B. Flanagan, J.P. Syvertsen, K.T. Hubick, S.C. Wong, and J.R. Ehleringer, Vegetation effects on the isotope composition of oxygen in atmospheric CO_2, *Nature*, *363*, 439-442, 1993.

Goulden, M.L., J.W. Munger, S.-M. Fan, B.C. Daube, and S.C. Wofsy, Exchange of carbon dioxide by a deciduous forest: response to interannual climate variability, *Science*, *271*, 1576-1578, 1996.

Reproduced with permission of the copyright owner. Further reproduction prohibited without permission.

CHAPTER 2

THE STABLE CARBON ISOTOPE COMPOSITION OF SOIL AND SOIL-RESPIRED CO_2 ACROSS A BIOCLIMATIC GRADIENT

Abstract

There is an increasing need to understand the role of the terrestrial biosphere in the global fluxes of carbon, water and energy. In order to make progress toward this goal, bottom-up approaches including comparative and process studies are needed in iteration with top-down modeling and remote-sensing approaches. Field and laboratory measurements are essential to understanding the spatial and temporal scales at which various processes operate. The work presented here aims to do just that. I examined soil processes along two transects of field sites in the Rocky Mountains of Colorado and assessed the spatial and temporal variability of the $\delta^{13}C$ values of the soil-to-atmosphere CO_2 flux. Measured rates of soil CO_2 efflux ranged from 0.62 $\mu mol/m^2/s$ in mid-November, 1998, to 7.9$\mu mol/m^2/s$ in mid-July, 1998. The isotopic composition of this flux was highly variable, in part due to variability in soil physical conditions. The $\delta^{13}C$ of the soil-atmosphere CO_2 flux ranged from -24.28‰ at a tundra site in early June to -15.0‰ at a steppe site in mid-August, with most growing season measurements falling between -24‰ to -20‰ for sites with only C_3 vegetation. A soil diffusion-equilibration model was shown to produce estimates of $\delta^{13}CO_2$ that differ by roughly 3‰ or more from the

Reproduced with permission of the copyright owner. Further reproduction prohibited without permission.

traditional two end-member mixing model approach. Regardless of the model used, the flux was roughly 9‰ more enriched in ^{13}C for steppe (mixed C_3-C_4 vegetation) as compared to the forested or tundra ecosystems studied.

2.1. Background and Introduction

Production of CO_2 in soils is a significant source to the atmospheric pool. Furthermore, the amount of CO_2 stored and released by soils has a large potential to vary as a function of environmental conditions. In order to improve our understanding of the exchange of carbon between the atmosphere and the terrestrial biosphere, there is a need for isotopic data from a variety of ecosystems to constrain regional and global models [e.g., *Ciais et al.*, 1997; *Ciais et al.*, 1995; *Fung et al.*, 1997]. Such modeling efforts have recently determined the contribution of terrestrial ecosystems to the global C budget, and addition of ^{18}O data is promising as a means to separate the processes that make up the terrestrial CO_2 flux. Although there are a large number of studies of the magnitude of the CO_2 flux from soil to the atmosphere, there is a paucity of isotopic data from the soil system. Examination of the processes controlling the variability in the isotopic composition of both soil CO_2 and soil-respired CO_2 over time and space will contribute to our ability to understand how the global carbon budget will respond to natural and imposed climate variability as well as to human-induced disturbances. The work presented here examines site-scale variability in the $\delta^{13}C$ of SOM, soil CO_2, and soil-respired CO_2. I also compare data across ecosystems and soil types in an effort to understand process level controls that may scale up to larger spatial domains.

Reproduced with permission of the copyright owner. Further reproduction prohibited without permission.

2.2. Methods

2.2.1 Field Sampling

2.2.1.1 Study sites

Six field sites located along the Front Range of the Rocky Mountains in Colorado were selected to represent three separate ecosystems and two soil textures (see Figure 2.1 and Table 2.1 for site locations).

Figure 2.1. Field sites sampled during this study. Site represent three ecosystems (shortgrass steppe, lodgepole pine, and alpine tundra) on soils of fine and coarse texture. Each photograph represents a textural pair of sites.

I selected sites using the state factor approach as outlined by Jenny [1941]. According to Jenny, soil development is conditioned by five factors: climate, organisms, relief (aspect and slope), parent material, and time. I was interested in both soil texture — a property largely determined by the parent material from which a soil develops — and bioclimate, or the combination of climate and its associated organisms [*Jenny*, 1980].

Reproduced with permission of the copyright owner. Further reproduction prohibited without permission.

Reproduced with permission of the copyright owner. Further reproduction prohibited without permission.

Table 2.1. Characterization of field sites.

Site name	Ecosystem type[&]	Parent material	Elevation (meters)	Location	Slope	Aspect	Climate*
CPER-Catena	Shortgrass steppe	Shale residuum	1646	40°48'N, 104°44'W	<5%	----	MAP 31 cm MAT 9.2°C
CPER-Meterological Station	Shortgrass steppe	Coarse alluvium	1646	40°48'N, 104°44'W	<1%	----	MAP 31 cm MAT 9.2°C
Ballard Road	Lodgepole pine	Mica schist	2720	40°34'N, 105°28'W	17%	105° (SE)	MAP 58.4 cm MAT 7.8°C
Allenspark	Lodgepole pine	Silver plume granite	2651	40°11'N, 105°32'W	22%	42° (NE)	MAP 52.6 cm MAT 4.7°C
Iceberg Pass	Alpine tundra	Biotite schist	3597	40°26'N, 105°45'W	22%	56° (NE)	MAP 191.5 cm MAT -8.3°C
Tombstone Ridge	Alpine tundra	Silver plume granite	3475	40°24'N, 105°41'W	14%	50° (NE)	MAP 180 cm MAT -8.3°C

[&] See Appendix I for details

* 30-yr average when available; data from http://ulysses.atmos.colostate.edu/Access.html

Accordingly, I selected field sites on uniform slopes on two parent material types along a bioclimatic gradient. The sites representing the shortgrass steppe ecosystem matched the other ecosystems in terms of soil texture, but the parent materials were coarse alluvium and shale residuum. Total clay content is much higher at each of the fine sites relative to that of its textural counterpart (Figures 2.2-2.4). See Appendix I for full soil descriptions.

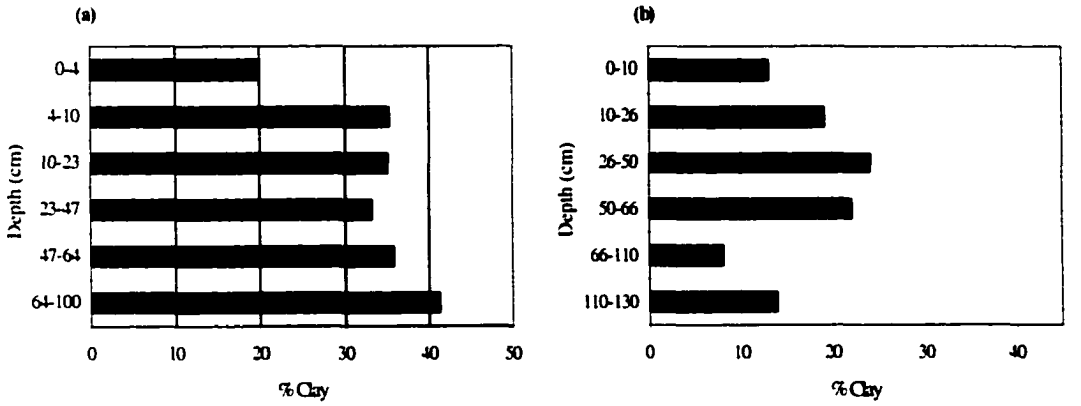

Figure 2.2. Soil texture as estimated by particle size analysis for the shortgrass steppe sites (a) "fine" soil, and (b) "coarse" soil.

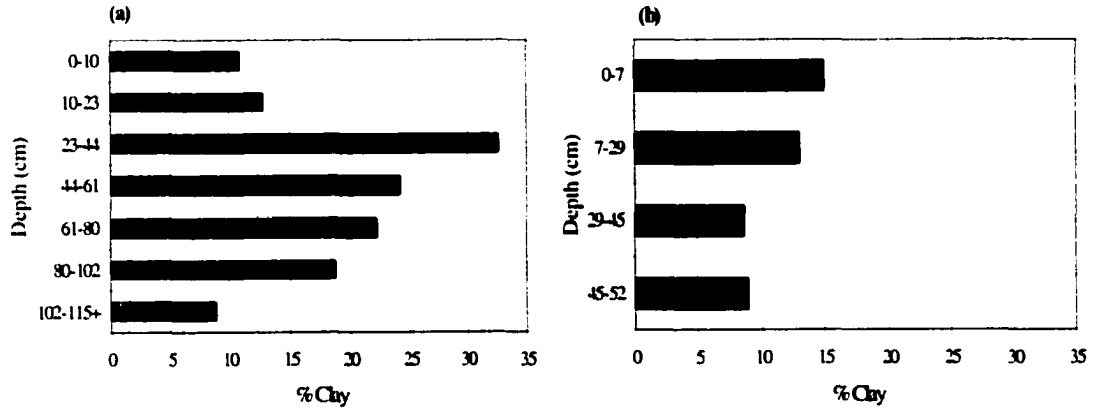

Figure 2.3. Soil texture as estimated by particle size analysis for the lodgepole pine sites (a) "fine" soil, and (b) "coarse" soil.

Reproduced with permission of the copyright owner. Further reproduction prohibited without permission.

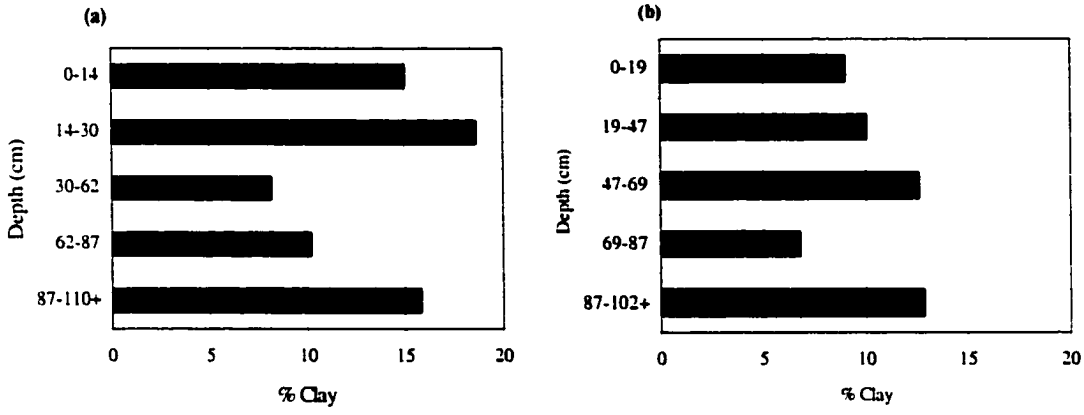

Figure 2.4. Soil texture as estimated by particle size analysis for the alpine tundra sites (a) "fine" soil, and (b) "coarse" soil.

Climate at the field sites was determined based on the longest available record from the closest official Colorado weather station (http://ulysses.atmos.colostate.edu/Access.html). Climatic graphs are presented in Appendix I. Sites range from roughly 100 m to 25 km from the nearest weather station. The shortgrass steppe (SS) sites were located within 5 km of each other within the Central Plains Experimental Range (CPER). One of these sites is co-located with the weather station. The alpine tundra (AT) sites were less than 10 km apart and were best represented by a single weather station ("Niwot Ridge Saddle," operated and maintained by the University of Colorado Boulder's Long-Term Ecological Research program. http://culter.colorado.edu:1030/ Niwot/Niwot_Ridge_LTER_climate.html). Although the weather station is about 25 km from the field sites studied in this work, the elevation match is good. The lodgepole (LP) sites were over 100 km apart. The nearest weather station for the site on coarse soil was 1 km away; that for the fine soil site was located about 12 km away. Data were not publicly available for the 1998 field season (as of February 2000) at any of the closest weather stations, and one station, that nearest the LP

Reproduced with permission of the copyright owner. Further reproduction prohibited without permission.

coarse site, was terminated in 1993. The climate at all sites is distinctly seasonal (Appendix I). At the shortgrass and lodgepole sites, rain falls primarily in the late spring and early summer, and temperatures peak in late summer (July-August). At the tundra sites there are only five months with above zero (°C) temperatures, and most of the precipitation falls as snow.

2.2.1.2 Sample types and sampling frequency

Field sampling was conducted over the 1997 and 1998 growing seasons, with an attempt made to capture pre-bud break and senescence (April-November). During the growing season (June-August), two field sites were visited each week. One site, lodgepole on coarse soil, was selected for intensive investigation because the 1997 CO_2 concentration and isotopic data suggested the LP sites were more variable than those in the other ecosystems. This site (LP-coarse) was visited every week. A total of 32 field visits were made during the 1998 season. Routine measurements/collections conducted during each field visit included air temperature and a soil temperature profile (every 5 cm to 30 cm, plus 50 cm: microprocessor thermometer, Omega Engineering), bulk soil from four depths, soil gases, and rainwater.

Bulk soil samples were taken from depths centered on 5, 10, 30, and 50 cm (± 2 cm). Samples were collected in 120 ml wide-mouth brown glass jars with a teflon-lined lid. After collection, the tops were wrapped in parafilm, and the jars were placed immediately in a cooler with ice for transport. Samples were stored in a cold room (5°C) until irradiated (1.15-1.20 Mrad) to stop all microbial activity. Duplicate samples were taken for analysis of gravimetric water content. These were stored in sealed plastic bags in the

Reproduced with permission of the copyright owner. Further reproduction prohibited without permission.

cooler, and then weighed moist immediately upon returning to the laboratory (usually within two hours of sampling).

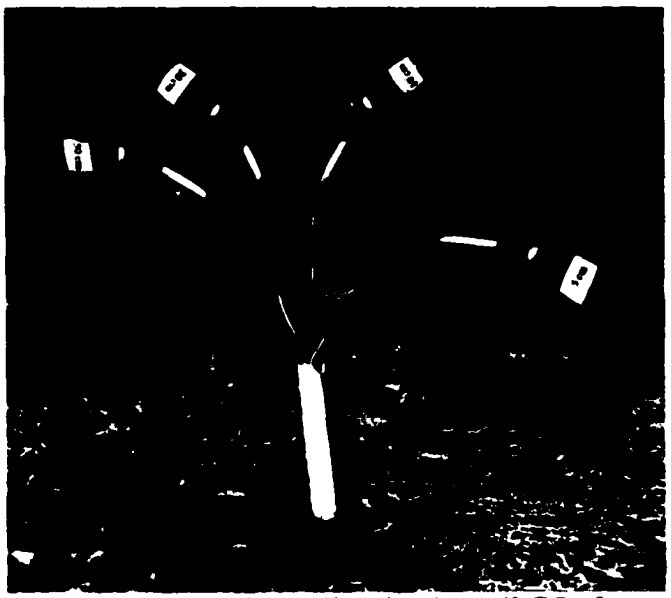

Figure 2.5. Apparatus used to collect in-situ soil CO_2 from each of the six field sites. Three of these PVC tubes, located approximately 1-m apart, were installed at each site.

Gas sampling tubes were installed in the field in June of 1997, three weeks prior to commencement of sample collection. The sampling apparatus, designed by A.Mosier and D.Valentine (pers. comm.), consisted of a 2.5 cm diameter PVC tube housing four 0.32 cm i.d. stainless steel tubes (Figure 2.5). The steel tubing extended from a hole in the PVC pipe at the desired gas sampling depth (5, 10, 30, and 50 cm) to several cm above the soil surface. The PVC pipe was filled with resin to hold the steel tubes at the desired depth. An auger of the same diameter as the PVC tube was used to install the tubes in the field with as little disturbance to the soil profile as possible. Three of these tubes were installed roughly 1 m apart at each field site (total of 18 tubes). A swagelock fitting holding a teflon-faced silicone rubber micro septa (Alltech Associates, Deerfield, IL) was connected to the top of each piece of steel tubing. Septa were replaced after each sampling.

Reproduced with permission of the copyright owner. Further reproduction prohibited without permission.

To begin sampling, a 25 ml gas sample was drawn by syringe from each tube and expelled to remove air that had built up and been in contact with the tubing and septa since the previous sampling. Gas was allowed to diffuse into the tubing and area surrounding the inlet of the tubing for 10 minutes. Soil gas was then drawn across a magnesium perchlorate water trap into pre-evacuated 25 ml glass serum vials via a double-sided precision glide blood collection needle (27½G) (Figure 2.5). New drying traps and new needles were used for each sample. Serum vials were left attached to the sampling tubes for 20 minutes to insure complete equilibration. Twelve samples were collected at each field site on each sampling date (4 depths x 3 PVC tubes). The radius of the hemisphere sampled by a 25 ml gas collection is 2.29 cm. Thus, the 5 cm sample actually represents the CO_2 concentration and isotopic composition of gases from 2.7 to 7.3 cm, and the sample representing the 10 cm depth increment actually covers a depth range of 7.7 to 12.3 cm. After the equilibration period, samples were removed from the sampling needles and their septa were sealed with Apiezon-M grease (Apiezon Products, Manchester, U.K.). The needles were then removed from the swagelock septa to allow gases to diffuse back into the sampling tubes and areas surrounding the sampling tube inlet. After 20 minutes, a second sample was taken from each tube and depth in the same manner as the first, but without the dry trap. Water content does not affect CO_2 concentration (it is removed prior to analysis), but storage of wet samples has been shown to alter their isotopic composition [*Gemery et al.*, 1996]. The samples collected for determination of CO_2 concentration were analyzed within two days post-sampling. All samples were stored cold (about 5°C) until analyzed for consistency (lab temperature

Reproduced with permission of the copyright owner. Further reproduction prohibited without permission.

highly variable) and to minimize any potential reactions between gas samples and water that might have been adsorbed to the glass vials.

Soil flux measurements were recorded using a dynamic closed chamber technique. A plexiglass cylindrical chamber (9-L volume: 20 cm height, 12 cm radius) was fitted with a small, 9V battery-powered fan and attached, via 2 m of 1 mm i.d. Tygon tubing, to a LI-6200 portable photosynthesis analyzer (LI-COR, Lincoln, Nebraska). Respired air samples were collected for later isotopic analysis during some of the soil flux measurements. In this case, the tubing was split, and a water trap (magnesium perchlorate and glass wool filter) and a 0.5-L pyrex flask with Teflon O-ring stopcocks at either end were inserted in-line between the chamber and the LI-COR instrument (see Figure 2.6).

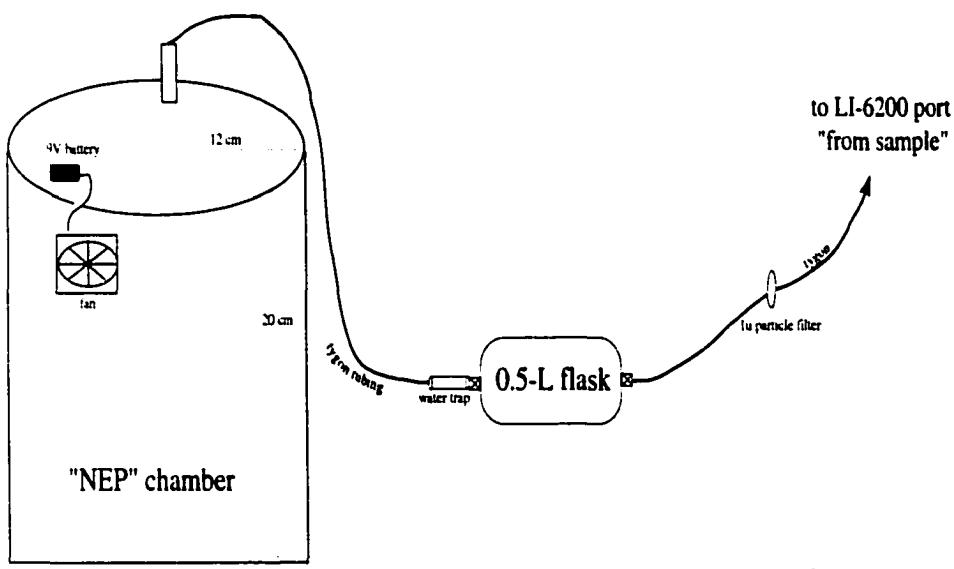

Figure 2.6. Chamber used to measure soil-respired CO_2 with capture for subsequent isotopic analysis.

The CO_2 analyzer was calibrated on each sampling date on-site (span gas 994 ppm). The calibration tank was taken into the field to account for pressure differences between the sites and the lab (sites range from about 630 to 850 mbar, lab pressure 848 mbar). The flow rate typical during sampling was 900 µmol/sec. Flow rates were lower at the higher

Reproduced with permission of the copyright owner. Further reproduction prohibited without permission.

elevation sites. Sampling was carried out in mid-day (usually between 12:00 and 14:00 hours) except during one diurnal study (not reported here). To begin measurements, the chamber was placed on a level spot with as little vegetation as possible (at the LP sites and AT-coarse, these were denuded) and forceful downward pressure was used to "seal" it in place. A black cloth was placed over the chamber to block all sunlight. CO_2 concentration and air flow rate were recorded every 15 seconds for a total of 90 seconds chamber closure (i.e., during the period of linear CO_2 increase). At the end of the CO_2 build-up period (final concentrations usually 450-500 ppm), the flask was closed (LI-COR end first, to prevent explosion), and then the LI-COR shut off and the chamber moved to a new spot. This was repeated in five locations at each field site, for each sampling date. Atmospheric samples were taken with the same protocol except that the chamber was held at shoulder height upwind from field personnel.

2.2.2. Laboratory Analysis

Laboratory analyses for the soil water samples included gravimetric analysis of water content, measurement of particle size distribution, and organic matter content analysis (necessary to calculate water amount on a volumetric basis). In addition, isotope ratio mass spectrometric analysis was carried out on rain water, soil water, and soil-respired CO_2 samples. The methods used for mass spectrometric analysis are described in separate sections, below. Measurement of soil water content was initiated on each sampling date by weighing moist samples immediately upon returning to the laboratory (as mentioned above). These samples were then oven dried for 48 hrs at 110°C, and re-weighed. Moisture content was calculated according to:

Reproduced with permission of the copyright owner. Further reproduction prohibited without permission.

$$\% \text{ water} = ((\text{wet weight-dry weight})/\text{dry weight}) \quad (1)$$

All soil samples for particle size and organic content analysis (six field sites, four depths, plus samples for each genetic soil horizon at each site, not reported here) were first sieved with 2 mm mesh sieve and gently crushed with a mortar and pestle. Each soil was then tested for the presence of carbonates by adding a few drops of 1N HCL to a few grams of dry soil. Carbonates were present only in soils from the shortgrass steppe sites below 45 cm (65 cm at the coarse-textured site). These samples were treated with weak acid (1M NaOAc) buffered at pH 5 for 1 hour in a warm (60°C) sand bath, then shaken and rinsed. This procedure was repeated until there was no reaction between strong acid and soil. Particle size distribution was determined by hydrometer method [*Gee and Bauder*, 1986].

A sub-sample of each soil was finely ground via a ball mill to assure complete homogenization. These homogenized samples were then analyzed via a LECO CHN 1000 Elemental Analyzer for organic content (%C and %N) (LECO Corporation, St. Joseph, MI). The %C information was used to estimate sample size needed for $\delta^{13}C$ analysis of the organic matter as well as for calculation of bulk density. The error associated with calculation of bulk density from particle size and organic matter content is 0.3 g/cm^3 or less [*Rawls*, 1983]. Water content expressed on a volumetric basis is the product of gravimetric water content and calculated bulk density.

CO_2 concentration of all gas samples was determined within two days of sampling via a LI-COR model LI-6252 infra-red gas analyzer (IRGA, LI-COR, Lincoln, NE). The system was calibrated prior to each set of field samples using two tanks of known concentration (1040 and 4824 ppm). Reference gas was injected in amounts ranging from 1 ml of the 1040 ppm tank to 7 ml of the 4824 ppm tank. The IRGA output was

Reproduced with permission of the copyright owner. Further reproduction prohibited without permission.

converted to μgC based on the ideal gas law:

$$\mu gC_{ref} = ((((a*(P_l/P_s))/(R*T))/1000)*C_s)*12.01, \quad (2)$$

Where a is the amount of reference tank gas injected (mls), P_l is the pressure in the lab, P_s is standard pressure, R is the ideal gas constant, T is the lab temperature (°C), and C_s is the CO_2 concentration of the reference tank (here, 1040 or 4824 ppm). A regression of analyzer output versus μgC for the reference gas was used to calculate the concentration of CO_2 in the sample gas via:

$$\mu gC_{sample} = (\text{IRGA output} + \text{Y-int})/\text{X-var}, \text{ and}$$

$$\text{ppm } CO_2 = (((\mu gC_{sample}/12.01)/3.46e^{-5})/a), \quad (3)$$

where a is again the amount of gas injected (this time the sample), and *Y-int* and *X-var* are the y-intercept and x-variable from the regression analysis of the reference gas, respectively.

2.2.2.1. Isotopic analyses of SOM

Well-homogenized, carbonate-free soil samples were loaded into tin foil cups and crimped into a bead and placed in a sample carousel. The carousel sequentially dropped each capsule into a slide, which, in turn, dropped the capsule into the vertical furnace tube of a Carlo Erba NA1500 elemental analyzer for combustion. The capsule and sample were flash-combusted in a stream of oxygen at 1800°C. Evolved gases were carried in a stream of helium through an oxidizing furnace tube at 1025°C, a reducing furnace tube at 650°C, and a water trap at ambient temperature. The emerging anhydrous CO_2 and nitrogen passed through a 2-m long packed chromatography column at 40°C, which separates the gases from each other due to their different affinities for the column's

Reproduced with permission of the copyright owner. Further reproduction prohibited without permission.

exchange medium, with nitrogen eluting from the column before CO_2. The gases were then carried in the helium stream to a Micromass Isochrom mass spectrometer (Micromass Inc., Manchester, U.K.) where they were analyzed by "continuous flow." To facilitate optimal peak height of sample runs ($1E^{-9}$ to $6E^{-9}$ amps), the amount of CO_2 produced by the combustion of high C samples is diluted with helium by selecting a "dilution" run, whereas pure CO_2 from the low C samples enters the mass spectrometer in a "normal" run. The isotopic composition of the sample is determined by comparison to the isotopic composition of a pulse of working reference carbon dioxide injected during the analysis. The final delta value of each sample is reported as $\delta^{13}C$ relative to PDB, as calculated by the mass spectrometer's computer software.

2.2.2.2. Isotopic analyses of soil CO_2

The gas samples collected for this study represented a tremendous methodological challenge because their CO_2 concentrations ranged from about 400 to over 12,000 ppm. Furthermore, the samples were collected at different atmospheric pressures, which meant that automating the sample runs was very difficult, and in the end, abandoned. As a consequence of the concentration and pressure issues, there was no single laboratory ideally equipped to process all of the gas samples. Thus, low concentration samples had to be processed in one lab, and high concentration samples were processed in another lab.

Soil gas samples were stored cold (5°C) until analyzed. Most samples were stored for about two weeks prior to analysis. Maximum storage time was 1-1/2 months. Samples were analyzed either at the Colorado State University (CSU) Stable Isotope Facility (the majority of the samples) or the Stable Isotope Facility for Ecological Research (SIRFER)

Reproduced with permission of the copyright owner. Further reproduction prohibited without permission.

at the University of Utah. The CSU facility is well-suited for high concentration samples whereas the Utah facility was better able to process the low concentration (ca. 400 to 3000 ppm) samples. The CSU hardware consists of a VG Microgas Injector (Micromass Inc., Manchester, U.K.) linked to an Optima mass spectrometer (formerly VG Scientific, now Micromass Inc., Manchester, U.K.) run in continuous flow mode. Gas samples were drawn from sample vials using a Series A-2 gas tight syringe (VICI Precision Sampling, Baton Rouge, LA). The needle was purged and the sample was over-pressured just prior to injection through a silicone septa into the gas chromatograph portion of the Microgas Injector. The amount of sample injected was calculated from the CO_2 concentration, based on an optimal peak height for the instrument (1-6 E^{-9} amps, most injections were 200 to 600 µl). Sample gases are separated on a PoraPak QS 80/00 packed column (0.2 cm i.d., 2 m length, column temperature 70°C), and enter the mass spectrometer via an open split (a heartcut valve sends column effluent to waste or to the MS). Over 230 samples plus duplicates and standards were processed using this manner. An average difference in isotopic composition between sample and reference gas was determined using the following general equation:

$$[(R_{sample}-R_{standard})/(R_{standard})] \times 1000 = \Delta_{sample\text{-}standard} \quad (4)$$

where R_{sample} is the ratio of heavy to light isotope of interest in the sample, $R_{standard}$ is the same ratio in the working reference gas, and $\Delta_{sample\text{-}standard}$ is the difference in isotopic composition of the sample relative to that of the reference, expressed in parts per thousand (per mill, or ‰). Twenty-eight injections of a working standard yielded a precision of 0.4‰ for C and 0.5‰ for O.

Reproduced with permission of the copyright owner. Further reproduction prohibited without permission.

Samples analyzed at the SIRFER facility (141 samples, plus duplicates and standards) were injected via gas-tight syringe (VICI Precision Sampling, Baton Rouge, LA) into a flow of helium carrier gas (flow rate of 20 ml/min). The samples passed through a PreCon trace gas preconcentrator (Finnigan MAT, Bremen, Germany), into a 55 m gas chromotograph column (GC column temp 30°C). The column effluents were sent to a Finnigan MAT 252 mass spectrometer (Finnigan MAT, Bremen, Germany) via moveable open split. Optimal sample size for the instrument is $1.8E^{-9}$ to $8.9E^{-9}$ moles CO_2, so the volume of gas injected varied as a function of its CO_2 concentration (usually 30 µl to 400 µl). External precision of the method is 0.2‰ for C and 0.3‰ for O.

2.2.3. Modeling

I used a soil diffusion model developed by Tans [1998] that calculates the simultaneous effects of CO_2 diffusion and equilibration with water on $\delta^{18}O$ values of CO_2 in a soil profile. The model also implicitly accounts for atmospheric invasion into the soil profile [*Miller et al.*, 1999; *Tans*, 1998], and one output of the model is the apparent isotopic composition ($\delta^{13}C$ and $\delta^{18}O$) of the flux of respired CO_2 to the atmosphere. At each model time step, CO_2 is produced in model layers according to a field-measured production rate. CO_2 also diffuses both into and from an atmospheric layer, here set at a height of 20 cm, that initially contains air of a measured CO_2 concentration and isotopic signature, which is flushed at the measured flow rate. The model reaches steady state when both the concentration and isotopic signature of the atmospheric layer no longer change. The model is shown schematically in Figure 2.7, and described in more detail in Chapter 3.

Reproduced with permission of the copyright owner. Further reproduction prohibited without permission.

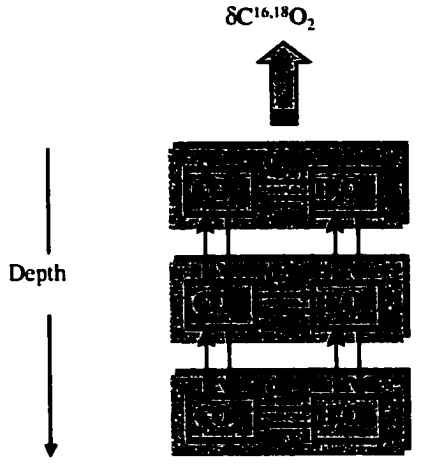

Figure 2.7. Schematic diagram of the soil diffusion-equilibration model developed by Tans [1998] and employed in this study. Each grey box represents a model layer. Small arrows indicate isotopic equilibration according to Brenninkmeijer et al. [1983], and larger arrows indicate diffusion according to Fick's 2nd law.

The model was initialized for field conditions on multiple sampling dates for each of the six field sites. A total of 19 simulations were undertaken to characterize site-dependent flux composition as well as its temporal variability. The model requires the following input as a function of depth in the soil: soil porosity, water volume, soil temperature, and the isotopic ($\delta^{18}O$) signature of soil water. Field measurements of these properties from 5, 10, 30, and 50 cm were entered into the model, and estimates, based on air temperature, rainwater $\delta^{18}O$, and field notes, were developed for surface (0 cm) characteristics. The model interpolates among the input measurements to complete the soil profile. Depth-independent input variables include background CO_2 concentration and isotopic composition, the rate of CO_2 evolution from the soil, and the rate of chamber flushing. Flushing rate is the measured flow rate of the LI-6200 during sample collection (converted to appropriate units using the ideal gas law). The flux rate was calculated directly from the LI-6200 output via plots of CO_2 concentration vs. time (separate plot for

Reproduced with permission of the copyright owner. Further reproduction prohibited without permission.

Reproduced with permission of the copyright owner. Further reproduction prohibited without permission.

Table 2.2 Calculation of the isotopic signature of the CO_2 flux from the soil to the atmosphere, using the Tans soil diffusion model (Tellus, 1998) in forward implicit mode, initialized with field data for a Lodgepole pine stand on fine soil in late July, 1998.

Site; sampling date	Depth-dependent model input					Depth-independent model input					
BR 728 Lodgepole pine, fine soil,	Depth	Porosity	Water volume	Soil Temp	Del Soil Water	Atmospheric flask			Flux rate	Depth-avg δ^{13}C-SOM	Other model parameters
28 July, 1998	0	0.460	0.15	16.0	-4.0	[CO2] "Cabg"	δ^{13}C "del13bg"	δ^{18}O "del18bg"	5.2 umol/m2/sec	-24.53 (‰PDB)	alpha18= 0.9913
	5	0.452	0.119	12.1	-4.69	371	-8.28	-1.14			
Production function written to match concentration profile	10	0.442	0.108	11.4	-6.4				.449 mol/m2/day		flush= 0.0472
	30	0.463	0.082	11.3	-12.5						ht of atm= 20 cm
	50	0.480	0.077	10.9	-13.2						atm press= 720 mbar

END OF RUN SUMMARY:

Total production (mol m-2 day-1): 0.44949999
Total production (mol cm-2 s-1): 5.2025462e-010
Flux from soil (mol cm-2 s-1): 5.2017371e-010 Flux from box: 5.2017395e-010
CO2, O18 and C13 into box: 371.00000 -1.14000 -8.28000
CO2, O18 and C13 from box: 389.39983 -1.5523330 -9.0464032
Apparent 18O signature of flux from soil: -9.8663330
Apparent 13C signature of flux from soil: -24.499991

18O signature of production (no invasion): -9.7208722

FLANAGAN model estimate of del-p: -6.42

Eeff= 9.8663330 - 4.0973922 = 5.77‰

each soil chamber closure, n=5, where the mean slope equals the flux in parts per million (ppm), which was then converted to units of mol/m^2/day). Production is assumed to equal the measured flux. Measured depth profiles of soil CO_2 concentration were used in conjunction with the total measured flux rate to constrain the CO_2 production function in the model. This added model constraint is an improvement over previous experiments with this model, which assumed constant production with depth [*Miller et al.*, 1999]. Table 2.2 lists the model input used for one of the simulations, and Appendix II includes the complete set of parameters used in each of the 19 simulations.

2.3. Results and Discussion

2.3.1. The $\delta^{13}C$ of soil organic matter

It is generally accepted that the ^{13}C signature of soil organic matter (SOM) increases with depth in the soil profile [e.g.,*Balesdent et al.*, 1993; *Desjardins et al.*, 1994; *Martin et al.*, 1990; *Nadelhoffer and Fry*, 1988; *Veldkamp*, 1993; *Volkoff and Cerri*, 1987]. However, there are competing processes that govern the carbon isotopic composition of SOM. First, selective utilization of nutrient-rich compounds such as carbohydrates, sugars, and proteins, which have relatively high $\delta^{13}C$ values, leaves $\delta^{13}C$-low compounds such as lignin, in the remaining organic material. Thus, over time there will be a tendency toward lighter ($\delta^{13}C$-low) values for bulk SOM as decomposition proceeds. Conversely, kinetic fractionation effects that accompany metabolism favor respiration of ^{12}C, leaving the remaining soil richer in ^{13}C [*Macko and Estep*, 1984]. An additional factor that will tend to make SOM rich in ^{13}C is the change in the $\delta^{13}C$ content of the atmosphere over time. Fossil fuel burning releases CO_2 with a $\delta^{13}C$ composition lower than that of the present

Reproduced with permission of the copyright owner. Further reproduction prohibited without permission.

atmosphere. Since the beginning of the Industrial Revolution the $\delta^{13}C$ of the atmosphere has dropped from roughly -6.7‰ to nearly -8‰ at the start of the 21st century [*Bird et al.*, 1996; *Farquhar et al.*, 1989; *Trolier et al.*, 1996]. Carbon derived from plants that lived further in the past will therefore be higher in ^{13}C than carbon from recently created organic matter. Note that both the change in the $\delta^{13}C$ of the atmosphere and metabolic fractionation are in direct opposition to the effect of preferential decomposition. Thus, it is not clear a priori what a $\delta^{13}C$-SOM versus depth profile will look like, especially under different vegetation types or soils of different physical characteristics.

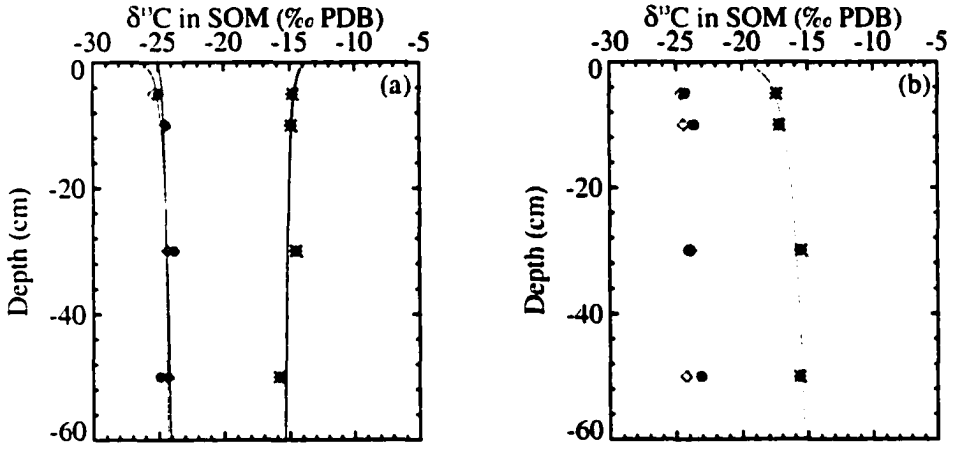

Figure 2.8. Carbon isotopic composition of soil organic matter by depth. (a) Three ecosystems on fine soil, (b) three ecosystems on coarse soil. Asterix represents shortgrass steppe, solid circle represents lodepole pine, and open diamond represents alpine tundra. (values expressed in units of per mil versus Pee Dee Belmnite)

Figures 2.8 and 2.9 explore the $\delta^{13}C$-SOM versus depth relationship for the three vegetation types and two soil textures studied. Average C_3 (e.g., forests and cool-season grasses) bulk plant $\delta^{13}C$ values are approximately –20 to –35‰, whereas those of C_4 plants (e.g., warm-season grasses) are –14 to –9‰ [*Galimov*, 1985] due to corresponding greater (C_3) and lesser (C_4) fractionation against ^{13}C during photosynthesis [*Lloyd and*

Reproduced with permission of the copyright owner. Further reproduction prohibited without permission.

Farquhar, 1994]. Thus, the large observed difference (Figure 2.8) in $\delta^{13}C$ of SOM between the pure C_3 and mixed C_3-C_4 ecosystems studied was expected. However, the difference in the slope of the curve for the shortgrass steppe site on fine soil, compared to the other five sites, was unexpected. The depth profiles for the shortgrass steppe sites suggest that either: (1) there has been a shift in the C_3-C_4 composition (recent increase in C_3 component at the coarse-textured site and perhaps the opposite at the fine-textured site), or (2) there is greater input of C_4 carbon at depth on sandy soils because of rooting depth differences in C_3 and C_4 plants, or (3) there is preferential decomposition of C_3 carbon. The last is not implausible. Santruckova et al. [2000] reported selective decomposition of C_3 over C_4 carbon in mixed grasslands in Australia. With the exception of the steppe sites, the $\delta^{13}C$ of bulk organic matter generally increases by roughly 2‰ between 5 and 50 cm depth (Figure 2.9, again, the difference in the slope of the curve for the two steppe sites is currently unexplained). The lodgepole pine site on fine soil may be an exception, as a smoothed representation of the data suggests essentially no increase in $\delta^{13}C$ with depth (Figure 2.9). von Fischer & Tieszen [1995] reported no increase in SOM $\delta^{13}C$ below the litter layer in four forests of Puerto Rico. In some forest and alpine systems, however, leaching of humic and fulvic acids leads to an increase in ^{13}C with depth. As shown in Figures 2.8 and 2.9, there is no distinct texture effect on the change in $\delta^{13}C$ with depth for these sites. This lack of textural effect is in contrast with the results of Kracht & Bird (unpublished data) and those of Desjardins et al. [1994], who found larger variations in $\delta^{13}C$ of SOM with depth in a finer-textured as compared to a sandier soil.

Reproduced with permission of the copyright owner. Further reproduction prohibited without permission.

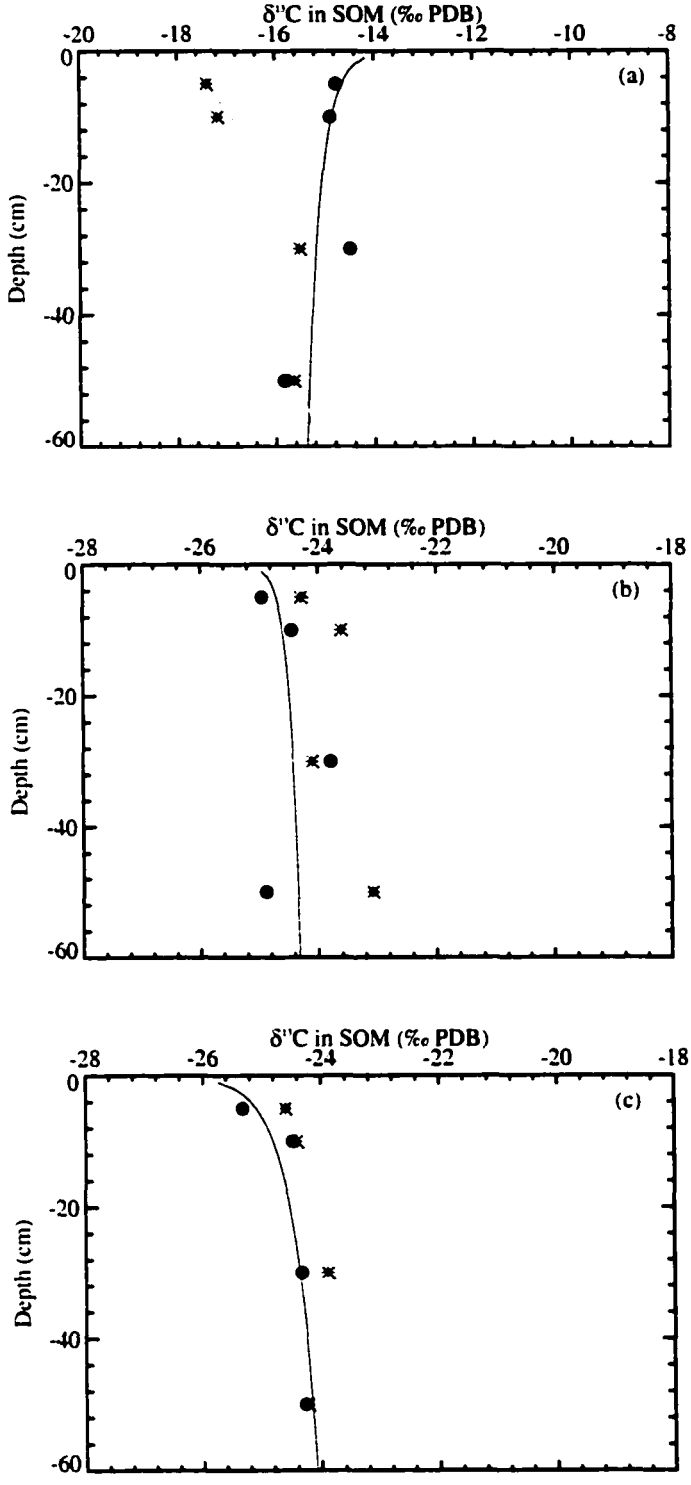

Figure 2.9. Depth profiles of soil organic matter carbon isotopic composition for the six field sites: (a) shortgrass steppe sites, (b) lodgepole pine sites, and (c) alpine tundra sites. Solid circle represents the data for fine soils, whereas the asterix represents the coarse soils. The smoothed curve is a log linear regression of the data (IDL Program, RSI, Inc.).

Reproduced with permission of the copyright owner. Further reproduction prohibited without permission.

2.3.2. The relationship between the $\delta^{13}C$ of SOM and that of soil CO_2

Soil CO_2 has three potential sources: root (autotrophic) respiration, heterotrophic respiration during decomposition, and diffusion from the atmosphere. Unless conditions are very dry and/or biological productivity is minimal, the atmospheric component will be small [*Hesterberg and Siegenthaler*, 1991; *Miller et al.*, 1999; *Tans*, 1998] and the isotopic composition of soil CO_2 will reflect the vegetation at the sampling location. A complication is that autotrophic respiration can account for as little as 10% to as much as 90% of total soil respiration [*Andrews et al.*, 1999; *Hanson et al.*, 2000; *Lin et al.*, 1999], suggesting that the match between in situ soil CO_2 the organic matter from which it is primarily derived will vary as a function of vegetation type and environmental conditions. de Camargo et al. [1999] reported differences between $\delta^{13}C$ of soil CO_2 and that of SOM ($\Delta_{CO_2\text{-}SOM}$) of 2‰ near the soil surface (0-10 cm), diminishing to 0.3‰ at 8 m depth in an Amazonian forest. Results from the current work also suggest that $\Delta_{CO_2\text{-}SOM}$ generally decreases with depth (Figure 2.10). Also in agreement with the Amazonian study [*de Camargo et al.*, 1999] and an Australian study [*Santruckova et al.*, 2000] is the nearly 1:1 relationship between the two variables. In both this study and that of de Camargo et al. [1999], soil CO_2 was slightly heavier (more ^{13}C) than the corresponding organic matter (Figure 2.11). In contrast, the results of Santruckova et al. [2000], suggest that whereas microbial C is enriched relative to the resultant CO_2, soil CO_2 is slightly depleted in ^{13}C. The current study cannot distinguish between microbially-derived and total soil CO_2.

Reproduced with permission of the copyright owner. Further reproduction prohibited without permission.

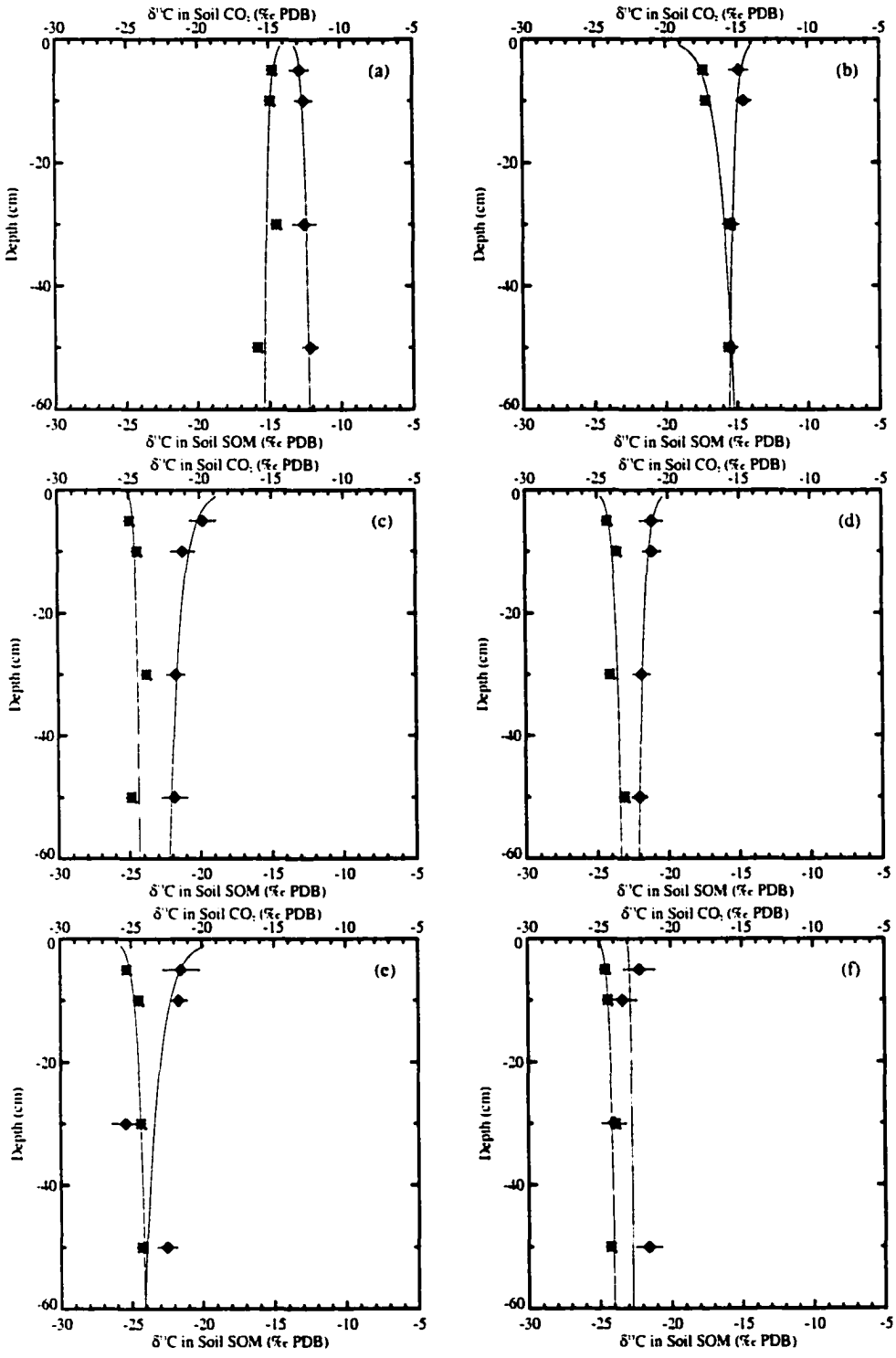

Figure 2.10. Seasonal mean values of $\delta^{13}C$ for soil CO_2 (open diamond) by depth compared with $\delta^{13}C$ of the soil organic matter (asterix) at the same depths. Error bars are standard error across all sampling dates. (a) Shortgrass steppe site on fine soil, (b) shortgrass steppe site on coarse soil, (c) lodgepole pine site on fine soil, (d) lodgepole pine site on coarse soil, (e) alpine tundra site on fine soil, (f) alpine tundra site on coarse soil.

Reproduced with permission of the copyright owner. Further reproduction prohibited without permission.

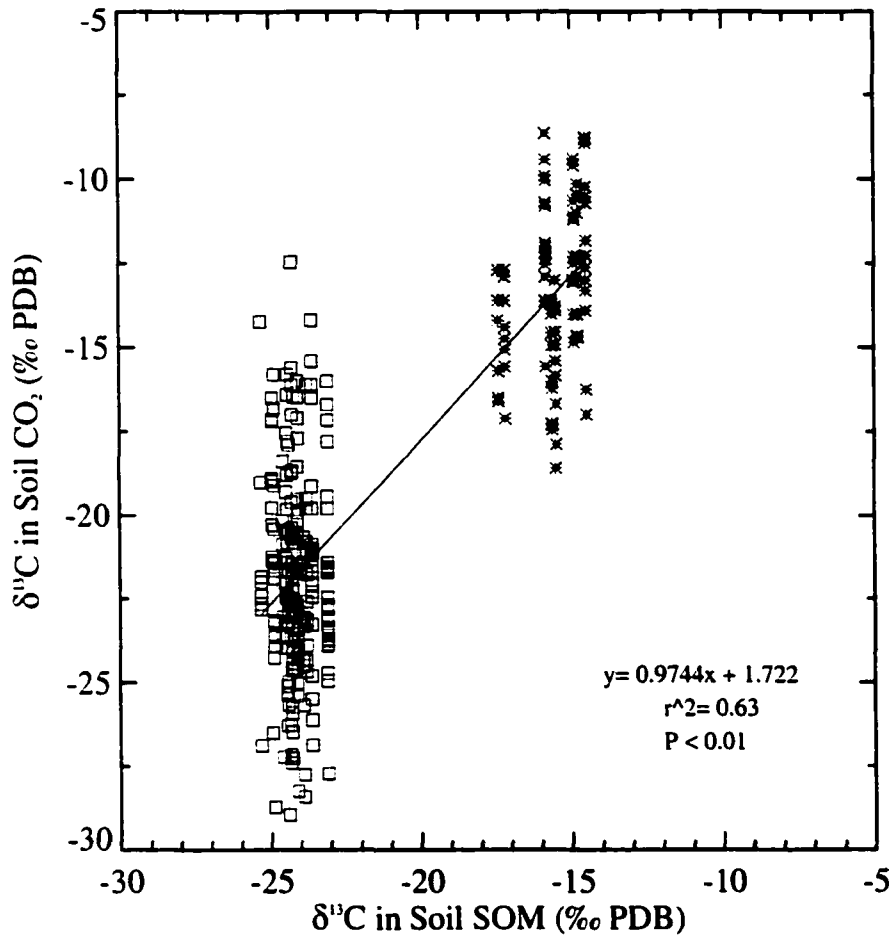

Figure 2.11. Comparison of the $\delta^{13}C$ composition of soil CO_2 with the $\delta^{13}C$ composition of soil organic matter (as elsewhere in the dissertation, all values for carbon isotopic composition expressed in units of per mil versus Pee Dee Belmnite). Open squares represent data from pure C_3 systems (lodgepole and tundra), and data from mixed C_3-C_4 sites (shortgrass steppe) are shown with an asterix.

As mentioned above, the isotopic composition of soil CO_2 will be affected by site-specific conditions. Figure 2.12 illustrates the differences in both the $\delta^{13}C$ value of soil CO_2 and in $\Delta_{CO_2\text{-}SOM}$ over time. The CO_2 emitted from these sites is isotopically most similar to SOM at the onset of the growing season (with the exception of the tundra site on fine soil) and least like SOM after senescence (note that there are no post-senescence measurements for the tundra sites).

Reproduced with permission of the copyright owner. Further reproduction prohibited without permission.

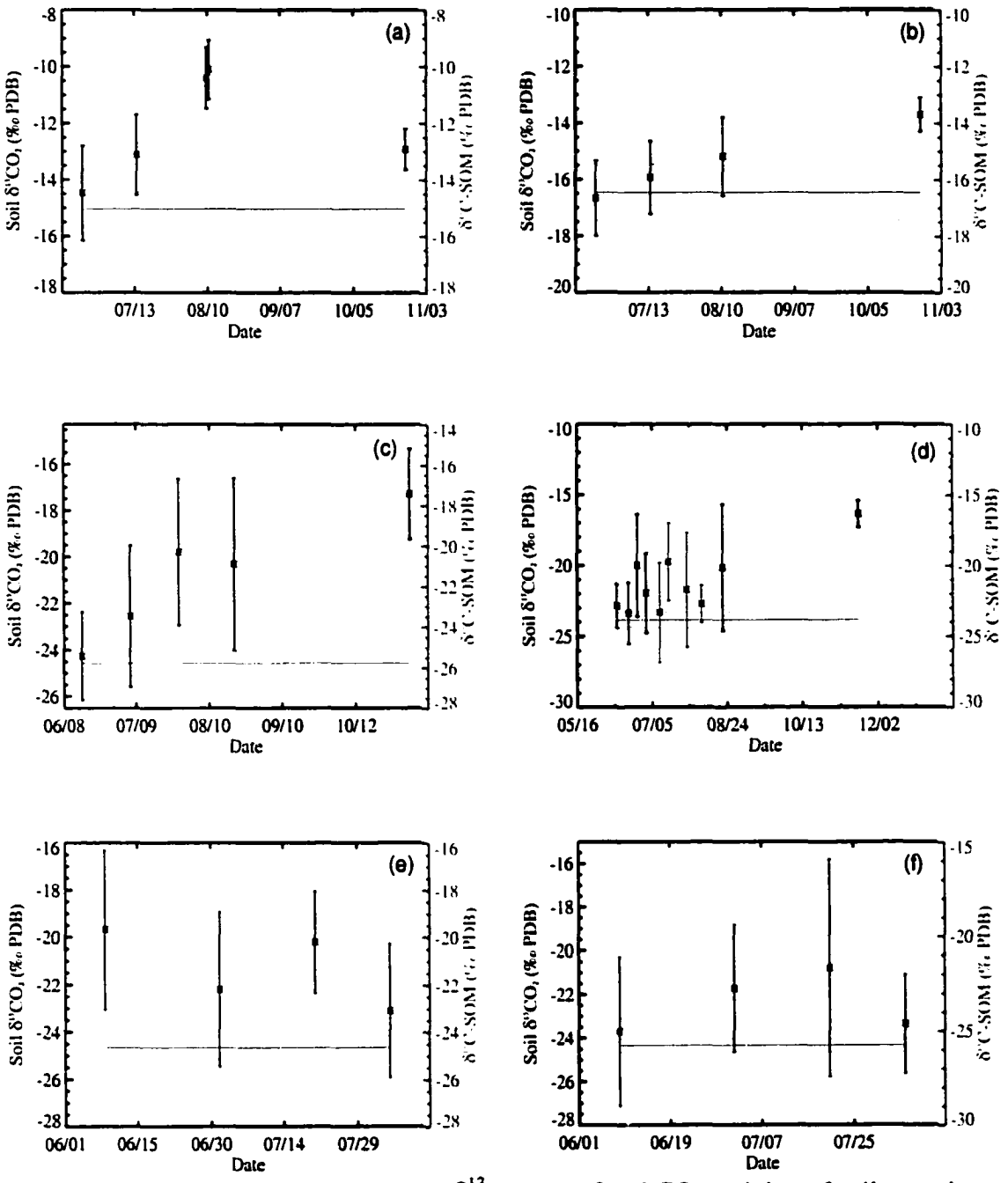

Figure 2.12. Relationship between the $\delta^{13}C$ value of soil CO_2 and that of soil organic matter. Asterix represents the mean value for all depths and across the three sampling tubes at a site. Error bars are standard deviation about the mean. Solid horizontal line represents the average $\delta^{13}C$ value for SOM from all depths, and dashed lines represent one standard deviation from the mean. It was assumed that the isotopic composition of the SOM did not vary over the growing season. (a) Shortgrass steppe site on fine soil, (b) shortgrass steppe site on coarse soil, (c) lodgepole pine, fine soil, (d) lodgepole pine, coarse soil, (e) alpine tundra, fine soil, (f) alpine tundra, coarse soil.

Reproduced with permission of the copyright owner. Further reproduction prohibited without permission.

At all but the alpine tundra site on fine soil, $\Delta_{CO_2\text{-}SOM}$ is very small at the start of the growing season. It then generally increases, but is highly variable. The cause for the change over the season needs further investigation. The change could suggest a shift in the contribution of root respiration to total respiration as primary productivity increases, a change in the amount of atmospheric invasion, or even a shift in the isotopic fractionation associated with diffusion of CO_2 out of the soil profile (there is less fractionation and more invasion under low production/dry conditions). For sites sampled after the end of the growing season (steppe and pine sites), the $\delta^{13}C$ value of soil CO_2 suggests a relatively large contribution of atmospheric origin ($\delta^{13}C$ much heavier, or less negative).

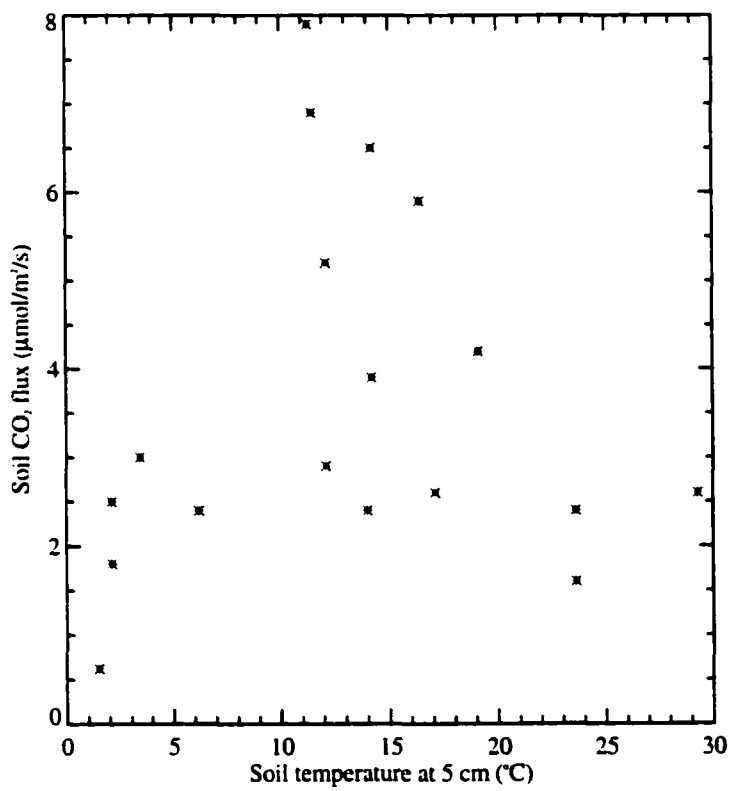

Figure 2.13. Relationship (not statistically significant at the 0.05 level, JMP IN, SAS Institute Inc.) between the soil CO_2 efflux rate and soil temperature at 5 cm depth. Data shown are for all field sites on all sampling dates for which data were available.

Reproduced with permission of the copyright owner. Further reproduction prohibited without permission.

2.3.3. The magnitude of the soil CO_2 flux

Measured flux rates for the 1998 growing season at the six field sites ranged from a low of 1.6 μmol/m^2/s to a high of 7.9 μmol/m^2/s (Table 2.3). The highest rates were associated with soil temperatures at 5 cm ranging from 10-20°C (Figure 2.13) and water-filled pore space at the same depth 0.2 or greater (Figure 2.14). Low CO_2 flux rates were associated with very dry conditions and cold soil surface temperature (Figures 2.13 and 2.14, Table 2.3). Flux rates were as low as 0.62 μmol/m^2/s during the fall sampling (lodgepole pine site on coarse soil, 5 cm soil temp 1.5°C). Davidson et al. [2000] argue that further progress is needed in defining temperature and moisture controls on the rate of soil respiration, and that measurements by soil horizon are more appropriate than are measurements taken at arbitrary depth increments.

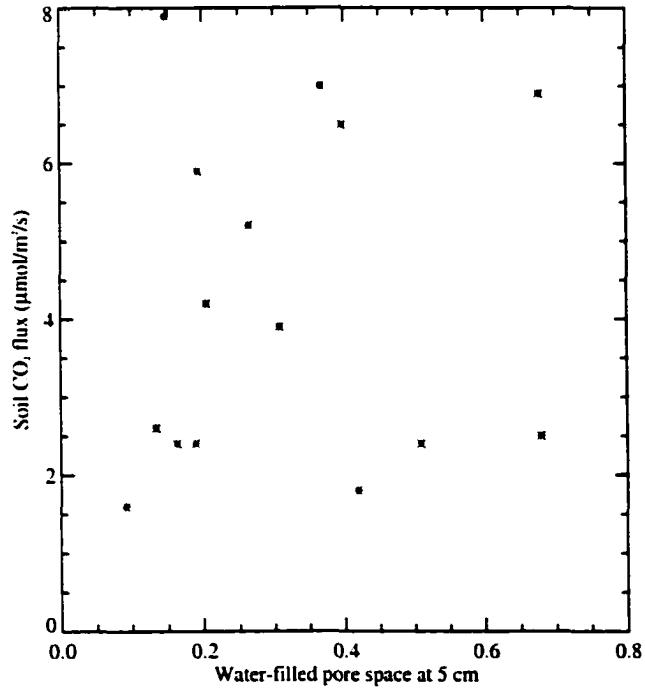

Figure 2.14. Relationship (not statistically significant at the 0.05 level, JMP IN, SAS Institute Inc.) between the soil CO_2 efflux rate and soil moisture content (expressed as water-filled pore space) at 5 cm depth. Data shown are for all field sites on all sampling dates for which data were available.

Reproduced with permission of the copyright owner. Further reproduction prohibited without permission.

Flux rate was weakly but significantly correlated with organic carbon content up to about 2% C; above this amount there was essentially no relationship between flux rate and C content (Figure 2.15). Considerable temporal variability in CO_2 flux rate was observed at each of the field sites, and spatial heterogeneity at each site was also high. Seasonal average flux rates were indistinguishable across ecosystems or soil textures (Figure 2.16). Additional sampling might reveal significantly lower fluxes from the shortgrass steppe site on coarse soil, but low sample numbers prevented establishment of significant differences across sites (Welch Anova test, JMP IN software, SAS Institute, Inc.).

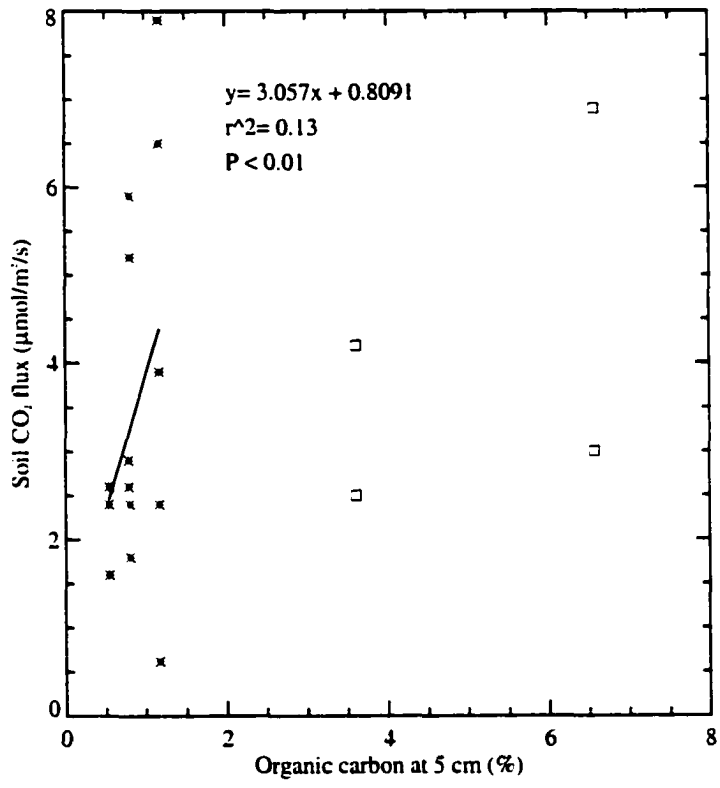

Figure 2.15. Relationship between the soil CO_2 efflux rate and soil organic carbon content (%) at 5 cm depth. At organic carbon contents below 2% (shown with an asterix) the relationship is statistically significant at the 0.01 level (JMP IN, SAS Institute Inc.). Above this content (data labeled with an open square), the relationship was not significant. Data shown are for all field sites on all sampling dates for which data were available.

Reproduced with permission of the copyright owner. Further reproduction prohibited without permission.

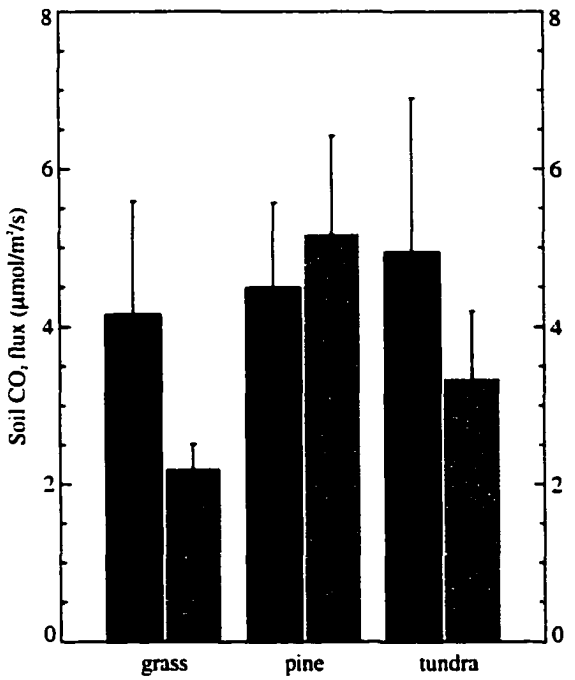

Figure 2.16. Seasonal average rates of soil CO_2 efflux. Data for coarse soils represented by the light bars, and data for fine soils by the dark bars. The differences across ecosystems and soil textures are not significant at the 0.05 level (Welch Anova test, JMP IN software, SAS Institute, Inc.).

My CO_2 flux rate measurements, and the patterns I observed, are in agreement with published data [*Davidson and Trumbore*, 1995; *Fang et al.*, 1998; *Gordon et al.*, 1987; *Lin et al.*, 1999; *Miranda et al.*, 1997; *Norman et al.*, 1992; *Ryan and Waring*, 1992; *Sommerfeld et al.*, 1993]. Buchmann & Schulze [1999] reviewed 116 studies of nighttime ecosystem fluxes using eddy covariance techniques (of which an estimated 80% or more is attributable to soil respiration [*Trumbore et al.*, 1990]). They reported a range of 2.7 to 8.3 $\mu mol/m^2/s$ across all ecosystem types examined, with lowest values from evergreen forests and the highest from C_4 crops and C_3 temperate grasslands.

Reproduced with permission of the copyright owner. Further reproduction prohibited without permission.

Table 2.3. Observed soil CO_2 efflux rates and associated field conditions.

Ecosystem	Texture	Date, 1998	Moisture content (% by wt, 5 cm)	Soil temperature (°C, 5 cm)	CO_2 efflux rate ($\mu mol/m^2/s$)
S. steppe	fine	6/5	na	12.1	2.9±0.3
S. steppe	fine	7/14	11	29.3	7.0±3.7
S. steppe	fine	8/11	4	29.3	2.6±0.8
S. steppe	coarse	6/5	na	17.1	2.6±0.2
S. steppe	coarse	7/14	4	23.6	2.4±0.2
S. steppe	coarse	8/11	2	23.6	1.6±0.3
L. pine	fine	6/16	16	6.2	2.4±0.7
L. pine	fine	7/7	6	16.4	5.9±0.4
L. pine	fine	7/28	8	12.1	5.2±1.5
L. pine	fine	11/5	13	2.1	1.8±0.5
L. pine	coarse	7/1	6	14.0	2.4±0.3
L. pine	coarse	7/10	5	11.3	7.9±2.8
L. pine	coarse	7/28	12	14.2	6.5±0.5
L. pine	coarse	8/7	10	14.2	3.9±0.9
L. pine	coarse	11/19	8	1.5	0.62±0.3
A. tundra	fine	6/9	62	3.4	3.0±0.4
A. tundra	fine	7/21	33	11.5	6.9±0.5
A. tundra	coarse	6/9	26	2.1	2.5±0.8
A. tundra	coarse	7/21	8	19.1	4.2±1.5

2.3.4. The $\delta^{13}C$ of the soil-respired CO_2 flux

Because it is very difficult, if not currently impossible, to collect actual samples of the soil-respired CO_2 flux to the atmosphere, one of two available approaches to estimate its isotopic composition must be used. The first approach, pioneered by C.D. Keeling [1958], assumes a simple two end-member mixing model between a biological source (here, total soil respiration) and the background atmosphere. Tans [1998] noted there can be problems with this method because of invasion of atmospheric CO_2 into the soil. The second approach [*Tans*, 1998] incorporates the soil physical and chemical processes of diffusion and isotopic equilibration. The model was developed primarily for assessment of soil-respired ^{18}O, because the assumption of a two end-member system in soil fails for

Reproduced with permission of the copyright owner. Further reproduction prohibited without permission.

this species (see Chapter 3). The "Keeling method" has been used extensively for profiles of CO_2 concentration and ^{13}C composition both in the free atmosphere and within the plant canopy [*Buchmann and Ehleringer*, 1998; *Dudziak and Halas*, 1996; *Flanagan et al.*, 1996; *Flanagan et al.*, 1997; *Friedli et al.*, 1987; *Keeling*, 1961; *Miranda et al.*, 1997; *Sternberg et al.*, 1998; *Yakir and Wang*, 1996]. However, the approach is much less frequently applied to soil profiles [*Amundson et al.*, 1998; *Cerling et al.*, 1991; *Dörr and Münnich*, 1980].

One consideration for using the Keeling approach in soils is that although theoretically CO_2 concentration should increase with depth as diffusion becomes more limited, because of both cracks or fissures and hot spots of decomposition, the observed pattern is not always everywhere smoothly increasing with depth (Figure 2.17). For example, one of the three sampling tubes at the shortgrass steppe, fine soil site appears to have been especially problematic (Figure 2.17) as was the case in late July, and again in late August, at the lodgepole pine site on coarse soil (Appendix III, Figures 1-5). A simple pattern with depth was neither expected nor observed for the relationship between the $\delta^{13}C$ of soil CO_2 and depth (Figure 2.18). The high degree of variability across the three sampling tubes on some, but not all, sampling dates, at some, but not all, depths was at first a little surprising. However, differential contributions of SOM decomposition (microbial respiration) and root respiration over time, even on the scale of a meter, have been observed by others [*Andrews et al.*, 1999; *Hanson et al.*, 2000; *Lin et al.*, 1999].

Calculation of the $\delta^{13}C$ of soil-respired CO_2 using the Keeling method was carried out for each sampling date for each of the six field sites (Figure 2.19). The $\delta^{13}C$ values

Reproduced with permission of the copyright owner. Further reproduction prohibited without permission.

and CO_2 concentrations were averaged across the three sampling tubes at each of the four sampling depths (5, 10, 30, and 50 cm) when CO_2 concentration increased with depth.

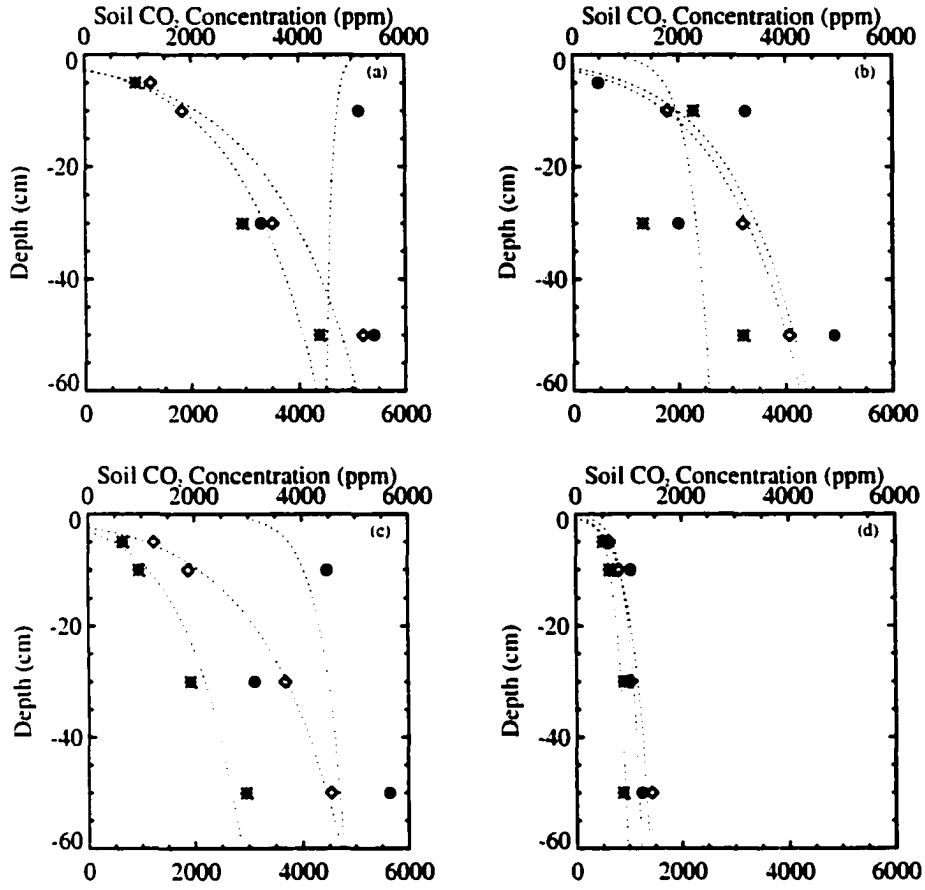

Figure 2.17. Representative plots of soil CO_2 concentration versus depth for the shortgrass steppe site on fine-textured soil. Different symbols represent different sampling tubes (placed 1-m apart). The smoothed curve is a log linear regression of the data (IDL program, RSI, Inc.). (a) Samples taken on June 23, 1998, (b) July 14, 1998, (c) August 11, 1998, and (d) October 26, 1998. Plots for the other field sites are presented in Appendix III, Figures 1-5.

When it did not, a filtering method was applied to replace the aberrant values with the average concentration from the depth above and below from the particular sampling tube in question. If the 5 cm concentration value was unusually high, or the 50 cm concentration value unusually low, the data point and its associated ^{13}C value were omitted. The y-intercept of a linear regression of the filtered CO_2 concentration data

Reproduced with permission of the copyright owner. Further reproduction prohibited without permission.

(plotted as inverse values by convention) and $^{13}CO_2$ values represents the biological source signature. Soil CO_2 is subject to kinetic fractionation during diffusion to the overlying atmosphere, and so the y-intercept of these plots must be shifted downward by roughly 4.4‰ to represent the signature of the soil CO_2 flux.

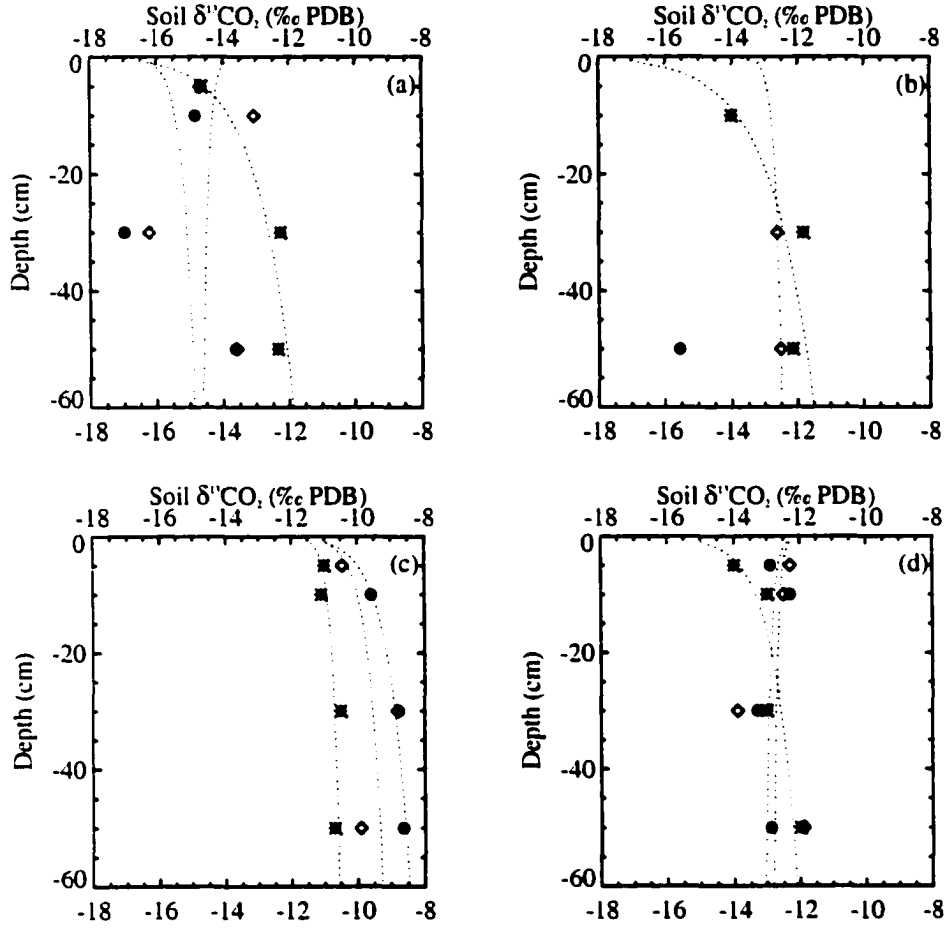

Figure 2.18. Representative plots of soil CO_2 $\delta^{13}C$ value versus depth for the shortgrass steppe site on fine-textured soil. Different symbols represent different sampling tubes (placed 1-m apart). The smoothed curve is a log linear regression of the data (IDL program, RSI, Inc.). (a) Samples taken on June 23, 1998, (b) July 14, 1998, (c) August 11, 1998, and (d) October 26, 1998. Plots for the other field sites are presented in Appendix III, Figures 6-10.

Davidson [1995] argues that although 4.4‰ is the theoretical maximum, the actual values are often less than this, and depend on the $\delta^{13}C$ of the soil-respired CO_2. Table 2.4

Reproduced with permission of the copyright owner. Further reproduction prohibited without permission.

summarizes the calculated $\delta^{13}C$ of the soil-respired flux assuming that the maximum value for diffusion applies in all cases (with the recognition that it most likely does not).

Table 2.4. Output of a two end-member mixing model ("Keeling plot") used to calculate the $\delta^{13}C$ of soil-respired CO_2.

Site	Date	Y-intercept	Slope	r^2	Estimated $\delta^{13}C$ of soil respired CO_2
1	6/23/98	-13.81	-971	0.14	-18.21
1	7/14/98	-11.93	-3726	0.14	-16.33
1	8/11/98	-9.267	-1296	0.81	-13.667
1	10/26/98	-12.46	-337	0.11	-16.86
2	6/23/98	-16.78	633	0.24	-21.18
2	7/14/98	-18.01	4512	0.74	-22.41
2	8/11/98	-14.22	-1215	0.07	-18.62
2	10/26/98	-13.91	231	0.64	-18.31
3	6/16/98	-24.93	2399	0.36	-29.33
3	7/7/98	-24.38	3064	0.47	-28.78
3	7/28/98	-22.56	1015	0.67	-26.96
3	8/21/98	-21.56	22.3	$3E^{-5}$	-25.96
3	11/5/98	-19.1	1643	0.36	-23.5
4	6/11/98	-23.42	1782	0.56	-27.82
4	6/19/98	-24.51	1399	0.66	-28.91
4	6/25/98	-23.32	5946	0.56	-27.72
4	7/1/98	-22.25	-481	0.00	-26.65
4	7/10/98	-24.1	751	0.23	-28.5
4	7/16/98	-21.63	2519	0.29	-26.03
4	7/28/98	-27.85	2519	0.39	-32.25
4	8/7/98	-23.09	2476	0.10	-27.49
4	8/21/98	-21.95	5146	0.23	-26.35
4	11/19/98	-15.68	-749	0.33	-20.08
5	6/9/98	-21.1	-5556	1.00	-25.5
5	7/2/98	-24.57	6055	0.62	-28.97
5	7/21/98	na	na	na	na
5	8/5/98	-23.74	1068	0.01	-28.14
6	6/9/98	-23.82	233	0.01	-28.22
6	7/2/98	-20.93	-5550	0.54	-25.33
6	7/21/98	-23.57	3411	0.05	-27.97
6	8/5/98	-24.04	2621	0.06	-28.44

Reproduced with permission of the copyright owner. Further reproduction prohibited without permission.

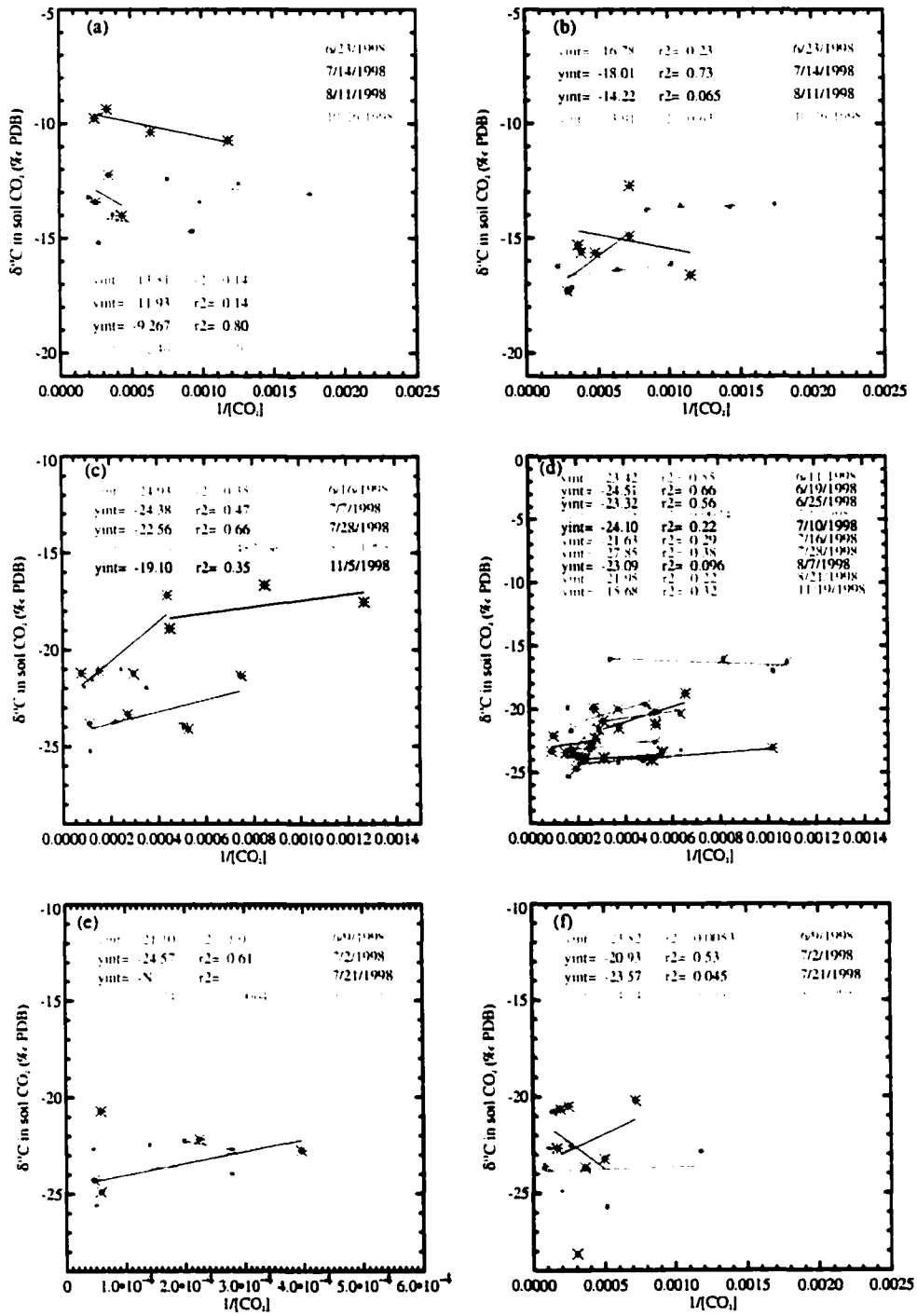

Figure 2.19. Soil CO_2 $\delta^{13}C$ values plotted against the inverse of soil CO_2 concentration. The y-intercept of this plot, minus 4.4‰ to account for diffusion, yields the isotopic composition of soil-respired CO_2. Each color represents a separate sampling date. Each asterix is a mean of the sample tubes for a particular depth on a given sampling date. (a) Shortgrass steppe site on fine soil, (b) shortgrass steppe site on coarse soil, (c) lodgepole pine site on fine soil, (d) lodgepole pine site on coarse soil, (e) alpine tundra site on fine soil, (f) alpine tundra site on coarse soil.

Reproduced with permission of the copyright owner. Further reproduction prohibited without permission.

The calculated $\delta^{13}C$ values of soil-respired CO_2 varied by more than 2‰ over the sampling period at each of the six sites (Figure 2.19, Table 2.4). Tans [1998] notes that under certain circumstances, including low soil CO_2 production and high diffusion, the actual relationship is curved near the y-axis, resulting in estimates of the $\delta^{13}C$ of soil-respired CO_2 that can deviate from the actual respired values by several per mil. At the four sites visited after the end of the growing season (all but the two tundra sites), the y-intercept of the regressed data was notably different from the value calculated for the other sampling dates (see Figure 2.19, especially panels c and d). A weak positive correlation ($P < 0.01$) was found between the ^{13}C of soil-respired CO_2 and soil temperature at 5 cm (Figure 2.20), whereas the correlation with soil moisture was also weak but negative ($P < 0.05$, Figure 2.21).

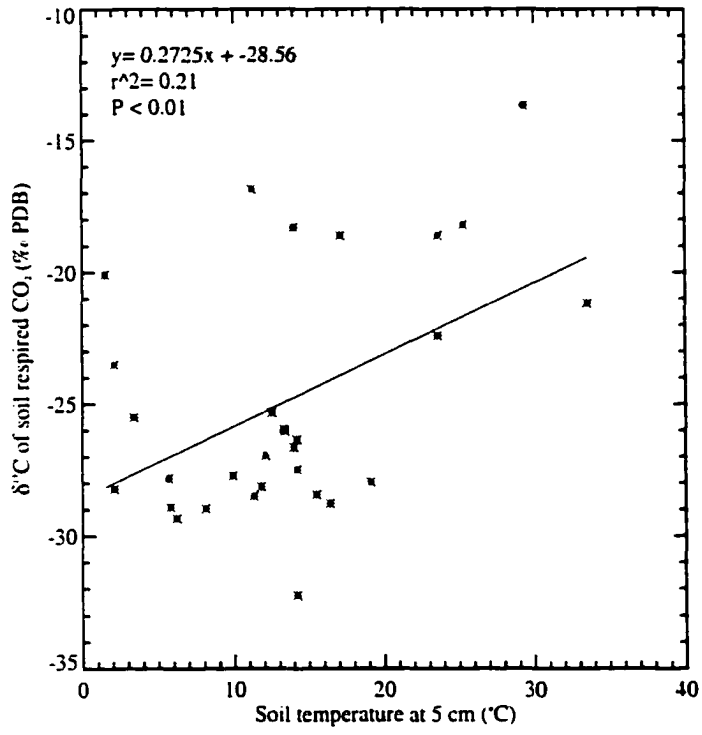

Figure 2.20. Relationship between the isotopic composition of soil-respired CO_2 (as calculated by the two end-member model) and soil temperature at 5 cm. This plot includes all sites and all sampling dates for which there are data.

Reproduced with permission of the copyright owner. Further reproduction prohibited without permission.

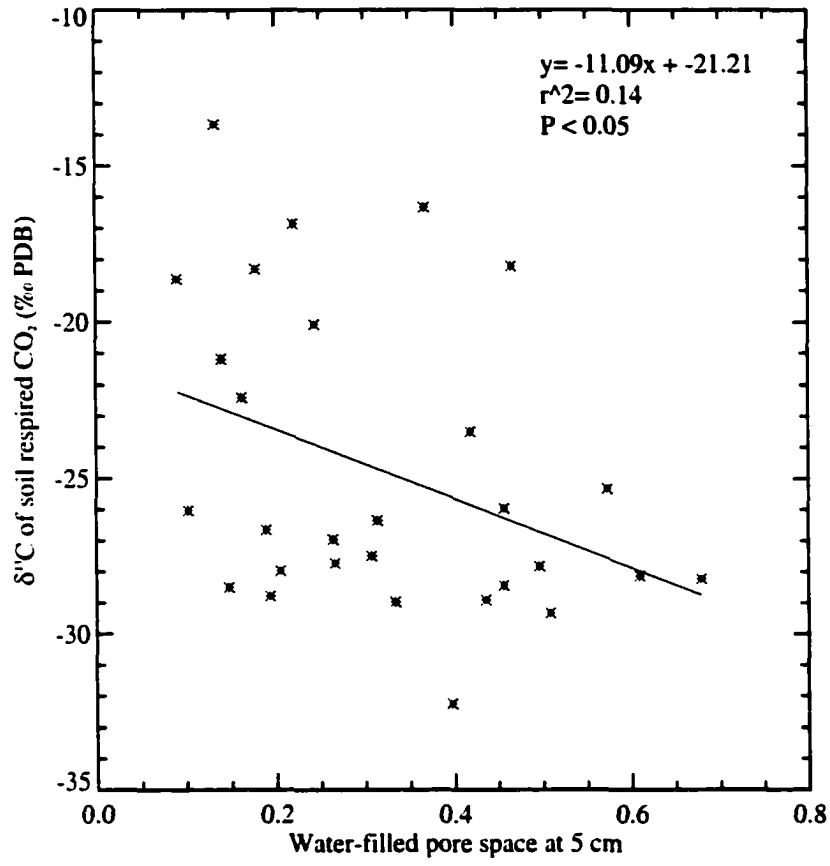

Figure 2.21. Relationship between the isotopic composition of soil-respired CO_2 (as calculated by the two end-member model) and soil moisture (as water-filled pore space) at 5 cm. This plot includes all sites and all sampling dates for which there are data.

When data are averaged over time there is a clear distinction between the $\delta^{13}C$ value of soil-respired CO_2 from a mixed C_3-C_4 system versus a pure C_3 system, but no clear differences among the four pure C_3 sites (Figure 2.22). There is a quantifiable difference in C_4 contribution to the total root-plus-organic matter respiration pool at the two shortgrass steppe sites. The ^{13}C content of the major plant species were not measured at these sites, but if one assumes values of –13‰ for the C_4 plants and –28‰ for the C_3 plants, then the average contribution of C_4 vegetation to the soil CO_2 flux can be calculated for each of the sites according to [*Miranda et al.*, 1997]:

Reproduced with permission of the copyright owner. Further reproduction prohibited without permission.

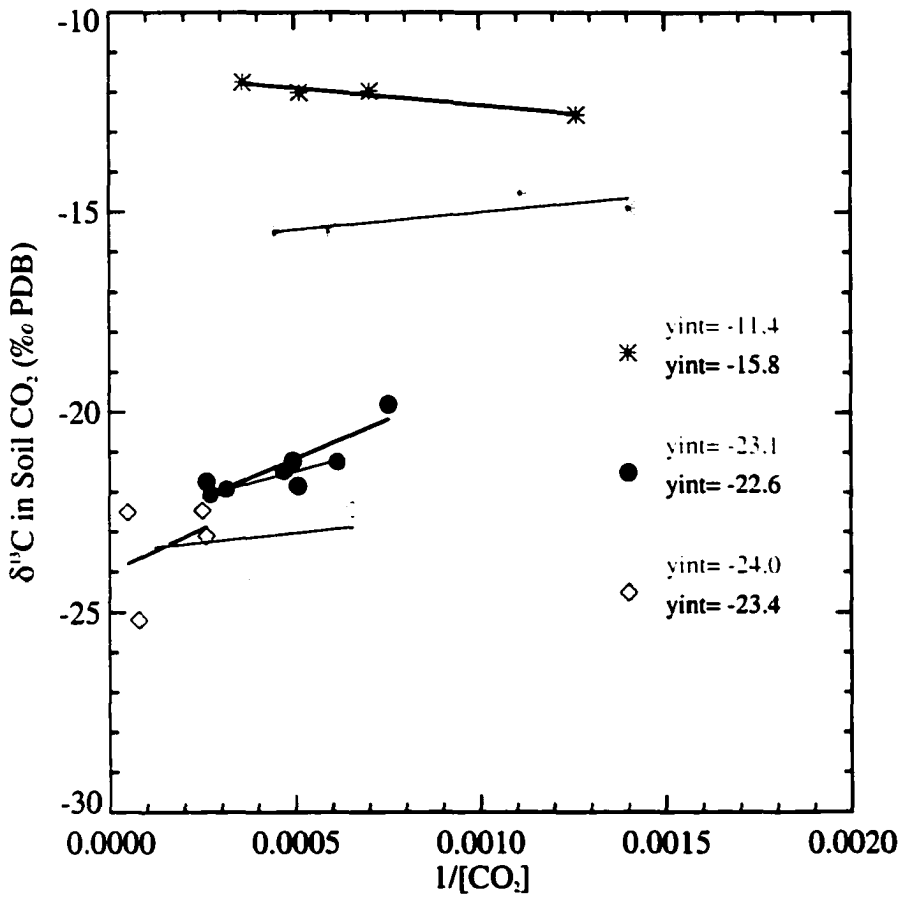

Figure 2.22. Isotopic composition of soil-respired CO_2 calculated as a seasonal average using the "Keeling" approach. The y-intercept of each regression line, minus 4.4‰ to account for diffusion, is the estimated signature of respiration. Shortgrass steppe sites are labeled with an asterix, lodgepole sites with a closed circle, and the tundra sites with an open diamond. Sites on coarse soils are labeled with dark symbols, sites on fine soils are light.

$$P_4 = (\delta^{13}_R - \delta^{13}_3)/(\delta^{13}_4 - \delta^{13}_3), \quad (5)$$

where δ^{13}_R is the carbon isotopic composition of the CO_2 flux to the atmosphere (for these calculations, the seasonal average with the assumption of 4.4‰ kinetic fractionation), δ^{13}_3 is the average carbon isotopic composition of the C_3 vegetation, and δ^{13}_4 is the average carbon isotopic composition of the C_4 vegetation. The results are presented in Table 2.5.

Reproduced with permission of the copyright owner. Further reproduction prohibited without permission.

Table 2.5. Proportion of C_4 vegetation contributing to the $\delta^{13}C$ composition of the soil-respired flux at the two field sites in the shortgrass steppe ecosystem (using eqn 5).

Soil texture	Average $\delta^{13}C_R$ (‰ vs. PDB)	P_4
Fine	-15.8	0.81
Coarse	-20.2	0.52

The use of the soil diffusion model to calculate the isotopic composition of the soil CO_2 flux to the atmosphere is explored in detail in Chapter 4. Appendix II lists model input and results for the 19 model runs performed. Table 2.6 compares the calculated seasonal-average $\delta^{13}C$ of the soil-respired flux based on the Keeling approach and the Tans approach. The two methods are in *relatively* good agreement on a seasonal-average basis. However, as discussed above, particularly under conditions of low CO_2 production or high diffusion (i.e., high atmospheric invasion into the soil profile), the Keeling approach is likely to seriously overestimate the $\delta^{13}C$ of the flux to the atmosphere. Under other conditions the correlation coefficient for the $\delta^{13}C$ vs. $1/[CO_2]$ is relatively high, but the y-intercept yields an estimate of the soil-respired $\delta^{13}C$ that is significantly lighter than that calculated by the soil diffusion model (Table 2.7).

Reproduced with permission of the copyright owner. Further reproduction prohibited without permission.

Table 2.6. Comparison of the seasonal, ecosystem-average $\delta^{13}C$ of the CO_2 flux to the atmosphere as calculated by the Tans approach and by the Keeling approach.

Ecosystem	Tans soil diffusion model	Keeling two end-member model
Shortgrass steppe	-15.57 ± 0.78 (n=5)	-18.20 ± 2.74 (n=8)
Lodgepole pine	-24.12 ± 0.38 (n=11)	-27.08 ± 2.75 (n=15)
Alpine tundra	-24.39 ± 0.18 (n=3)	-27.51 ± 1.47 (n=7)

Table 2.7. Comparison of the $\delta^{13}C$ of the CO_2 flux to the atmosphere as calculated by the Tans approach and by the Keeling approach for specific sample sites and dates.

Field site	Date	Tans soil diffusion model	Keeling two end-member model
Shortgrass steppe, fine soil	8/11/98 (hot and dry)	-15.00	-9.27 (r^2=0.80)
Shortgrass steppe, coarse soil	7/14/98 (hot and dry)	-16.43	-22.41 (r^2=0.73)
Lodgepole pine, fine soil	7/28/98 (high flux rate)	-24.50	-27.00 (r^2=0.66)
Lodgepole pine, coarse soil	11/19/98 (low flux rate)	-23.78	-20.08 (r^2=0.32)

2.4. Conclusions

Distinctions in the $\delta^{13}C$ of SOM were significant across sites only as a function of the proportion of C_4 photosynthetic pathway (from 0 to an estimated 81%) at the site.

Reproduced with permission of the copyright owner. Further reproduction prohibited without permission.

Regardless of SOM isotopic composition, the observed $\delta^{13}CO_2$ values were heavier than the SOM from which they are derived (with a variable root respiration component of 10-90% of the total soil respiration flux). The apparent kinetic fractionation that contributes to the observed difference between CO_2 and SOM isotopic composition was often less that the theoretical value of 4.4‰, and varied over time according to site-specific conditions (e.g., soil temperature and moisture content). CO_2 flux from these sites can be large, especially when soil temperatures are from 10-20°C and water-filled pore space at 5 cm is greater than 0.2. A two end-member mixing model was used to calculate the $\delta^{13}C$ of the soil-respired CO_2 flux. Results suggest high temporal variability at each of the six sites, likely due in part to changes in soil temperature and moisture. A comparison of results from the two end-member model with those of a model of soil diffusion and isotopic equilibration reveals discrepancies of roughly 3‰ for seasonal average values from each ecosystem, with results of the simple model always more enriched in ^{13}C. Differences between the two methods were sometimes even greater for specific field conditions.

Literature Cited

Amundson, R., L. Stern, T. Baisden, and Y. Wang, The isotopic composition of soil and soil-respired CO_2, *Geoderma*, *82*, 83-114, 1998.

Andrews, J.A., K.G. Harrison, R. Matamala, and W.H. Schlesinger, Separation of root respiration from total soil respiration using carbon-13 labeling during Free-Air Carbon Dioxide Enrichment (FACE), *Soil Science Society of America Journal*, *63* (5), 1429-1435, 1999.

Balesdent, J., C. Girardin, and A. Mariotti, Site-related $\delta^{13}C$ of tree leaves and soil organic matter in a temperate forest, *Ecology*, *74*, 1713-1721, 1993.

Reproduced with permission of the copyright owner. Further reproduction prohibited without permission.

Bird, M.I., A.R. Chivas, and J. Head, A latitudinal gradient in carbon turnover times in forest soils, *Nature*, *381*, 143-146, 1996.

Buchmann, N., and J.R. Ehleringer, CO_2 concentration profiles, and carbon and oxygen isotopes in C_3 and C_4 crop canopies, *Agricultural and Forest Meteorology*, *89*, 45-58, 1998.

Buchmann, N., and E.-D. Schulze, Net CO_2 and H_2O fluxes of terrestrial ecosystems, *Global Biogeochemical Cycles*, *13* (3), 751-760, 1999.

Cerling, T.E., D.K. Solomon, J. Quade, and J.R. Bowman, On the isotopic composition of carbon in soil carbon dioxide, *Geochimica et Cosmochimica Acta*, *55*, 3403-3405, 1991.

Ciais, P., A.S. Denning, P.P. Tans, J.A. Berry, D.A. Randall, G.J. Collatz, P.J. Sellers, J.W.C. White, M. Trolier, H.A.J. Meijer, R.J. Francey, M. Patrick, and M. Heimann, A three dimensional synthesis study of $\delta^{18}O$ in atmospheric CO_2 Part I: Surface fluxes, *Journal of Geophysical Research*, *102* (D5), 5857-5872, 1997.

Ciais, P., P. Tans, J.W. White, M. Trolier, R. Francey, J. Berry, D. Randall, P. Sellers, J.G. Collatz, and D. Schimel, Partitioning of ocean and land uptake of CO_2 as inferred by $\delta^{13}C$ measurements from the NOAA/Climate Monitoring and Diagnostics Laboratory Global Air Sampling Network, *Journal of Geophysical Research*, *100D* (D3), 5051-5070, 1995.

Davidson, E.A., and S.E. Trumbore, Gas diffusivity and production of CO_2 in deep soils of the eastern Amazon, *Tellus*, *47B*, 550-565, 1995.

Davidson, E.A., L.V. Verchot, J.H. Cattanio, I.L. Ackerman, and J.E.M. Carvalho, Effects of soil water content on soil respiration in forests and cattle pastures of eastern Amazonia, *Biogeochemistry*, *48* (1), 53-69, 2000.

Davidson, G.R., The stable isotopic composition and measurement of carbon in soil CO_2, *Geochimica et Cosmochimica Acta*, *59* (12), 2485-2489, 1995.

de Camargo, P.B., S.E. Trumbore, L.A. Martinelli, E.A. Davidson, D.C. Nepstad, and R.L. Victoria, Soil carbon dynamics in regrowing forest of eastern Amazonia, *Global Change Biology*, *5*, 693-702, 1999.

Desjardins, T., F. Andreaux, B. Volkoff, and C.C. Cerri, Organic carbon and ^{13}C contents in soils and soil size-fractions, and their changes due to deforestation and pasture installation in eastern Amazonia, *Geoderma*, *61*, 103-118, 1994.

Dörr, H., and K.O. Münnich, Carbon-14 and caron-13 in soil CO_2, *Radiocarbon*, *22*, 909-918, 1980.

Reproduced with permission of the copyright owner. Further reproduction prohibited without permission.

Dudziak, A., and S. Halas, Diurnal cycle of carbon isotope ratio in soil CO_2 in various ecosystems, *Plant and Soil, 183*, 291-299, 1996.

Fang, C., J.B. Moncrieff, H.L. Gholz, and K.L. Clark, Soil CO_2 efflux and its spatial variation, *Plant & Soil, 205* (2), 135-146, 1998.

Farquhar, G.D., J.R. Ehleringer, and K.T. Hubick, Carbon isotope discrimination and photosynthesis, *Annual Reviews of Plant Physiology and Plant Molecular Biology, 40*, 503-537, 1989.

Flanagan, L.B., J.R. Brooks, G.T. Varney, S.C. Berry, and J.R. Ehleringer, Carbon isotope discrimination during photosynthesis and the isotope ratio of respired CO_2 in boreal forest ecosystems, *Global Biogeochemical Cycles, 10* (4), 629-640, 1996.

Flanagan, L.B., J.R. Brooks, G.T. Varney, and J.R. Ehleringer, Discrimination against $C^{18}O^{16}O$ during photosynthesis and the oxygen isotope ratio of respired CO_2 in boreal forest ecosystems, *Global Biogeochemical Cycles, 11* (1), 83-98, 1997.

Friedli, H., U. Siegenthaler, D. Rauber, and H. Oeschger, Measurements of concentration, $^{13}C/^{12}C$ and $^{18}O/^{16}O$ ratios of tropospheric carbon dioxide over Switzerland, *Tellus, 39B*, 80-88, 1987.

Fung, I., C.B. Field, J.A. Berry, M.V. Thompson, J.T. Randerson, C.M. Malmstrom, P.M. Vitousek, G.J. Collatz, P.J. Sellers, D.A. Randall, A.S. Denning, F. Badeck, and J. John, Carbon 13 exchanges between the atmosphere and biosphere, *Global Biogeochemical Cycles, 11* (4), 507-533, 1997.

Galimov, E.M., *The Biological Fractionation of Isotopes*, Academic Press, New York, 1985.

Gee, G.W., and J.W. Bauder, Particle size analysis, in *Methods of Soil Analysis. Part I. Physical and Mineralogical Methods*, edited by A. Klute, pp. 383-411, Soil Science Society of America, Madison, WI, 1986.

Gemery, P.A., M. Trolier, and J.W.C. White, Oxygen isotope exchange between carbon dioxide and water following atmospheric sampling using glass flasks, *Journal of Geophysical Research, 101* (D9), 14,415-14,420, 1996.

Gordon, A.M., R.E. Schlentner, and K. van Cleve, Seasonal patterns of soil respiration and CO_2 evolution following harvesting in the white spruce forests of interior Alaska, *Canadian Journal of Forest Research, 17*, 304-310, 1987.

Reproduced with permission of the copyright owner. Further reproduction prohibited without permission.

Hanson, P.J., N.T. Edwards, C.T. Garten, and J.A. Andrews, Separating root and soil microbial contributions to soil respiration: A review of methods and observations, *Biogeochemistry*, *48* (1), 115-146, 2000.

Hesterberg, R., and U. Siegenthaler, Production and stable isotopic composition of CO_2 in a soil near Bern, Switzerland, *Tellus*, *43B*, 197-205, 1991.

Jenny, H., *Factors of Soil Formation*, McGraw Hill, New York, 1941.

Jenny, H., *The Soil Resource*, Springer-Verlag, New York, 1980.

Keeling, C.D., The concentration and isotopic abundances of atmospheric carbon dioxide in rural areas, *Geochimica et Cosmochimica Acta*, *13*, 322-334, 1958.

Keeling, C.D., The concentration and isotopic abundances of atmospheric carbon dioxide in rural and marine air, *Geochimica et Cosmochimica Acta*, *24*, 277-298, 1961.

Lin, G., J.R. Ehleringer, P.T. Rygiewicz, M.G. Johnson, and D.T. Tingey, Elevated CO_2 and temperature impacts on different components of soil CO_2 efflux in Douglas-fir terracosms, *Global Change Biology*, *5*, 157-168, 1999.

Lloyd, J., and G.D. Farquhar, ^{13}C discrimination during CO_2 assimilation by the terrestrial biosphere, *Oecologia*, *99*, 201-215, 1994.

Macko, S.A., and M.L.F. Estep, Microbial alteration of stable nitrogen and carbon isotopic composition of organic matter, *Organic Geochemistry*, *6*, 787-790, 1984.

Martin, A., A. Mariotti, J. Balesdent, P. Lavelle, and R. Vuattoux, Estimate of organic matter turnover rate in savanna soil by ^{13}C natural abundance measurements, *Soil Biology and Biochemistry*, *22*, 517-523, 1990.

Miller, J.B., D. Yakir, J.W.C. White, and P.P. Tans, Measurement of $^{18}O/^{16}O$ in the soil atmosphere CO_2 flux, *Global Biogeochemical Cycles*, *13* (3), 761-774, 1999.

Miranda, A.C., H.S. Miranda, J. Lloyd, J. Grace, R.J. Francey, J.A. Mcintyre, P. Meir, P. Riggan, R. Lockwood, and J. Brass, Fluxes of carbon, water and energy over Brazilian cerrado: an analysis using eddy covariance and stable isotopes, *Plant, Cell and Environment*, *20*, 315-328, 1997.

Nadelhoffer, K.J., and B. Fry, Controls on natural nitrogen-15 and carbon-13 abundances in forest soil organic matter, *Soil Science Society of America Journal*, *52*, 1633-1640, 1988.

Norman, J.M., R. Garcia, and S.B. Verma, Soil surface CO_2 fluxes and the carbon budget of a grassland, *Journal of Geophysical Research*, *97* (D17), 18,845-18,853, 1992.

Reproduced with permission of the copyright owner. Further reproduction prohibited without permission.

Rawls, W.J., Estimating soil bulk density from particle size analysis and organic matter content, *Soil Science*, *135* (2), 123-125, 1983.

Ryan, M.G., and R.H. Waring, Maintenance respiration and stand development in a subalpine lodgepole pine forest, *Ecology*, *73* (6), 2100-2108, 1992.

Santruckova, H., M.I. Bird, and J. Lloyd, Microbial processes and carbon-isotope fractionation in tropical and temperate grassland soils, *Functional Ecology*, *14* (1), 108-114, 2000.

Sommerfeld, R.A., A.R. Mosier, and R.C. Musselman, CO_2, CH_4 and N_2O flux through a Wyoming snowpack and implications for global budgets, *Nature*, *361*, 140-142, 1993.

Sternberg, L.d.S.L., M.Z. Moreira, L.A. Martinelli, R.L. Victoria, E.M. Barbosa, L.C.M. Bonates, and D. Nepstad, The relationship between $^{18}O/^{16}O$ and $^{13}C/^{12}C$ ratios of ambient CO_2 in two Amazonian tropical forests, *Tellus*, *50B*, 366-376, 1998.

Tans, P.P., Oxygen isotopic equilibrium between carbon dioxide and water in soils, *Tellus*, *50B*, 163-178, 1998.

Trolier, M., J.W.C. White, P.P. Tans, K.A. Masarie, and P.A. Gemery, Monitoring the isotopic composition of atmospheric CO_2: measurements from the NOAA global air sampling network, *Journal of Geophysical Research*, *101* (D20), 25,897-25,916, 1996.

Trumbore, S.E., M. Keller, S.C. Wofsy, and J.M. da Costa, Measurements of soil canopy exchange rates in the Amazon rain forest using ^{222}Rn, *Journal of Geophysical Research*, *95* (D10), 16,865-16,873, 1990.

Veldkamp, E., Soil organic carbon dynamics in pastures established after deforestation in the humid tropics of Costa Rica, PhD. Dissertation thesis, Wageningen Agricultural University, Wageningen, The Netherlands, 1993.

Volkoff, B., and C.C. Cerri, Carbon isotopic fractionation in subtropical Brazilian grassland soils: comparison with tropical forest soils, *Plant and Soil*, *102*, 27-31, 1987.

von Fischer, J.C., and L.L. Tieszen, Carbon isotope characterization of vegetation and soil organic matter in subtropical forests in Luquillo, Puerto Rico, *Biotropica*, *27* (2), 138-148, 1995.

Yakir, D., and X.-F. Wang, Fluxes of CO_2 and water between terrestrial vegetation and the atmosphere estimated from isotope measurements, *Nature*, *380*, 515-517, 1996.

Reproduced with permission of the copyright owner. Further reproduction prohibited without permission.

CHAPTER 3

THE TEMPORAL AND SPATIAL VARIABILITY OF OXYGEN ISOTOPIC COMPOSITION OF SOIL WATER IN THREE COLORADO ECOSYSTEMS

Abstract

I measured the isotopic composition of oxygen in soil water across a bioclimatic gradient in the Rocky Mountains of Colorado to assess whether depth profiles reflect ecosystem type and/or soil physical properties. Seasonal variability in these profiles was also of interest, particularly as it may be transferred to the atmosphere via soil respiration. Soil water content (expressed as water-filled pore space) ranged from 0.03 in mid-July in a lodgepole pine forest on coarse-textured soil to 0.49 in early-June in an alpine tundra system on fine-textured soil. The isotopic composition of precipitation collected along the bioclimatic gradient ranged from −14.73‰ in early June to −0.03‰ in mid-August. The corresponding $\delta^{18}O$ in soil water at the sites ranged from −15.74‰ in June (lodgepole forest, fine soil) to −1.03‰ in August (shortgrass steppe, fine soil). Seasonal mean values for $\delta^{18}O$ were considerably more enriched at the grassland, as compared to lodgepole and tundra sites, and seasonal mean water content was lower on coarse than on fine soils. Results presented in Chapter 4 indicate that the differences in isotopic composition of soil water presented in this chapter translate into unique signatures of soil-respired CO_2.

Reproduced with permission of the copyright owner. Further reproduction prohibited without permission.

3.1. Introduction and Background

The isotopic composition of soil water has been of interest in the past for studies of groundwater recharge [*Mathieu and Bariac*, 1996; *Maule et al.*, 1994; *Zimmermann et al.*, 1967], analysis of water sources for plant uptake [*Brunel et al.*, 1997; *Dawson and Ehleringer*, 1991; *Walker and Richardson*, 1991], and study of local evaporation and transpiration [*Allison et al.*, 1983; *Barnes and Allison*, 1988; *Brunel et al.*, 1992; *Hsieh et al.*, 1998a]. The soil water profiles studied here were used to model the isotopic composition of soil-respired CO_2 (Sulzman et al., in prep, Chapter 4).

Soil water is the result of precipitation inputs and groundwater sources minus evaporated and transpired water. Evaporation is highly fractionating [*Craig and Gordon*, 1965] but transpiration is not [*White et al.*, 1985; *Zimmermann et al.*, 1967]. Precipitation amount varies greatly at any given location, and the source of the rainwater also varies. Measurements of the isotopic signature of oxygen in rainwater have been correlated to temperature, latitude, continentality, precipitation amount and intensity, and storm track and source region [*Cole et al.*, 1999; *Dansgaard*, 1964; *Gat*, 1980; *Koster et al.*, 1993; *Rozanski et al.*, 1982; *Yapp*, 1982]. The resulting spatial variability in the isotopic signature of soil water is high [*Brunel et al.*, 1997; *Mathieu and Bariac*, 1996]. Given the same amount of kinetic energy, molecules of lighter mass react more quickly than do those of heavier mass [*Galimov*, 1985]. This leads to an observed enrichment near the soil surface [*Barnes and Allison*, 1983]. Thus, spatial variability in both the vertical and the horizontal direction are important for an isotopic characterization of soil water.

Reproduced with permission of the copyright owner. Further reproduction prohibited without permission.

3.2. Methods

3.2.1. Field Sampling

Six field sites located along the Front Range of the Rocky Mountains in Colorado (Figure 3.1) were selected to represent three separate ecosystems (shortgrass steppe, lodgepole pine forest, and alpine tundra) and two soil textures (fine and coarse). The sites were selected utilizing the state factor approach as outlined by Jenny [*Jenny*, 1941]. According to Jenny, soil development is influenced by five factors: climate, organisms, relief (aspect and slope), parent material, and time. I was interested in both soil texture — a property largely determined by the parent material from which a soil develops — and bioclimate, or the combination of climate and its associated organisms [*Jenny*, 1980]. See Chapter 2 and Appendix I for further details regarding the field sites.

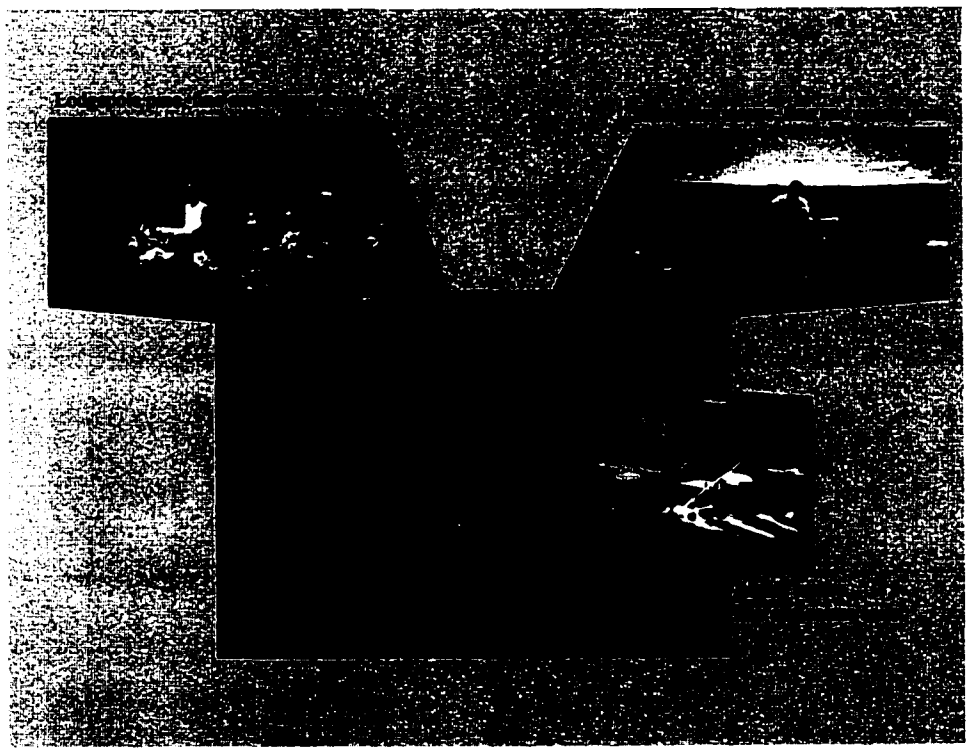

Figure 3.1. Field sites sampled during this study. Site represent three ecosystems (shortgrass steppe, lodgepole pine, and alpine tundra) on soils of fine and coarse texture. Each photograph represents a textural pair of sites.

Reproduced with permission of the copyright owner. Further reproduction prohibited without permission.

Field sampling was conducted over the 1997 and 1998 growing seasons, with an attempt made to capture pre-bud break and senescence (April-November). During the growing season (June-August), two field sites were visited each week. One site, lodgepole on coarse soil, was selected for intensive investigation because the 1997 data suggested the LP sites were more variable than those in the other ecosystems. This site (LP-coarse) was visited every week. A total of 32 field visits were made during the 1998 season. Routine measurements/collections conducted during each field visit included air temperature and a soil temperature profile (every 5 cm to 30 cm, plus 50 cm: microprocessor thermometer, Omega Engineering), bulk soil from four depths, soil gases, and rainwater. Details of methods used in sample collection are presented in Chapter 2. Methods specific to rain water and soil water analysis are presented here.

Bulk soil samples were taken from depths centered on 5, 10, 30, and 50 cm (± 2 cm). Samples were collected in 120 ml wide-mouth brown glass jars with a teflon-lined lid. After collection, the tops were wrapped in parafilm, and the jars were placed immediately in a cooler with ice for transport. Samples were stored in a cold room (5°C) until irradiated (1.15-1.20 Mrad) to stop all microbial activity. Duplicate samples were taken for analysis of gravimetric water content. These were stored in sealed plastic bags in the cooler, and then weighed moist immediately upon returning to the laboratory (usually within two hours of sampling).

To collect rainwater, a ring clamp attached to a re-bar stake was placed at breast height roughly 100-300 m away from the soil pit. A 100 mm diameter plastic funnel was set in the ring and Tygon tubing was fed from the funnel to a 1L high density polyethylene (HDPE) bottle, with a hole cut in the lid just barely big enough for the

Reproduced with permission of the copyright owner. Further reproduction prohibited without permission.

tubing. A loop was made in the tubing between the bottle and the funnel to prevent evaporation. Care was taken when removing the bottle to avoid contamination with water from the funnel and tubing (this water, if any, could have been fractionated by evaporation).

3.2.2. Laboratory Analyses

Laboratory analyses for the soil water samples included gravimetric analysis of water content, measurement of particle size distribution, and organic matter content analysis (necessary to calculate water amount on a volumetric basis). In addition, isotope ratio mass spectrometric analysis was carried out on rainwater, soil water, and soil-respired CO_2 samples. The methods used for mass spectrometric analysis are described in separate sections, below.

Measurement of soil water content was initiated on each sampling date by weighing moist samples immediately upon returning to the laboratory (as mentioned above). These samples were then oven dried for 48 hrs at 110°C, and re-weighed. Moisture content was calculated according to:

$$\% \text{ water} = ((\text{wet weight-dry weight})/\text{dry weight}) \quad (1)$$

Particle size distribution was determined by hydrometer method [*Gee and Bauder*, 1986]. A sub-sample of each soil was finely ground via a ball mill to assure complete homogenization. These homogenized samples were then analyzed via a LECO CHN 1000 Elemental Analyzer for organic content (%C and %N) (LECO Corporation, St. Joseph, MI). The %C information was used for calculation of bulk density. The error associated with calculation of bulk density from particle size and organic matter content

Reproduced with permission of the copyright owner. Further reproduction prohibited without permission.

is 0.3 g/cm^3 or less [*Rawls*, 1983]. Water content expressed on a volumetric basis is the product of gravimetric water content and calculated bulk density.

3.2.3. Isotopic Analyses

3.2.3.1 Method selection for isotopic analysis of soil water samples

To begin, a test was carried out of available methods for soil water isotopic analysis. An overview of the test and the chosen method is presented here. Working reference waters were mixed with a homogenized oven-dried (48 hrs at 110°C) clay loam soil in an amount sufficient to reach 10% moisture. The moist soil samples were loaded into seal-top sampling vials and topped with 0.5% CO_2 in helium. Samples were allowed to equilibrate for 24 h on an autosampler tray (temperature stability <0.1°C) at 30°C (Combi PAL, CTC, Switzerland). After equilibration, the concentric double wall needle of a Gas Bench II autoanalyzer (Finnigan MAT, Germany) sequentially pierces a sample septa and helium carrier gas is injected into the sampling vial at a flushing rate of 0.3 ml/min. The overpressure continuously passes the headspace gas (CO_2 plus helium) via the output portion of the needle over a Nafion drying trap via a Valco 6-port valve into a 100 µl sample loop for injection into the gas chromatograph column. After separation by a PoraPLOT Q capillary GC column (90 sec pass time), the individual gases are passed across a second Nafion drying trap into a MAT 252 isotope ratio mass spectrometer (Finnigan MAT, Bremen, Germany) via a moveable open split (see Figure 3.2).

Ten replicates (i.e., loop switches) of each sample headspace were made and the mean sample peak value was compared to two reference gases for computation of a preliminary delta value. This preliminary value was then converted to a value relative to

Reproduced with permission of the copyright owner. Further reproduction prohibited without permission.

Standard Mean Ocean Water (SMOW) reference material [*Coplen et al.*, 1983] by comparing to standard water samples run concurrently with the soil water samples. An average difference in isotopic composition between sample and reference gas is determined using the following general equation:

$$[(R_{sample}-R_{standard})/(R_{standard})] \times 1000 = \Delta_{sample\text{-}standard} \quad (2)$$

where R_{sample} is the ratio of heavy to light isotope of interest in the sample, $R_{standard}$ is the same ratio in the working reference gas, and $\Delta_{sample\text{-}standard}$ is the difference in isotopic composition of the sample relative to that of the reference, expressed in parts per thousand (per mill, or ‰). Analyses with the Gas Bench II instrument used here yielded an external precision of 0.14‰. Water samples were analyzed in the same manner as the moist soils. The results of this test are listed in Table 3.1.

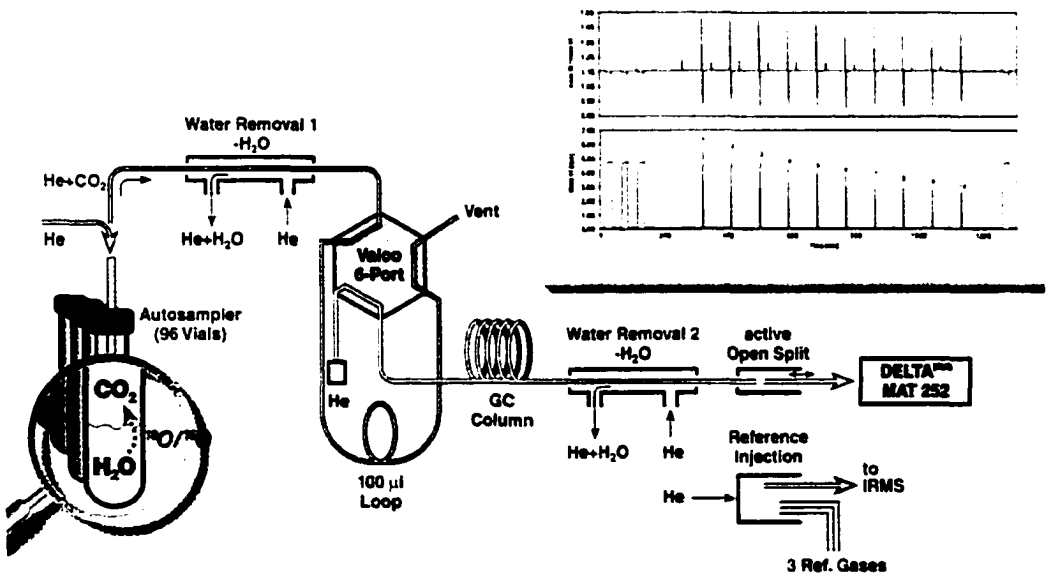

Figure 3.2. Design of the Finnigan MAT Gas Bench II device. Example output (reference gas and sample peaks) is shown in the upper right. I placed a moist soil sample in the test tube (lower left), where water is shown in this diagram.

Reproduced with permission of the copyright owner. Further reproduction prohibited without permission.

Table 3.1. Test of the direct equilibration method for determining the oxygen isotopic signature of soil water using the Finnigan MAT Gas Bench II device.

Water 1	Clay loam + Water 1	Difference	Water 2	Clay loam + Water 2	Difference
−15.31 ± 0.13	−15.26 ± 0.36	0.05±0.38	−2.74 ± 0.07	−3.15 ± 0.07	0.41±0.10

Part of the difference between soil water and the added water shown above may be due to the texture of the soil chosen for the test (the finest texture of all my field samples). Hsieh et al. [1998b] reported incomplete equilibration between water and CO_2 in soils of fine texture, such as the clay loam used for this test, because part of the water within these soils is adsorbed to mineral surfaces and/or is structurally-bound and therefore not available for equilibration. The amount of water used in the test may also have affected the results. Scrimgeour [1995] reported an effect of water amount on the signature of soil water measured, with the signature measured for soil water approaching that of the added water as water content increased. At 11% moisture (10% was used in this test as it was the modal value of all my field samples), Scrimgeour [1995] measured a difference of 0.6‰ between soil water and the added water. In an inter-laboratory comparison of methods to determine the stable isotope composition of soil water, Walker et al. [1994] found that all of the 14 laboratories involved measured soil water values significantly lighter (often more than 2‰) than the water added to those soils. Thus, the 0.4‰ or less difference (see Table 3.1) between the soil water and water analyses presented here suggests that the method used is perhaps the best available for measurement of the isotopic signature of the oxygen in soil water.

Reproduced with permission of the copyright owner. Further reproduction prohibited without permission.

3.2.3.2 Isotopic analysis of soil water

Field-moist soil (based on water content, water amount 0.3 ml) was loaded into 10 ml seal cap vials and shipped, along with two working standard waters, to Jena, Germany, for analysis on a Gas Bench II analyzer at the Max-Planck-Institut für Biogeochemie. Including duplicate samples, over 200 analyses were carried out. The direct equilibration method described above under "Method Selection for Isotopic Analysis of Soil Water Samples" was used to analyze the oxygen isotopic signature of the samples. Duplicates, and in some cases, triplicates, were randomly selected from all site—sampling date—depth combinations and were analyzed to assess "working precision" of the measurement technique. That is, I tried to quantify the uncertainty in the measured isotopic signature associated with storing, transferring, and shipping samples, in addition to the uncertainty due to internal instrument precision. Replicate measurements varied from 0.00 to 0.24‰, with standard deviations for duplicates of about 0.15‰ most common.

3.2.3.3 Isotopic analysis of rain water

Rain samples collected via the funnel system described above were carefully sealed to prevent evaporation and stored cold (5°C) until analyzed. Sub-samples of 0.2 ml were transferred with a disposable pipette into 1-ml glass chromatography vials fitted with a lid holding a Kel-f lined septa (new septa for each analysis) and placed into a sample rack. The rack of samples was then placed in a glove bag and evacuated gently (enough to remove the majority of the air from the glove bag), and then flushed with pure CO_2. The evacuation-flushing process was repeated three times. The vial lids were then sealed

Reproduced with permission of the copyright owner. Further reproduction prohibited without permission.

within the pure CO_2 atmosphere, and the samples were removed from the glove bag and placed on the equilibration block of a Multiprep automated sample preparation device (Micromass Inc., Manchester, U.K.). The samples were held at 40°C (controlled to ±0.1°C) for 10 hours to allow complete equilibration. A time series test showed that 10 hours is sufficient for this temperature and sample size (D. Reuss, personal communication). After equilibration a needle sequentially punctures each vial's septum, injecting carbon dioxide into the vials containing the water samples. The CO_2 that has equilibrated with the water sample then enters a side port in the same needle and passes through a water trap prior to being frozen into a cold finger (-80°C trap for five minutes). The pure CO_2 is then released into the dual inlet of an Optima gas-source triple-collector mass spectrometer (Micromass Inc., Manchester, U.K.), where it is analyzed by comparing its stable isotopic composition to that of a reference gas repeatedly during a seven-minute analysis.

Because the number of oxygen atoms in the CO_2 are far outnumbered by the number in each water sample (0.01 mol O from water vs. 0.00006 mol from CO_2), the isotopic composition of the CO_2 measured after equilibration is not affected by the signature of the CO_2 used for the equilibration (within instrument precision, 0.15‰ for the equilibration). The fractionation of the oxygen-18 between the gaseous CO_2 phase and the liquid water phase was accounted for by analyzing a series of waters with known ^{18}O signatures (SMOW, SLAP, GISP) and regressing the actual delta versus the observed delta, where:

$$\text{actual } \delta = 0.999889 * \text{observed } \delta - 6.25998$$

Reproduced with permission of the copyright owner. Further reproduction prohibited without permission.

3.3. Results and Discussion

3.3.1 Comparison of $\delta^{18}O$ Depth Profiles by Ecosystem Type

The isotopic signature of soil water, although highly variable over time, is distinct among ecosystems. Figure 3.3 shows the seasonal mean values for the pattern of $\delta^{18}O$ of soil water with depth, and compares those means across ecosystems. On fine-textured soils (Figure 3.3a), the seasonally-averaged values are distinct at all depths (with the possible exception of the 10 cm depth in pine and tundra ecosystems). From 5 to 50 cm the soil water is most enriched in the shortgrass steppe, intermediate in the lodgepole pine, and the least enriched (most negative) in the alpine tundra ecosystem. On coarse-textured soils there were no distinct differences between the two pure C_3 ecosystems for all but the near-surface measurements (Figure 3.3b), but the shortgrass steppe is again most enriched at all depths, and the tundra system is most depleted of the three near the soil surface. In the seasonal average, the $\delta^{18}O$ of soil water in the alpine tundra ecosystem on coarse-textured soil is characterized by an opposite pattern than that expected, with lighter water near the surface. This result is especially surprising because there are many bare-soil patches at this site, which would be expected to cause high evaporative water loss. The pattern of lighter water toward the soil surface might be due to rapid infiltration of frequent storm events at this site.

Differences in soil water $\delta^{18}O$ among ecosystems is not a function of their soil water content. Soil water content does not predict either the isotopic composition of soil water or its pattern with depth, something that would be expected in the simple case of evaporation with no recharge. Figure 3.4 explores the effect of soil water content (expressed in g water/g soil) on the average $\delta^{18}O$ values. The figure shows that although

Reproduced with permission of the copyright owner. Further reproduction prohibited without permission.

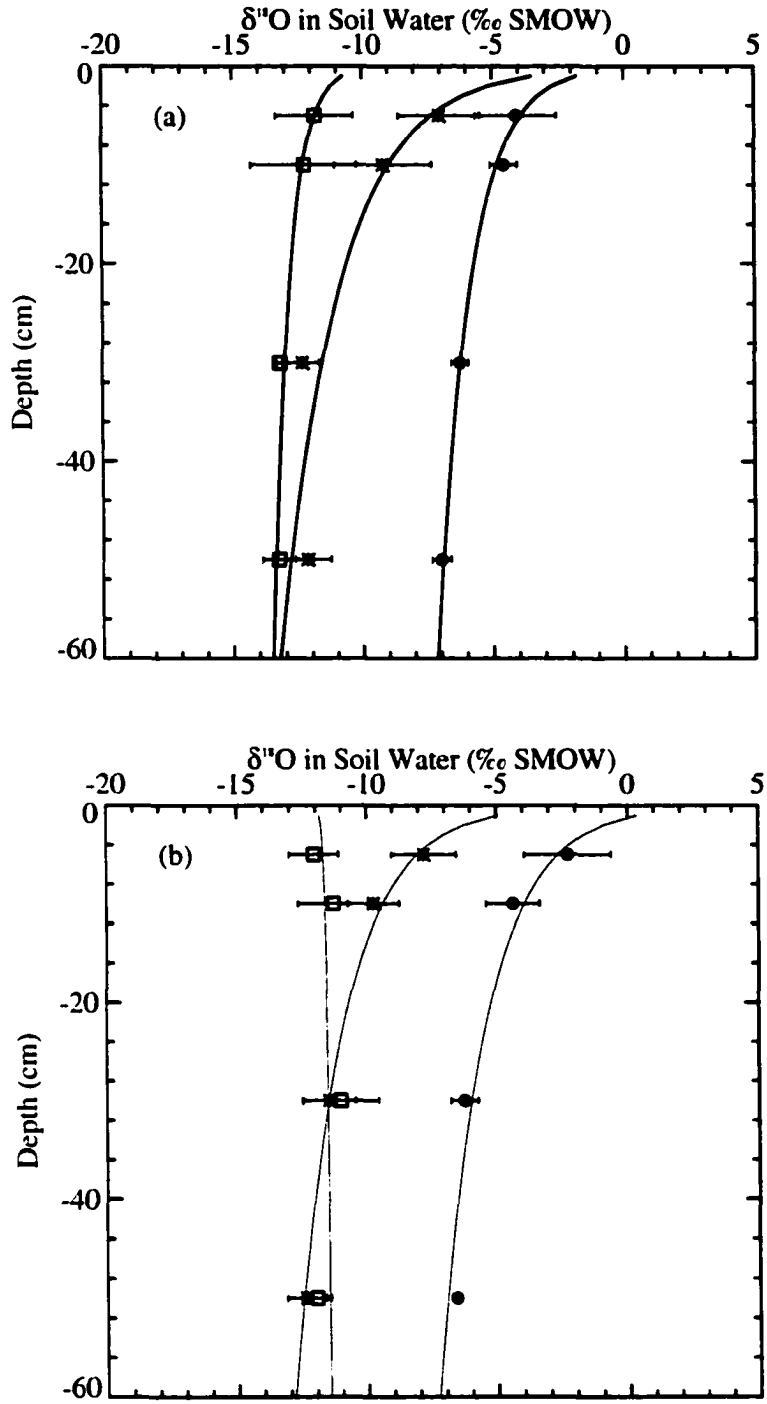

Figure 3.3. Seasonal-average $\delta^{18}O$ values of soil water by depth at each of the six field sites. Symbols are mean ± standard error; the smoothed fit is a log linear regression of the data (IDL software, RSI, Inc.). (a) Three ecosystems on fine-textured soil, (b) three ecosystems on coarse-textured soil. Solid circle represents shortgrass steppe, asterix represents lodgepole pine, and open square represents alpine tundra systems.

Reproduced with permission of the copyright owner. Further reproduction prohibited without permission.

soil water signature versus depth is consistently enriched toward the surface (except for the tundra ecosystem on coarse soil, mentioned above), the seasonal average of water content shows no consistent pattern across sites. The large error associated with taking the mean of a parameter with high temporal variability (here, soil water content) obscures the overall relationship between isotopic signature and water content. Part of the apparent lack of relationship may be due to the high variability in source water (see below). Summer storm tracks in Colorado have two distinct sources: the Pacific Northwest, and the Gulf of Mexico. Cole and others [*Cole et al.*, 1999; *Koster et al.*, 1993; *Rozanski et al.*, 1982] have shown that the difference in source region and storm track result in rain events of distinct isotopic signature. The depth to which each of the rain events infiltrated is also highly variable, and so more enriched soil water at any depth cannot be linked to either an enriched rain event or to evaporation without additional information. What is clear is that water content alone cannot be used as a proxy for estimation of isotopic signature.

I expected differences in CO_2 concentration and isotopic signature across ecosystems because of differences in plant rooting depth, associated microbial communities, and organic matter decomposition rates. In tundra and grassland ecosystems 80-90% of all roots are in the top 30 cm of soil, compared to only 50% in a temperate coniferous forest [*Jackson et al.*, 1996]. If lodgepole pine are capable of hydraulic lift [*Richards and Caldwell*, 1987], water from depth (presumably lighter) would be brought to the surface and could be lost to evaporation, leading to greater surface enrichment in this ecosystem [*Dawson*, 1993]. In contrast, in ecosystems with the majority of roots near the soil surface, evaporative enrichment might be limited by transpirational water loss. Data from

Reproduced with permission of the copyright owner. Further reproduction prohibited without permission.

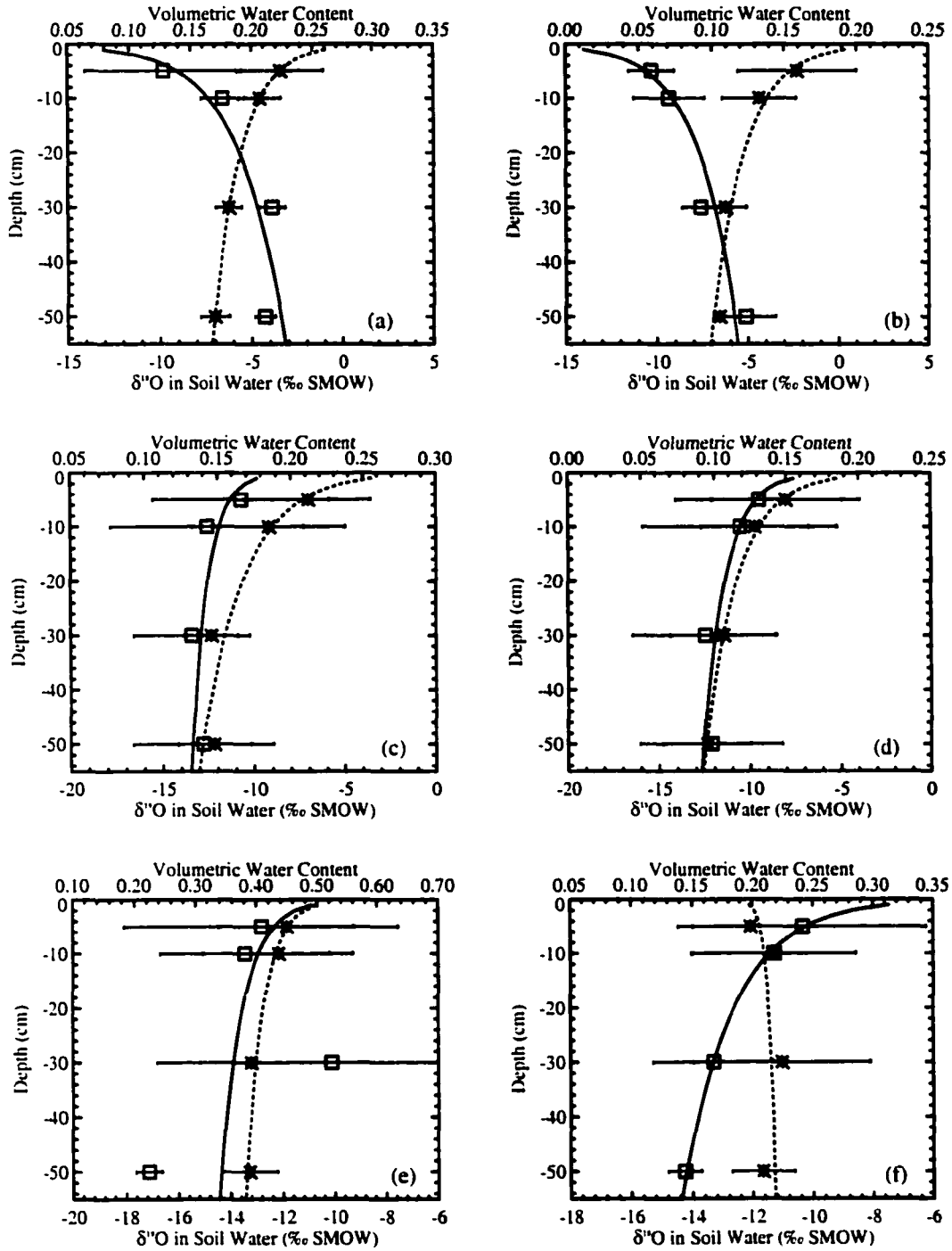

Figure 3.4. Seasonal average values of $\delta^{18}O$ and volumetric water content versus depth for each of the six field sites. Symbols are means ± standard error; smoothed lines are log linear regressions of the data (IDL software, RSI Inc.). Open squares and solid lines are for volumetric water content (top axis); asterix and dashed lines represent $\delta^{18}O$ data (bottom axis). (a) Shortgrass steppe on fine soil, (b) shortgrass steppe on coarse soil, (c) lodgepole pine on fine soil, (d) lodgepole pine on coarse soil, (e) alpine tundra on fine soil, (f) alpine tundra on coarse soil.

Reproduced with permission of the copyright owner. Further reproduction prohibited without permission.

our field sites suggest greater surface enrichment in the pine, compared to the tundra and grassland ecosystems (Figure 3.3), but the ability of lodgepole pine to hydraulically lift groundwater is unknown. Caldwell et al. [1998] suggest that hydraulic lift is likely to be a common phenomenon, although it is currently documented in only 27 species.

3.3.2 Comparison of $\delta^{18}O$ Depth Profiles as a Function of Soil Texture

There were no significant differences in the $\delta^{18}O$ of soil water between textural site pairs. Differences in clay content and distribution in each of the field site textural pairs suggest that depth profiles of the isotopic composition of soil water from these sites should be distinct if water amount, or even the strength with which water is held, influences isotopic signature. Because soils of coarse texture drain more quickly than do finer soils, there is the possibility for greater expression of isotopic enrichment near the soil surface in fine soils, where the surface water is held long enough for evaporation to take place. Conversely, soils with higher water-holding capacity could have greater losses of water due to transpiration (non-fractionating) than to evaporation [*Amundson et al.*, 1998; *Hsieh et al.*, 1998a]. However, water amount does not predict isotopic composition. Water content was significantly higher at the sites with fine-textured soils, especially in the grassland pair (Figure 3.5), whereas the seasonal average isotopic composition of soil water was not distinct at any depth among the textural pairs (Figure 3.6), perhaps as a result of piston flow. Rainfall is of the same isotopic signature at the grassland sites but is not exactly the same at the two pine (Figure 3.7, discussed below) or two tundra sites (data not shown). Another important distinction between paired sites is the proportion of vegetation cover. The greatest difference in amount of vegetation cover between site

Reproduced with permission of the copyright owner. Further reproduction prohibited without permission.

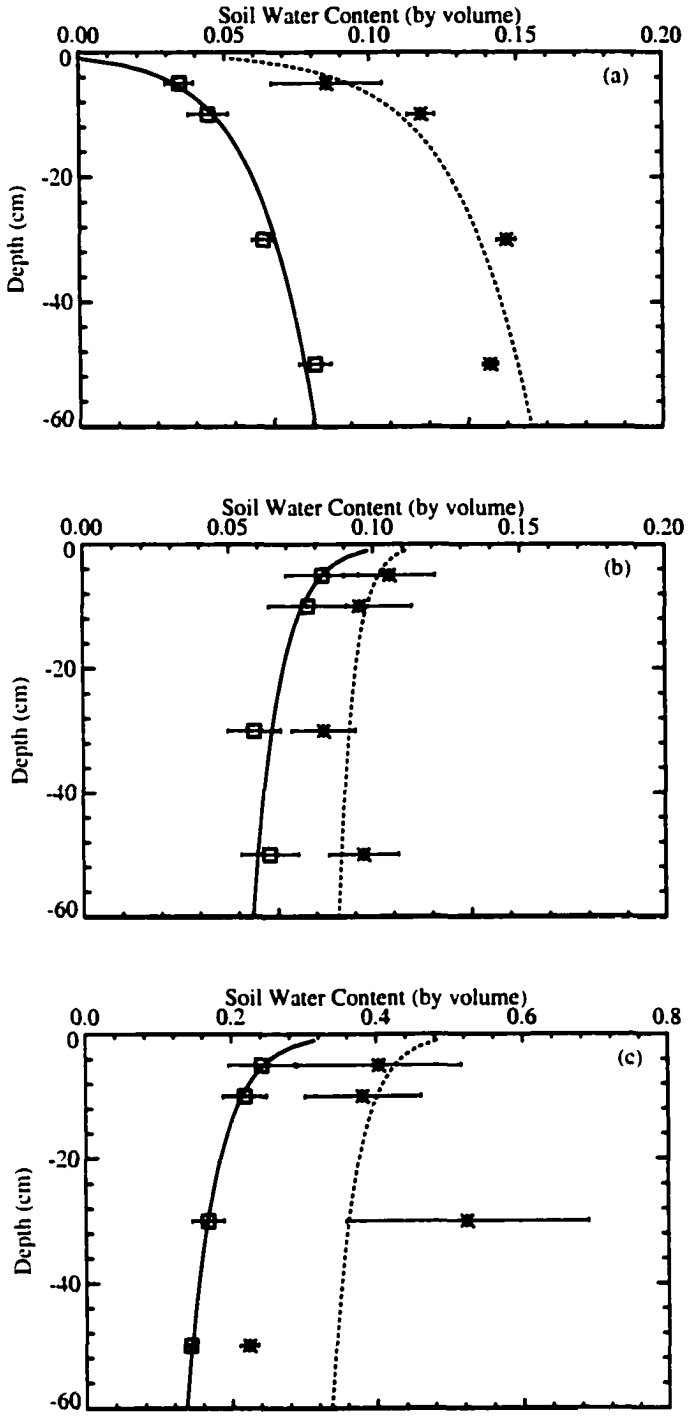

Figure 3.5. Comparisons across soil textural pairs for seasonal mean (± standard error) volumetric water content as a function of depth in the soil profile. Data from sites with fine-textured soil are labeled with an asterix, those from coarse-textured soil are labeled with an open square. Smoothed lines are log-linear regressions of the data. (a) Shortgrass steppe, (b) lodgepole pine, (c) alpine tundra.

Reproduced with permission of the copyright owner. Further reproduction prohibited without permission.

pairs is in the tundra ecosystem. Figure 3.6 indicates that the grassland sites are the most similar with respect to soil water $\delta^{18}O$, whereas those in the tundra ecosystem are the least similar. Therefore, it is likely that precipitation inputs and the proportion of soil water lost to evaporation are the dominant factors influencing the isotopic composition of soil water.

3.3.3 Temporal Variability in Rain Water $\delta^{18}O$

The isotopic composition of rainfall varies both as a function of season (as expected from temperature differences), but also in response to different source regions. Rainfall data for the lodgepole pine sites are instructive. Although samples do not contain information about individual storms because collection was not carried out on an event basis, the data do contain information about seasonal means and even about source regions. Weekly samples from the LP-coarse site (Figure 3.7b) suggest that in July of 1998 there were storms from two sources: one source yielded rain with an oxygen-18 signature of about -8‰ (Pacific Northwest?), whereas the other yielded rain of about –5‰ (Gulf of Mexico?). Furthermore, the data indicate that average July rainfall has a signature between –10‰ and –4‰ at both sites. Because the July precipitation is likely to be the most enriched of the year, surface soil water values more enriched than -4‰ can be attributed to evaporative water loss.

Are the precipitation data collected plausible for sites of this latitude and elevation? The oxygen isotope signature for rainfall at a given site can be calculated from a regression equation relating signature to mean annual temperature, mean annual precipitation, and elevation [*International Atomic Energy Agency (IAEA)*, 1981].

Reproduced with permission of the copyright owner. Further reproduction prohibited without permission.

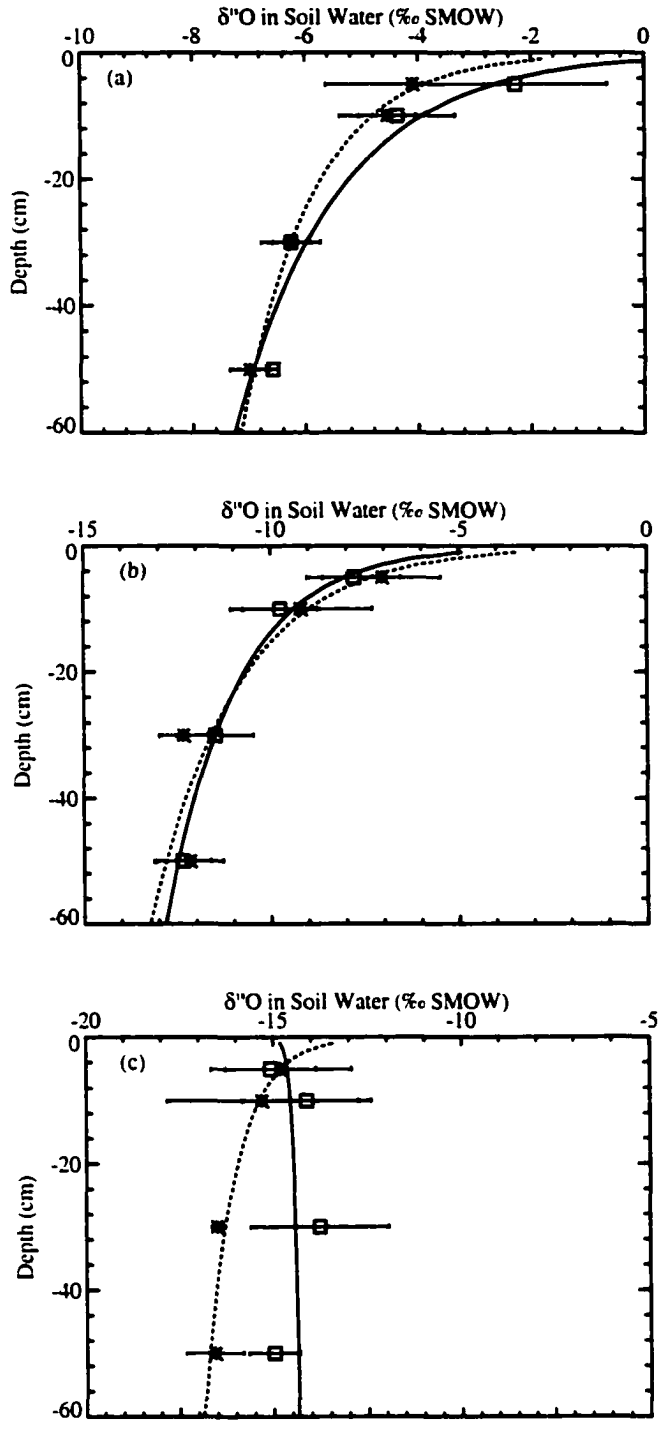

Figure 3.6. Comparisons of $\delta^{18}O$ values in soil water across soil textural pairs (seasonal mean ± standard error) as a function of depth in the soil profile. Data from sites with fine-textured soil are labeled with an asterix, those from coarse-textured soil are labeled with an open square. Smoothed lines are log-linear regressions of the data. (a) Shortgrass steppe, (b) lodgepole pine, (c) alpine tundra.

Reproduced with permission of the copyright owner. Further reproduction prohibited without permission.

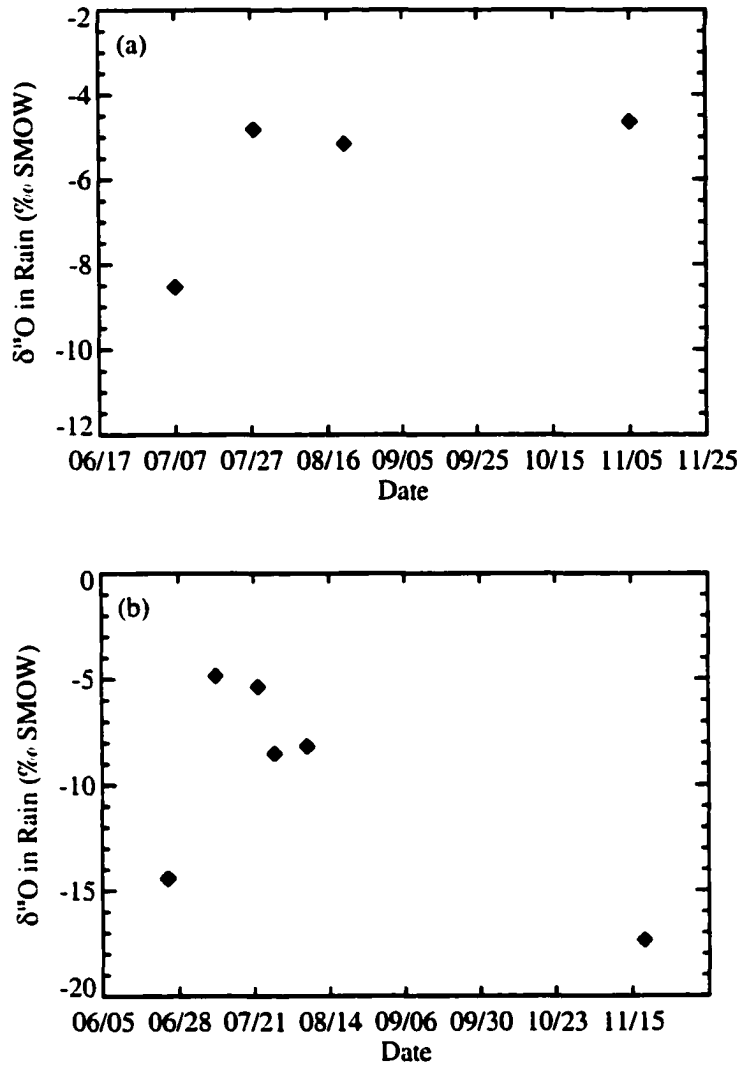

Figure 3.7. Temporal variability in oxygen isotopic composition of rainfall at two field sites in 1998. (a) Lodgepole site on fine-textured soil, (b) lodgepole pine site on coarse-textured soil.

Using the IEAE formulation[1], the annual mean isotopic signature of rainfall at the LP-fine site is –12.91‰, and that for the coarse site is –14.37‰. The $\delta^{18}O$ of snowfall is much lighter than is that for summer rain due to greater isotopic fractionation at colder

[1] δ (‰ SMOW) = $(0.579T-0.0114T^2-1.35P+4.47P^2-0.147(E)^{-1/2}-9.80)$, where T is mean annual temperature in °C, P is mean annual precipitation in meters, and E is elevation in meters.

Reproduced with permission of the copyright owner. Further reproduction prohibited without permission.

temperature [*Bottinga and Craig*, 1969; *Brenninkmeijer et al.*, 1983]; thus, the mean annual values calculated with the IEAE regression equation are plausible. Although the November samples are of questionable value because they represent a mixture of all rain events since the 21 August sampling, the fall sample from the LP-fine site (but not the LP-coarse site) lends further credence to the calculated annual mean value. The relationship between rainfall data and soil water profiles is discussed below.

3.3.4 Temporal Variability in Soil Water $\delta^{18}O$ and in Soil Water Content

Analysis of individual sampling days indicates that the oxygen isotopic signature of soil water near the soil surface ranges from only slightly enriched relative to precipitation inputs (1‰ at 5 cm) to very enriched as a result of evaporative water loss. However, the relationship between isotopic signature, water content, and soil temperature is not straightforward (Figures 3.8, 3.9). At the soil surface, one expects soil water to be enriched by evaporation, but if the time since the last rain event is short, surface enrichment will not be expressed (depending on solar radiation input and relative humidity). Figure 3.8 illustrates that the isotopic composition of soil water near the surface reflects recent rainfall, whereas deeper in the soil profile the water retains a lighter signature derived in part from winter precipitation. Figure 3.8 also shows that in the shortgrass ecosystem the data often are best modeled by a curve of increasing enrichment toward the soil surface corresponding to decreasing water content (Figure 3.8), but that this is not the case in the more mesic lodgepole and tundra sites (Appendix III, Figures 11-15). Note in these figures that a logarithmic fit of the data was used to aid pattern recognition.

Reproduced with permission of the copyright owner. Further reproduction prohibited without permission.

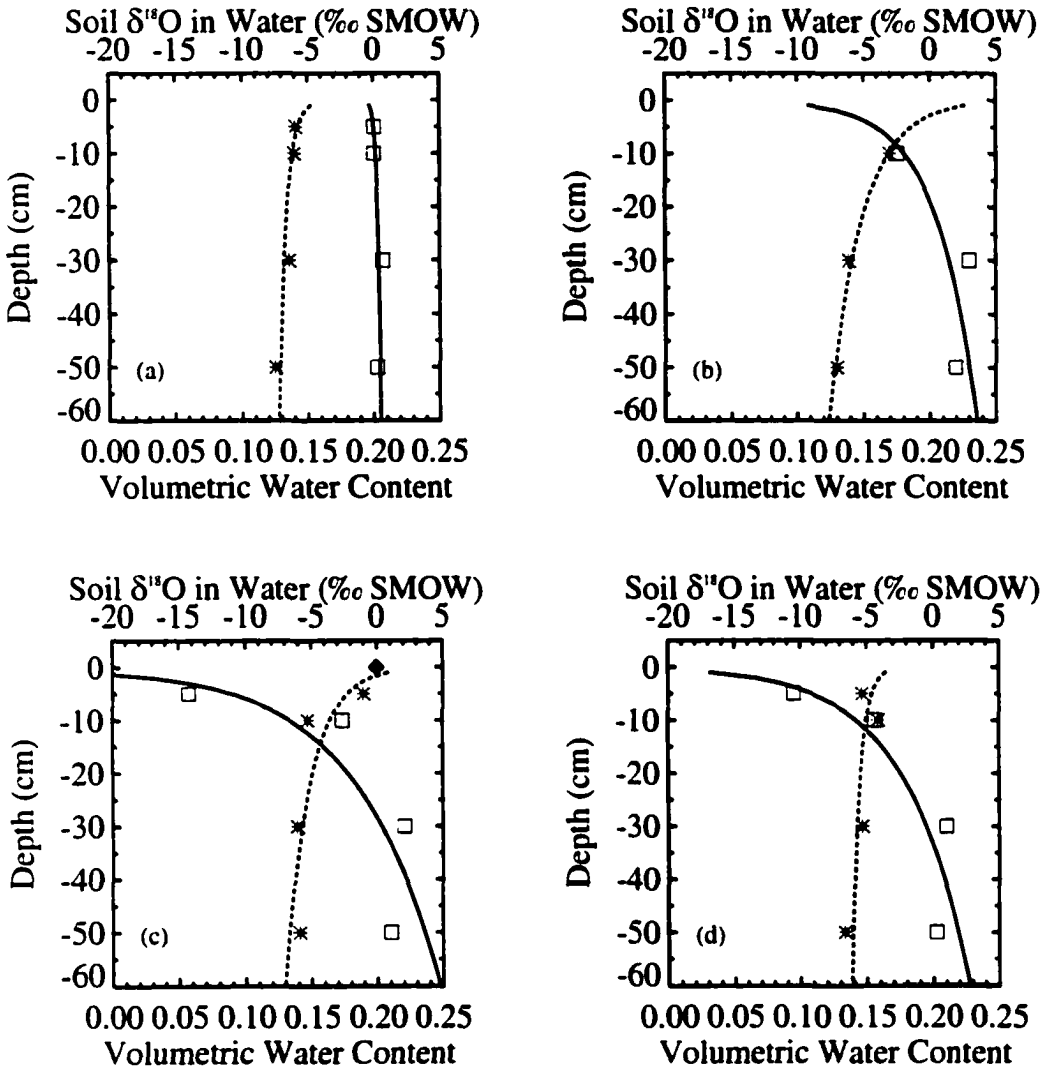

Figure 3.8. Oxygen isotopic composition of soil water (asterix) and rainfall (solid diamond), as well as soil water content (open square, expressed as g H_2O/g soil) versus depth for each sampling date. Smoothed curves are a log linear regression of the data (IDL software, RSI, Inc.). These graphs are for the shortgrass steppe site on fine soil. (a) June 23, 1998, (b) July 14, 1998, (c) August 11, 1998, (d) October 26, 1998. The same analyses are presented for the other field sites in Appendix III (Figures 11-15).

Reproduced with permission of the copyright owner. Further reproduction prohibited without permission.

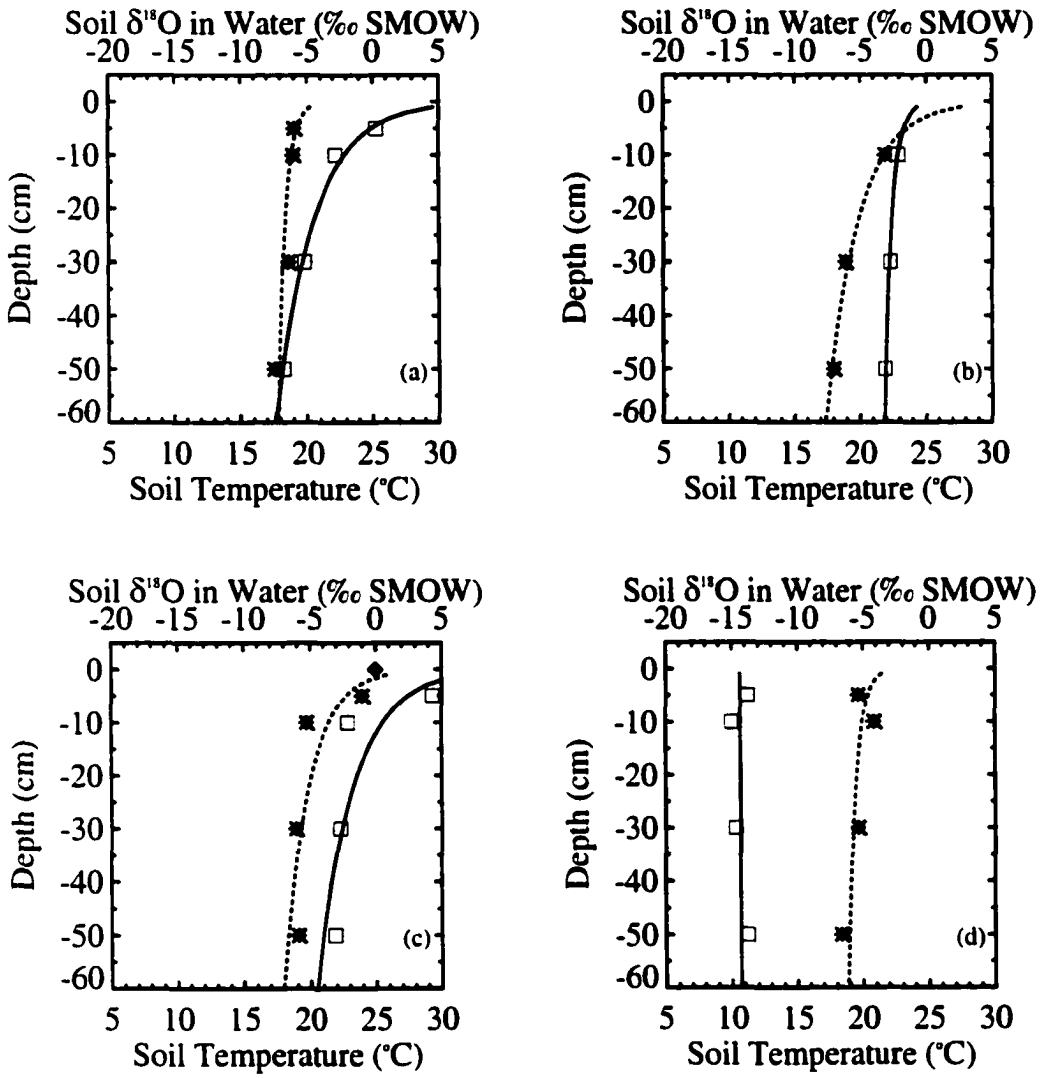

Figure 3.9. Oxygen isotopic composition of soil water (asterix) and rainfall (solid diamond), as well as soil temperature (open square) versus depth for each sampling date. These graphs are for the shortgrass steppe site on fine soil. Smoothed curves are a log linear regression of the data (IDL software, RSI, Inc.). (a) June 23, 1998, (b) July 14, 1998, (c) August 11, 1998, (d) October 26, 1998. The same analyses are presented for the other field sites in Appendix III (Figures 16-20).

Reproduced with permission of the copyright owner. Further reproduction prohibited without permission.

It is hypothesized that the frequency, intensity, and variable source region of recharge events all affect the pattern of isotopic signature of soil water. Data presented in Figure 3.9 (and Appendix III, Figures 16-20) suggest that soil temperature alone cannot yield much information about isotopic composition of soil water, although the amount of warming toward the surface is sometimes an indicator of the degree of surface enrichment. Fractionation is greater at colder temperatures [*Bottinga and Craig*, 1969; *Brenninkmeijer et al.*, 1983; *Galimov*, 1985]; thus, the amount of change in $\delta^{18}O$ with depth would be larger than is measured if the temperature profile were constant with depth. However, it is likely that the range of soil temperatures measured in this study is too small to exert an appreciable influence on fractionation due to diffusion (at most about 3‰).

Although it was shown above that soil water content cannot be used as a predictor of isotopic composition, it does hold that under conditions of stable water content over time, $\delta^{18}O$ over time is also relatively stable. Figure 3.10 and Figure 3.11 show the time evolution of $\delta^{18}O$ in soil water at each sampling site by depth increment for a shortgrass steppe site and a lodgepole pine site, respectively. It is clear from this analysis that there are frequent inputs and losses at the 5 cm depth that affect both isotope signature and soil water content. Data suggest that the greater rainfall at the lodgepole site relative to the grassland site means penetratation to greater depth, thereby increasing temporal variability of soil water ^{18}O in this ecosystem (e.g., compare Figure 3.10 and Figure 3.11, see also Appendix III). The greater variability is expressed to the 10 cm depth in the lodgepole pine sites, and perhaps throughout the profile (as measured, 50 cm) at the alpine tundra sites (Appendix III, Figures 21-24). Similarly, data are more variable over

Reproduced with permission of the copyright owner. Further reproduction prohibited without permission.

time for each depth increment in coarse-textured, as compared to fine-textured sites, again implicating infiltration characteristics as an influence on isotopic depth profiles.

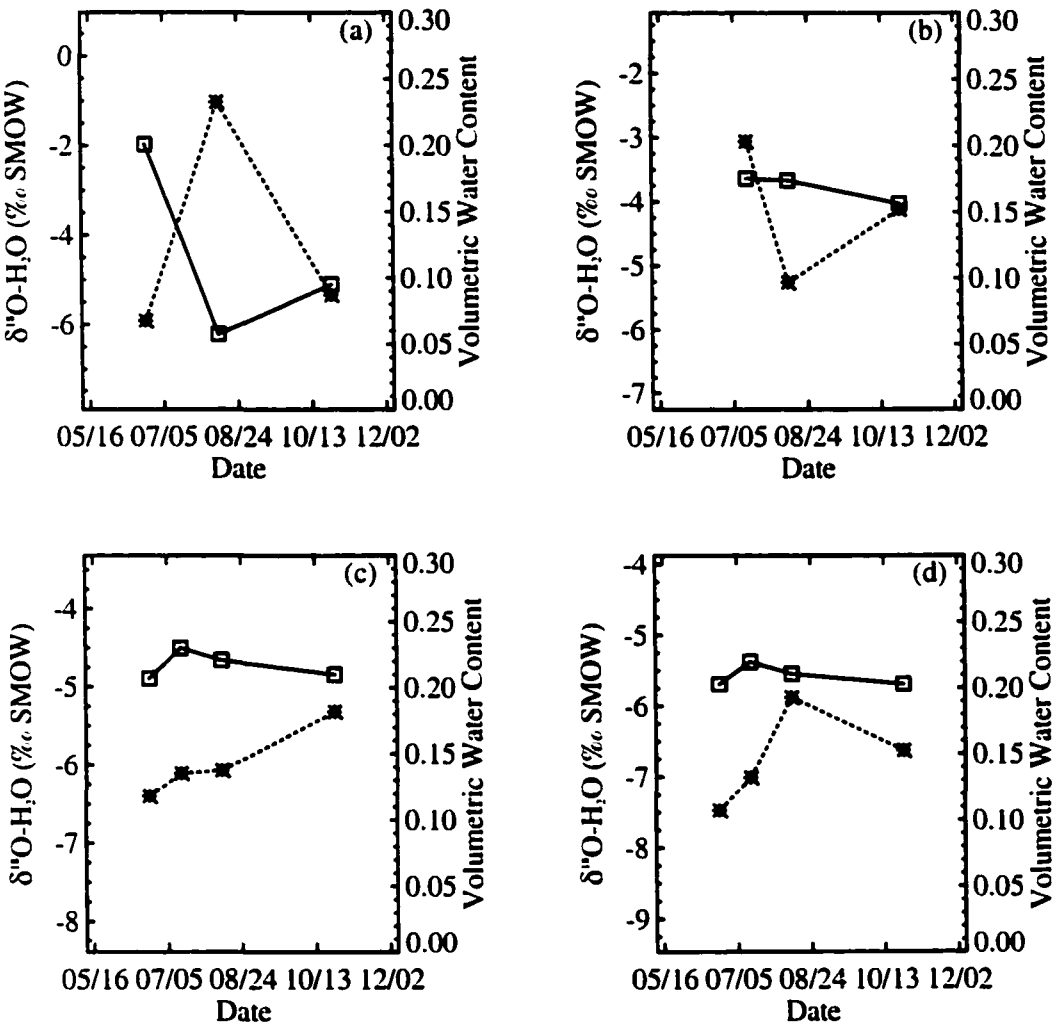

Figure 3.10. Patterns of soil water content (open square) and soil water $\delta^{18}O$ values (asterix) over the sampling period in 1998 for the shortgrass steppe site on fine soil. Data are for the following depths: (a) 5 cm, (b) 10 cm, (c) 30 cm, (d) 50 cm. Data are not continuous in time; points are connected merely for visualization.

Reproduced with permission of the copyright owner. Further reproduction prohibited without permission.

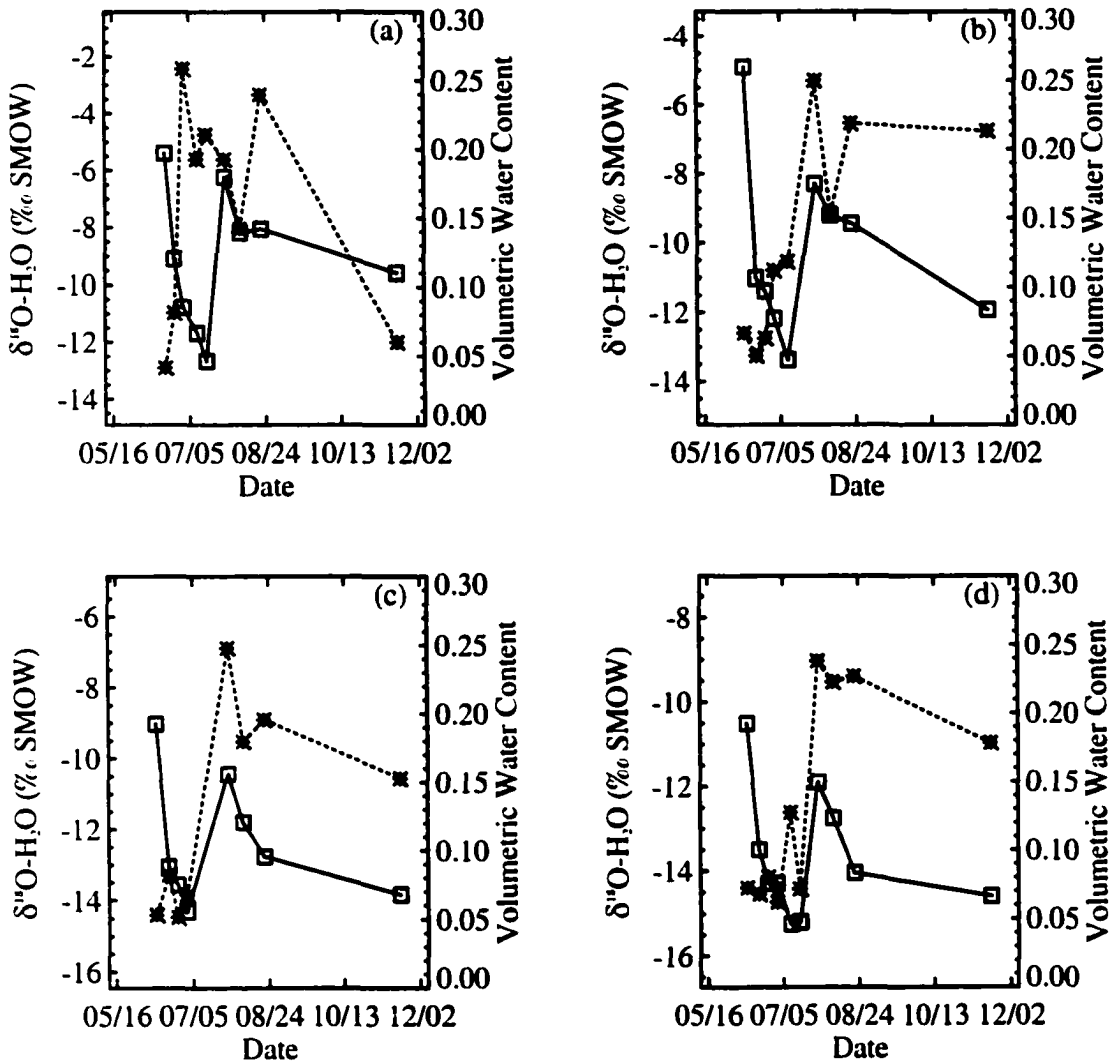

Figure 3.11. Patterns of soil water content (open square) and soil water $\delta^{18}O$ values (asterix) over the sampling period in 1998 for the lodgepole pine site on coarse soil. Data are for the following depths: (a) 5 cm, (b) 10 cm, (c) 30 cm, (d) 50 cm. Data are not continuous in time; points are connected merely for visualization.

Reproduced with permission of the copyright owner. Further reproduction prohibited without permission.

Figures 3.12 and 3.13 illustrate the temporal variability in the depth profiles of soil water content and isotopic composition. Figure 3.13 shows a clear trend toward isotopic enrichment at all depths in the tundra sites. This pattern is explained by the fact that over the course of the growing season snow melt and cold (and therefore lighter) precipitation events are replaced by warmer, heavier rain. As the growing season progresses evaporation is expected to become increasingly dominant. Changes in the proportion of evaporation and transpiration are likely to have a large impact on the isotopic value of soil water.

3.4. Conclusions

A new means of directly equilibrating CO_2 and soil water was shown to provide relatively rapid and accurate results for soil water $\delta^{18}O$ analyses. I used this method to analyze soil water samples from three ecosystems. Data reveal high temporal variability in both soil water content and soil water isotopic composition over the growing season. Isotopic composition of soil water was distinct across grassland, pine, and tundra systems on fine-textured soils, but the $\delta^{18}O$ values for soil water were less distinct across the same ecosystems on coarse-textured soils. Although water content was much higher on fine-textured soils, there were no significant differences in the isotopic composition of soil water between textural site pairs; changes in water content alone do not explain the observed patterns in $\delta^{18}O$ values. Variation in source region of precipitation inputs contributes to the observed variability. In addition, some variability in soil water $\delta^{18}O$ is explained by changes in the proportion of water loss to evaporation versus that lost to transpiration over the course of the growing season.

Reproduced with permission of the copyright owner. Further reproduction prohibited without permission.

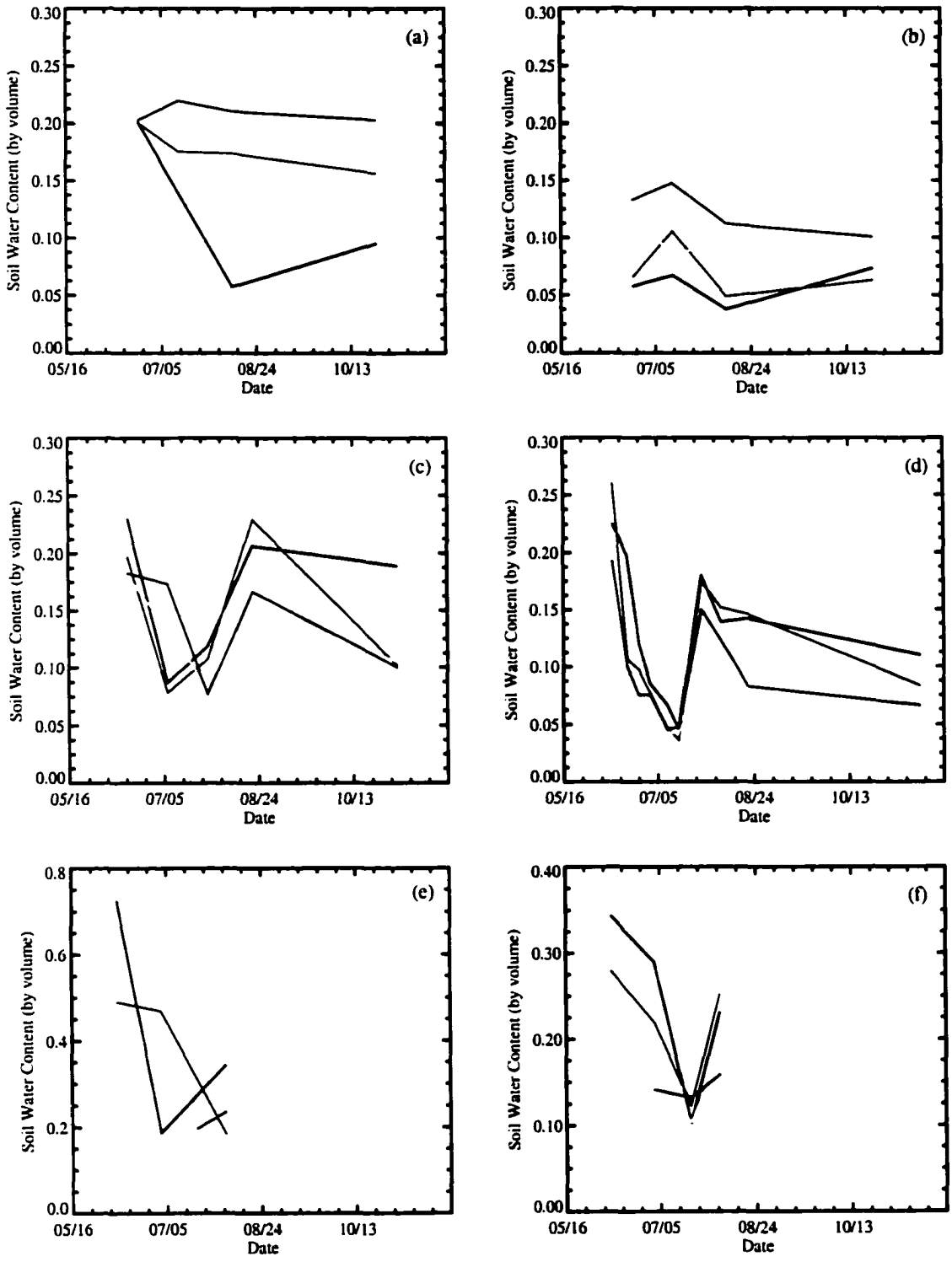

Figure 3.12. Seasonal variability in volumetric water content at each of the six field sites. Data for 5 cm depth are in blue, 10 cm depth data are green, 30 cm depth data are yellow, and 50 cm depth data are red. (a) Shortgrass steppe on fine soil, (b) shortgrass steppe on coarse soil, (c) lodgepole pine on fine soil, (d) lodgepole pine on coarse soil, (e) alpine tundra on fine soil, (f) alpine tundra on coarse soil.

Reproduced with permission of the copyright owner. Further reproduction prohibited without permission.

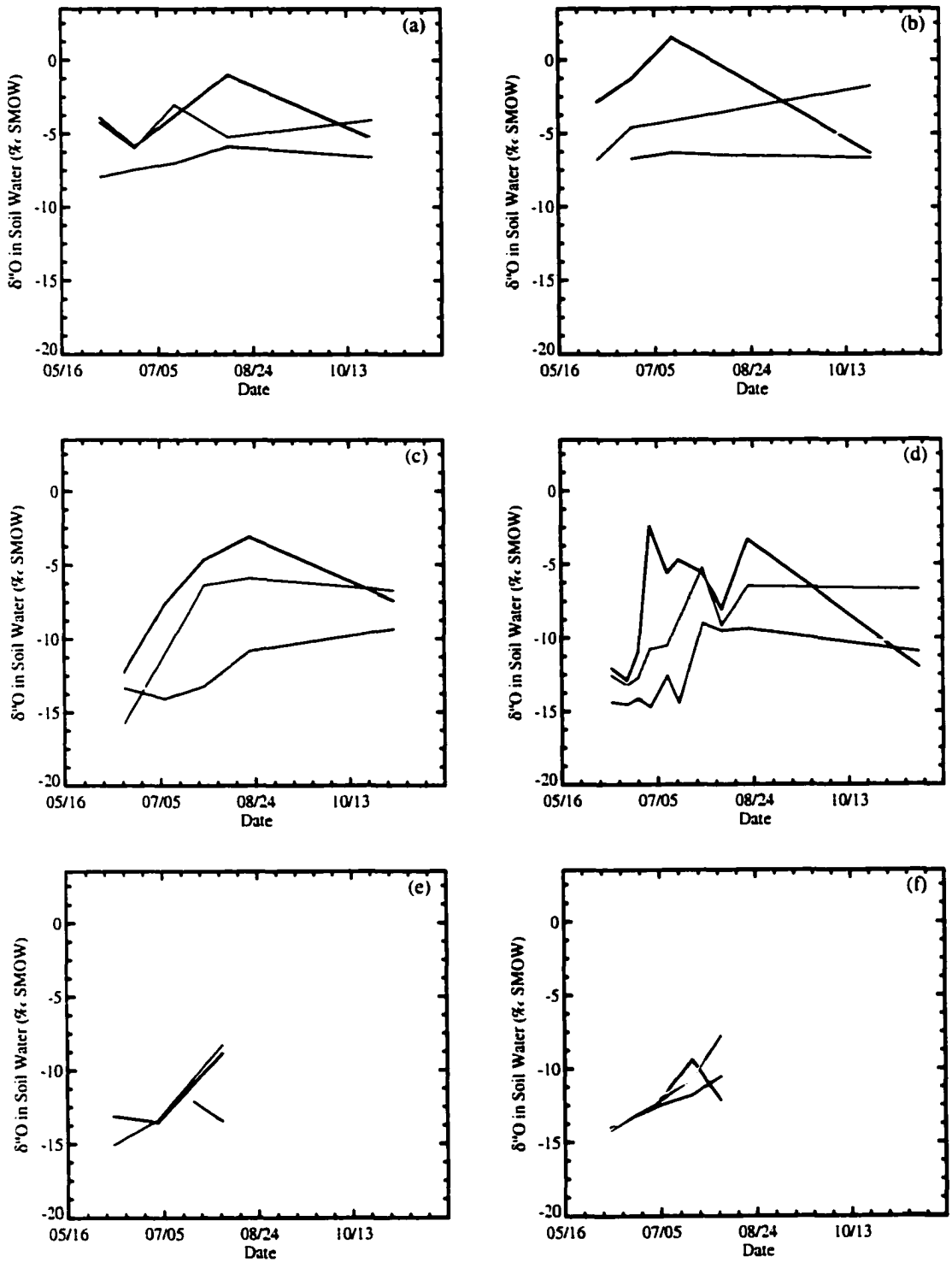

Figure 3.13. Seasonal variability in $\delta^{18}O$ values of soil water at each of the six field sites. Data for 5 cm depth are in blue, 10 cm depth data are green, 30 cm depth data are yellow, and 50 cm depth data are red. (a) Shortgrass steppe on fine soil, (b) shortgrass steppe on coarse soil, (c) lodgepole pine on fine soil, (d) lodgepole pine on coarse soil, (e) alpine tundra on fine soil, (f) alpine tundra on coarse soil.

Reproduced with permission of the copyright owner. Further reproduction prohibited without permission.

Literature Cited

Allison, G.B., C.J. Barnes, and M.W. Hughes, The distribution of deuterium and ^{18}O in dry soils, 2, Experimental, *Journal of Hydrology*, *64*, 377-397, 1983.

Amundson, R., L. Stern, T. Baisden, and Y. Wang, The isotopic composition of soil and soil-respired CO_2, *Geoderma*, *82*, 83-114, 1998.

Barnes, C.J., and G.B. Allison, The distribution of deuterium and ^{18}O in dry soils., 1.Theory, *Journal of Hydrology*, *60*, 141-156, 1983.

Barnes, C.J., and G.B. Allison, Tracing of water movement in the unsaturated zone using using stable isotopes of hydrogen and oxygen, *Journal of Hydrology*, *100*, 143-176, 1988.

Bottinga, Y., and H. Craig, Oxygen isotope fractionation between CO_2 and water, and the isotopic composition of marine atmospheric air, *Earth and Planetary Science Letters*, *5*, 285-295, 1969.

Brenninkmeijer, C.A.M., P. Kraft, and W.G. Mook, Oxygen isotope fractionation between CO_2 and H_2O, *Isotope Geoscience*, *1*, 181-190, 1983.

Brunel, J.P., H.J. Simpson, A.L. Herczeg, R. Whitehead, and G.R. Walker, Stable isotope composition of water vapor as an indicator of transpiration fluxes from rice crops, *Water Resources Research*, *28* (5), 1407-1416, 1992.

Brunel, J.P., G.R. Walker, J.C. Dighton, and B. Monteny, Use of stable isotopes of water to determine the origin of water used by the vegetation and to partition evapotranspiration. A case study from the HAPEX-Sahel, *Journal of Hydrology*, *188-189*, 466-481, 1997.

Caldwell, M.M., T.E. Dawson, and J.H. Richards, Hydraulic lift: consequences of water efflux from the roots of plants, *Oecologia*, *113* (2), 151-161, 1998.

Cole, J.E., D. Rind, R.S. Webb, J. Jouzel, and R. Healy, Climatic controls on interannual variability of precipitation $\delta^{18}O$: simulated influence of temperature, precipitation amount, and vapor source region, *Journal of Geophysical Research*, *104* (D12), 14,223-14,235, 1999.

Coplen, T.B., C. Kendall, and J. Hopple, Comparison of stable isotope reference samples, *Nature*, *302* (5905), 236-238, 1983.

Craig, H., and L. Gordon, Deuterium and oxygen-18 variation in the ocean and the marine atmosphere, in *Proceedings of the Conference on Stable Isotopes in Oceanographic Studies and Paleotemperatures, Spoleto, Italy*, edited by E. Tongiorgi, pp. 9-130, Pisa, 1965.

Reproduced with permission of the copyright owner. Further reproduction prohibited without permission.

Dansgaard, W., Stable isotopes in precipitation, *Tellus*, *26* (4), 436-468, 1964.

Dawson, T.E., Water sources of plants as determined from xylem-water isotopic composition: perspectives on plant competition, distribution, and water relations, in *Stable Isotopes and Plant Carbon-Water Relations*, edited by J.R. Ehleringer, A.E. Hall, and G.D. Farquhar, pp. 465-496, Academic Press, San Diego, 1993.

Dawson, T.E., and J.R. Ehleringer, Streamside trees that do not use stream water, *Nature*, *350*, 335-337, 1991.

Galimov, E.M., *The Biological Fractionation of Isotopes*, Academic Press, New York, 1985.

Gat, J.R., The isotopes of hydrogen and oxygen in precipitation, in *Handbook of Environmental Isotope Geochemistry*, edited by P. Fritz, and J.C. Fontes, pp. 21-47, Elsevier Scientific, New York, 1980.

Gee, G.W., and J.W. Bauder, Particle size analysis, in *Methods of Soil Analysis. Part I. Physical and Mineralogical Methods*, edited by A. Klute, pp. 383-411, Soil Science Society of America, Madison, WI, 1986.

Hsieh, J.C.C., O.A. Chadwick, E.F. Kelly, and S.M. Savin, Oxygen isotopic composition of soil water: quantifying evaporation and transpiration, *Geoderma*, *82*, 269-293, 1998a.

Hsieh, J.C.C., S.M. Savin, E.F. Kelly, and O.A. Chadwick, Measurement of soil water $\delta^{18}O$ values by direct equilibration with CO_2, *Geoderma*, *82*, 225-268, 1998b.

International Atomic Energy Agency (IAEA), Statistical treatment of environmental isotope data in precipitation, pp. 1-256, IAEA, Vienna, 1981.

Jackson, R.B., J. Canadell, J.R. Ehleringer, H.A. Mooney, O.E. Sala, and E.D. Schulze, A global analysis of root distributions for terrestrial biomes, *Oecologia*, *108*, 389-411, 1996.

Jenny, H., *Factors of Soil Formation*, McGraw Hill, New York, 1941.

Jenny, H., *The Soil Resource*, Springer-Verlag, New York, 1980.

Koster, R.D., D.P. de Valpine, and J. Jouzel, Continental water recycling and $H_2{}^{18}O$ concentrations, *Geophysical Research Letters*, *20*, 2215-2218, 1993.

Mathieu, R., and T. Bariac, An isotopic study (^2H and ^{18}O) of water movements in clayey soils under a semiarid climate, *Water Resources Research*, *32* (4), 779-789, 1996.

Reproduced with permission of the copyright owner. Further reproduction prohibited without permission.

Maule, C.P., D.S. Chanasyk, and K. Muehlenbachs, Isotopic determination of snow-water contribution to soil water and groundwater, *Journal of hydrology*, *155*, 73-91, 1994.

Rawls, W.J., Estimating soil bulk density from particle size analysis and organic matter content, *Soil Science*, *135* (2), 123-125, 1983.

Richards, J.H., and M.M. Caldwell, Hydraulic lift: substantial nocturnal water transport between soil layers by *Artemisia tridentata* roots, *Oecologia*, *73*, 486-489, 1987.

Rozanski, K., C. Sonntag, and K.O. Muennich, Factors controlling the stable isotope concentration of European precipitation, *Tellus*, *34*, 142-150, 1982.

Scrimgeour, C.M., Measurement of plant and soil water isotope composition by direct equilibration methods, *Journal of Hydrology*, *172*, 261-274, 1995.

Walker, C.D., and S.B. Richardson, The use of stable isotopes of water in characterizing the sources of water in vegetation, *Chemical Geology, Isotope Geosciences Section*, *94*, 145-158, 1991.

Walker, G.R., P.H. Woods, and G.B. Allison, Interlaboratory comparison of methods to determine the stable isotope composition of soil water, *Chemical Geology (Isotope Geoscience Section)*, *111*, 297-306, 1994.

White, J.W.C., E.R. Cook, J.R. Lawrence, and W.S. Broecker, The D/H ratios of sap in trees: implications for water sources and tree ring D/H ratios, *Geochimica et Cosmochimica Acta*, *49*, 237-246, 1985.

Yapp, C.J., A model for the relationships between precipitation D/H ratios and precipitation intensity, *Journal of Geophysical Research*, *87*, 9614-9620, 1982.

Zimmermann, U., D. Ehhalt, and K.O. Muennich, Soil-water movement and evapotranspiration: changes in the isotopic composition of the water, *Proceedings of the I.A.E.A. Symposium on Isotopes in Hydrology, Vienna*, 567-585, 1967.

Reproduced with permission of the copyright owner. Further reproduction prohibited without permission.

CHAPTER 4

THE $\delta^{18}O$ OF SOIL-RESPIRED CO_2:

ISOTOPIC EQUILIBRATION BETWEEN SOIL WATER AND SOIL CO_2

Abstract

Soil respired CO_2 is an important influence on the carbon and oxygen isotopic composition of the atmosphere. The oxygen isotopic composition of this flux can be used to partition gross primary productivity and ecosystem respiration, thereby lending insight to patterns of ecosystem response in time and space and in response to environmental disturbances. I explored the connection between the depth profile of soil water $\delta^{18}O$ and soil CO_2 $\delta^{18}O$ and used a soil diffusion and isotopic equilibration model to calculate the oxygen isotope composition of the CO_2 flux from soil to the atmosphere. Work presented here suggests that soil CO_2 and soil water are sometimes, but not always, in complete isotopic equilibrium, and that the expressed, or "effective" fractionation factor varies as a function of local conditions (from 3.40 to 7.47‰). Model sensitivity to input was explored, and model output compared to estimates based on large-scale patterns in rainfall as well as to an empirical formulation that does not allow diffusive fractionation to vary with soil conditions. Seasonal average values of the isotopic composition of soil-respired CO_2 were 34.20‰ from the shortgrass steppe sites, 30.27‰ from the lodgepole pine sites, and 27.50‰ from the tundra sites studied. Estimates of ^{18}O in soil respired CO_2 based on a method that does not take into account the competition between

Reproduced with permission of the copyright owner. Further reproduction prohibited without permission.

equilibration and diffusion deviate significantly from the composition as computed with a full equilibrium-diffusion model. Further, the full diffusion-equilibration model is needed to capture temporal variability in the isotopic composition of the soil flux, which can be as large as 8‰ over the course of the growing season at a single location.

4.1. Background and Introduction

Soils are one of three major components of the carbon budget and have a large potential both to store carbon and to emit carbon to the atmosphere in magnitude that could affect the global environment. Stable isotopes of carbon and oxygen are proving invaluable tools for quantifying the exchanges of the global carbon budget. For example, $\delta^{13}C$ values have been used to partition terrestrial and oceanic sources and sinks of CO_2 [*Ciais et al.*, 1995; *Francey et al.*, 1995; *Fung et al.*, 1997]. Recent work suggests that the isotopic composition of oxygen in atmospheric CO_2 can be used to partition the amount of carbon taken up or emitted within terrestrial systems, because soil and vegetation contribute isotopically distinct fractions to the atmospheric budget [*Yakir and Wang*, 1996]. This further partitioning is critical because in order to assess response of the carbon cycle to small-scale variability in climate or other disturbances the net flux between the atmosphere and terrestrial biosphere must be partitioned into its components: gross primary production and ecosystem respiration. In principle this is possible because the isotopic composition of oxygen in water in the chloroplasts of leaves is different from that in the soil [*Flanagan et al.*, 1997; *Hesterberg and Siegenthaler*, 1991; *Hsieh et al.*, 1998a; *Yakir et al.*, 1994]. Previous attempts to calculate the isotopic composition of the flux of CO_2 from soil to the atmosphere was based on the assumption that soil water and

Reproduced with permission of the copyright owner. Further reproduction prohibited without permission.

soil CO_2 are in isotopic equilibrium. Thus, the isotopic composition of the flux was the $\delta^{18}O$ value of soil water plus a factor to account for fractionation during diffusion. The assumption of CO_2-water isotopic equilibrium arises because of the known isotopic exchange during the CO_2 hydration reaction [*Mills and Urey*, 1940]:

$$H_2{}^{18}O\ (l) + CO_2\ (g) \leftrightarrow H^+ + [HCO_2{}^{18}O]\ (aq) \leftrightarrow H_2O\ (l) + CO^{18}O\ (g) \qquad (1)$$

Previous studies have included the assumption of equilibrium between soil CO_2 and average annual precipitation [*Farquhar et al.*, 1993], equilibrium between soil CO_2 and soil surface water [*Ciais et al.*, 1997], and equilibrium between soil CO_2 and soil water at depth [*Flanagan et al.*, 1997]. Each of these studies used a different value of expressed diffusional fractionation (from 5.0 to 8.8‰). Work presented here suggests that soil CO_2 and soil water are sometimes, but not always in isotopic equilibrium, and that the expressed, or "effective" fractionation factor varies as a function of local conditions (range 3.40-7.47‰ in 19 cases examined).

4.2. Methods

4.2.1. Field Sampling

4.2.1.1. Site characteristics

Six field sites located along the Front Range of the Rocky Mountains in Colorado were selected to represent three separate ecosystems (shortgrass steppe, lodgepole pine forest, and alpine tundra, see Figure 4.1) and two soil textures (fine and coarse). The sites were selected utilizing the state factor approach as outlined by Jenny [*Jenny*, 1941]. According to Jenny, soil development is affected by five factors: climate, organisms, relief (aspect and slope), parent material, and time. I was interested in both soil texture — a property

Reproduced with permission of the copyright owner. Further reproduction prohibited without permission.

largely determined by the parent material from which a soil develops — and bioclimate, or the combination of climate and its associated organisms [*Jenny*, 1980].

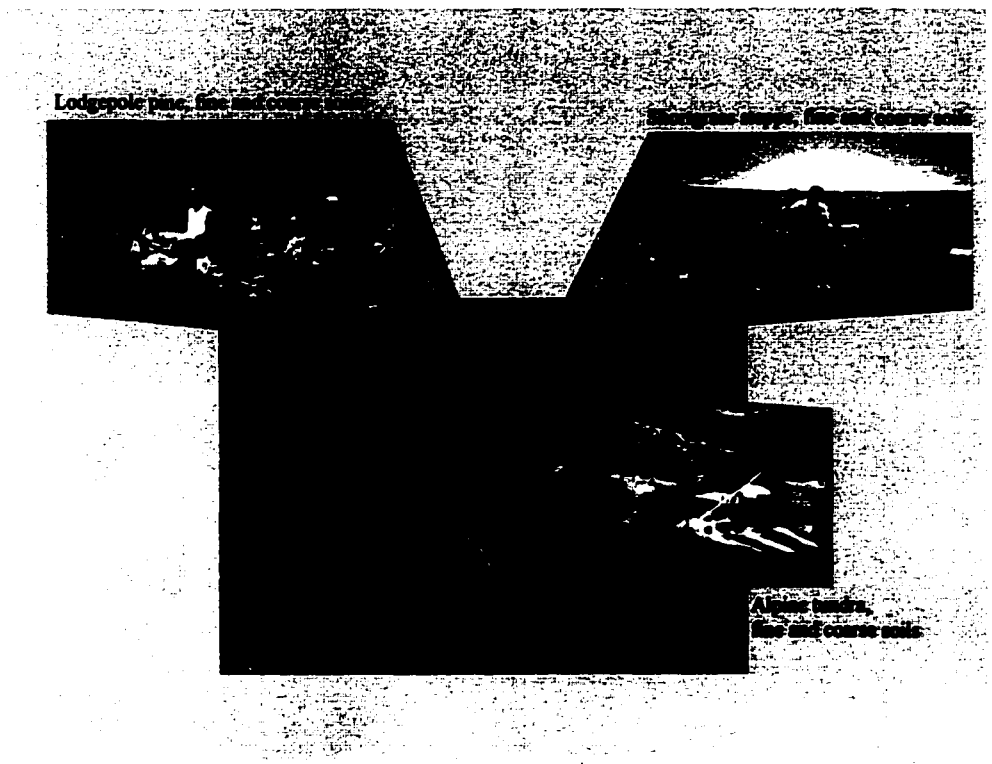

Figure 4.1. Field sites sampled during this study. Site represent three ecosystems (shortgrass steppe, lodgepole pine, and alpine tundra) on soils of fine and coarse texture. Each photograph represents a textural pair of sites.

Accordingly, I selected my field sites to be as level as possible (maximum slope 22%, see Table 4.1), and to represent the same aspect when possible (all sites 42-56° NE, except one, which was 105° SE). The two parent material types, schist and granite, were of roughly the same age. The sites representing the shortgrass steppe ecosystem matched the other ecosystems in terms of soil texture, but the parent materials were coarse alluvium and shale residuum. Climate at the field sites was determined based on the longest available record from the closest official Colorado State weather station (http://ulysses.atmos.colostate.edu/Access.html). Climate data for the six sites are

Reproduced with permission of the copyright owner. Further reproduction prohibited without permission.

summarized in Appendix I. Vegetation at the sites was not the focus of the current study; representative species are listed in Appendix I. The primary vegetational difference between the two shortgrass steppe sites was a greater abundance of prickly pear cactus (*Opuntia polyacantha*), yucca (*Yucca glauca*), and evening primrose (*Oenothera caespitosa*) at the coarse site. The coarse lodgepole site differed from the fine lodgepole site in a paucity of ground cover, and the coarse tundra site had many more patches of sparse or no vegetation than did the very biologically rich fine tundra site.

Table 4.1. Characterization of field sites.

Site name	Ecosystem type[&]	Parent material	Elevation (meters)	Location	Slope	Aspect	Climate*
CPER-Catena	Shortgrass steppe	Shale residuum	1646	40°48'N, 104°44'W	<5%	----	MAP 31 cm, MAT 9.2°C
CPER-Meterological Station	Shortgrass steppe	Coarse alluvium	1646	40°48'N, 104°44'W	<1%	----	MAP 31 cm, MAT 9.2°C
Ballard Road	Lodgepole pine	Mica schist	2720	40°34'N, 105°28'W	17%	105° (SE)	MAP 58.4 cm, MAT 7.8°C
Allenspark	Lodgepole pine	Silver plume granite	2651	40°11'N, 105°32'W	22%	42° (NE)	MAP 52 cm, MAT 4.7°C
Iceberg Pass	Alpine tundra	Biotite schist	3597	40°26'N, 105°45'W	22%	56° (NE)	MAP 191 cm, MAT -8.3°C
Tombstone Ridge	Alpine tundra	Silver plume granite	3475	40°24'N, 105°41'W	14%	50° (NE)	MAP 180 cm, MAT -8.3°C

[&] See Appendix I for details

* 30-yr average when available; data from http://ulysses.atmos.colostate.edu/Access.html

4.2.1.2. Sample types and sampling frequency

Field sampling was conducted over the 1997 and 1998 growing seasons, with an attempt made to capture pre-bud break and senescence (April-November). As methods were not consistent between years, only the 1998 data are discussed here. During the growing

Reproduced with permission of the copyright owner. Further reproduction prohibited without permission.

season (June-August), two field sites were visited each week. One site, lodgepole on coarse soil, was selected for intensive investigation because the 1997 data suggested the lodgepole sites were more variable than those in the other ecosystems. This site (lodgepole-coarse) was visited every week. A total of 32 field visits were made during the 1998 season. Routine measurements/collections conducted during each field visit included air temperature and a soil temperature profile (every 5 cm to 30 cm, plus 50 cm: micro-processor thermometer, Omega Engineering), bulk soil from four depths, soil gases, and rainwater. On some, but not all, sampling dates the soil CO_2 flux was also measured.

Bulk soil samples were taken from depths centered on 5, 10, 30, and 50 cm. Samples were collected in 120 ml wide-mouth brown glass jars with a teflon-lined lid. After collection, the tops were wrapped in parafilm, and the jars were placed immediately in a cooler with ice for transport. Samples were stored in a cold room (10°C) until irradiated (1.15-1.20 Mrad) to stop all microbial activity. Duplicate samples were taken for analysis of gravimetric water content. These were stored in sealed plastic bags in the cooler, and then weighed moist immediately upon returning to the laboratory (usually within two hours of sampling). On the rare occasion when condensation was noticed on the bag walls, samples were thoroughly shaken to incorporate this moisture prior to weighing.

Gas sampling tubes were installed in the field in June of 1997, three weeks prior to commencement of sample collection. The sampling apparatus, designed by A.Mosier (pers. comm.), consisted of a 2.5 cm diameter PVC tube housing four 0.32 cm i.d. stainless steel tubes (Figure 4.2). The steel tubing extended from a hole in the PVC pipe

Reproduced with permission of the copyright owner. Further reproduction prohibited without permission.

at the desired gas sampling depth (5, 10, 30, and 50 cm) to several cm above the soil surface. The PVC pipe was filled with resin to hold the steel tubes at the desired depth. An auger of the same diameter as the PVC tube was used to install the tubes in the field with as little disturbance to the soil profile as possible. Three of these tubes were installed roughly 1 m apart at each field site (total of 18 tubes). A swagelock fitting holding a teflon-faced silicone rubber micro septa (Alltech Associates, Deerfield, IL) was connected to the top of each piece of steel tubing. Septa were replaced after each sampling.

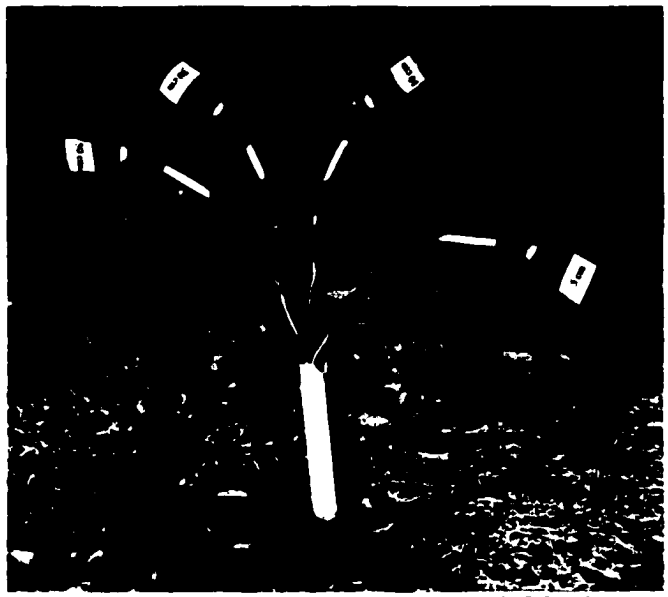

Figure 4.2. Apparatus used to collect in-situ soil CO_2 from each of the six field sites. Three of these PVC tubes, located approximately 1-m apart, were installed at each site.

To begin sampling, a 25 ml gas sample was drawn by syringe from each tube and expelled to remove air that had built up and been in contact with the tubing and septa since the previous sampling. Gas was allowed to diffuse into the tubing and area surrounding the inlet of the tubing for 10 minutes. Soil gas was then drawn across a magnesium perchlorate water trap into pre-evacuated 25 ml glass serum vials via a

Reproduced with permission of the copyright owner. Further reproduction prohibited without permission.

double-sided precision glide blood collection needle (27½G) (Figure 4.2). New drying traps and new needles were used for each sample. Serum vials were left attached to the sampling tubes for 20 minutes to insure complete equilibration. Twelve samples were collected at each field site on each sampling date (4 depths x 3 PVC tubes). The radius of the hemisphere sampled by a 25 ml gas collection is 2.29 cm. Thus, the 5 cm sample actually represents the CO_2 concentration and isotopic composition of gases from 2.7 to 7.3 cm, and the sample representing the 10 cm depth increment actually covers a depth range of 7.7 to 12.3 cm. After the equilibration period, samples were removed from the sampling needles and their septa were sealed with Apiezon-M grease (Apiezon Products, Manchester, U.K.). The needles were then removed from the swagelock septa to allow gases to diffuse back into the sampling tubes and areas surrounding the sampling tube inlet. After 20 minutes, a second sample was taken from each tube and depth in the same manner as the first, but without the dry trap. Water content does not affect CO_2 concentration (it is removed prior to analysis), but storage of wet samples has been shown to alter their isotopic composition [*Gemery et al.*, 1996]. The samples collected for determination of CO_2 concentration were analyzed within two days post-sampling. All samples were stored cold (about 5°C) until analyzed for consistency and to minimize any potential reactions between gas samples and water that might have been adsorbed to the glass vials.

Soil flux measurements were recorded using a dynamic closed chamber technique. A plexiglass cylindrical chamber (9-L volume: 20 cm height, 12 cm radius) was fitted with a small, 9V battery-powered fan and attached, via 2 m of 1 mm i.d. Tygon tubing, to a LI-6200 portable photosynthesis analyzer (LI-COR, Lincoln, Nebraska). Respired air

Reproduced with permission of the copyright owner. Further reproduction prohibited without permission.

samples were collected for later isotopic analysis during some of the soil flux measurements. In this case, the tubing was split, and a water trap (magnesium perchlorate and glass wool filter) and a 0.5-L pyrex flask with Teflon O-ring stopcocks at either end were inserted in-line between the chamber and the LI-COR instrument (see Figure 4.3).

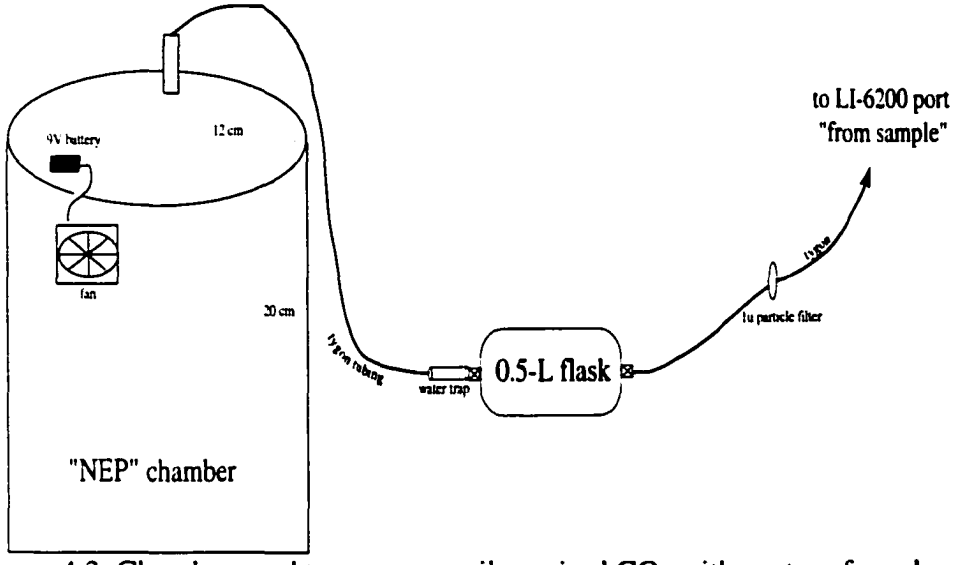

Figure 4.3. Chamber used to measure soil-respired CO_2 with capture for subsequent isotopic analysis.

The CO_2 analyzer was calibrated on each sampling date on-site (span gas 994 ppm). The calibration tank was taken into the field to account for pressure differences between the sites and the lab (sites range from about 630 to 850 mbar, lab pressure 848 mbar). The flow rate typical during sampling was 900 µmol/sec. Flow rates were lower at the higher elevation sites. Sampling was carried out in mid-day (usually between 12 and 2 p.m.) except during one diurnal study (not reported here). To begin measurements, the chamber was placed on a level spot with as little vegetation as possible (at the lodgepole sites and tundra-coarse, these were denuded) and forceful downward pressure was used to "seal" it in place. A black cloth was placed over the chamber to block all sunlight. CO_2

Reproduced with permission of the copyright owner. Further reproduction prohibited without permission.

concentration and air flow rate were recorded every 15 seconds for a total of 90 seconds chamber closure (i.e., during the period of linear CO_2 increase). At the end of the CO_2 build-up period (final concentrations usually 450-500 ppm), the flask was closed (LI-COR end first, to prevent explosion), and then the LI-COR shut off and the chamber moved to a new spot. This was repeated in five locations at each field site, for each sampling date. Atmospheric samples were taken with the same protocol except that the chamber was held at shoulder height upwind from field personnel.

4.2.2. Laboratory Analysis

Laboratory analyses for the soil water samples included gravimetric analysis of water content, measurement of particle size distribution, and organic matter content analysis (necessary to calculate water amount on a volumetric basis). In addition, isotope ratio mass spectrometric analysis was carried out on rain water, soil water, and soil-respired CO_2 samples. The methods used for mass spectrometric analysis are described in separate sections, below. Measurement of soil water content was initiated on each sampling date by weighing moist samples immediately upon returning to the laboratory (as mentioned above). The samples were oven dried for 48 hrs at 110°C and re-weighed. All soil samples for particle size and organic content analysis (six field sites, four depths, plus samples for each genetic soil horizon at each site) were first sieved with 2 mm mesh sieve and gently crushed with a mortar and pestle. Each soil was then tested for the presence of carbonates by adding a few drops of 1N HCL to a few grams dry soil. Carbonates were present only in soils from the shortgrass steppe sites below 45 cm (65 cm at the coarse-textured site). These samples were treated with weak acid (1M NaOAc) buffered at pH 5

Reproduced with permission of the copyright owner. Further reproduction prohibited without permission.

for 1 hour in a warm (60°C) sand bath, then shaken and rinsed. This procedure was repeated until there was no reaction between strong acid and soil. Particle size distribution was determined by hydrometer method [*Gee and Bauder*, 1986].

A sub-sample of each soil was finely ground via a ball mill to assure complete homogenization. These homogenized samples were then analyzed via a LECO CHN 1000 Elemental Analyzer for organic content (%C and %N) (LECO Corporation, St. Joseph, MI). The %C information was used to estimate sample size needed for $\delta^{13}C$ analysis of the organic matter (reported elsewhere), as well as for calculation of bulk density. The error associated with calculation of bulk density from particle size and organic matter content is 0.3 g/cm^3 or less [*Rawls*, 1983]. Water content expressed on a volumetric basis is the product of gravimetric water content and calculated bulk density.

CO_2 concentration of all gas samples was determined within two days of sampling via a LI-COR model LI-6252 infra-red gas analyzer (IRGA, LI-COR, Lincoln, NE). The system was calibrated prior to each set of field samples using two tanks of known concentration (1040 and 4824 ppm). Reference gas was injected in amounts ranging from 1 ml of the 1040 ppm tank to 7 ml of the 4824 ppm tank. The IRGA output was converted to μgC based on the ideal gas law:

$$\mu gC_{ref} = ((((a*(P_l/P_s))/(R*T))/1000)*C_s)*12.01, \quad (2)$$

Where a is the amount of reference tank gas injected (mls), P_l is the pressure in the lab, P_s is standard pressure, R is the ideal gas constant, T is the lab temperature (°C), and C_s is the CO_2 concentration of the reference tank (here, 1040 or 4824 ppm). A regression of analyzer output versus μgC for the reference gas was used to calculate the concentration of CO_2 in the sample gas via:

Reproduced with permission of the copyright owner. Further reproduction prohibited without permission.

$$\mu gC_{sample} = (\text{IRGA output} + \text{Y-int})/\text{X-var}, \text{ and}$$

$$\text{ppm } CO_2 = (((\mu gC_{sample}/12.01)/3.46e^{-5})/a), \quad (3)$$

where *a* is again the amount of gas injected (this time the sample), and *Y-int* and *X-var* are the y-intercept and x-variable from the regression analysis of the reference gas, respectively.

4.2.3. Isotopic Analyses

4.2.3.1. Irm-CGMS of soil water samples

Field-moist soil (amount based on water content, water amount 0.3 ml) was loaded into 10 ml seal cap exetainers and shipped, along with two working standard waters, to Jena, Germany, for analysis on a Gas Bench II analyzer at the Max-Planck-Institut für Biogeochemie. Including duplicate samples, over 200 analyses were carried out. In Germany, the moist soil samples were topped with 0.5% CO_2 in helium and allowed to equilibrate for 24 h on an autosampler tray (temperature stability <0.1°C) at 30°C (Combi PAL, CTC, Switzerland). After equilibration, the concentric double wall needle of the Gas Bench II autoanalyzer (Finnigan MAT, Bremen, Germany) sequentially pierced a sample septa and helium carrier flushed the exetainer (flow rate 0.3 ml/min). The overpressure continuously passed the headspace gas (CO_2 plus helium) via the output portion of the needle over a Nafion drying trap into a PoraPLOT Q capillary gas chromatograph column via a Valco 6-port valve and a 100 µl sample loop. After separation (90 sec pass time) the individual gases were passed across a second Nafion drying trap into a Delta-Plus isotope ratio mass spectrometer (Finnigan MAT, Bremen, Germany) via a movable open split. Ten replicates (i.e., loop switches) of each sample

Reproduced with permission of the copyright owner. Further reproduction prohibited without permission.

headspace were made and the mean sample peak value was compared to two reference gases for computation of a delta value relative to Vienna Standard Mean Ocean Water (VSMOW) reference material [*Coplen et al.*, 1983]. An average difference in isotopic composition between sample and reference gas is determined using the following general equation:

$$[(R_{sample}-R_{standard})/(R_{standard})] \times 1000 = \Delta_{sample\text{-}standard} \quad (4)$$

where R_{sample} is the ratio of heavy to light isotope of interest in the sample, $R_{standard}$ is the same ratio in the working reference gas, and $\Delta_{sample\text{-}standard}$ is the difference in isotopic composition of the sample relative to that of the reference, expressed in parts per thousand (per mil, or ‰). Analyses with the Gas Bench II instrument used here yielded an external precision of 0.14‰. Water and water-plus-soil tests of the method indicated that the value of the water added to a soil can be determined within 0.41±0.10 (see Ch.2). Duplicates, and in some cases, triplicates, were randomly selected from all site—sampling date—depth combinations and were analyzed to assess "working precision" of the measurement technique. That is, I tried to quantify the uncertainty in the measured isotopic signature associated with storing, transferring, and shipping samples, in addition to the uncertainty due to internal instrument precision. Replicate measurements varied from 0.00 to 0.24‰, with standard deviations for duplicates of about 0.15‰ most common.

4.2.3.2. Irm-GCMS of soil CO_2

The gas samples collected for this study represented a tremendous methodological challenge because their CO_2 concentrations ranged from about 400 to over 12,000 ppm.

Reproduced with permission of the copyright owner. Further reproduction prohibited without permission.

Furthermore, the samples were collected at different atmospheric pressures, which meant that automating the sample runs was very difficult, and in the end, abandoned. As a consequence of the concentration and pressure issues, there was no single laboratory ideally equipped to process all of the gas samples. Thus, low concentration samples had to be processed in one lab, and high concentration samples were processed in another lab.

Soil gas samples were stored cold (5°C) until analyzed. Most samples were stored for about two weeks prior to analysis. Maximum storage time was 1-1/2 months. Samples were analyzed either at the Colorado State University (CSU) Stable Isotope Facility (the majority of the samples) or the Stable Isotope Facility for Ecological Research (SIRFER) at the University of Utah. The CSU facility is well-suited for high concentration samples whereas the Utah facility was better able to process the low concentration (ca. 400 to 3000 ppm) samples. The CSU hardware consists of a VG Microgas Injector (Micromass Inc., Manchester, U.K.) linked to an Optima mass spectrometer (formerly VG Scientific, now Micromass Inc., Manchester, U.K.) run in continuous flow mode. Gas samples were drawn from sample vials using a Series A-2 gas tight syringe (VICI Precision Sampling, Baton Rouge, LA). The needle was purged and the sample was over-pressured just prior to injection through a silicone septa into the gas chromatograph portion of the Microgas Injector. The amount of sample injected was calculated from the CO_2 concentration, based on an optimal peak height for the instrument (1-6 E^{-9} amps, most injections were 200 to 600 µl). Sample gases are separated on a PoraPak QS 80/00 packed column (0.2 cm i.d., 2 m length, column temperature 70°C), and enter the mass spectrometer via an open split (a heartcut valve sends column effluent to waste or to the MS). Over 230

Reproduced with permission of the copyright owner. Further reproduction prohibited without permission.

samples plus duplicates and standards were processed using this manner. Twenty-eight injections of a working standard yielded a precision of 0.4‰ for C and 0.5‰ for O.

Samples analyzed at the SIRFER facility (141 samples, plus duplicates and standards) were injected via gas-tight syringe (VICI Precision Sampling, Baton Rouge, LA) into a flow of helium carrier gas (flow rate of 20 ml/min). The samples passed through a PreCon trace gas preconcentrator (Finnigan MAT, Bremen, Germany), into a 55 m gas chromotograph column (GC column temp 30°C). The column effluents were sent to a Finnigan MAT 252 mass spectrometer (Finnigan MAT, Bremen, Germany) via moveable open split. Optimal sample size for the instrument is $1.8E^{-9}$ to $8.9E^{-9}$ moles CO_2, so the volume of gas injected varied as a function of its CO_2 concentration (usually 30 µl to 400 µl). External precision of the method is 0.2‰ for C and 0.3‰ for O. As there had been no prior formal intercomparison between the CSU and Utah facility, the same working standard was transported and processed with all samples. A detailed analysis of differences between the two facilities is presented in Appendix IV.

4.2.4. Modeling Analysis

I used a soil diffusion model developed by Tans [1998] that calculates the simultaneous effects of CO_2 diffusion and equilibration with water on $\delta^{18}O$ of CO_2 in a soil profile. The model also implicitly accounts for atmospheric invasion into the soil profile [*Miller et al.*, 1999; *Tans*, 1998], and one output of the model is the apparent isotopic composition of the flux of respired CO_2 to the atmosphere. At each model time step, CO_2 is produced in model layers according to a field-measured production rate. The CO_2 hydration rate in soil is:

Reproduced with permission of the copyright owner. Further reproduction prohibited without permission.

$$k_s = k_h \cdot B \cdot \theta_w, \quad (5)$$

where k_h is the rate constant for the oxygen exchange between CO_2 and water (eqn 1, $0.037 s^{-1}$) [*Skirrow*, 1975], B is the volumetric Bunsen solubility coefficient (0.76), and θ_w is water-filled pore space. The rate of isotopic hydration is 1/3 of k_s because there are three oxygen atoms involved in the exchange reaction (see Miller et al. [1999] and Stern et al. [1999]). The half-life for the isotopic equilibration for CO_2 in water in soil pores is:

$$t_{1/2} = \ln 2 / k_s \quad (6)$$

Oxygen equilibration between water and CO_2 also results in a temperature-dependent fractionation [*Brenninkmeijer et al.*, 1983]. In the model the hydrated CO_2 diffuses to soil layers above and below at a rate determined by:

$$D_s = D_{air} \cdot \kappa \cdot \theta_a, \quad (7)$$

where D_{air} is the diffusivity of $C^{16}O^{18}O$ in air (0.164 cm^2/s, [*Hillel*, 1998]), θ_a is air-filled pore space, and κ is soil tortuosity (set at a constant 0.66 for these simulations). CO_2 also diffuses both into and from an atmospheric layer, here set at a height of 20 cm, that initially contains air of a measured CO_2 concentration and isotopic signature, which is flushed at the measured flow rate. The model reaches steady state when both the concentration and isotopic signature of the atmospheric layer no longer change.

The model was initialized for field conditions on multiple sampling dates for each of the six field sites. A total of 19 simulations were undertaken to characterize site-dependent flux composition as well as its temporal variability. The model requires the following input as a function of depth in the soil: soil porosity, water volume, soil temperature, and the isotopic ($\delta^{18}O$) signature of soil water. Field measurements of these properties from 5, 10, 30, and 50 cm were entered into the model, and estimates, based on

Reproduced with permission of the copyright owner. Further reproduction prohibited without permission.

air temperature, rainwater $\delta^{18}O$, and field notes, were developed for surface (0 cm) characteristics. The model interpolates among the input measurements to complete the soil profile.

Depth-independent input variables include background CO_2 concentration and isotopic composition, the rate of CO_2 evolution from the soil, and the rate of chamber flushing. Flushing rate is the measured flow rate of the LI-6200 during sample collection (converted to appropriate units using the ideal gas law). The flux rate was calculated directly from the LI-6200 output via plots of CO_2 concentration vs. time (separate plot for each soil chamber closure, n=5, where the mean slope equals the flux in parts per million (ppm), which was then converted to units of $mol/m^2/day$). Production is assumed to equal the measured flux. Measured depth profiles of soil CO_2 concentration were used in conjunction with the total measured flux rate to constrain the CO_2 production function in the model. This added model constraint is an improvement over previous experiments with this model, which assumed constant production with depth [*Miller et al.*, 1999]. Appendix II includes the complete set of parameters used in each of the 19 simulations.

After each model simulation a second simulation was carried out to calculate the effective kinetic fractionation affecting the composition of respired-CO_2. For these simulations the model was run with background CO_2 concentration set to zero, maximal flushing rate, and the assumption of no isotopic fractionation (model parameter "alpha18" set to 1.0). The difference in the apparent signature of the soil CO_2 flux from this run and a standard run (with fractionation fully expressed) is the effective kinetic fractionation under the given field conditions.

Reproduced with permission of the copyright owner. Further reproduction prohibited without permission.

4.3. Results and Discussion

4.3.1. $\delta^{18}O$ in Soil Water and in Soil CO_2

Results of the analysis of soil water isotopic composition suggest that it is highly variable over time (Figure 4.4), reflecting both recharge by precipitation from different sources or at least of different isotopic composition, and fractionation due to evaporative water loss [*Sulzman et al.*, in prep]. The isotopic composition of oxygen in soil CO_2 varies in a similar fashion (Figure 4.5), although there is generally less variability in $\delta^{18}O$ values with depth in soil CO_2 as compared to that in soil water. Interestingly, whereas soil water closest to the surface is often the most enriched, soil CO_2 is often less enriched at 5 cm than deeper in the profile. The reasons for this are unclear, especially as one would expect a greater influence of atmospheric CO_2 at the 5 cm depth. As predicted by Farquhar et al. [1993], when the seasonal mean values of $\delta^{18}O$ in soil water are compared across ecosystems, they are distinct, reflecting similar source water and evaporative fraction (Figure 4.6). However, the seasonally-averaged depth profiles of soil CO_2 are not unique across ecosystems (Figure 4.7). Differences in soil texture can result in great differences in diffusivity (via differences in air- vs. water-filled pore space), rates and patterns of water infiltration, and even the proportion of water available for loss via transpiration (non-fractionating) or evaporation (fractionating). However, there were no distinct differences in $\delta^{18}O$ values of either soil water or soil CO_2 among the textural site-pairs studied (Figure 4.8).

Reproduced with permission of the copyright owner. Further reproduction prohibited without permission.

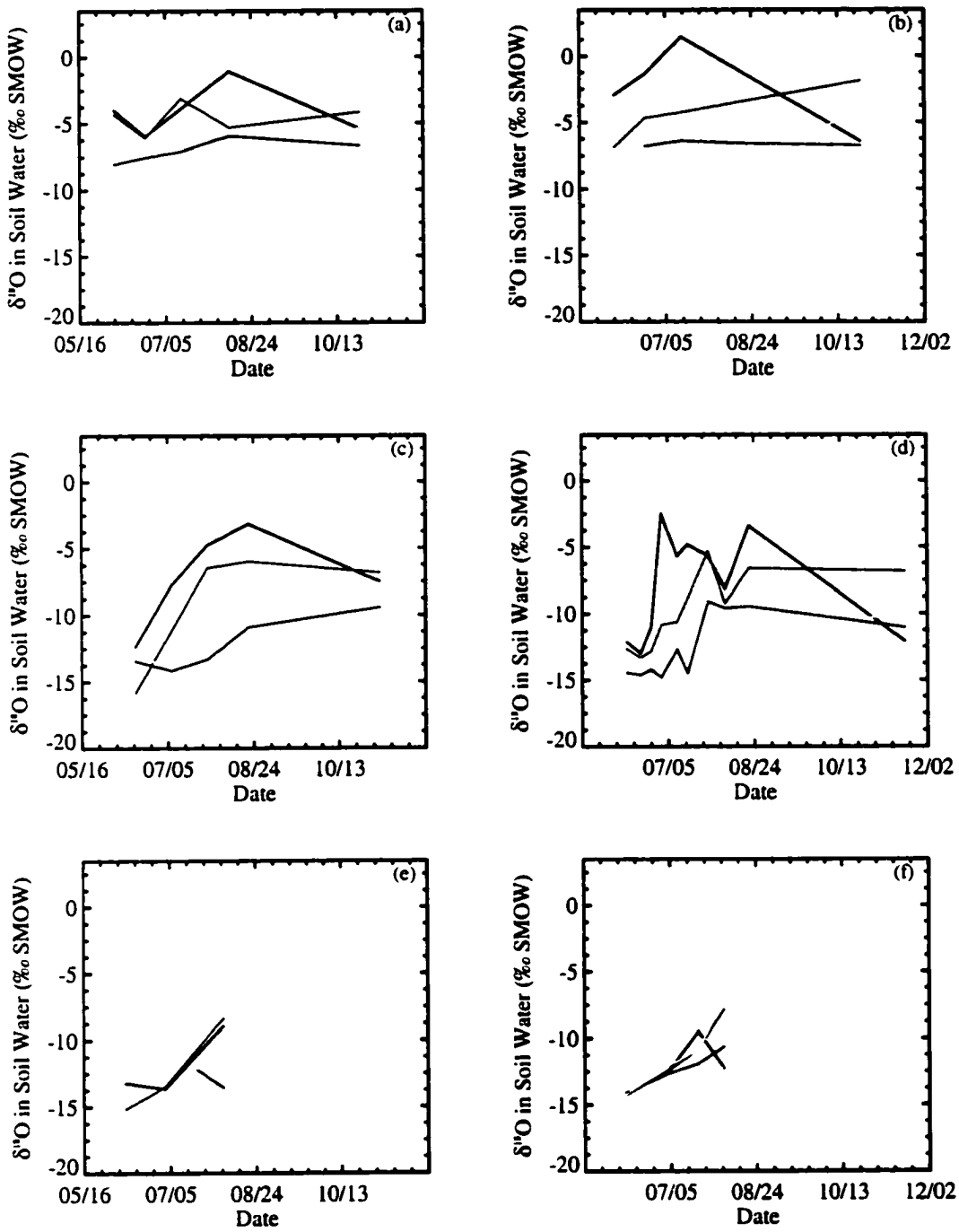

Figure 4.4. Seasonal variability in $\delta^{18}O$ values of soil water at each of the six field sites. Data for 5 cm depth are in blue, 10 cm depth data are green, 30 cm depth data are yellow, and 50 cm depth data are red. Lines connect data points – data are not continuous. (a) Shortgrass steppe on fine soil, (b) shortgrass steppe on coarse soil, (c) lodgepole pine on fine soil, (d) lodgepole pine on coarse soil, (e) alpine tundra on fine soil, (f) alpine tundra on coarse soil.

Reproduced with permission of the copyright owner. Further reproduction prohibited without permission.

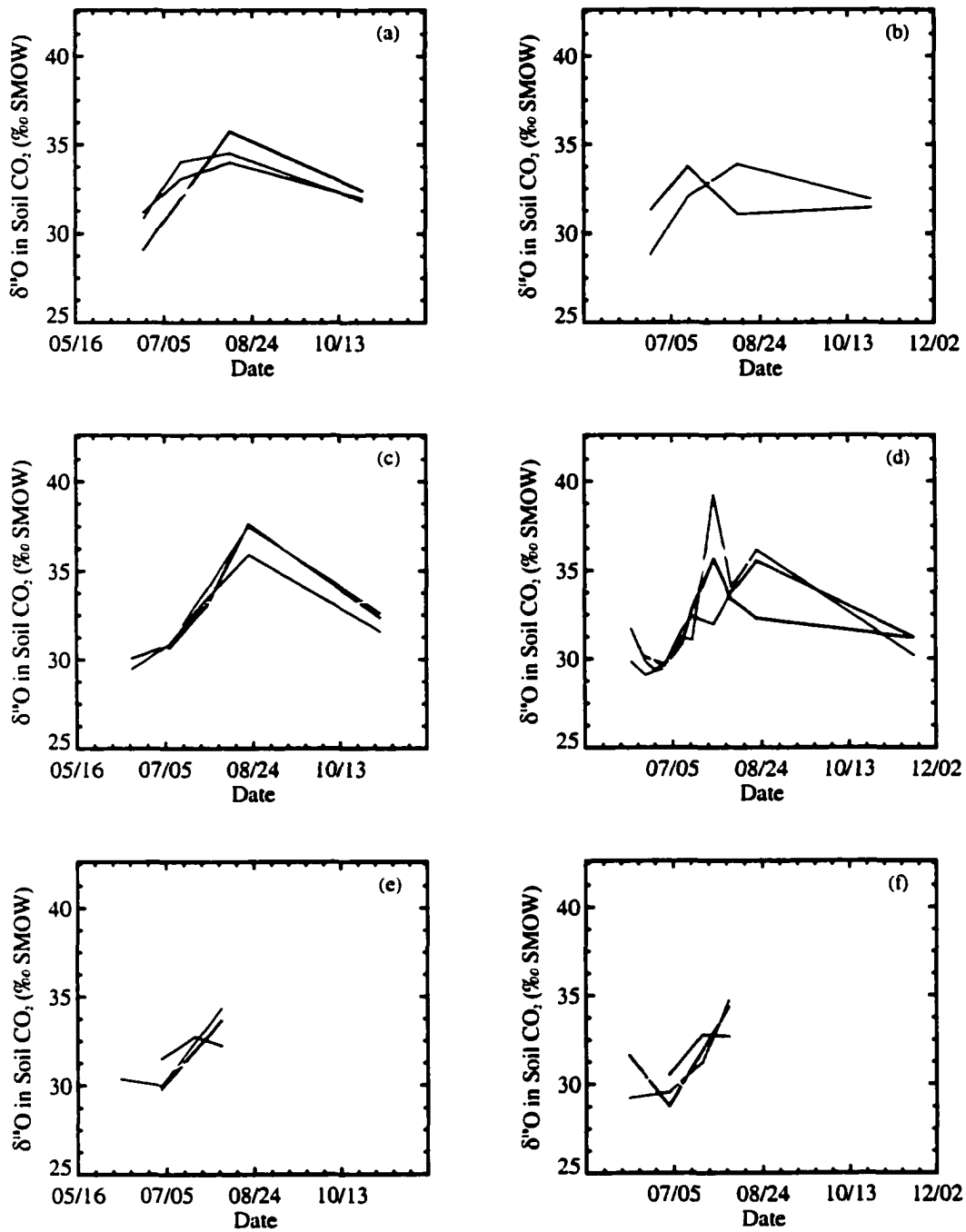

Figure 4.5. Seasonal variability in $\delta^{18}O$ values of soil CO_2 at each of the six field sites. Data for 5 cm depth are in blue, 10 cm depth data are green, 30 cm depth data are yellow, and 50 cm depth data are red. Lines connect data points – data are not continuous. (a) Shortgrass steppe on fine soil, (b) shortgrass steppe on coarse soil, (c) lodgepole pine on fine soil, (d) lodgepole pine on coarse soil, (e) alpine tundra on fine soil, (f) alpine tundra on coarse soil.

Reproduced with permission of the copyright owner. Further reproduction prohibited without permission.

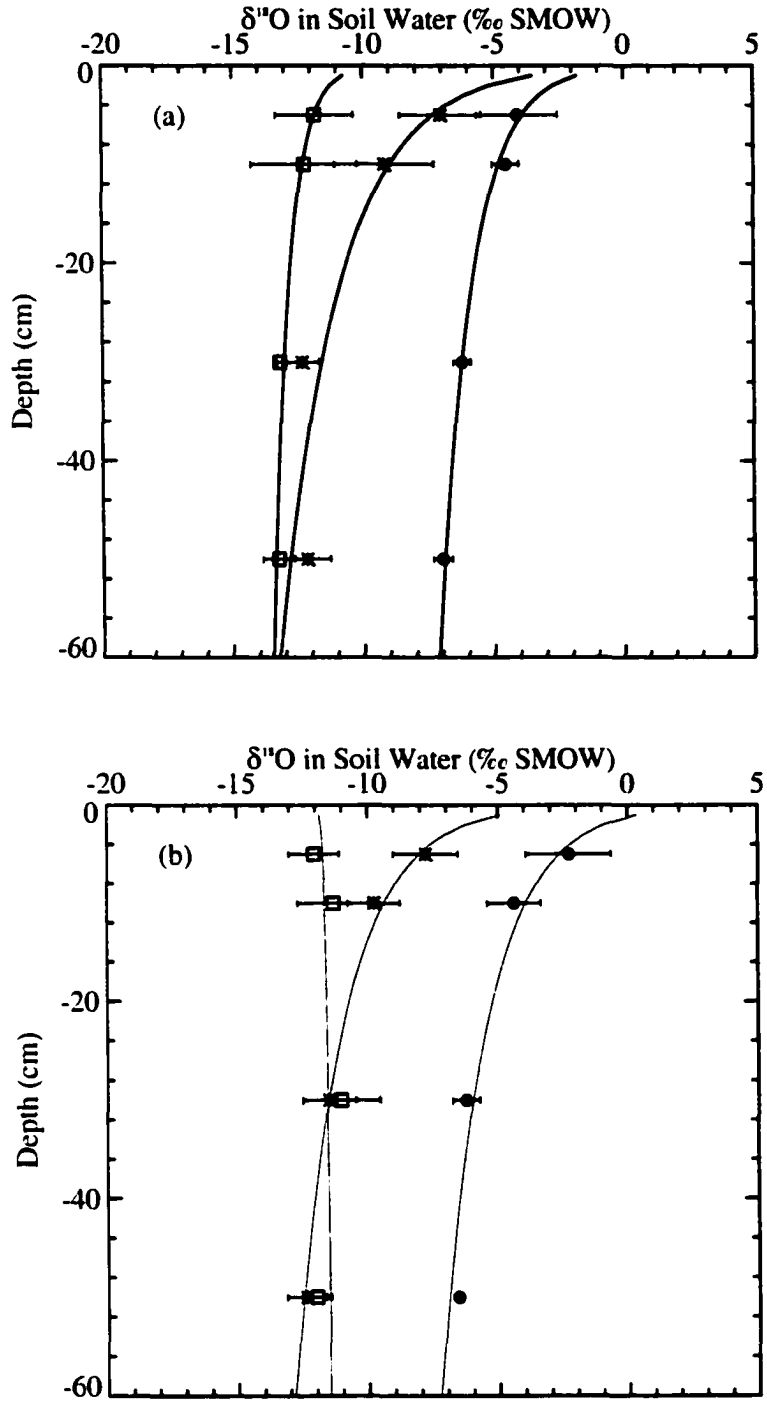

Figure 4.6. Seasonal-average $\delta^{18}O$ values of soil water by depth at each of the six field sites. Symbols are mean ± standard error; the smoothed fit is a log linear regression of the data (IDL software, RSI, Inc.). (a) Three ecosystems on fine-textured soil, (b) three ecosystems on coarse-textured soil. Solid circle represents shortgrass steppe, asterix represents lodgepole pine, and open square represents alpine tundra systems.

Reproduced with permission of the copyright owner. Further reproduction prohibited without permission.

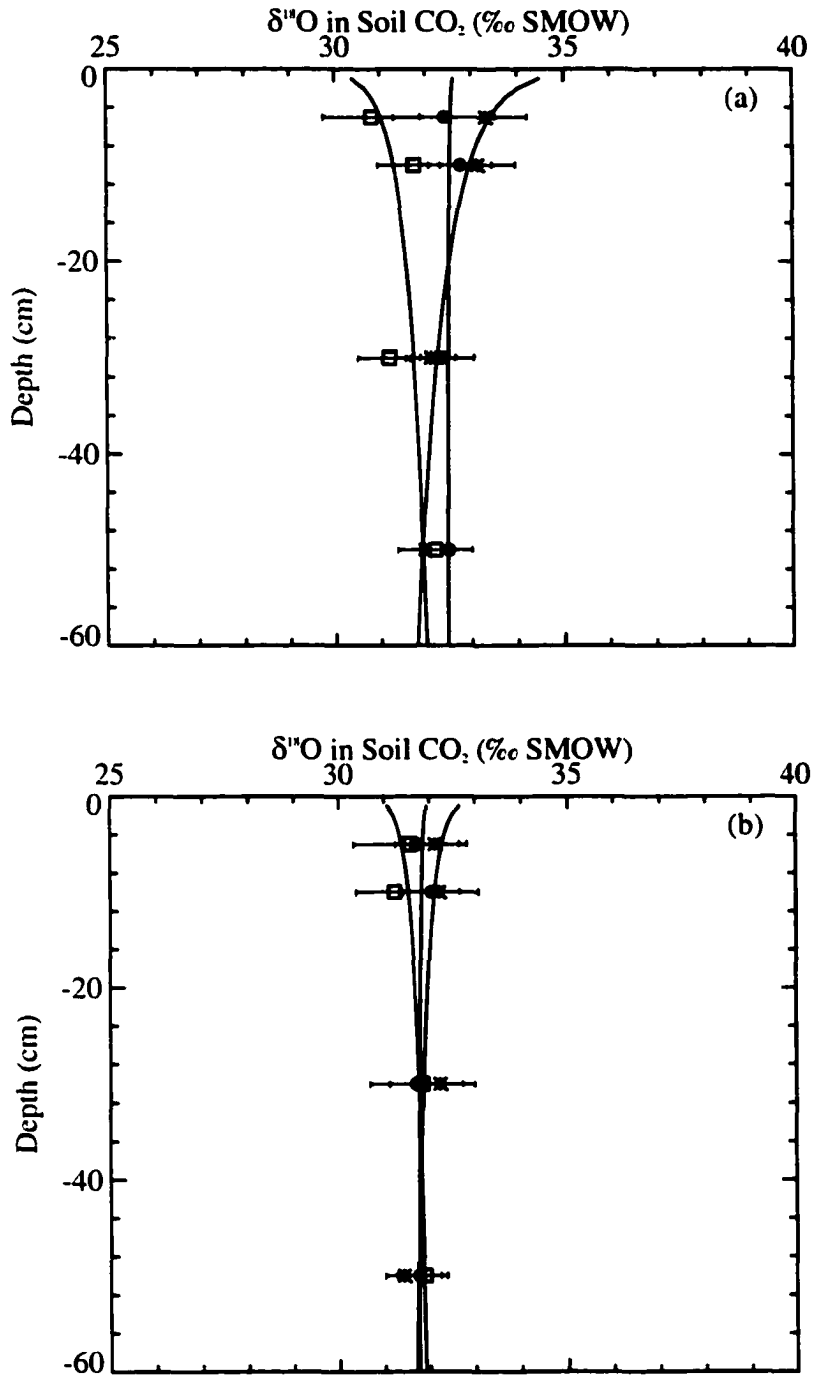

Figure 4.7. Seasonal-average $\delta^{18}O$ values of soil CO_2 by depth at each of the six field sites. Symbols are mean ± standard error; the smoothed fit is a log linear regression of the data (IDL software, RSI, Inc.). (a) Three ecosystems on fine-textured soil, (b) three ecosystems on coarse-textured soil. Solid circle represents shortgrass steppe, asterix represents lodgepole pine, and open square represents alpine tundra systems.

Reproduced with permission of the copyright owner. Further reproduction prohibited without permission.

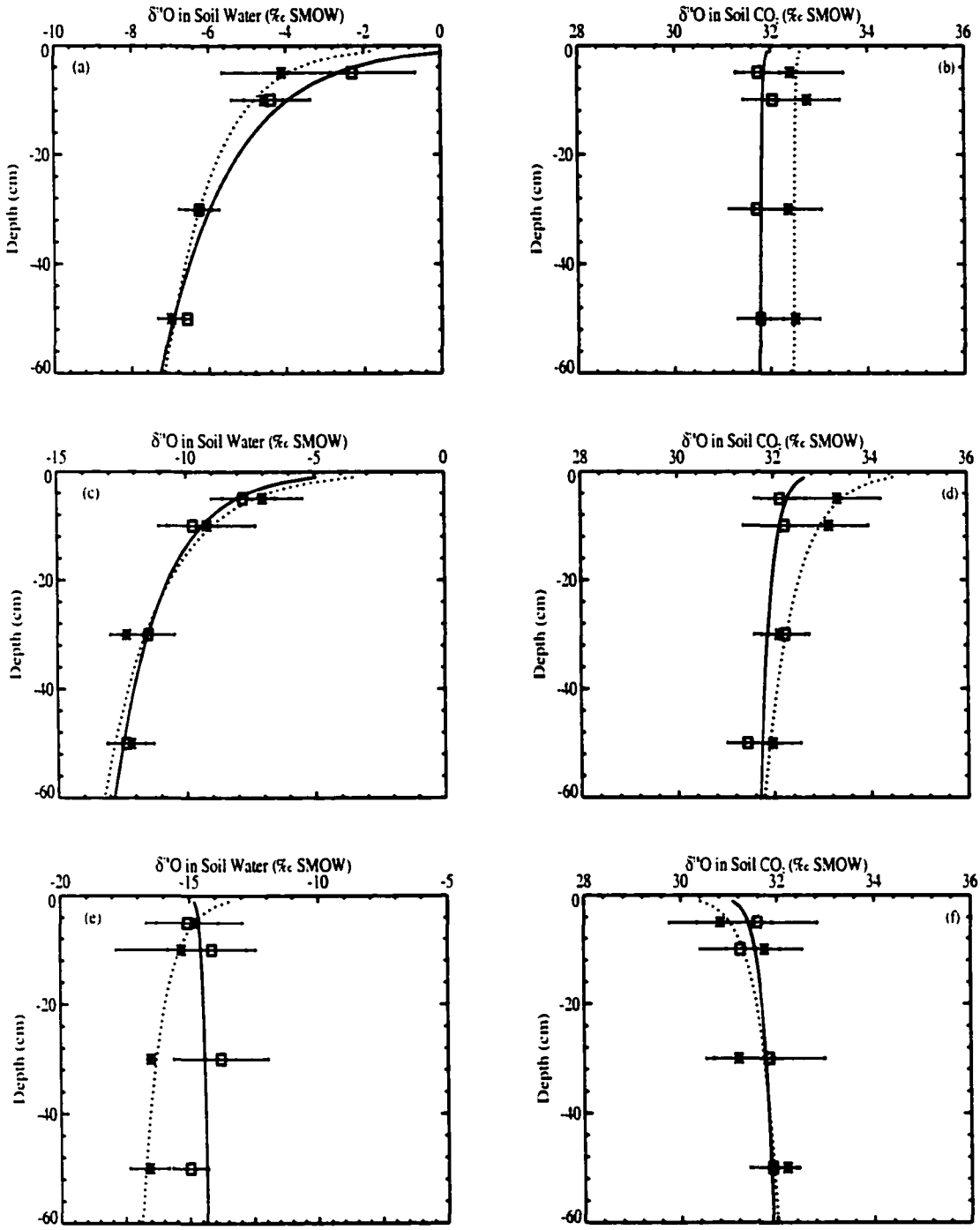

Figure 4.8. Comparison of the $\delta^{18}O$ values in soil water (panels a, c, e) with those in soil CO_2 (panels b, d, f) across the six field sites. Data are presented as mean ± standard error for all sampling dates. Data from fine-textured soils are represented by an asterix, those from coarse-textured soils are shown with an open square. Smoothed lines are a log linear regression of the data (IDL software, RSI, Inc.). Panels (a) and (b) are shortgrass steppe, (c) and (d) are lodgepole pine, and (e) and (f) are alpine tundra.

Reproduced with permission of the copyright owner. Further reproduction prohibited without permission.

4.3.2. Isotopic Equilibration Between Soil CO_2 and Soil Water

CO_2 and water have been shown to come to isotopic equilibrium in the laboratory [*Bottinga and Craig*, 1969; *Brenninkmeijer et al.*, 1983; *Hsieh et al.*, 1998b; *Mills and Urey*, 1940]. Pioneering work by Hesterberg and Siegenthaler [1991] suggested that water and CO_2 also are in equilibrium at 30 and 80 cm depths in the soil. In order to assess whether there was isotopic equilibrium at the depths, sites, and dates studied here, I used the equilibration equation of Brenninkmeijer et al. [1983]. This equation allowed me to calculate what the isotopic composition of soil CO_2 *would be* if it were in full equilibrium with soil water from the same depth and measured temperatures. Next, I compared these "calculated equilibrium" values to the actual measured values. Figure 4.9 shows the fit of observed CO_2 values to the equilibrium assumption.

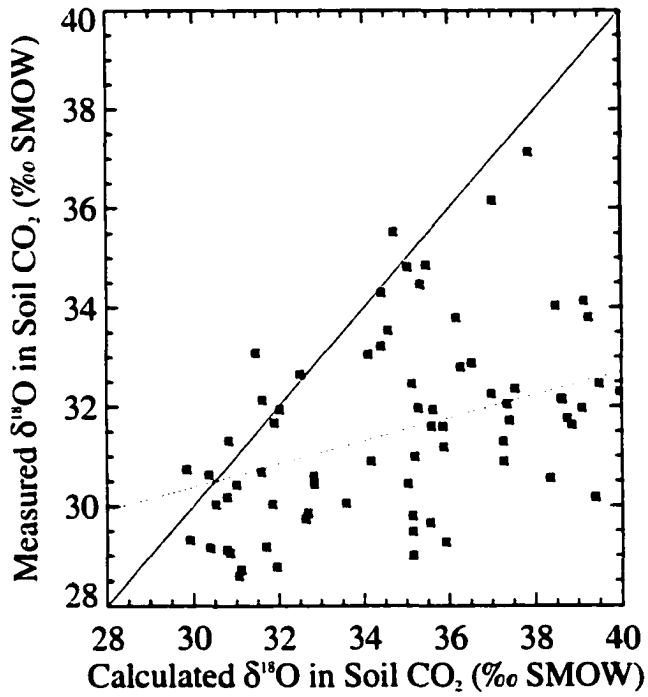

Figure 4.9. Comparison of $\delta^{18}O$ values measured in soil CO_2 and those calculated with the Brenninkmeijer et al. [1983] model based on $\delta^{18}O$ values measured in soil water. The 1:1 line is solid, a linear regression of the data (r^2=0.15, P<0.01) is dashed.

Reproduced with permission of the copyright owner. Further reproduction prohibited without permission.

The majority of data points (n=74) fall below the 1:1 line, suggesting that observed soil CO_2 is less enriched than that in full equilibrium with soil water. In a study in the Sierra Nevada mountains of California, Amundson and Wang [1996] found the opposite result: soil CO_2 in their study was slightly enriched (ca. 1‰) relative to soil water. One problem with both the current work and previous work of this nature [*Allison et al.*, 1987; *Amundson and Wang*, 1996; *Hesterberg and Siegenthaler*, 1991], is that soil CO_2 and soil water samples can not be perfectly co-located, as sampling for soil water is destructive. It is possible that some of the offset from full equilibrium can be explained by this fact. In a laboratory study including novel techniques that allowed soil CO_2 and soil water to be measured from exactly the same location [*Miller et al.*, 1999], soil CO_2 was found to be sometimes slightly enriched, and sometimes slightly lighter than, co-located soil water (see Figure 11 of [*Miller et al.*, 1999]).

The suggestion that soil CO_2 and soil water are not always in full equilibrium under field conditions challenges our ability to use information on soil water to constrain models of soil-respired CO_2, and so needs to be examined further. Table 4.2 presents the suite of soil CO_2 and soil water measurements for one of the six field sites over the 1998 sampling season (lodgepole pine, fine soil). Tables for each of the other sites are presented in Appendix III. The final column in this table, "Mod-Obs," contains the differences between calculated and observed values for soil CO_2. Figure 4.10 illustrates the information in Table 4.2 for one of the six field sites (lodgepole pine, coarse soil). In this figure it is clear that disequilibrium tends to dominate close to the soil surface, whereas at depth there is often, but not always, convergence between the calculated (bottom axis, open square) and measured (top axis, asterix) soil CO_2. This figure and the

Reproduced with permission of the copyright owner. Further reproduction prohibited without permission.

companion figures in Appendix III (Figures 25-29) also suggest that soil CO_2 and soil water were usually closer to equilibrium in lodgepole and tundra ecosystems than at the grassland sites studied. Furthermore, all measurements made in the fall (October and November) reflect considerable deviation from equilibrium, with the difference as great as 10‰ on the grassland site on coarse soil (Table 4.2 and Appendix III).

Table 4.2. Calculation of the difference between the $\delta^{18}O$ measured in soil CO_2 and that in equilibrium with soil water (last column, Modeled-Observed) for each sampling date. Eq@stemp is the calculated value of soil CO_2 in equilibrium with measured soil water at the measured soil temperature.

Lodgepole pine, Fine Soil 6/16/98							
Site	Depth	Soil CO2	Std err	Soil water	Soil temp	Eq@stemp	Mod-Obs
3	5	-99.000	0.000	-12.260	6.200	45.088	na
3	10	29.513	0.304	-15.740	6.100	45.110	-0.143
3	30	30.161	0.214	-12.600	5.600	45.223	2.462
3	50	30.090	0.057	-13.360	5.700	45.201	1.750
Lodgepole pine, Fine Soil 7/798							
Site	Depth	Soil CO2	Std err	Soil water	Soil temp	Eq@stemp	Mod-Obs
3	5	30.695	0.295	-7.680	16.400	42.868	4.493
3	10	30.869	0.925	-11.100	12.900	43.612	1.643
3	30	31.096	0.124	-14.130	9.600	44.330	-0.896
3	50	30.817	0.206	-14.080	9.100	44.440	-0.457
Lodgepole pine, Fine Soil 7/28/98							
Site	Depth	Soil CO2	Std err	Soil water	Soil temp	Eq@stemp	Mod-Obs
3	5	33.051	1.079	-4.690	12.100	43.78	6.040
3	10	33.960	1.237	-6.400	11.400	43.936	3.576
3	30	33.291	0.206	-12.500	11.300	43.958	-1.834
3	50	33.408	1.050	-13.230	10.900	44.045	-2.593
Lodgepole pine, Fine Soil 8/21/98							
Site	Depth	Soil CO2	Std err	Soil water	Soil temp	Eq@stemp	Mod-Obs
3	5	37.632	0.495	-3.110	13.300	43.526	2.784
3	10	37.525	0.393	-5.920	12.100	43.784	0.339
3	30	33.132	2.448	-12.350	11.400	43.936	-1.546
3	50	35.920	0.000	-10.820	11.300	43.958	-2.782
Lodgepole pine, Fine Soil 11/5/98							
Site	Depth	Soil CO2	Std err	Soil water	Soil temp	Eq@stemp	Mod-Obs
3	5	32.393	0.243	-7.430	2.100	46.026	6.203
3	10	32.640	0.774	-6.770	2.600	45.910	6.500
3	30	33.263	0.819	-10.100	4.100	45.565	2.202
3	50	31.597	0.942	-9.360	2.700	45.887	4.931

Reproduced with permission of the copyright owner. Further reproduction prohibited without permission.

Figure 4.10. Comparison of $\delta^{18}O$ values measured in soil CO_2 (asterix, mean ± standard error, three sample tubes) with those calculated (open square) based on the assumption of full isotopic equilibrium with soil water measured at the same depths (accounting for temperature-dependent fractionation [*Brenninkmeijer et al.*, 1983]). Smoothed lines are log linear regressions of the data. Plots are for the lodgepole pine site on coarse soil. Each panel represents an individual sampling date: (a) June 11, 1998, (b) June 19, 1998, (c) June 25,1998, (d) July 1, 1998, (e) July 10, 1998, (f) July 16, 1998, (g) July 28, 1998, (h) August 7, 1998, (i) August 21, 1998, (j) November 19, 1998. Companion figures for the other field sites are in Appendix III, Figures 25-29.

Reproduced with permission of the copyright owner. Further reproduction prohibited without permission.

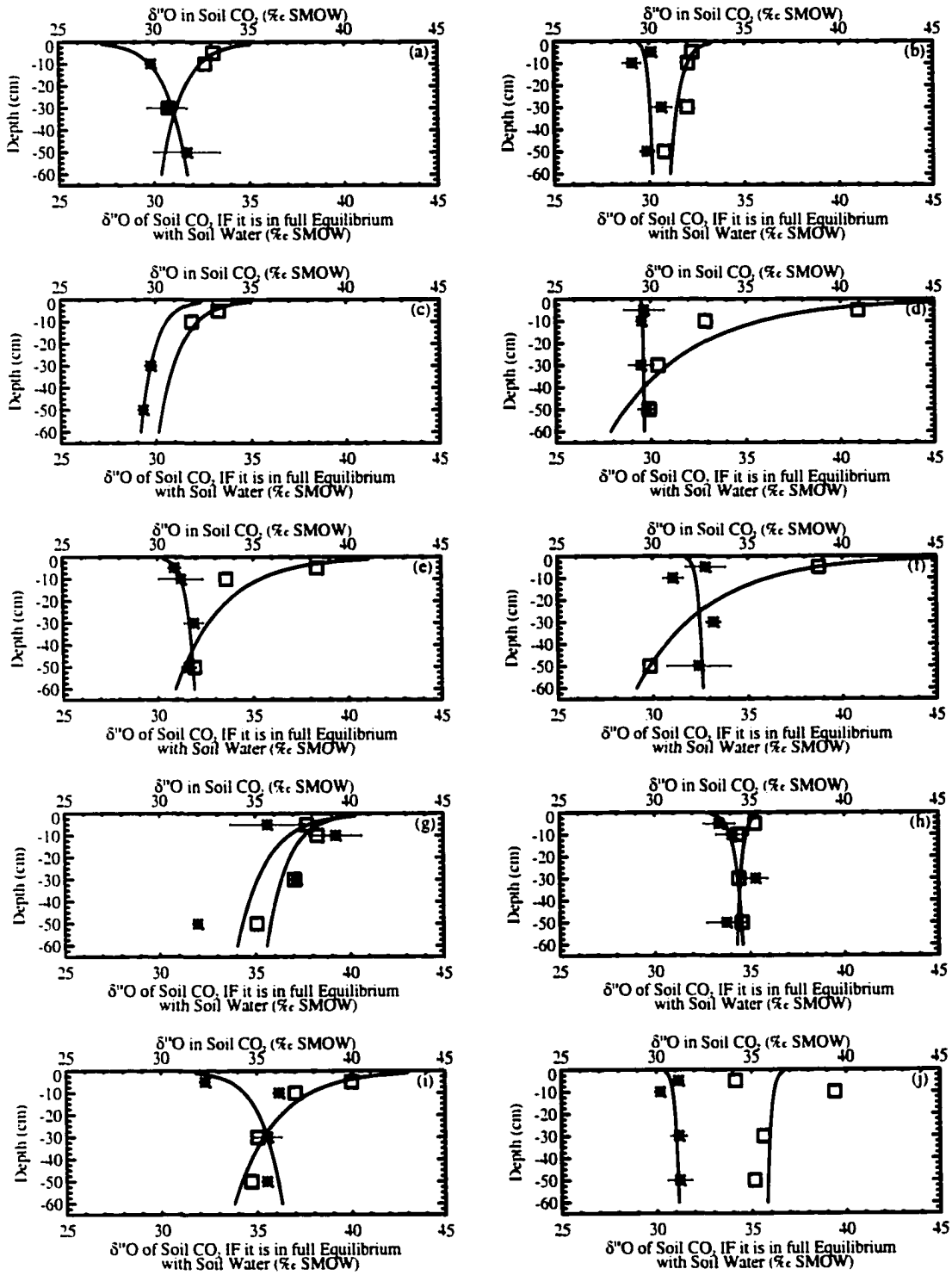

Reproduced with permission of the copyright owner. Further reproduction prohibited without permission.

One explanation for the difference among field sites and the greater disequilibrium near the soil surface is that when water content is low, diffusion times (D_s) are rapid and equilibration times (t_{ie}) slow (see equations 6 and 7, Section 4.2.4; $t_{ie} = 3.5*t_{1/2}$). For example, if θ_a is 0.23, t_{ie} is 145 seconds and D_s is 501 seconds, but if θ_a is 0.4, then t_{ie} is 1040 seconds, and D_s drops to 289 seconds. Calculations for all field sites indicate that only rarely did conditions exist at that permit CO_2-H_2O equilibration right near the soil surface; this occured only when air-filled pore space was 0.22 or less (seven out of 31 cases). In addition, there were seven cases where equilibrium was prevented by the difference in time to reach isotopic equilibrium versus that for diffusion from 10 cm. Stern et al. [1999], argue that effective values of t_{ie} may be lower than those used here, explaining disequilibrium as deep as 10 cm in more cases. Figure 4.11 indicates that low water content alone does not explain lack of equilibrium between soil CO_2 and soil water observed on some sampling dates at some field locations. Low soil CO_2 production, allowing a large proportion of atmospheric CO_2 to invade the soil profile, could partially explain the disequilibrium, especially in the fall. Unfortunately, there are too few sampling dates with reliable flux measurements to adequately test this hypothesis.

Explanation of the seven cases in which there is apparent disequilibrium below the depth where $D_s = t_{ie}$ (from here on, z*) is slightly more complicated than a comparison of diffusion versus equilibration time, because as the CO_2 diffuses, it encounters water of potentially different isotopic composition (see Figure 4.4). Miller et al. [1999] found that the signature of CO_2 diffusing out of the soil profile carried the isotopic signature of water from 5 to 10 cm below the soil surface (average for their experiments 7 cm). Unfortunately, these authors did not measure the isotopic composition of co-located soil

Reproduced with permission of the copyright owner. Further reproduction prohibited without permission.

CO_2 and soil water below 8 cm. Theoretically, at depths below those where one finds significant variation in the isotopic composition of soil water, soil CO_2 and soil water will be in equilibrium. However, under conditions when the isotopic composition of soil water is changing due to infiltration and capillary water removal, soil CO_2 and soil water might not be in isotopic equilibrium, even though the time for CO_2 diffusion is greater than the time for isotopic equilibration. This conclusion is supported by the work of Hesterberg and Siegenthaler [1991]. Their data reveal much less rapid change in isotopic composition of soil water at the 80 cm, as compared to 30 cm, depth. In addition, the measured $\delta^{18}O$ of soil CO_2 was very close to that predicted by full equilibrium at the 80 cm depth, but was less often in full equilibrium at the 30 cm depth [*Hesterberg and Siegenthaler*, 1991].

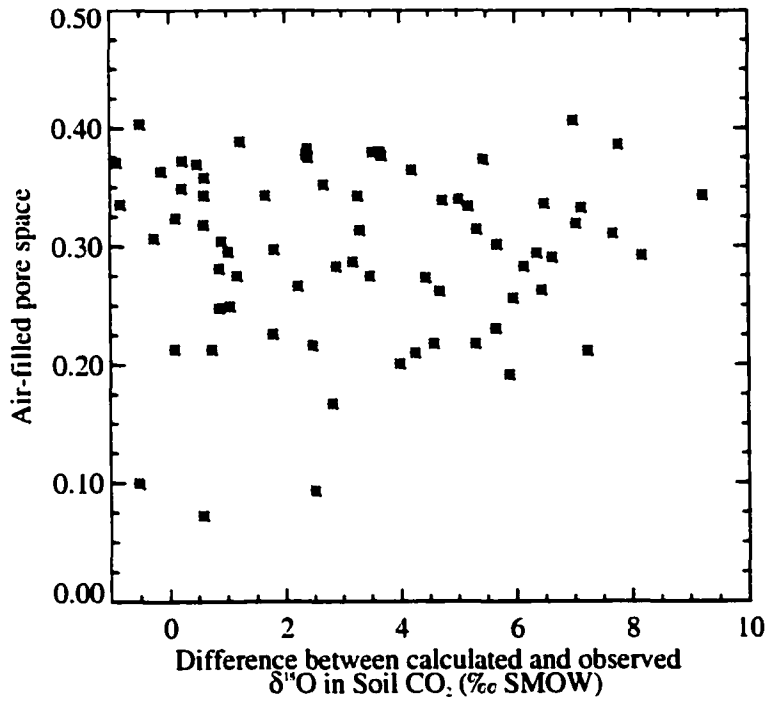

Figure 4.11. Difference between $\delta^{18}O$ values observed in soil CO_2 and those calculated from soil water $\delta^{18}O$ values [Brenninkmeijer et al., 1983] as a function of air-filled pore space. The relationship is not significant ($P>0.05$).

Reproduced with permission of the copyright owner. Further reproduction prohibited without permission.

An alternative hypothesis that could explain cases of apparent disequilibrium below z* is that under some conditions there is physical separation between soil CO_2 and soil water. This could happen, for instance, on the drying arm of the soil water hysteresis curve, in which water is held in the fine pores whereas air is in the coarse pores. In contrast, on the wetting arm of the hysteresis curve, water fills the coarse pores, and soil CO_2 must diffuse through this water, and presumably, acquire its isotopic signature, on its way out of the soil profile. Hysteresis is more pronounced in coarse, than in fine-textured soils [*Hillel*, 1980], so if hysteresis is an explanation for the observed cases of disequilibrium below z*, I should observe more cases at sites on coarse than on fine soil. Of the seven cases where there is apparent disequilibrium below z*, four are on coarse soil and three are on fine soil. Thus, laboratory experiments to test this hypothesis are needed. A companion explanation including physical separation occurs in soils of fine texture. Some clay soils contain water that is chemically or physically bound (e.g., montmorillonitic soils or soils containing halloysite), thereby preventing full isotopic equilibration [*Hsieh et al.*, 1998b]. Laboratory studies to assess whether or not there are separable water fractions of different isotopic composition within soil are feasible.

Disequilibrium only exists under some sampling conditions. For example, see Figure 4.10(h), and Appendix III. There is often at least one sampling date for each of the six field sites where equilibrium does not exist between soil CO_2 and soil water, even at depth. Seasonally averaged values (Table 4.3 and Figure 4.12) indicate that there is equilibrium below z* at four of the six field sites. The seasonal-average (n=4) at the grassland sites is most likely dominated by the late October measurements, which are out of equilibrium by roughly 8‰. While the fall measurements deviate significantly from

Reproduced with permission of the copyright owner. Further reproduction prohibited without permission.

equilibrium at the lodgpole sites as well (Table 4.2 and Appendix III), the offset from equilibrium is smaller at the fine site (n=5), and there are many more sampling dates at the coarse site (n=10).

4.3.3. Model Results

There are several significant results from the modeling effort. First, the model is insensitive to background conditions and production rate, but quite sensitive to the $\delta^{18}O$ of soil water near the surface and to the shape of the CO_2 production function. Second, the oxygen isotopic composition of the soil CO_2 flux was unique across ecosystems, but not across soil type. Finally, while a simpler model [*Flanagan et al.*, 1997] is capable of capturing the average signal of CO_2 produced in the soil, the full diffusion-equilibration model is needed to compute the temporal variability in the $\delta^{18}O$ of respired CO_2. In addition, I verified that the Keeling plot method of calculating the composition of respired CO_2 does not work for ^{18}O because there are more than two end-members (an assumption of that method). This is despite the fact that the plots themselves do not look worse than those for ^{13}C, where the method is well-established.

4.3.3.1. Sensitivity tests

Model sensitivity tests were conducted with regard to initial conditions, flux rate, soil CO_2 production function, and surface (0-5 cm) soil water amount and oxygen isotopic composition (Table 4.4). The test case used was a lodgepole pine site on fine textured soils under fairly moist conditions (5 cm volumetric water content 0.19g/cm^3). When the initial conditions of the atmosphere were set at values used in Tans [1998] rather than the

Reproduced with permission of the copyright owner. Further reproduction prohibited without permission.

Table 4.3. Calculation of the difference between the $\delta^{18}O$ measured in soil CO_2 and that in equilibrium with soil water (last column, Modeled-Observed) as a seasonal average.

Shortgrass Steppe, Fine Soil

Depth	Soil CO2	std err	n	Soil Water	std err	n	Soil temp	Eq@stemp	Mod-Obs
5	32.41	1.11	7	-3.30	1.35	4	21.9	41.73	6.02
10	32.76	0.69	7	-4.55	0.51	5	16.6	42.82	5.50
30	32.36	0.70	10	-6.25	0.32	5	16.5	42.84	4.24
50	32.50	0.51	11	-6.99	0.36	5	17.1	42.72	3.24

Shortgrass Steppe, Coarse Soil

Depth	Soil CO2	std err	n	Soil Water	std err	n	Soil temp	Eq@stemp	Mod-Obs
5	31.74	0.47	3	-2.28	1.64	4	22.1	41.70	7.69
10	32.05	0.63	8	-4.38	1.03	4	19.1	42.31	5.88
30	31.69	0.58	10	-6.25	0.53	5	16.9	42.76	4.82
50	31.77	0.48	10	-6.58	0.09	4	17.0	42.74	4.39

Lodgepole pine, Fine Soil

Depth	Soil CO2	std err	n	Soil Water	std err	n	Soil temp	Eq@stemp	Mod-Obs
5	33.33	0.89	9	-7.03	1.56	5	10.0	44.24	3.88
10	33.14	0.82	14	-9.19	1.88	5	9.0	44.46	2.13
30	32.11	0.54	12	-12.34	0.65	5	8.4	44.60	0.15
50	31.96	0.59	12	-12.17	0.89	5	7.9	44.70	0.56

Lodgepole pine, Coarse Soil

Depth	Soil CO2	std err	n	Soil Water	std err	n	Soil temp	Eq@stemp	Mod-Obs
5	32.13	0.54	16	-8.02	1.37	9	9.5	44.36	4.20
10	32.22	0.86	16	-9.74	0.99	9	8.6	44.54	2.58
30	32.23	0.50	24	-11.49	1.02	8	7.6	44.77	1.06
50	31.43	0.42	24	-12.38	0.76	10	7.1	44.87	1.07

Alpine tundra, Fine Soil

Depth	Soil CO2	std err	n	Soil Water	std err	n	Soil temp	Eq@stemp	Mod-Obs
5	30.82	1.07	4	-11.84	1.50	3	8.7	44.53	1.87
10	31.74	0.79	8	-12.16	1.44	4	6.5	45.03	1.12
30	31.20	0.68	3	-13.20	0.12	3	4.4	45.49	1.09
50	32.19	0.26	7	-13.26	0.61	3	3.7	45.66	0.21

Alpine tundra, Coarse Soil

Depth	Soil CO2	std err	n	Soil Water	std err	n	Soil temp	Eq@stemp	Mod-Obs
5	31.59	1.25	5	-12.06	0.96	4	12.3	43.74	0.09
10	31.24	0.84	8	-11.29	1.37	4	9.2	44.42	1.89
30	31.84	1.15	6	-11.02	1.47	4	5.1	45.34	2.48
50	31.90	0.49	8	-11.99	0.55	4	4.3	45.52	1.63

Reproduced with permission of the copyright owner. Further reproduction prohibited without permission.

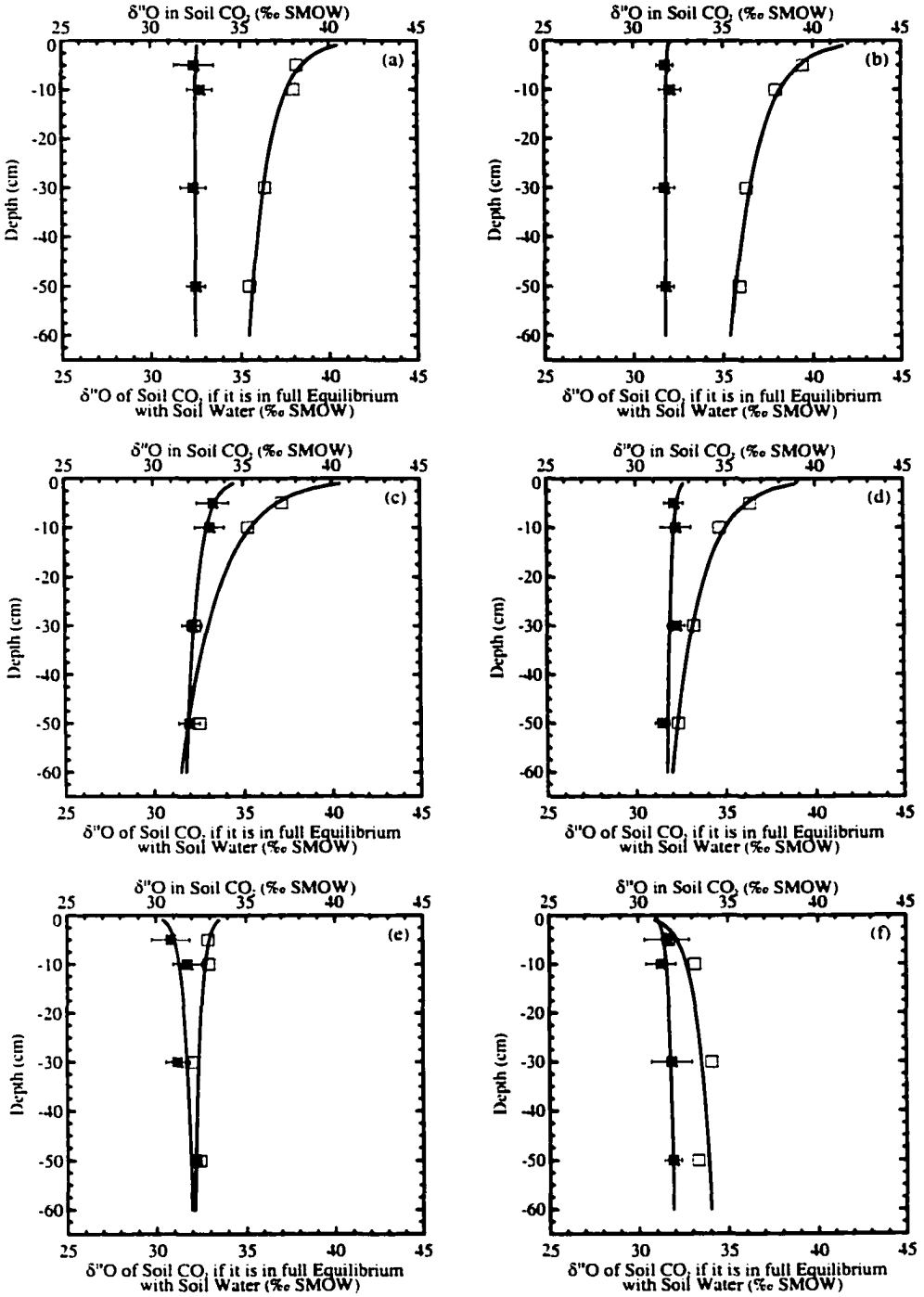

Figure 4.12. Comparison of seasonal mean $\delta^{18}O$ values measured in soil CO_2 (asterix, mean ± standard error) with those calculated (open square) based on the assumption of full isotopic equilibrium with soil water measured at the same depths (accounting for temperature-dependent fractionation [*Brenninkmeijer et al.*, 1983]). Smoothed lines are log linear regressions of the data. (a) Shortgrass steppe, fine soil, (b) shortgrass steppe, coarse soil, (c) lodgepole pine, fine soil, (d) lodgepole pine, coarse soil, (e) alpine tundra, fine soil, (f) alpine tundra, coarse soil.

Reproduced with permission of the copyright owner. Further reproduction prohibited without permission.

measured values for atmospheric flasks collected on that sampling date, the apparent signature of the $\delta^{18}O$ flux from soil was essentially unchanged (Table 4.4). This is despite the fact that the difference between the flask and original $\delta^{18}O$ of the atmosphere was 3‰. A test of the sensitivity to the flux rate used in the model was conducted using the lowest, and then the highest of my measured flux rates for the entire sampling period (0.12 and 0.52 mol/m^2/day). Published flux rates indicate that the range selected captures normal field variability [*Davidson and Trumbore*, 1995; *Fang et al.*, 1998; *Gordon et al.*, 1987; *Ryan and Waring*, 1992; *Sommerfeld et al.*, 1993]. The model is not very sensitive to the efflux rate: model output only varied by 0.8‰ over the range of efflux rates tested (Table 4.4).

The model was also tested for sensitivity to the distribution of CO_2 production within the soil profile. Hesterberg and Siegenthaler [1991] assumed an exponential decline in production in their model, which is supported by data indicating an exponential decline in microbial numbers with depth [*Severson et al.*, 1991]. Previous work using this model [*Miller et al.*, 1999] assumed constant production with depth based on a laboratory incubation (J.Miller, pers. comm., April, 2000). Root distribution data suggest constant production with depth is unlikely in grassland and tundra ecosystems [*Jackson et al.*, 1996], although it might be plausible in lodgepole systems. For the lodgepole case tested the modeled isotopic composition of the soil-respired CO_2 was 2.62‰ more enriched when the constant production function was used as compared to the customized case of production matched to the measured concentration profile. Sensitivity to the use of a constant production function was 4‰ in a grassland case. A comparison between the exponential production decline and site-specific production indicated that for the

Reproduced with permission of the copyright owner. Further reproduction prohibited without permission.

lodgepole test case sensitivity was nearly the same as for the constant production case (2.91‰). In all model runs it was discovered that a deep (>30 cm to the deepest model layer) source of CO_2 was needed to match the shape and magnitude of the observed CO_2 concentration profiles. Keller and Bacon [1998] argue that about 2% of total (soil plus geo-) respiration originates from the zone just above the water table, supporting the need for a "deep" source in the current modeling exercise.

The model also was found to be very sensitive to conditions at the soil surface. This sensitivity test was conducted using values for 0 and 5 cm depths used in model development versus values measured at 5 cm and interpolated to the surface based on rainfall composition (see Table 4.4). The values interpolated to the surface are comparable to those measured under laboratory conditions by Miller et al. [1999]. Under the conditions used for model development, which assumed strong evaporative fractionation in surface soil layers, the modeled flux from soil was 2.88‰ heavier than in the case using conditions measured in the field.

Table 4.4. Sensitivity tests of the soil diffusion model [*Tans*, 1998].

Conditions tested	Test	Model sensitivity
Atmospheric background	360 ppm, 0‰ $\delta^{18}O$, -8‰ $\delta^{13}C$ vs. 393 ppm,-3.26 $\delta^{18}O$, -9.06 $\delta^{13}C$	very low (0.5‰)
Flux rate	0.12 mol/m^2/day vs. 0.52 mol/m^2/day	low (0.8‰)
Soil CO_2 production function	Constant production vs. matched to measured [CO_2] depth profile	very high (2.62‰)
Surface soil water signature	+5.0‰ at 0 cm and –4.0‰ at 5 cm vs. -4.0‰ at 0 cm and –7.4‰ at 5 cm	very high (2.88‰)

Reproduced with permission of the copyright owner. Further reproduction prohibited without permission.

4.3.3.2. Model-generated apparent isotopic composition of the flux to the atmosphere

Model simulations were carried out for each field site on every sampling date for which soil water $\delta^{18}O$ data were available. As model sensitivity to this input parameter was high, sampling dates without complete isotope profiles of soil water were not simulated. However, simulations sometimes included estimates for the magnitude of the flux or background conditions because of model insensitivity to these parameters (see Appendix II). This suite of simulations allowed me to assess both differences in the isotopic composition of the soil flux across sites, and also to assess its temporal variability at a single location. Table 4.5 presents the modeled "del-f," or oxygen isotope composition of the CO_2 flux from the soil. Results are presented relative to two different international standards (PDB-CO_2 and SMOW) because although all values of $\delta^{18}O$ should be expressed relative to SMOW, there is strong precedent in the literature to use PDB-CO_2 when referring to CO_2 [*Ciais et al.*, 1997; *Farquhar et al.*, 1993; *Flanagan et al.*, 1997; *Friedli et al.*, 1987; *Miller et al.*, 1999; *Sternberg et al.*, 1998; *Tans*, 1998]. (To convert values from PBD-CO_2 to SMOW, multiply by 1.04142 and add 41.42.) Simulations indicate that the $\delta^{18}O$ composition of each ecosystem studied was unique, as suggested by Farquhar et al. [1993]. Average values range from -13.37‰ (27.50‰ SMOW) at the tundra sites to –6.93‰ (34.20‰ SMOW) at the grassland sites, reflecting the unique isotopic composition of soil water in these different locales. The lack of difference across soil texture confirms that composition of precipitation is more important than is water content or even mode of water loss (evaporation vs. transpiration) as a control on the $\delta^{18}O$ of the soil flux, at least when sampling sites and dates are averaged.

Reproduced with permission of the copyright owner. Further reproduction prohibited without permission.

Table 4.5. The oxygen isotope composition of the flux of CO_2 from soil to the atmosphere ("del-f"). Simulation results are presented relative to two international standards because although $\delta^{18}O$ technically should be reported against SMOW, there is precedent in the literature for the use of PDB-CO_2.

Ecosystem	Sample size (model runs)	Del-f ± std err (‰ PDB-CO_2)	Del-f (‰ SMOW)
Grass	5	-6.93 ± 0.93	34.20
Pine	11	-10.71 ± 0.84	30.27
Tundra	3	-13.37 ± 0.15	27.50

Soil Texture	Sample size (model runs)	Del-f ± std err (‰ PDB-CO_2)	Del-f (‰ SMOW)
Coarse	10	-9.73 ± 0.97	31.29
Fine	9	-10.18 ± 1.2	30.82

Results of simulations for the same field site parameterized for different sampling dates indicate that there is considerable temporal variability in the isotopic composition of the flux from soil to atmosphere (Figure 4.13). This finding is consistent with the variability observed in the isotopic composition of precipitation (not shown) and that in soil water (Figure 4.4), especially in the zone from which the soil respired CO_2 flux appears to be obtaining its isotopic signature (5-15 cm). Although there is a tendency towards greater isotopic enrichment in the soil flux under drier field conditions at a single site, the relationship is weak (r^2=0.20) and does not account for the fact that there can be large rain events that are relatively enriched, due, for example, to local storm generation. Figure 4.14 shows results for one field site on three different sampling dates. The figure illustrates the fact that the composition of the flux to the atmosphere is not necessarily dependent on whether or not there is local equilibrium between $\delta^{18}O$ in soil water and

Reproduced with permission of the copyright owner. Further reproduction prohibited without permission.

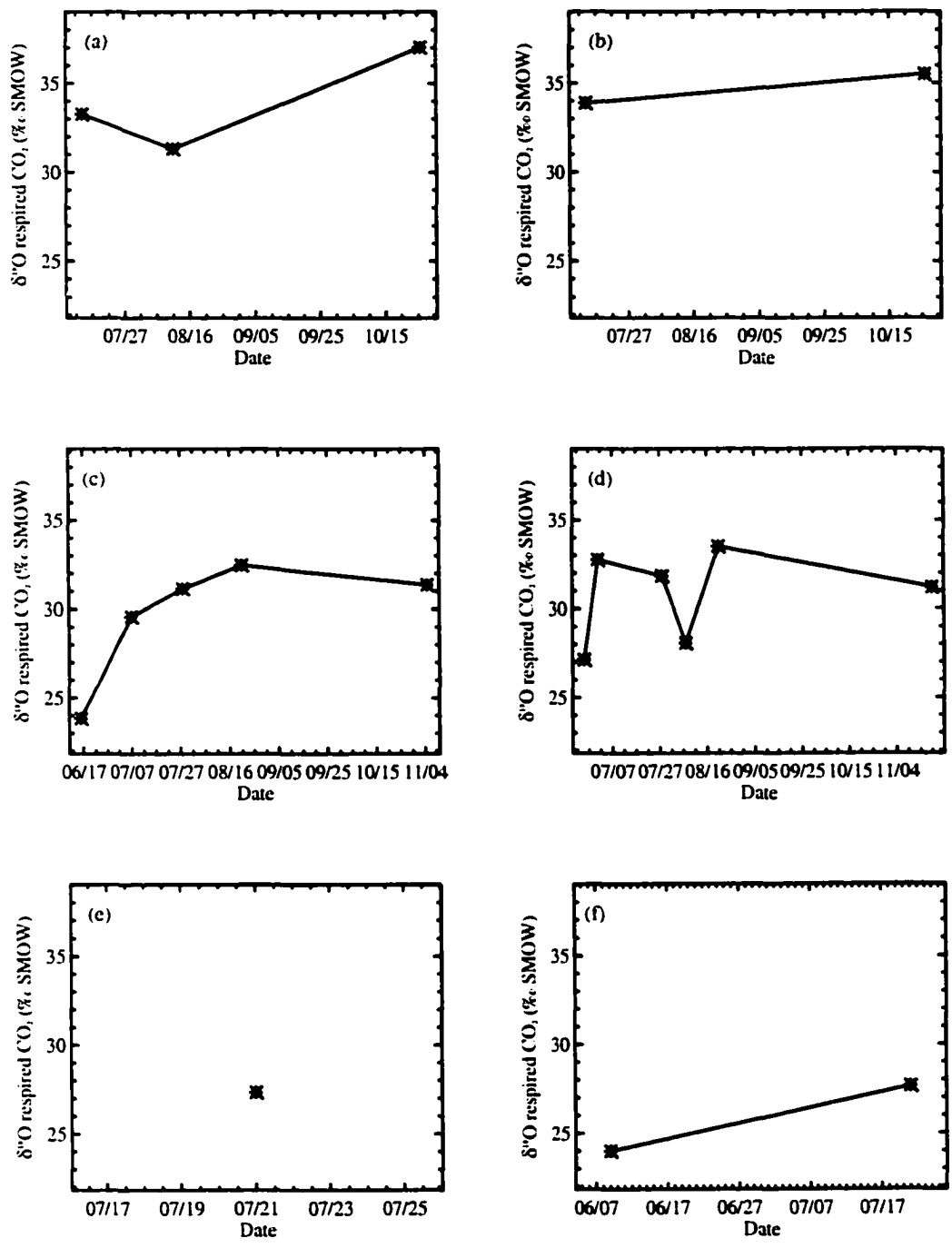

Figure 4.13. Model-generated oxygen isotopic composition of soil-respired CO_2 as a function of time for each of the six field sites. Flux values based on field measurements of soil water $\delta^{18}O$ values and other soil properties (see text). (a) Shortgrass steppe, fine soil, (b) shortgrass steppe, coarse soil, (c) lodgepole pine, fine soil, (d) lodgepole pine, coarse soil, (e) alpine tundra, fine soil, (f) alpine tundra, coarse soil. Measurements are not continuous; points connected for visualization.

Reproduced with permission of the copyright owner. Further reproduction prohibited without permission.

Figure 4.14. Three case studies of isotopic equilibrium (or lack thereof) in field soils. (a) Equilibrium near the soil surface under "wet" conditions (air-filled pore space (θ_a) at 5 cm = 0.314, data from 7 August, 1998), (b) equilibrium at depth under "dry" conditions (5 cm θ_a = 0.367, 1 July, 1998), and (c) apparent disequilibrium following recent snow on a dry profile (50 cm θ_a = 0.352, 19 November, 1998). All data are from the lodgepole pine site on coarse soil. Asterix represent field measurements of soil CO_2 $\delta^{18}O$ values, open square represents $\delta^{18}O$ values for CO_2 calculated from soil water $\delta^{18}O$ values (based on the Brenninkmeijer et al. [1983] model). Solid circle indicates the soil diffusion-equilibrium model calculation of the $\delta^{18}O$ value of soil CO_2 that becomes the soil-respired flux to the atmosphere (i.e., the $\delta^{18}O$ value of the flux minus a condition-specific term for diffusion).

Reproduced with permission of the copyright owner. Further reproduction prohibited without permission.

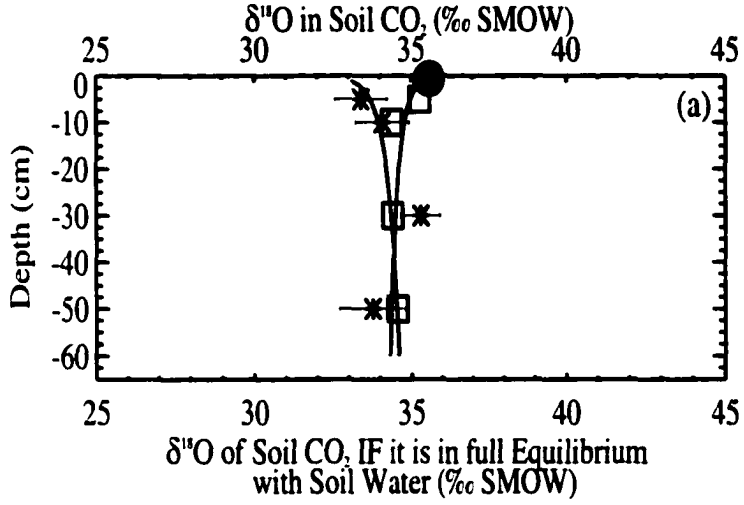

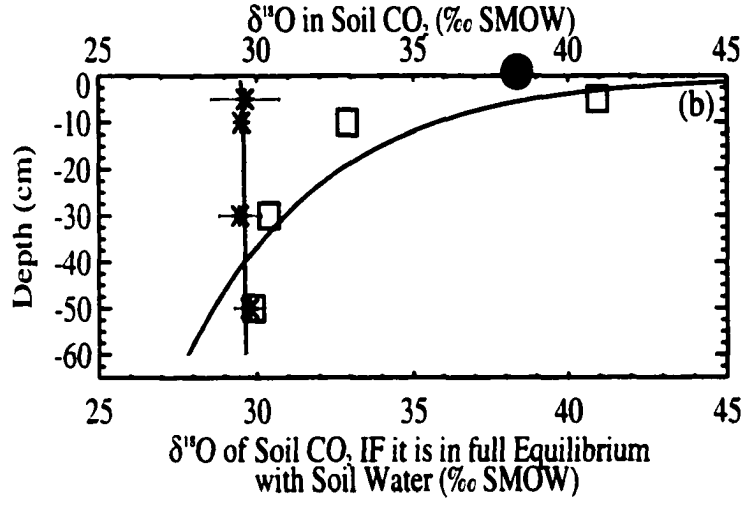

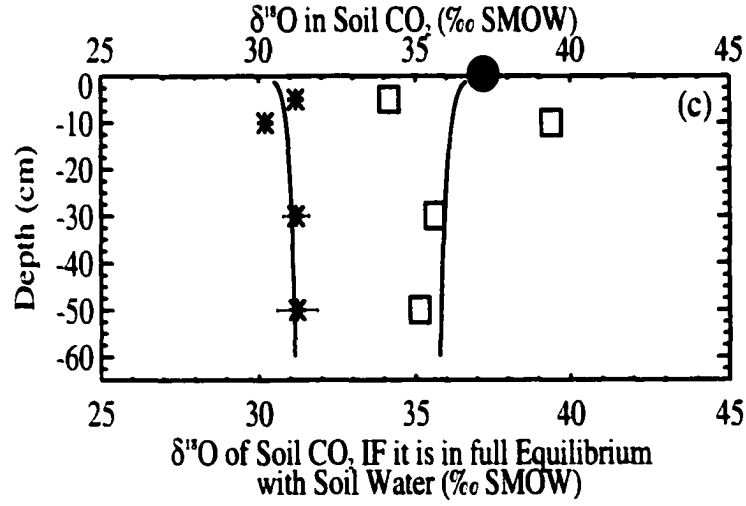

Reproduced with permission of the copyright owner. Further reproduction prohibited without permission.

that in soil CO_2 at the time of sampling. For all three sampling dates the modeled flux depends most strongly on the isotopic composition of the soil water at a depth between 5 and 10 cm. This result agrees with results of Miller et al. [1999] and confirms the model of Flanagan et al. [1997]. At the same time, it argues against the approach taken by Farquhar et al. [1993] and Ciais et al. [1997]. A more detailed assessment of their approach is discussed in Section 4.3.3.3, below.

One factor that plays an important role in any model that includes diffusion of a gas from the soil is the isotopic fractionation that diffusion causes. Although the theoretical fractionation factor resulting from the difference in mass between ^{18}O and ^{16}O is 8.8‰, this factor is only fully expressed if water and CO_2 are in complete isotopic equilibrium from depth all the way to the soil surface. As calculations above show that this cannot be the case in any but extremely wet conditions, the CO_2 remaining in the soil profile will be enriched relative to its value in equilibrium with water (because the lighter CO_2 molecules diffuse out of the soil faster). The result is that the observed kinetic fractionation factor is less than the theoretical value. Various studies have reported a range of values for "effective" kinetic fractionation ("Eeff"), from 3.29‰ [*Flanagan et al.*, 1997] to 7.6‰ [*Farquhar et al.*, 1993]. Stern et al. [1999] argue that this factor is likely to vary as a function of field conditions. The simulations presented here produced values of Eeff ranging from 3.4‰ to 7.47‰, with a mean value of 5.58‰ (n=19). Note that the values of Eeff are negative, because they reflect the fact that the CO_2 respired from the soil is lighter than that which remains in the soil. The time-averaged value for each ecosystem was not unique, nor was the value computed for the two soil textures (Table 4.6). There was, however, a significant effect of near-surface water content on the

Reproduced with permission of the copyright owner. Further reproduction prohibited without permission.

strength of kinetic fractionation, as would be expected based on the dependence of equilibration and diffusion times on this soil characteristic (Figure 4.15).

Table 4.6. The observed kinetic fractionation ("Eeff") that arises during diffusion of CO_2 out of the soil profile, as computed with the soil diffusion-equilibration model.

Ecosystem	Sample size (model runs)	Eeff ± std err (‰)
Grass	5	5.09 ± 1.51
Pine	11	5.65 ± 0.92
Tundra	3	6.01 ± 1.27

Soil Texture	Sample size (model runs)	Eeff ± std err (‰)
Coarse	10	5.45 ± 1.12
Fine	9	5.68 ± 1.18

4.3.3.3. Inter-model comparison

A test of the soil diffusion model was conducted by comparing model output to values generated by a simple, one-dimensional model [*Flanagan et al.*, 1997][2], and to the $\delta^{18}O$ of soil respired CO_2 calculated using the approach of Farquhar et al.[3] [1993] (Table 4.7). There are several striking features of this comparison. First, the approach taken in recent

[2] $\delta_{R\text{-}Soil}$ (PDB-CO_2) = ((α_{BC}[1 + δ_{stem}(SMOW)]/1.04142)-1.0088), where α_{BC} is the temperature-sensitive H_2O-CO_2 equilibration factor ($\ln\alpha = 16.60T^{-1} - 1.519*10^{-2}$: from [*O'Neil and Adami*, 1969]).

[3] The approach of Ciais et al. [1997] is esssentially the same as that of Farquhar et al. [1993]. The only difference is that in the Ciais et al. paper the $\delta^{18}O$ of precipitation was calculated using a GCM (general circulation model), and the kinetic fraction factor they used was 5.0‰ instead of 7.6‰.

Reproduced with permission of the copyright owner. Further reproduction prohibited without permission.

global calculations [*Ciais et al.*, 1997; *Farquhar et al.*, 1993] yields estimates of the $\delta^{18}O$ of soil respired CO_2 that are 1 to 11‰ lighter than estimates based on the full equilibration-diffusion model. Further, differences are greatest in grassland systems, which occupy a very significant portion of the terrestrial biosphere. The estimates for soil temperature (used in the calculation of equilibrium fractionation [*Brenninkmeijer et al.*, 1983]) are biased high due to lack of data for the winter months. This bias could cause the estimates presented here to be 1-2‰ lower than if data for the entire year were used (greater equilibrium fractionation at colder temperature). Previously reported values of the soil respired contribution to the atmospheric ^{18}O budget in midlatitudes range from about −15‰ [*Farquhar et al.*, 1993] to −12‰ [*Friedli et al.*, 1987]. These estimates clearly do not capture the spatial variability depicted by the data presented here.

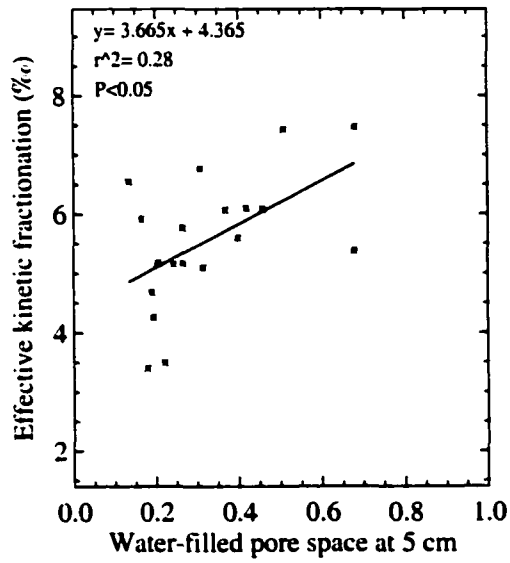

Figure 4.15. Effect of water content on effective kinetic fractionation. The relationship is significant at the $P < 0.05$ level, but other factors clearly have a strong influence on the degree to which kinetic fractionation is expressed.

Reproduced with permission of the copyright owner. Further reproduction prohibited without permission.

The empirical calculation [*Flanagan et al.*, 1997] provides a very reasonable estimate of the $\delta^{18}O$ of soil respired CO_2 when compared to the full diffusion-equilibrium model. Note, however, that the input used to obtain these results ($\delta^{18}O$ of soil water at 10 cm), is labor intensive to obtain, so this method does not present an advantage over use of the full model. Figure 4.16 suggests that although the difference between the empirical calculation and full model is sometimes quite small or even negligible, on other sampling dates there are large differences between the two approaches. This finding demonstrates that factors such as atmospheric invasion and variability in the exact depth of z*, which are not included in the simple empirical approach [*Flanagan et al.*, 1997], can have a significant impact on the $\delta^{18}O$ of soil respired CO_2 under some field conditions. The full model, therefore, is a meaningful improvement over the purely empirical approach.

Table 4.7. Average $\delta^{18}O$ of soil respired CO_2 (‰ PDB-CO_2).

Modeled system	Calculation based on precipitation[S] plus fractionation	Empirical calculation using soil water at 10 cm*	Soil diffusion model[&]
Grassland	-17.54	-3.71	-6.53
Lodgepole forest	-17.61	-8.83	-10.32
Alpine tundra	-14.92	-12.31	-13.52

[S]Rainfall calculated using the IEAE regression equation [1981] plus an equilibrium fractionation factor based on measured soil temperature [*Brenninkmeijer et al.*, 1983] and a kinetic fractionation factor of -7.6‰ (this is the Farquhar et al. [1993] approach).
* Flanagan et al. [1997] equation using soil water data from 10 cm in place of stem water
[&] [*Tans*, 1998]

Reproduced with permission of the copyright owner. Further reproduction prohibited without permission.

In order to bypass the dependence on knowing the $\delta^{18}O$ of soil water, a two end-member mixing model [*Keeling*, 1961] was used as an alternative method to calculate the $\delta^{18}O$ of soil respired CO_2. The "Keeling" approach is well-accepted as a method to determine the $\delta^{13}C$ of soil respired CO_2, and has been used for air samples collected in the plant canopy for ^{18}O [*Flanagan et al.*, 1997; *Flanagan et al.*, 1999; *Friedli et al.*, 1987; *Sternberg et al.*, 1998; *Yakir and Wang*, 1996]. Figure 4.17 presents plots of $\delta^{18}O$ in soil CO_2 against $1/[CO_2]$ for all sampling dates at each field site. The correlation between variables is much higher (r^2=.95) in some cases than in others (r^2=.01). The y-intercept of these plots represents the signature of the source of ^{18}O to the atmosphere. To calculate the $\delta^{18}O$ of soil respiration, these values would be shifted by a factor up to 8.8‰ to account for kinetic fractionation. Although there is tremendous temporal variability, the time- and ecosystem-averaged values are not unique (y-intercepts of about –9‰). The fact that work by Sternberg et al. [1998] in the canopy of the Amazon forest resulted in the same value (-9.35‰) is not comforting. Furthermore, if the empirical approach presented above is used with soil water data for the Amazon field site [*Sternberg et al.*, 1998], the resulting signature of respired CO_2 is –12.6‰. Sternberg et al. [1998] conclude that it is not possible to determine the isotopic identity of ecosystem respired CO_2 based on the $\delta^{18}O$ of soil water and a constant fractionation factor. Through calculations presented here I argue that the two end-member mixing model does not apply to soil CO_2 profiles, and that profiles within the canopy must reflect a significant enrichment in ^{18}O due to exchange with plant leaves.

Reproduced with permission of the copyright owner. Further reproduction prohibited without permission.

4.4. Conclusions

Incomplete isotopic equilibration between soil water and soil CO_2 frequently was observed under field conditions. Near the soil surface (less than 5 to 10 cm) the time it takes CO_2 to diffuse out of the soil profile is less than that required for isotope equilibrium. This means that the isotopic composition of the soil flux to the atmosphere will originate from soil water below 5 to 10 cm. At depths greater than this, there is the possibility for isotopic disequilibrium if the isotopic composition of soil water is changing. Such change might occur, for example, with infiltration of a storm event that has an isotopic composition different from that of the previous event. An alternative hypothesis that could explain cases of apparent disequilibrium below the depth of equal time for diffusion and equilibration is that under some conditions there is physical separation between soil CO_2 and soil water. Further research is needed to determine the mechanisms that lead to isotopic disequilibrium deep in the soil profile.

A full diffusion-equilibration model [*Tans*, 1998] was used to calculate the $\delta^{18}O$ composition of the soil flux. Results indicate that the $\delta^{18}O$ of soil respiration was unique for each ecosystem studied. The calculated composition of the flux to the atmosphere was not dependent on whether or not there was local equilibrium between $\delta^{18}O$ in soil water and that in soil CO_2 at the time of sampling; instead, it depends most strongly on the isotopic composition of the soil water at a depth between 5 and 10 cm. The magnitude of observed kinetic fractionation, which, like the composition of the flux, cannot be directly measured, was found to vary with local conditions. A weak dependence of this factor on near-surface soil water content was indicated.

Reproduced with permission of the copyright owner. Further reproduction prohibited without permission.

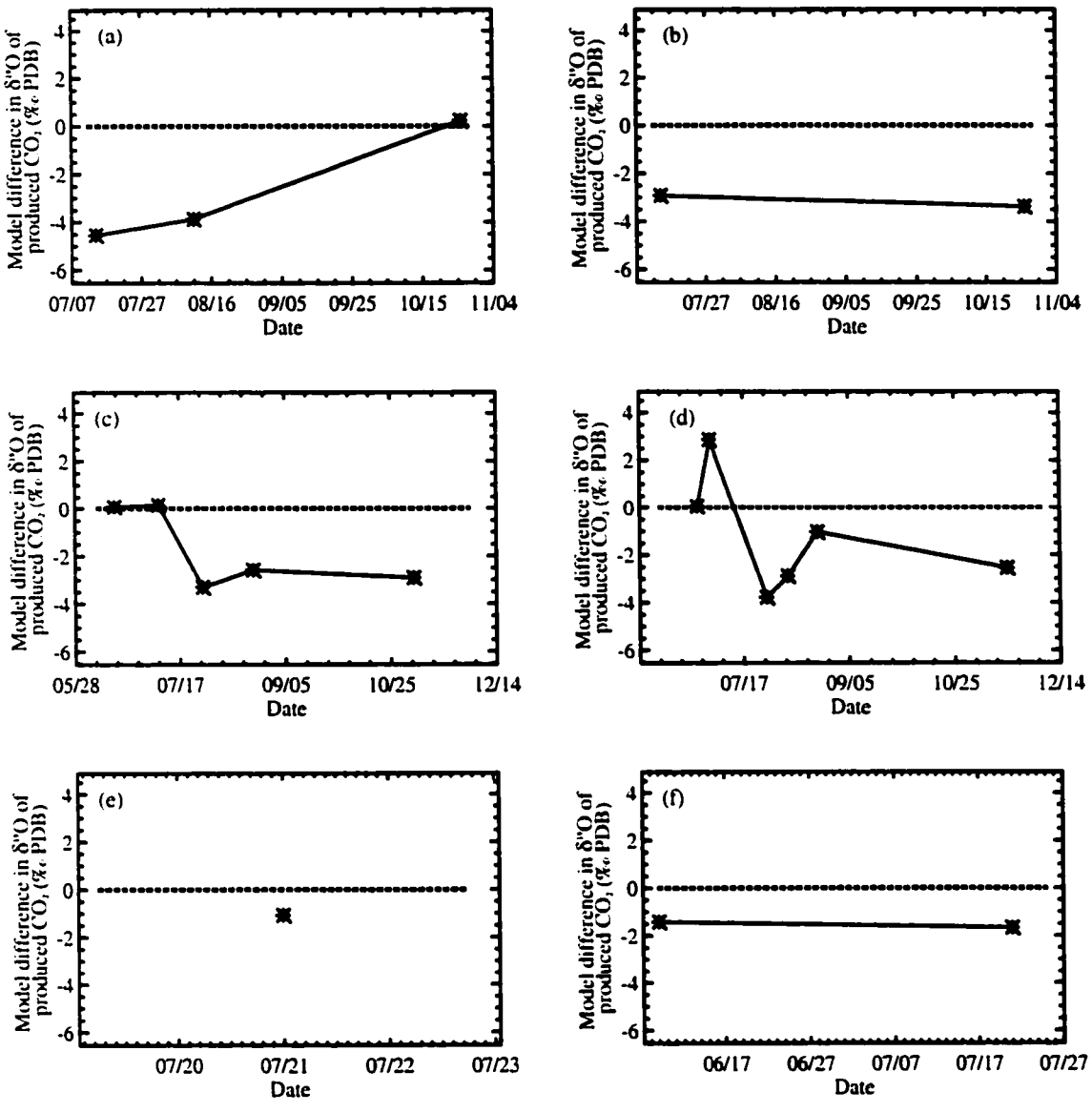

Figure 4.16. The isotopic signature of CO_2 produced in the soil. Differences between estimates calculated using the Tans [1998] model versus those calculated using the Flanagan et al. [1997] model. (a) Shortgrass steppe, fine soil, (b) shortgrass steppe, coarse soil, (c) lodgepole pine, fine soil, (d) lodgepole pine, coarse soil, (e) alpine tundra, fine soil, (f) alpine tundra, coarse soil. Measurements are not continuous; points connected for visualization.

Reproduced with permission of the copyright owner. Further reproduction prohibited without permission.

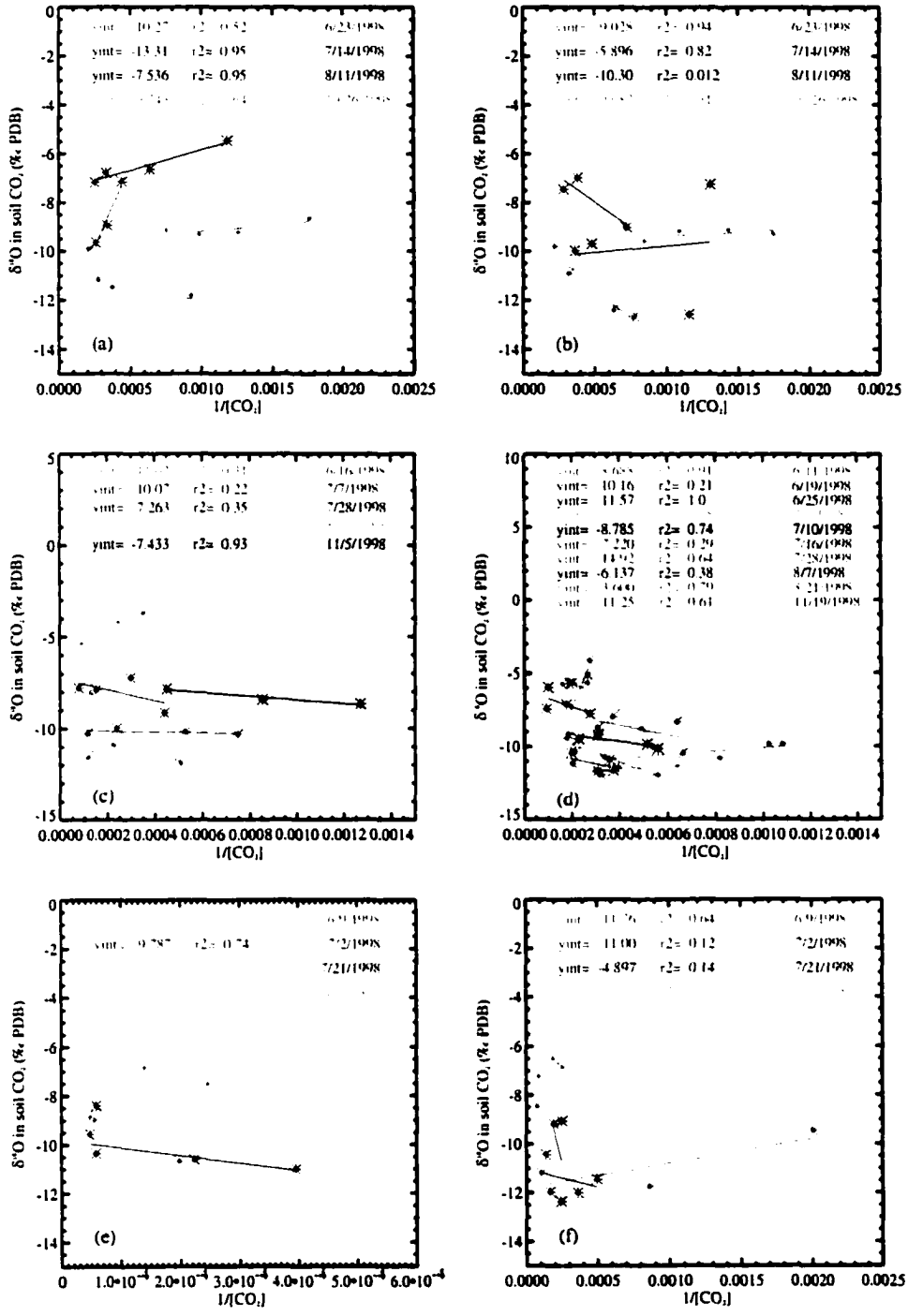

Figure 4.17. Soil CO_2 $\delta^{18}O$ values plotted against the inverse of soil CO_2 concentration. The y-intercept of this plot, minus 8.8‰ to account for diffusion, yields the isotopic composition of soil-respired CO_2. Each color represents a separate sampling date. Each asterix is a mean of the sample tubes for a particular depth on a given sampling date. (a) Shortgrass steppe site on fine soil, (b) shortgrass steppe site on coarse soil, (c) lodgepole pine site on fine soil, (d) lodgepole pine site on coarse soil, (e) alpine tundra site on fine soil, (f) alpine tundra site on coarse soil.

Reproduced with permission of the copyright owner. Further reproduction prohibited without permission.

Comparison of model output with other methods illustrates that temporal variability in the isotopic composition of the soil flux, which can be as large as 8‰ over the course of the growing season at a single location, could not be captured with the other available means. The approach taken in recent global calculations [*Ciais et al.*, 1997; *Farquhar et al.*, 1993] yielded estimates of the $\delta^{18}O$ of soil respired CO_2 that are 1 to 11‰ lighter than estimates based on the full equilibration-diffusion model. In part this is because they fail to take into account the fact that fractionation due to diffusion is expressed to a greater or lesser degree depending on soil physical conditions, such as moisture status and porosity. The inclusion of soil properties and condition is clearly an improvement over prior work, especially as differences across methods were greatest in grassland systems, which occupy a significant portion of the terrestrial biosphere.

Literature Cited

Allison, G.B., C. Colin-Kaczala, A. Filly, and J.C. Fontes, Measurement of isotopic equilibrium between water, water vapor, and soil CO_2 in arid zone soils, *Journal of Hydrology*, *95*, 131-141, 1987.

Amundson, R., and Y. Wang, The relationship between the oxygen isotopic composition of soil CO_2 and water, in *International Symposium on Isotopes in Water Resources Management*, pp. 315-332, International Atomic Energy Agency, Vienna, 1996.

Bottinga, Y., and H. Craig, Oxygen isotope fractionation between CO_2 and water, and the isotopic composition of marine atmospheric air, *Earth and Planetary Science Letters*, *5*, 285-295, 1969.

Brenninkmeijer, C.A.M., P. Kraft, and W.G. Mook, Oxygen isotope fractionation between CO_2 and H_2O, *Isotope Geoscience*, *1*, 181-190, 1983.

Ciais, P., A.S. Denning, P.P. Tans, J.A. Berry, D.A. Randall, G.J. Collatz, P.J. Sellers, J.W.C. White, M. Trolier, H.A.J. Meijer, R.J. Francey, M. Patrick, and M. Heimann, A three dimensional synthesis study of $\delta^{18}O$ in atmospheric CO_2 Part I: Surface fluxes, *Journal of Geophysical Research*, *102* (D5), 5857-5872, 1997.

Reproduced with permission of the copyright owner. Further reproduction prohibited without permission.

Ciais, P., P.P. Tans, M. Trolier, J.W.C. White, and R.J. Francey, A large northern hemisphere terrestrial CO_2 sink indicated by $^{13}C/^{12}C$ of atmospheric CO_2, *Science*, *269*, 1098-1102, 1995.

Coplen, T.B., C. Kendall, and J. Hopple, Comparison of stable isotope reference samples, *Nature*, *302* (5905), 236-238, 1983.

Davidson, E.A., and S.E. Trumbore, Gas diffusivity and production of CO_2 in deep soils of the eastern Amazon, *Tellus*, *47B*, 550-565, 1995.

Fang, C., J.B. Moncrieff, H.L. Gholz, and K.L. Clark, Soil CO_2 efflux and its spatial variation, *Plant & Soil*, *205* (2), 135-146, 1998.

Farquhar, G.D., J. Lloyd, J.A. Taylor, L.B. Flanagan, J.P. Syvertsen, K.T. Hubick, S.C. Wong, and J.R. Ehleringer, Vegetation effects on the isotope composition of oxygen in atmospheric CO_2, *Nature*, *363*, 439-442, 1993.

Flanagan, L.B., J.R. Brooks, G.T. Varney, and J.R. Ehleringer, Discrimination against $C^{18}O^{16}O$ during photosynthesis and the oxygen isotope ratio of respired CO_2 in boreal forest ecosystems, *Global Biogeochemical Cycles*, *11* (1), 83-98, 1997.

Flanagan, L.B., D.S. Kubien, and J.R. Ehleringer, Spatial and temporal variation in the carbon and oxygen stable isotope ratio of respired CO_2 in a boreal forest ecosystem, *Tellus*, *51B*, 367-384, 1999.

Francey, R.J., P.P. Tans, C.E. Allison, I.G. Enting, J.W.C. White, and M. Trolier, Changes in oceanic and terrestrial carbon uptake since 1982, *Nature*, *373* (26 Jan), 326-330, 1995.

Friedli, H., U. Siegenthaler, D. Rauber, and H. Oeschger, Measurements of concentration, $^{13}C/^{12}C$ and $^{18}O/^{16}O$ ratios of tropospheric carbon dioxide over Switzerland, *Tellus*, *39B*, 80-88, 1987.

Fung, I., C.B. Field, J.A. Berry, M.V. Thompson, J.T. Randerson, C.M. Malmstrom, P.M. Vitousek, G.J. Collatz, P.J. Sellers, D.A. Randall, A.S. Denning, F. Badeck, and J. John, Carbon 13 exchanges between the atmosphere and biosphere, *Global Biogeochemical Cycles*, *11* (4), 507-533, 1997.

Gee, G.W., and J.W. Bauder, Particle size analysis, in *Methods of Soil Analysis. Part I. Physical and Mineralogical Methods*, edited by A. Klute, pp. 383-411, Soil Science Society of America, Madison, WI, 1986.

Gemery, P.A., M. Trolier, and J.W.C. White, Oxygen isotope exchange between carbon dioxide and water following atmospheric sampling using glass flasks, *Journal of*

Reproduced with permission of the copyright owner. Further reproduction prohibited without permission.

Geophysical Research, 101 (D9), 14,415-14,420, 1996.

Gordon, A.M., R.E. Schlentner, and K. van Cleve, Seasonal patterns of soil respiration and CO_2 evolution following harvesting in the white spruce forests of interior Alaska, *Canadian Journal of Forest Research, 17*, 304-310, 1987.

Hesterberg, R., and U. Siegenthaler, Production and stable isotopic composition of CO_2 in a soil near Bern, Switzerland, *Tellus, 43B*, 197-205, 1991.

Hillel, D., *Fundamentals of Soil Physics*, 413 pp., Academic Press, San Diego, 1980.

Hillel, D., *Environmental Soil Physics*, 771 pp., Academic Press, San Diego, 1998.

Hsieh, J.C.C., O.A. Chadwick, E.F. Kelly, and S.M. Savin, Oxygen isotopic composition of soil water: quantifying evaporation and transpiration, *Geoderma, 82*, 269-293, 1998a.

Hsieh, J.C.C., S.M. Savin, E.F. Kelly, and O.A. Chadwick, Measurement of soil water $\delta^{18}O$ values by direct equilibration with CO_2, *Geoderma, 82*, 225-268, 1998b.

International Atomic Energy Agency (IAEA), Statistical treatment of environmental isotope data in precipitation, pp. 1-256, IAEA, Vienna, 1981.

Jackson, R.B., J. Canadell, J.R. Ehleringer, H.A. Mooney, O.E. Sala, and E.D. Schulze, A global analysis of root distributions for terrestrial biomes, *Oecologia, 108*, 389-411, 1996.

Jenny, H., *Factors of Soil Formation*, McGraw Hill, New York, 1941.

Jenny, H., *The Soil Resource*, Springer-Verlag, New York, 1980.

Keeling, C.D., The concentration and isotopic abundances of atmospheric carbon dioxide in rural and marine air, *Geochimica et Cosmochimica Acta, 24*, 277-298, 1961.

Keller, C.K., and D.H. Bacon, Soil respiration and georespiration distinguished by transport analyses of vadose CO_2, $^{13}CO_2$, and $^{14}CO_2$, *Global Biogeochemical Cycles, 12* (2), 361-372, 1998.

Miller, J.B., D. Yakir, J.W.C. White, and P.P. Tans, Measurement of $^{18}O/^{16}O$ in the soil atmosphere CO_2 flux, *Global Biogeochemical Cycles, 13* (3), 761-774, 1999.

Mills, G.A., and H.C. Urey, The kinetics of isotopic exchange between carbon dioxide, biocarbonate ion and water, *Journal of the American Chemical Society, 62*, 1019-1026, 1940.

Reproduced with permission of the copyright owner. Further reproduction prohibited without permission.

O'Neil, J.R., and L.H. Adami, The oxygen isotope partition function ratio of water and the structure of liquid water, *Journal of Physical Chemistry, 73*, 1553-1558, 1969.

Rawls, W.J., Estimating soil bulk density from particle size analysis and organic matter content, *Soil Science, 135* (2), 123-125, 1983.

Ryan, M.G., and R.H. Waring, Maintenance respiration and stand development in a subalpine lodgepole pine forest, *Ecology, 73* (6), 2100-2108, 1992.

Severson, K.J., D.L. Johnstone, C.K. Keller, and B.D. Wood, Hydrogeologic parameters affecting vadose-zone microbial distributions, *Geomicrobiology, 9* (4), 197-216, 1991.

Skirrow, G., The dissolved gases: carbon dioxide, in *Chemical Oceanography*, edited by J.P. Riley, and G. Skirrow, pp. 1-92, Academic Press, San Diego, 1975.

Sommerfeld, R.A., A.R. Mosier, and R.C. Musselman, CO_2, CH_4 and N_2O flux through a Wyoming snowpack and implications for global budgets, *Nature, 361*, 140-142, 1993.

Stern, L., W.T. Baisden, and R. Amundson, Processes controlling the oxygen isotope ratio of soil CO_2: Analytic and numerical modeling, *Geochimica et Cosmochimica Acta, 63* (6), 799-814, 1999.

Sternberg, L.d.S.L., M.Z. Moreira, L.A. Martinelli, R.L. Victoria, E.M. Barbosa, L.C.M. Bonates, and D. Nepstad, The relationship between $^{18}O/^{16}O$ and $^{13}C/^{12}C$ ratios of ambient CO_2 in two Amazonian tropical forests, *Tellus, 50B*, 366-376, 1998.

Sulzman, E.W., E.F. Kelly, D.S. Schimel, and W.A. Brand, The isotopic composition of oxygen in soil water, *Journal of Hydrology*, in prep.

Tans, P.P., Oxygen isotopic equilibrium between carbon dioxide and water in soils, *Tellus, 50B*, 163-178, 1998.

Yakir, D., J.A. Berry, L. Giles, and C.B. Osmond, Isotopic heterogeneity of water in transpiring leaves: identification of the component that controls the $\delta^{18}O$ of atmospheric O_2 and CO_2, *Plant, Cell and Environment, 17* (1), 73-80, 1994.

Yakir, D., and X.-F. Wang, Fluxes of CO_2 and water between terrestrial vegetation and the atmosphere estimated from isotope measurements, *Nature, 380*, 515-517, 1996.

Reproduced with permission of the copyright owner. Further reproduction prohibited without permission.

APPENDIX I

CLIMATE DATA, SOIL DESCRIPTIONS, AND VEGETATION CHARACTERISTICS FOR THE SIX FIELD SITES

Reproduced with permission of the copyright owner. Further reproduction prohibited without permission.

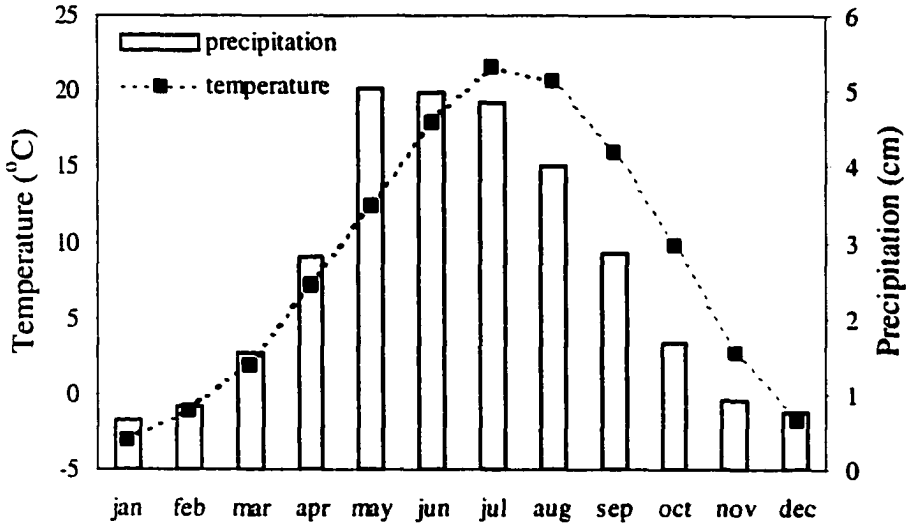

Figure I.1. Climate data for the shortgrass steppe sites, 1912-1990. Data from the Central Plains Experimental Range Long-Term Ecological Research site weather station, 40°48'N 104°44'W.

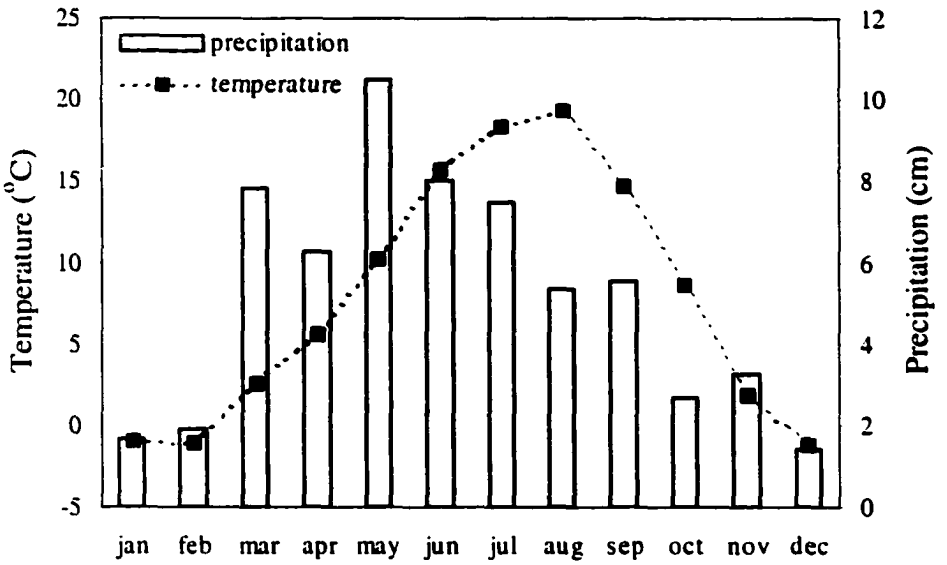

Figure I.2. Climate data for the lodgepole pine site on fine soil, 1988-1995. Data from Colorado weather station #51060, 40°37'N 105°17'W (http://ulysses.colostate.edu).

Reproduced with permission of the copyright owner. Further reproduction prohibited without permission.

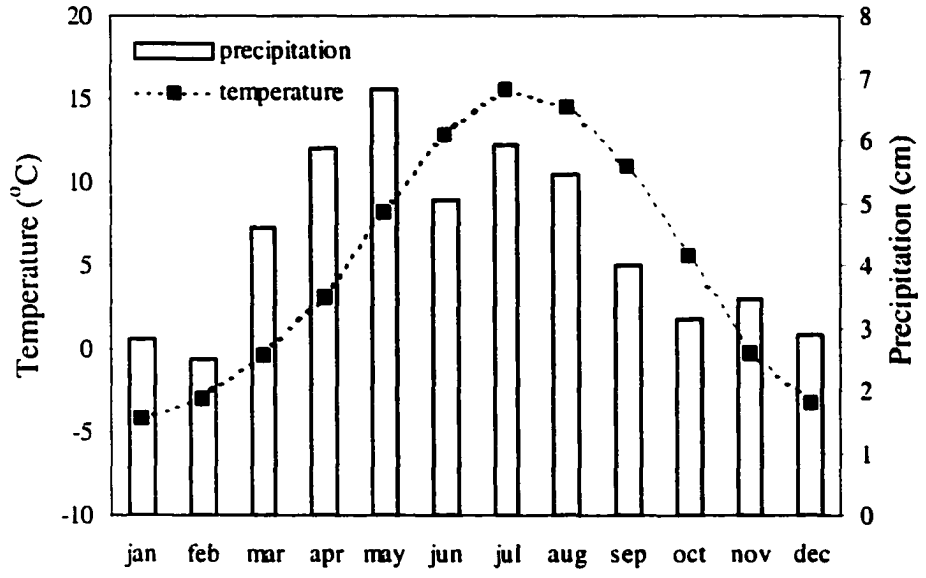

Figure I.3. Climate data for the lodgepole pine site on coarse soil, 1978-1993. Data from Colorado weather station #50183, 40°12'N 105°32'W (http://ulysses.colostate.edu).

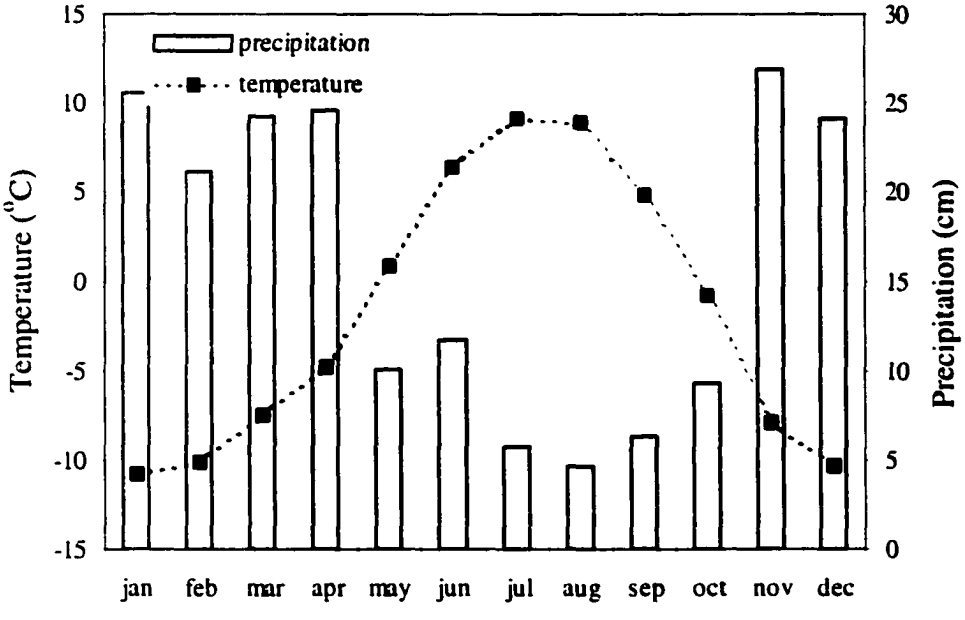

Figure I.4. Climate data for the alpine tundra sites, 1988-1997. Data from the Niwot Ridge Long-Term Ecological Research site "saddle" weather station located at 40° 03'N, 105° 36'W: http://culter.colorado.edu:1030/Niwot/Niwot_Ridge_LTER_climate.html.

Reproduced with permission of the copyright owner. Further reproduction prohibited without permission.

Table I.1. Soil data for the CPER-Catena field site. Soil classification: fine, montmorillonitic, mesic Ustic Haplargid.

Horizon	Depth (cm)	Moist color	Sand (%)	Silt (%)	Clay (%)	OC (%)	$\delta^{13}C$ value (‰)
A1	0-4	10YR 3/2	74.3	5.9	19.8	.914	-17.32
A2	4-10	10YR 4/2	49.2	15.7	35.1	.787	-13.58
Bt1	10-23	10YR 4/3	33.9	31.1	35.0	.600	-13.81
Bt2	23-47	10YR 4/2	49.4	17.5	33.1	.292	-13.33
BCk1	47-64	10YR 4/3	46.6	17.8	35.6	.257	-14.20
BCk2	64-100	10YR 5/2	27.5	31.3	41.2	.313	-12.85

Table I.2. Soil data for the CPER-Meteorological Station field site. Soil classification: fine-loamy, mixed, mesic Ustic Haplargid.

Horizon	Depth (cm)	Moist color	Sand (%)	Silt (%)	Clay (%)	OC (%)	$\delta^{13}C$ value (‰)
A	0-10	10YR 3/3	72.0	15.0	13.0	.539	-16.68
Bt1	10-26	10YR 4/2	70.0	11.0	19.0	.536	-14.36
Bt2	26-50	10YR 4/2	64.0	12.0	24.0	.342	-14.80
Bt3	50-66	10YR 4/2	66.0	12.0	22.0	.278	-15.87
BCk1	66-110	10YR 5/2	74.2	17.9	7.9	.588	Na
BCk2	110-130	10YR 5/2	74.3	11.9	13.8	.374	Na

Table I.3. Soil data for the Ballard Road field site. Soil classification: fine-loamy, paramicaceous, Typic Cryoboralf.

Horizon	Depth (cm)	Moist color	Sand (%)	Silt (%)	Clay (%)	OC (%)	$\delta^{13}C$ value (‰)
Oe	3-0						-24.82
E	0-10	10YR 4/3	65.2	24.0	10.8	.800	-24.03
E/B	10-23	10YR 4/4	62.4	24.8	12.8	.497	-23.77
Bt1	23-44	7.5YR 4/4	49.6	17.8	23.6	.363	-23.39
Bt2	44-61	7.5YR 3/4	57.2	18.6	24.2	.312	-22.96
BC1	61-80	7.5YR 4/6	59.2	18.6	22.2	.147	-23.92
BC2	80-102	10YR 3/6	52.4	28.8	18.8	.158	-26.01
Cr	102-115+		79.2	12.0	8.8	.047	

Table I.4. Soil data for the Allenspark field site. Soil classification: loamy-skeletal, mixed, Typic Cryorthent.

Horizon	Depth (cm)	Moist color	Sand (%)	Silt (%)	Clay (%)	OC (%)	$\delta^{13}C$ value (‰)
Oe	2-0						-25.19
A	0-7	7.5YR 4/3	61.6	23.4	15.0	1.17	-24.35
E	7-29	7.5YR 4/3	67.6	19.4	13.0	.34	-23.79
E/B	29-45	10YR 5/4	61.6	29.8	8.6	.339	-23.75
BC	45-52	10YR 5/4	76.4	14.8	8.8	.103	-21.81
R	52+						

Reproduced with permission of the copyright owner. Further reproduction prohibited without permission.

Table I.5. Soil data for the Iceberg Pass field site. Soil classification: loamy-skeletal, mixed, Typic Cryumbrept.

Horizon	Depth (cm)	Moist color	Sand (%)	Silt (%)	Clay (%)	OC (%)	$\delta^{13}C$ value (‰)
A1	0-14	10YR 2/2	73.6	11.4	15.0	6.57	-25.14
A2	14-30	10YR 3/3	63.6	17.8	18.6	1.83	-24.54
Bw1	30-62	10YR 4/4	63.2	28.6	8.2	.495	-23.43
Bw2	62-87	10YR 4/3	63.2	26.6	10.2	.226	-23.04
BC	87-110+	10YR 5/3	62.4	21.8	15.8	.019	-23.81

Table I.6. Soil data for the Tombstone Ridge field site. Soil classification: sandy-skeletal, mixed, Typic Cryumbrept.

Horizon	Depth (cm)	Moist color	Sand (%)	Silt (%)	Clay (%)	OC (%)	$\delta^{13}C$ value (‰)
A	0-19	7.5YR 3/2	83.6	7.4	9.0	3.61	-24.59
Bw1	19-47	7.5YR 4/4	70	20	10.0	.09	-23.89
Bw2	47-69	10YR 4/4	67.6	19.8	12.6	.314	-23.12
BC1	69-87	10YR 4/4	91.2	2	6.8	.027	-22.81
BC2	87-102+	10YR 5/3	67.2	20	12.8	.042	-22.93

Table I.7. Dominant vegetation species at the six field sites.

Site name	Dominant vegetation
CPER Shortgrass steppe, fine soil	(C_4) Blue grama (*Bouteloua gracilis*), buffalograss (*Buchloe dactyloides*), ring muhly (*Muhlenbergia torreyi*); (C_3) western wheatgrass (*Agropyron smithii*), green needlegrass (*Stipa viridula*); (succulents) prickly pear cactus (*Opuntia polyacantha*)
CPER Shortgrass steppe, coarse soil	(C_4) Blue grama (*Bouteloua gracilis*), buffalograss (*Buchloe dactyloides*); (C_3) western wheatgrass (*Agropyron smithii*); (forbs) white stemless evening primrose (*Oenothera caespitosa*); (shrubs) fourwing saltbush (*Atriplex canescens*); (succulents) prickly pear cactus (*Opuntia polyacantha*), yucca (*Yucca glauca*)
Ballard Road Lodgepole pine, fine soil	Rocky Mountain lodgepole pine (*Pinus contorta* var. *latifolia*), kinnikinick (*Arctostaphylos adenotricha*), Rocky Mountain juniper (*Juniperus scopulorum*)
Allenspark Lodgepole pine, coarse soil	Rocky Mountain lodgepole pine (*Pinus contorta* var. *latifolia*) (no understory)
Iceberg Pass* Alpine tundra, fine soil	Alpine avens (*Acomastylis rossii*), alpine primrose (*Primula angustifolia*), alpine bunchgrass (*Deschampsia caespitosa*), alpine clover (*Trifolium dasyphyllum*)
Tombstone Ridge* Alpine tundra-coarse soil	Alpine avens (*Acomastylis rossii*), alpine sedge (*Kobresia myosuroides*), Little clubmoss (*Selaginella densa*), Moss campion (*Silene acaulis*)

* Identified with the help of http://culter.colorado.edu:1030/Niwot/Niwot_Ridge_LTER_vegetation.html

Reproduced with permission of the copyright owner. Further reproduction prohibited without permission.

APPENDIX II

THE SOIL DIFFUSION-EQUILIBRATION MODEL DATA INPUT FOR EACH SITE AND SAMPLING DATE ANALYZED AND RESULTING $\delta^{13}C$ AND $\delta^{18}O$ VALUES FOR THE SOIL CO_2 FLUX TO THE ATMOSPHERE

Reproduced with permission of the copyright owner. Further reproduction prohibited without permission.

Reproduced with permission of the copyright owner. Further reproduction prohibited without permission.

Table II.1. Calculation of the isotopic signature of the CO_2 flux from the soil to the atmosphere, using the Tans soil diffusion model (Tellus, 1998) in forward implicit mode, initialized with field data for a lodgepole pine stand on coarse soil in June, 1998.

Site; sampling date	Depth-dependent model input					Depth-independent model input					
AP 625 Lodgepole pine, coarse soil,	Depth	Porosity	Water volume	Soil Temp	Del Soil Water	Atmospheric flask*			Flux rate*	Depth-avg δ^{13}C-SOM	Other model parameters
25 June, 1998	0	.440	.095	11.0	-10.0	[CO2] "Cabg"	δ^{13}C "del13bg"	δ^{18}O "del18bg"	2.4 umol/m2/sec	-23.77 (‰PDB)	alpha18= 0.9913
	5	.453	.120	9.9	-11.0	390	-8.37	-1.49			
	10	.427	.097	8.3	-12.7				.207 mol/m2/day		flush= 0.0472
Production function written to match concentration profile	30	.445	.075	6.7	-14.5						ht of atm= 20 cm
	50	.418	.076	7.0	-14.1						atm press= 748 mbar

END OF RUN SUMMARY:

Total production (mol m-2 day-1): 0.20659999
Total production (mol cm-2 s-1): 2.3912036e-010
Flux from soil (mol cm-2 s-1): 2.3911494e-010 Flux from box: 2.3911518e-010
CO2, O18 and C13 into box: 390.00000 -1.49000 -8.37000
CO2, O18 and C13 from box: 398.00070 -1.7356459 -8.6795627
Apparent 18O signature of flux from soil: -13.710004
Apparent 13C signature of flux from soil: -23.770311

18O signature of production (no invasion): -12.677549
FLANAGAN model estimate of del-p: -12.74 (using data for 10 cm)

Eeff= 13.710004 - 8.5404917 = 5.17‰

*estimated

Reproduced with permission of the copyright owner. Further reproduction prohibited without permission.

Table II.2. Calculation of the isotopic signature of the CO_2 flux from the soil to the atmosphere, using the Tans soil diffusion model (Tellus, 1998) in forward implicit mode, initialized with field data for a lodgepole pine stand on coarse soil in July, 1998.

Site; sampling date	Depth-dependent model input					Depth-independent model input					
AP 71 Lodgepole pine, coarse soil,	Depth	Porosity	Water volume	Soil Temp	Del Soil Water	Atmospheric flask*			Flux rate	Depth-avg δ^{13}C-SOM	Other model parameters
	0	.440	.060	20.4	0.0*	[CO2] "Cabg"	δ^{13}C "del13bg"	δ^{18}O "del18bg"	2.4 umol/m2/sec	-23.77 (‰PDB)	alpha18= 0.9913
1 July, 1998	5	.453	.086	14.0	-2.44	390	-8.37	-1.49			
	10	.427	.077	12.6	-10.8				.207 mol/m2/day		flush= 0.0442
Production function written to match concentration profile	30	.445	.056	10.0	-13.9						
	50	.418	.076	8.2	-14.7						ht of atm= 20 cm
											atm press= 748 mbar

END OF RUN SUMMARY:

Total production (mol m-2 day-1): 0.20659999
Total production (mol cm-2 s-1): 2.3912036e-010
Flux from soil (mol cm-2 s-1): 2.3911738e-010 Flux from box: 2.3911705e-010
CO2, O18 and C13 into box: 390.00000 -1.49000 -8.37000
CO2, O18 and C13 from box: 398.82644 -1.6409891 -8.7108014
Apparent 18O signature of flux from soil: -8.3126392
Apparent 13C signature of flux from soil: -23.770027

18O signature of production (no invasion): -7.9542873

FLANAGAN model estimate of del-p: -10.82

Eeff= 8.3126392 - 3.6311750 = 4.68‰

*estimated

Reproduced with permission of the copyright owner. Further reproduction prohibited without permission.

Table II.3. Calculation of the isotopic signature of the CO_2 flux from the soil to the atmosphere, using the Tans soil diffusion model (Tellus, 1998) in forward implicit mode, initialized with field data for a lodgepole pine stand on coarse soil in July, 1998.

Site; sampling date	Depth-dependent model input					Depth-independent model input					
AP 728 Lodgepole pine, coarse soil	Depth	Porosity	Water volume	Soil Temp	Del Soil Water	Atmospheric flask			Flux rate	Depth-avg δ^{13}C-SOM	Other model parameters
	0	.440	.180	14.0	-8.0	[CO2] "Cabg"	δ^{13}C "del13bg"	δ^{18}O "del18bg"	6.4 umol/m2/sec	-23.77 (‰PDB)	alpha18= 0.9913
July 28, 1998	5	.453	.180	14.2	-5.62	366	-8.27	-2.05			
	10	.427	.175	13.2	-5.29				0.553 mol/m2/day		flush= 0.0455
Production function written to match concentration profile	30	.445	.156	11.4	-6.89						ht of atmos= 20 cm
	50	.418	.149	10.7	-9.03						atm press= 748 mbar*

END OF RUN SUMMARY:

Total production (mol m-2 day-1): 0.55449999
Total production (mol cm-2 s-1): 6.4178240e-010
Flux from soil (mol cm-2 s-1): 6.4039055e-010 Flux from box: 6.4038878e-010
CO2, O18 and C13 into box: 365.99999 -2.05000 -8.27000
CO2, O18 and C13 from box: 388.46239 -2.4633867 -9.1689154
Apparent 18O signature of flux from soil: -9.1993544
Apparent 13C signature of flux from soil: -23.815292

18O signature of production (no invasion): -9.0862368

FLANAGAN model estimate of del-p: -5.31‰

Eeff= 9.1993544 - 3.6021315 = 5.60‰

"soildif_ap728" *NOTE: light rain while sampling

Reproduced with permission of the copyright owner. Further reproduction prohibited without permission.

Table II.4. Calculation of the isotopic signature of the CO_2 flux from the soil to the atmosphere, using the Tans soil diffusion model (Tellus, 1998) in forward implicit mode, initialized with field data for the lodgepole pine, coarse soil site, in August, 1998.

Site; sampling date	Depth-dependent model input					Depth-independent model input					
AP 87 Lodgepole pine, coarse soil	Depth	Porosity	Water volume	Soil Temp	Del Soil Water	Atmospheric flask			Flux rate	Depth-avg δ^{13}C-SOM	Other model parameters
	0	.440	.12	17.5	-6.0	[CO2] "Cabg"	δ^{13}C "del13bg"	δ^{18}O "del18bg"	3.5 umol/m2/sec	-23.8 (‰PDB)	alpha18= 0.9913
August 7, 1998	5	.453	.139	14.2	-8.06	436	-8.56	-0.5			
	10	.427	.152	13.2	-9.16				.302 mol/m2/day		flush= 0.0389
Production function written to match concentration profile	30	.445	.121	11.4	-9.53						
	50	.418	.123	10.7	-9.53						ht of atmos= 20 cm
											atm press= 748 mbar

END OF RUN SUMMARY:

Total production (mol m-2 day-1): 0.30224999
Total production (mol cm-2 s-1): 3.4982638e-010
Flux from soil (mol cm-2 s-1): 3.4927936e-010 Flux from box: 3.4927890e-010
CO2, O18 and C13 into box: 436.00000 -0.500000 -8.56000
CO2, O18 and C13 from box: 450.50468 -0.89676419 -9.0509542
Apparent 18O signature of flux from soil: -12.822521
Apparent 13C signature of flux from soil: -23.808590

18O signature of production (no invasion): -12.063014

FLANAGAN model estimate of del-p: -9.18

Eeff= 12.822521 - 6.0561221 = 6.77‰

"soildif_ap87.pro"

Reproduced with permission of the copyright owner. Further reproduction prohibited without permission.

Table II.5. Calculation of the isotopic signature of the CO_2 flux from the soil to the atmosphere, using the Tans soil diffusion model (Tellus, 1998) in forward implicit mode, initialized with field data for a lodgepole pine stand on coarse soil in August, 1998.

Site; sampling date	*Depth-dependent model input*					*Depth-independent model input*					
AP 821 Lodgepole pine, coarse soil,	Depth	Porosity	Water volume	Soil Temp	Del Soil Water	Atmospheric flask*			Flux rate*	Depth-avg δ^{13}C-SOM	Other model parameters
	0	.440	.100	17.7	-2.0*	[CO2] "Cabg"	δ^{13}C "del13bg"	δ^{18}O "del18bg"	6.5 umol/m2/sec	-23.77 (‰PDB)	alpha18= 0.9913
21 August, 1998	5	.453	.142	14.2	-3.35	379	-8.33	-1.71			
	10	.427	.146	13.2	-6.53				.562 mol/m2/day		flush= 0.0465
Production function written to match concentration profile	30	.445	.096	11.4	-8.91						
	50	.418	.083	10.7	-9.39						ht of atm= 20 cm
											atm press= 748 mbar

END OF RUN SUMMARY:

Total production (mol m-2 day-1): 0.56174999
Total production (mol cm-2 s-1): 6.5017360e-010
Flux from soil (mol cm-2 s-1): 6.5022697e-010 Flux from box: 6.5022724e-010
CO2, O18 and C13 into box: 379.00000 -1.71000 -8.33000
CO2, O18 and C13 from box: 401.60458 -2.0409995 -9.1990381
Apparent 18O signature of flux from soil: -7.5907503
Apparent 13C signature of flux from soil: -23.769997

18O signature of production (no invasion): -7.5848732

FLANAGAN model estimate of del-p: -6.55‰

Eeff= 7.5907503 - 2.4954985 = 5.10‰

*estimated

Reproduced with permission of the copyright owner. Further reproduction prohibited without permission.

Table II.6. Calculation of the isotopic signature of the CO_2 flux from the soil to the atmosphere, using the Tans soil diffusion model (Tellus, 1998) in forward implicit mode, initialized with field data: lodgepole pine stand on coarse soil in November, 1998.

Site; sampling date	Depth-dependent model input					Depth-independent model input					
AP 1119 Lodgepole pine, coarse soil,	Depth	Porosity	Water volume	Soil Temp	Del Soil Water	Atmospheric flask			Flux rate	Depth-avg δ^{13}C-SOM	Other model parameters
	0	.440	.110	-0.1	-13.0	[CO2] "Cabg"	δ^{13}C "del13bg"	δ^{18}O "del18bg"	0.62 umol/m2/sec	-23.77 (‰PDB)	alpha18= 0.9913
19 November, 1998	5	.453	.110	1.5	-12.0	379	-8.33	-1.71			
	10	.427	.084	1.6	-6.75				0.054 mol/m2/day		flush= 0.0454
	30	.445	.068	1.7	-10.6						
Production function written to match concentration profile	50	.418	.066	1.8	-11.0						ht of atm= 20 cm
											atm press= 748 mbar

END OF RUN SUMMARY:

Total production (mol m-2 day-1): 0.086549998
Total production (mol cm-2 s-1): 1.0017361e-010
Flux from soil (mol cm-2 s-1): 1.0017227e-010 Flux from box: 1.0017217e-010
CO2, O18 and C13 into box: 379.00000 -1.71000 -8.33000
CO2, O18 and C13 from box: 382.34849 -1.7811007 -8.4652062
Apparent 18O signature of flux from soil: -9.8289290
Apparent 13C signature of flux from soil: -23.769990

18O signature of production (no invasion): -9.0126012

FLANAGAN model estimate of del-p: -6.46 ‰

Eeff= 9.8289290-4.6704411= 5.16 ‰

Reproduced with permission of the copyright owner. Further reproduction prohibited without permission.

Table II.7. Calculation of the isotopic signature of the CO_2 flux from the soil to the atmosphere, using the Tans soil diffusion model (Tellus, 1998) in forward implicit mode, initialized with field data for a lodgepole pine stand on fine soil in June, 1998.

Site; sampling date	Depth-dependent model input					Depth-independent model input					
BR 616 Lodgepole pine, fine soil,	Depth	Porosity	Water volume	Soil Temp	Del Soil Water	Atmospheric flask			Flux rate	Depth-avg δ^{13}C-SOM	Other model parameters
16 June, 1998	0	0.460	.230	9.2	-12.0*	[CO2] "Cabg"	δ^{13}C "del13bg"	δ^{18}O "del18bg"	2.4 umol/m2/sec	-24.53 (‰PDB)	alpha18= 0.9913
	5	0.452	.230	6.2	-12.3	371	-8.28	-1.14			
	10	0.442	.197	6.1	-15.7				.207 mol/m2/day		flush= 0.0487
Production function written to match concentration profile	30	0.463	.181	5.6	-12.6						ht of atm= 20 cm
	50	0.480	.183	5.7	-13.4						atm press= 720 mbar

END OF RUN SUMMARY:

Total production (mol m-2 day-1): 0.20654999
Total production (mol cm-2 s-1): 2.3906249e-010
Flux from soil (mol cm-2 s-1): 2.3908551e-010 Flux from box: 2.3908559e-010
CO2, O18 and C13 into box: 371.00000 -1.14000 -8.28000
CO2, O18 and C13 from box: 379.00380 -1.4723678 -8.6231486
Apparent 18O signature of flux from soil: -16.878679‰
Apparent 13C signature of flux from soil: -24.530071‰

18O signature of production (no invasion): -15.674765‰

FLANAGAN model estimate of del-p: -15.75‰

Eeff= 16.878679 - 9.4464534 = 7.43‰

*estimated

Reproduced with permission of the copyright owner. Further reproduction prohibited without permission.

Table II.8. Calculation of the isotopic signature of the CO_2 flux from the soil to the atmosphere, using the Tans soil diffusion model in forward implicit mode, initialized with field data: lodgepole pine stand, fine soil, July, 1998.

Site; sampling date	Depth-dependent model input					Depth-independent model input					
BR 77 Lodgepole pine, fine soil, 7 July, 1998	Depth	Porosity	Water volume	Soil Temp	Del Soil Water	Atmospheric flask*			Flux rate	Depth-avg δ^{13}C-SOM	Other model parameters
						[CO2] "Cabg"	δ^{13}C "del13bg"	δ^{18}O "del18bg"			
	0	0.460	.070	20.2	-7.0	393	-9.06	-3.25	5.9 umol/m2/sec	-24.53 (‰PDB)	alpha18= 0.9913
	5	0.452	.082	16.4	-7.68				0.510 mol/m2/day		flush= 0.0506
	10	0.442	.078	12.9	-11.1						
Production function written to match concentration profile	30	0.463	.134	9.6	-14.1						ht of atm= 20 cm
	50	0.480	.174	9.1	-14.1						atm press= 720 mbar

END OF RUN SUMMARY:

C:/Libbit/PhDdata/output/tans_model/soildif_br77.pro
Total production (mol m-2 day-1): 0.51074995
Total production (mol cm-2 s-1): 5.9114578e-010
Flux from soil (mol cm-2 s-1): 5.9132982e-010 Flux from box: 5.9133011e-010
CO2, O18 and C13 into box: 371.00000 -1.14000 -8.28000
CO2, O18 and C13 from box: 390.79474 -1.6578843 -9.1030828
Apparent 18O signature of flux from soil: -11.364292‰
Apparent 13C signature of flux from soil: -24.529991‰

18O signature of production (no invasion): -10.962241‰

FLANAGAN model estimate of del-p: -11.12‰

Eeff= 11.364292 - 7.1045570 = 4.26‰

*estimated

Reproduced with permission of the copyright owner. Further reproduction prohibited without permission.

Table II.9. Calculation of the isotopic signature of the CO_2 flux from the soil to the atmosphere, using the Tans soil diffusion model (Tellus, 1998) in forward implicit mode, initialized with field data for a lodgepole pine stand on fine soil in late July, 1998.

Site; sampling date	Depth-dependent model input					Depth-independent model input					
BR 728 Lodgepole pine, fine soil,	Depth	Porosity	Water volume	Soil Temp	Del Soil Water	Atmospheric flask			Flux rate	Depth-avg δ^{13}C-SOM	Other model parameters
28 July, 1998	0	0.460	0.15	16.0	-4.0	[CO2] "Cabg"	δ^{13}C "del13bg"	δ^{18}O "del18bg"	5.2 umol/m2/sec	-24.53 (‰PDB)	alpha18= 0.9913
	5	0.452	0.119	12.1	-4.69	371	-8.28	-1.14			
	10	0.442	0.108	11.4	-6.4				.449 mol/m2/day		flush= 0.0472
Production function written to match concentration profile	30	0.463	0.082	11.3	-12.5						
	50	0.480	0.077	10.9	-13.2						ht of atm= 20 cm
											atm press= 720 mbar

END OF RUN SUMMARY:

Total production (mol m-2 day-1): 0.44949999
Total production (mol cm-2 s-1): 5.2025462e-010
Flux from soil (mol cm-2 s-1): 5.2017371e-010 Flux from box: 5.2017395e-010
CO2, O18 and C13 into box: 371.00000 -1.14000 -8.28000
CO2, O18 and C13 from box: 389.39983 -1.5523330 -9.0464032
Apparent 18O signature of flux from soil: -9.8663330
Apparent 13C signature of flux from soil: -24.499991

18O signature of production (no invasion): -9.7208722

FLANAGAN model estimate of del-p: -6.42

Eeff= 9.8663330 - 4.0973922 = 5.77‰

Reproduced with permission of the copyright owner. Further reproduction prohibited without permission.

Table II.10. Calculation of the isotopic signature of the CO_2 flux from the soil to the atmosphere, using the Tans soil diffusion model (Tellus, 1998) in forward implicit mode, initialized with field data: lodgepole pine stand on fine soil in late August, 1998.

Site; sampling date	Depth-dependent model input					Depth-independent model input					
BR 821 Lodgepole pine, fine soil,	Depth	Porosity	Water volume	Soil Temp	Del Soil Water	Atmospheric flask*			Flux rate*	Depth-avg δ^{13}C-SOM	Other model parameters
	0	0.460	.220	17.2	-4.0	[CO2] "Cabg"	δ^{13}C "del13bg"	δ^{18}O "del18bg"	5.2 umol/m2/sec	-24.53 (‰PDB)	alpha18= 0.9913
21 August, 1998	5	0.452	.206	13.3	-3.11	393	-9.06	-3.25			
	10	0.442	.229	12.1	-5.92				.449 mol/m2/day		flush= 0.0472
Production function written to match concentration profile	30	0.463	.159	11.4	-12.4						ht of atm= 20 cm
	50	0.480	.167	11.3	-10.8						atm press= 720 mbar

END OF RUN SUMMARY

Total production (mol m-2 day-1): 0.40950000
Total production (mol cm-2 s-1): 4.7395833e-010
Flux from soil (mol cm-2 s-1): 4.7393185e-010 Flux from box: 4.7393208e-010
CO2, O18 and C13 into box: 371.00000 -1.14000 -8.28000
CO2, O18 and C13 from box: 387.83372 -1.4633003 -8.9840001
Apparent 18O signature of flux from soil: -8.5885864‰
Apparent 13C signature of flux from soil: -24.499994‰

18O signature of production (no invasion): -8.5188152‰

FLANAGAN model estimate of del-p: -5.94

Eeff= 8.5885864 - 2.4976866 = 6.09‰

*estimated

Reproduced with permission of the copyright owner. Further reproduction prohibited without permission.

Table II.11. Calculation of the isotopic signature of the CO_2 flux from the soil to the atmosphere, using the Tans soil diffusion model (Tellus, 1998) in forward implicit mode, initialized with field data: lodgepole pine stand, fine-textured soil, November, 1998.

Site; sampling date	Depth-dependent model input					Depth-independent model input					
BR 115 Lodgepole pine, fine soil	Depth	Porosity	Water volume	Soil Temp	Del Soil Water	Atmospheric flask			Flux rate	Depth-avg δ^{13}C-SOM	Other model parameters
5 November, 1998	0	0.460	.21	1.2	-8.0	[CO2] "Cabg"	δ^{13}C "del13bg"	δ^{18}O "del18bg"	1.8 umol/m2/sec	-24.53 (‰PDB)	alpha18= 0.9913
	5	0.452	.189	2.1	-7.43	393	-9.06	-3.26			
	10	0.442	.102	2.6	-6.77				0.156 mol/m2/day		flush= 0.0478
Production function written to match concentration profile	30	0.463	.105	4.1	-10.10						
	50	0.480	.101	2.7	-9.36						ht of atmos= 20 cm
											atm press= 720 mbar*

END OF RUN SUMMARY:

Total production (mol m-2 day-1): 0.15454999
Total production (mol cm-2 s-1): 1.7887731e-010
Flux from soil (mol cm-2 s-1): 1.7885159e-010 Flux from box: 1.7885197e-010
CO2, O18 and C13 into box: 392.99999 -3.26000 -9.06000
CO2, O18 and C13 from box: 398.92727 -3.3551425 -9.2894322
Apparent 18O signature of flux from soil: -9.6623646‰
Apparent 13C signature of flux from soil: -24.499993‰

18O signature of production (no invasion): -9.6999140‰

FLANAGAN model estimate of del-p: -6.80‰

Calculated effective kinetic fractionation= 9.6623646 - 3.5658609 = 6.10‰

"soildif_br115.pro"; *NOTE: ca. 5 cm new, wet snow

Reproduced with permission of the copyright owner. Further reproduction prohibited without permission.

Table II.12. Calculation of the isotopic signature of the CO_2 flux from the soil to the atmosphere, using the Tans soil diffusion model in forward implicit mode, initialized with field data for a shortgrass steppe site on fine soil in July, 1998.

Site; sampling date	Depth-dependent model input					Depth-independent model input					
CC 714 Shortgrass steppe, fine soil,	Depth	Porosity	Water volume	Soil Temp	Del Soil Water	Atmospheric flask*			Flux rate	Depth-avg δ^{13}C-SOM	Other model parameters
14 July, 1998	0	.430	.100	33.8	1.00*	[CO2] "Cabg"	δ^{13}C "del13bg"	δ^{18}O "del18bg"	5.1 umol/m2/sec	-15.00 (‰PDB)	alpha18= 0.9913
	5	.431	.158	29.3	-0.89	367	-8.05	-0.33			
	10	.449	.175	22.9	-3.06				.441 mol/m2/day		flush= 0.0475
Production function written to match concentration profile	30	.42	.230	22.3	-6.11						ht of atm= 20 cm
	50	.420	.220	21.9	-7.01				modeled production .344 mol/m2/day		atm press= 848 mbar

END OF RUN SUMMARY:

Total production (mol m-2 day-1): 0.34424999
Total production (mol cm-2 s-1): 3.9843749e-010
Flux from soil (mol cm-2 s-1): 3.9862057e-010 Flux from box: 3.9862041e-010
CO2, O18 and C13 into box: 367.00000 -0.330000 -8.05000
CO2, O18 and C13 from box: 379.59886 -0.57882385 -8.2806935
Apparent 18O signature of flux from soil: -7.8278016‰
Apparent 13C signature of flux from soil: -14.999990‰

18O signature of production (no invasion): -7.6055822‰

FLANAGAN model estimate of del-p: -3.07‰

Eeff= 7.8278016 - 1.7548197= 6.07‰

*estimated

Reproduced with permission of the copyright owner. Further reproduction prohibited without permission.

Table II.13. Calculation of the isotopic signature of the CO_2 flux from the soil to the atmosphere, using the Tans soil diffusion model in forward implicit mode, initialized with field data for a shortgrass steppe site on fine soil in August, 1998.

Site; sampling date	Depth-dependent model input					Depth-independent model input					
CC 811 Shortgrass steppe, fine soil,	Depth	Porosity	Water volume	Soil Temp	Del Soil Water	Atmospheric flask			Flux rate	Depth-avg δ13C-SOM	Other model parameters
	0	.430	.05	30.0	-0.03	[CO2], "C_{abg}"	d13C, "del13bg"	d18O, "del18bg"			
11 August, 1998	5	.431	.057	29.3	-1.03	367	-8.28	-0.33	2.6 umol/m2/sec	-15.00 (‰ PDB)	alpha18= 0.9913
	10	.449	.174	22.9	-5.26						flush= 0.0385
Production function written to match concentration profile	30	.42	.221	22.3	-6.07				=		
	50	.420	.210	21.9	-5.88				0.22 mol/m2/day		ht of atmos= 20 cm
											atm press= 848 mbar

END OF RUN SUMMARY:

Total production (mol m-2 day-1): 0.21972500
Total production (mol cm-2 s-1): 2.5431134e-010
Flux from soil (mol cm-2 s-1): 2.5432149e-010 Flux from box: 2.5432144e-010
CO2, O18 and C13 into box: 367.00000 -0.330000 -8.05000
CO2, O18 and C13 from box: 376.79439 -0.57320375 -8.2306819
Apparent 18O signature of flux from soil: -9.6872236‰
Apparent 13C signature of flux from soil: -14.999991‰

18O signature of production (no invasion): -9.1360109‰

FLANAGAN model estimate of del-p: -5.27‰

Eeff= 9.6872236 - 3.1398132 = 6.55‰

Reproduced with permission of the copyright owner. Further reproduction prohibited without permission.

Table II.14. Calculation of the isotopic signature of the CO_2 flux from the soil to the atmosphere, using the Tans soil diffusion model in forward implicit mode, initialized with field data: shortgrass steppe on fine soil site, October, 1998.

Site; sampling date	Depth-dependent model input					Depth-independent model input					
CC 1026 Shortgrass Steppe, fine soil,	Depth	Porosity	Water volume	Soil Temp	Del Soil Water	Atmospheric flask*			Flux rate*	Depth-avg δ^{13}C-SOM	Other model parameters
	0	.430	.08	15.0	-0.03*	[CO2] "Cabg"	δ^{13}C "del13bg"	δ^{18}O "del18bg"	1.4 umol/m2/sec	-15.0 (‰PDB)	alpha18= 0.9913
26 October, 1998	5	.431	.095	11.2	-5.34	374	-8.56	0.12			
	10	.449	.156	10.0	-4.12				.121 mol/m2/day		flush= 0.0402
Production function written to match concentration profile	30	.422	.210	10.3	-5.32						ht of atmos= 20 cm
	50	.420	.203	11.2	-6.63						atm press= 848 mbar**

END OF RUN SUMMARY:

Total production (mol m-2 day-1): 0.12080000
Total production (mol cm-2 s-1): 1.3981481e-010
Flux from soil (mol cm-2 s-1): 1.3984474e-010 Flux from box: 1.3984522e-010
CO2, O18 and C13 into box: 374.00000 0.120000 -8.56000
CO2, O18 and C13 from box: 378.91429 0.063862089 -8.6435244
Apparent 18O signature of flux from soil: -4.2118332‰
Apparent 13C signature of flux from soil: -14.999991‰

18O signature of production (no invasion): -3.9116828‰

FLANAGAN model estimate of del-p: -4.14

Eeff= 4.2118332 - 0.71624618 = 3.50‰

"soildif_cc1026.pro", *estimated ** NOTE: estimated background and flux

Reproduced with permission of the copyright owner. Further reproduction prohibited without permission.

Table II.15. Calculation of the isotopic signature of the CO_2 flux from the soil to the atmosphere, using the Tans soil diffusion model in forward implicit mode, initialized with field data for a shortgrass steppe site on coarse soil in July, 1998.

Site; sampling date	Depth-dependent model input					Depth-independent model input					
CM 714 Shortgrass steppe, coarse soil,	Depth	Porosity	Water volume	Soil Temp	Del Soil Water	Atmospheric flask*			Flux rate	Depth-avg δ^{13}C-SOM	Other model parameters
	0	.416	.050	29.3	3.0*	[CO2] "Cabg"	δ^{13}C "del13bg"	δ^{18}O "del18bg"	2.4 umol/m2/sec	-16.43 (‰PDB)	alpha18= 0.9913
14 July, 1998	5	.412	.067	23.6	1.48	376	-8.73	0.27			
	10	.407	.105	22.5	-4.21				.207 mol/m2/day		flush= 0.0482
Production function written to match concentration profile	30	.402	.089	23.1	-5.92						ht of atm= 20 cm
	50	.395	.147	22.2	-6.35						atm press= 848 mbar

END OF RUN SUMMARY:

Total production (mol m-2 day-1): 0.20900000
Total production (mol cm-2 s-1): 2.4189814e-010
Flux from soil (mol cm-2 s-1): 2.4190463e-010 Flux from box: 2.4190446e-010
CO2, O18 and C13 into box: 376.00001 0.270000 -8.73000
CO2, O18 and C13 from box: 383.44169 0.12444553 -8.8794329
Apparent 18O signature of flux from soil: -7.2303213‰
Apparent 13C signature of flux from soil: -16.429991‰

18O signature of production (no invasion): -7.1445698‰

FLANAGAN model estimate of del-p: -4.22‰

Eeff= 7.2303213 - 1.3128911 = 5.92‰

*estimated

Reproduced with permission of the copyright owner. Further reproduction prohibited without permission.

Table II.16. Calculation of the isotopic signature of the CO_2 flux from the soil to the atmosphere, using the Tans soil diffusion model in forward implicit mode, initialized with field data: shortgrass steppe site, coarse soil, October, 1998.

Site; sampling date	Depth-dependent model input					Depth-independent model input					
CM 1026 Shortgrass steppe, coarse soil,	Depth	Porosity	Water volume	Soil Temp	Del Soil Water*	Atmospheric flask*			Flux rate*	Depth-avg δ^{13}C-SOM	Other model parameters
26 October, 1998	0	.416	.060	16.0	-4.0	[CO2] "Cabg"	δ^{13}C "del13bg"	δ^{18}O "del18bg"	1.6 umol/m2/sec	-16.43 (‰PDB)	alpha18= 0.9913
	5	.412	.073	14.0	-6.39	376	-8.73	0.27			
	10	.407	.063	11.9	-1.82				0.138 mol/m2/day		flush= 0.0438
Production function written to match concentration profile	30	.402	.082	10.2	-4.70						ht of atm= 20 cm
	50	.395	.101	11.3	-6.69						atm press= 848 mbar

END OF RUN SUMMARY:

Total production (mol m-2 day-1): 0.13825000
Total production (mol cm-2 s-1): 1.6001158e-010
Flux from soil (mol cm-2 s-1): 1.6004880e-010 Flux from box: 1.6004903e-010
CO2, O18 and C13 into box: 376.00001 0.270000 -8.73000
CO2, O18 and C13 from box: 381.17993 0.18916282 -8.8346307
Apparent 18O signature of flux from soil: -5.6793130
Apparent 13C signature of flux from soil: -16.429991

18O signature of production (no invasion): -5.2099358‰

FLANAGAN model estimate of del-p: -1.83‰

Eeff= 5.6793130 - 2.2820912 = 3.40‰

*estimated

Reproduced with permission of the copyright owner. Further reproduction prohibited without permission.

Table II.17. Calculation of the isotopic signature of the CO_2 flux from the soil to the atmosphere, using the Tans soil diffusion model in forward implicit mode, initialized with field data: alpine tundra site on coarse soil in early June, 1998.

Site; sampling date	Depth-dependent model input					Depth-independent model input					
TO 69 Alpine tundra, coarse soil,	Depth	Porosity	Water volume	Soil Temp	Del Soil Water	Atmospheric flask			Flux rate*	Depth-avg $\delta^{13}C$-SOM	Other model parameters
9 June, 1998	0	.510	.343	3.9	-14.0*	[CO2] "Cabg"	$\delta^{13}C$ "del13bg"	$\delta^{18}O$ "del18bg"	2.5 umol/m2/sec	-24.28 (‰PDB)	alpha18= 0.9913
	5	.506	.343	2.1	-14.0	387	-12.28	-0.50			
	10	.506	.279	1.8	-14.2				.216 mol/m2/day		flush= 0.0424
Production function written to match concentration profile	30	.445	.221	0	-14.1						ht of atm= 20 cm
	50	.408	.221	0	-14.1						atm press= 665mbar

END OF RUN SUMMARY:

Total production (mol m-2 day-1): 0.21625000
Total production (mol cm-2 s-1): 2.5028935e-010
Flux from soil (mol cm-2 s-1): 2.5030280e-010 Flux from box: 2.5030304e-010
CO2, O18 and C13 into box: 387.00001 -0.500000 -12.2800
CO2, O18 and C13 from box: 397.22477 -0.91777030 -12.588873
Apparent 18O signature of flux from soil: -16.729205‰
Apparent 13C signature of flux from soil: -24.279987‰
CO2, O18 and C13 into box: 387.00001 -0.500000 -8.00000
CO2, O18 and C13 from box: 397.22477 -0.91777021 -8.4190707
Apparent 18O signature of flux from soil: -16.729205‰
Apparent 13C signature of flux from soil: -24.279997‰
18O signature of production (no invasion): -15.680583‰
FLANAGAN model estimate of del-p: -14.26‰

Eeff= 16.729205 - 9.2614821 = 7.47‰

*estimated

Reproduced with permission of the copyright owner. Further reproduction prohibited without permission.

Table II.18. Calculation of the isotopic signature of the CO_2 flux from the soil to the atmosphere, using the Tans soil diffusion model in forward implicit mode, initialized with field data for a alpine tundra site on coarse soil in late July, 1998.

Site; sampling date	*Depth-dependent model input*					*Depth-independent model input*					
TO 721 Alpine tundra, coarse soil,	Depth	Porosity	Water volume	Soil Temp	Del Soil Water	Atmospheric flask			Flux rate	Depth-avg δ^{13}C-SOM	Other model parameters
	0	.510	.100	19.6	-9.0	[CO2] "Cabg"	δ^{13}C "del13bg"	δ^{18}O "del18bg"	4.2 umol/m2/sec	-24.28 (‰PDB)	alpha18= 0.9913
21 July, 1998	5	.506	.103	19.1	-9.4	387	-12.28	-0.50			
	10	.506	.123	13.2	-10.7				.363 mol/m2/day		flush= 0.0446
Production function written to match concentration profile	30	.445	.105	9.3	-10.7						
	50	.408	.132	8.2	-11.8						ht of atm= 20 cm
											atm press= 665mbar

END OF RUN SUMMARY:

Total production (mol m-2 day-1): 0.36349999
Total production (mol cm-2 s-1): 4.2071758e-010
Flux from soil (mol cm-2 s-1): 4.2074233e-010 Flux from box: 4.2074239e-010
CO2, O18 and C13 into box: 387.00001 -0.500000 -12.2800
CO2, O18 and C13 from box: 404.26527 -1.0432638 -12.792481
Apparent 18O signature of flux from soil: -13.219969‰
Apparent 13C signature of flux from soil: -24.279991‰

18O signature of production (no invasion): -12.388992‰

FLANAGAN model estimate of del-p: -10.72‰

Eeff= 13.219969 - 8.0378438 = 5.18‰

Reproduced with permission of the copyright owner. Further reproduction prohibited without permission.

Table II.19. Calculation of the isotopic signature of the CO_2 flux from the soil to the atmosphere, using the Tans soil diffusion model (Tellus, 1998) in forward implicit mode, initialized with field data: alpine tundra site, fine soil, July, 1998.

Site; sampling date	Depth-dependent model input					Depth-independent model input					
IP 721 Alpine tundra, fine soil, 21 July, 1998 Production function written to match concentration profile	Depth	Porosity	Water volume	Soil Temp	Del Soil Water	Atmospheric flask			Flux rate	Depth-avg δ^{13}C-SOM	Other model parameters
	0	.565	.380	12.7	-10.5	[CO2] "Cabg"	δ^{13}C "del13bg"	δ^{18}O "del18bg"	6.9 umol/m2/sec .596 mol/m2/day	-24.60 (‰PDB)	alpha18= 0.9913 flush= 0.0437 ht of atm= 20 cm atm press= 653mbar
	5	.563	.381	11.5	-11.0	387	-12.28	-0.50			
	10	.563	.379	8.6	-11.9						
	30	.453	.362	6.1	-13.3						
	50	.449	.198	4.2	-12.1						

END OF RUN SUMMARY:

Total production (mol m-2 day-1): 0.59569997
Total production (mol cm-2 s-1): 6.8946756e-010
Flux from soil (mol cm-2 s-1): 6.8953311e-010 Flux from box: 6.8953344e-010
CO2, O18 and C13 into box: 387.00001 -0.500000 -12.2800
CO2, O18 and C13 from box: 415.71545 -1.3986235 -13.130990
Apparent 18O signature of flux from soil: -13.509125‰
Apparent 13C signature of flux from soil: -24.600010‰

18O signature of production (no invasion): -13.010520‰

FLANAGAN model estimate of del-p: -11.94‰

Eeff= 13.509125 - 8.1281609 = 5.38‰

APPENDIX III

DATA NOT PRESENTED IN THE TEXT

Reproduced with permission of the copyright owner. Further reproduction prohibited without permission.

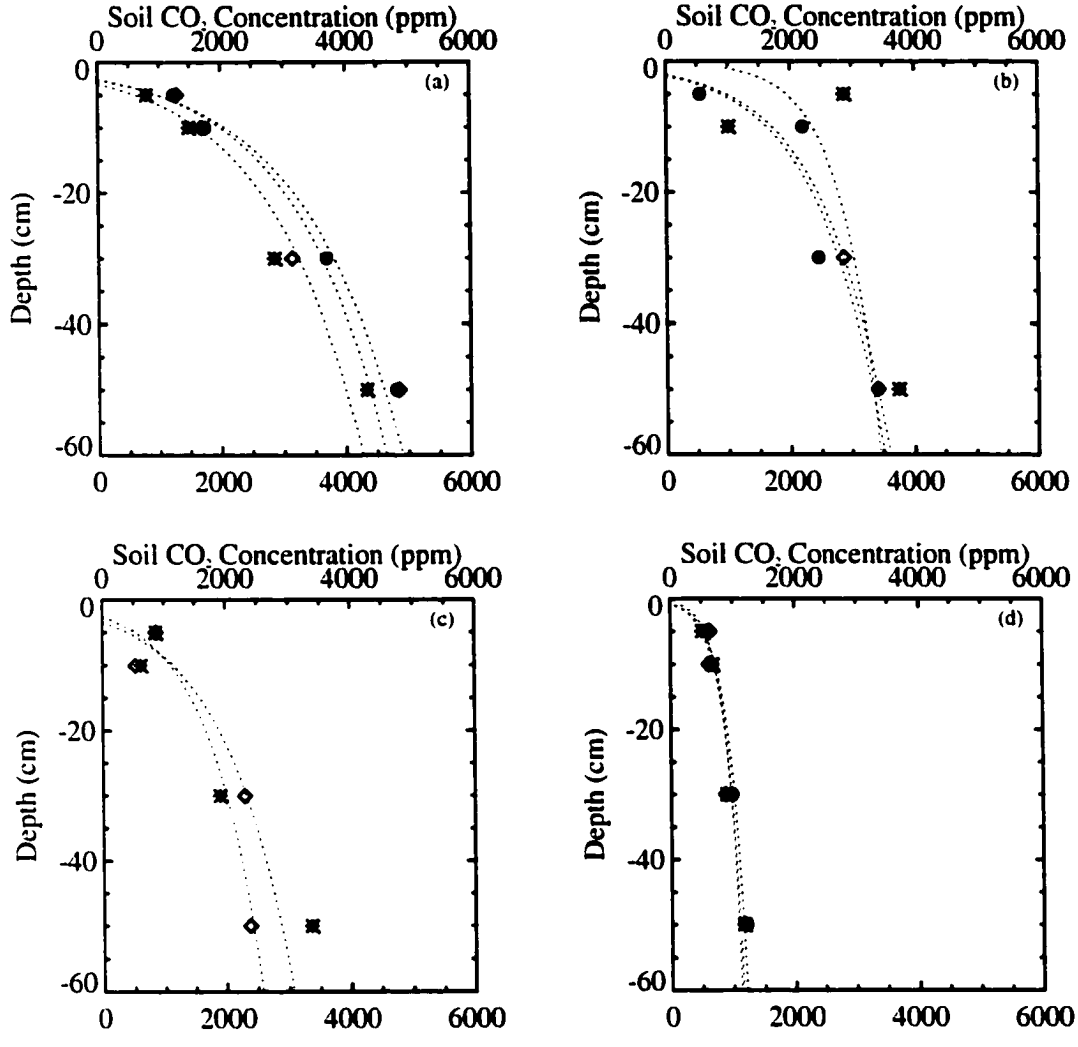

Figure III.1. Soil CO_2 concentration versus depth for the shortgrass steppe site on coarse-textured soil. Different symbols represent different sampling tubes (placed 1-m apart). The smoothed curve is a log linear regression of the data (IDL program, RSI, Inc.). Samples taken (a) June 23, 1998, (b) July 14, 1998, (c) August 11, 1998, and (d) October 26, 1998.

Reproduced with permission of the copyright owner. Further reproduction prohibited without permission.

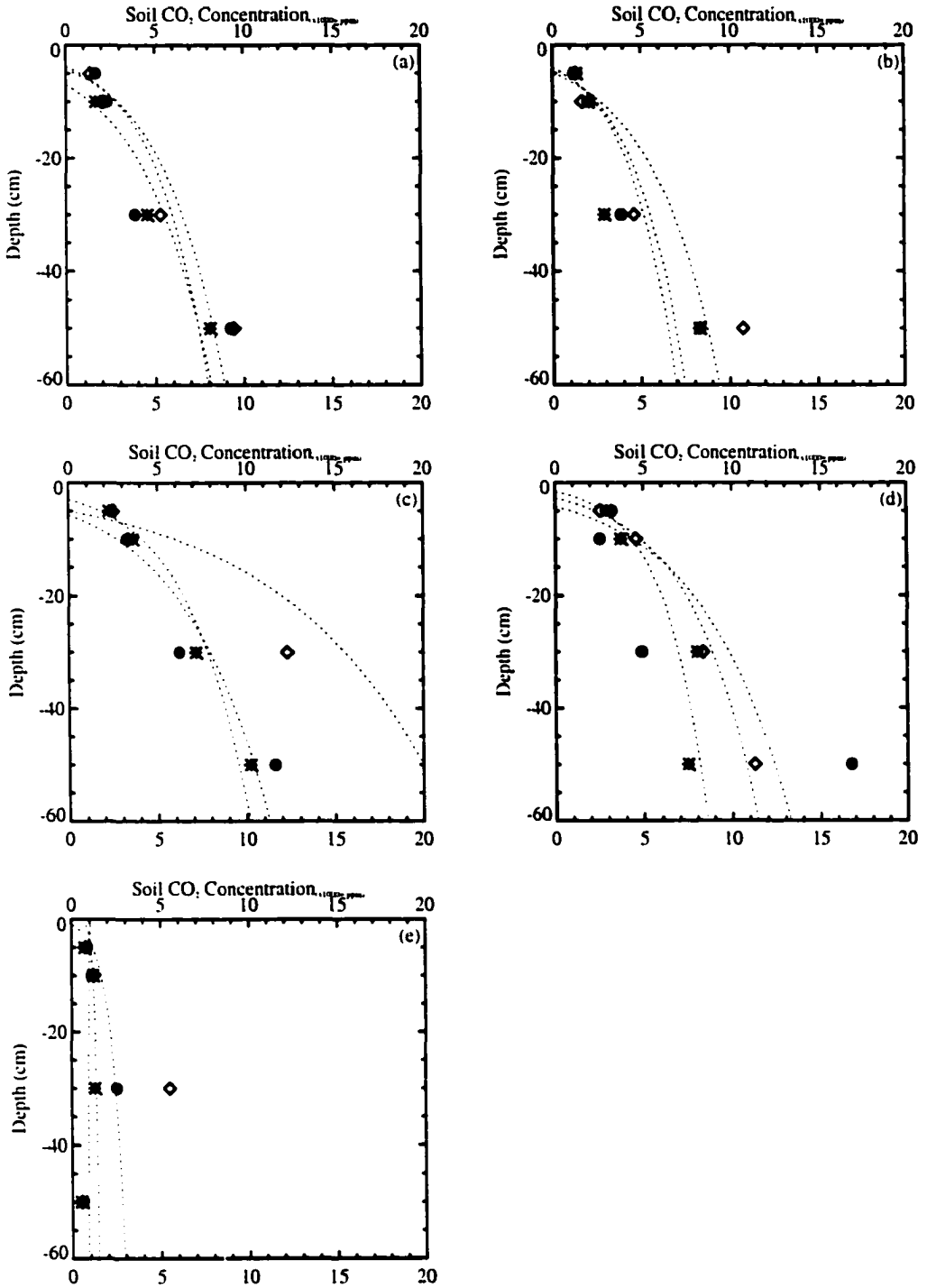

Figure III.2. Soil CO_2 concentration versus depth for the lodgepole pine site on fine-textured soil. Different symbols represent different sampling tubes (placed 1-m apart). The smoothed curve is a log linear regression of the data (IDL program, RSI, Inc.). Samples taken (a) June 16, 1998, (b) July 7, 1998, (c) July 28, 1998, (d) August 21, 1998, (e) November 5, 1998.

Reproduced with permission of the copyright owner. Further reproduction prohibited without permission.

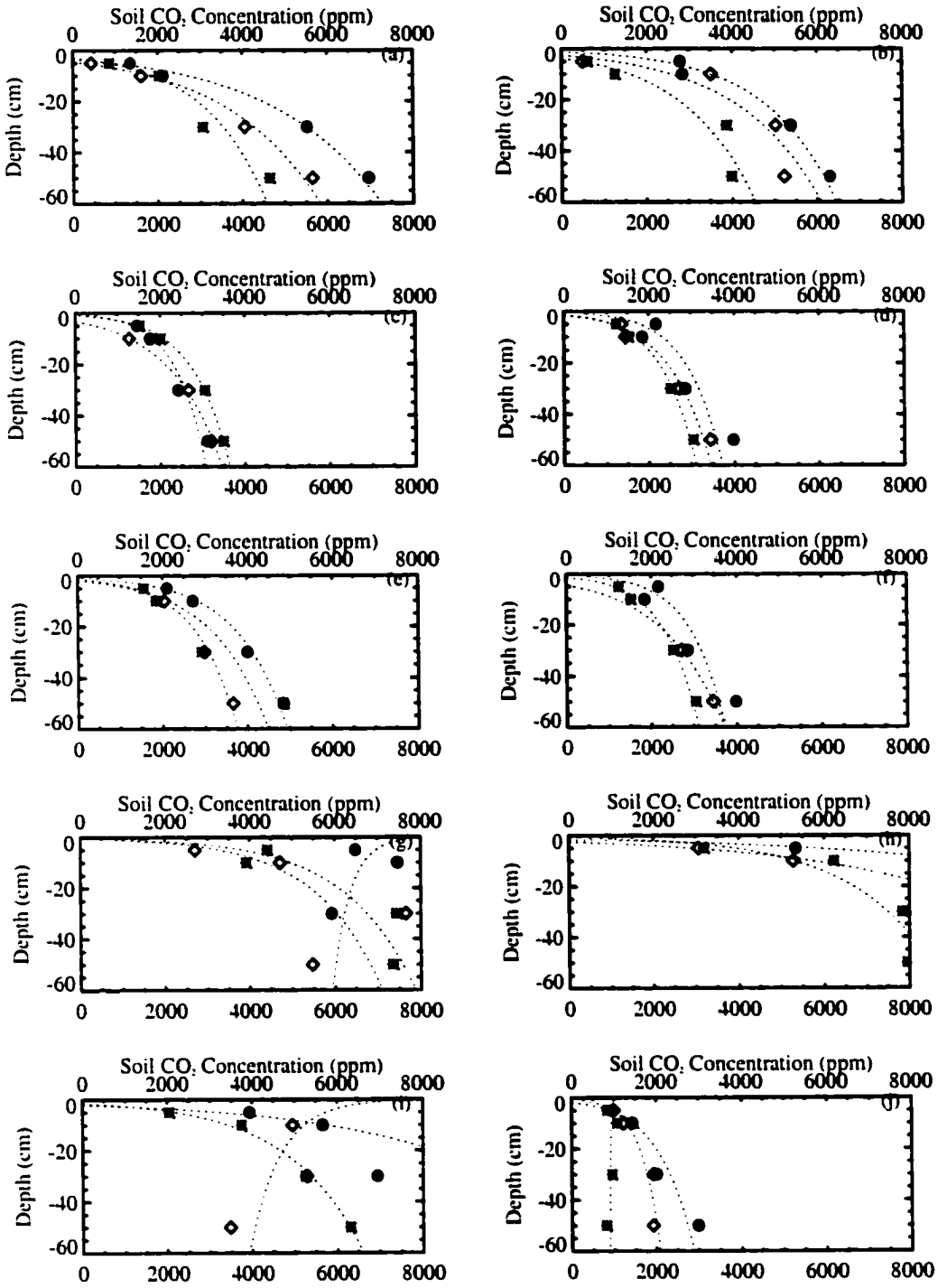

Figure III.3. Soil CO_2 concentration versus depth for the lodgepole pine site on coarse-textured soil. Different symbols represent different sampling tubes (placed 1-m apart). The smoothed curve is a log linear regression of the data (IDL program, RSI, Inc.). Samples taken (a) June 11, 1998, (b) June 19, 1998, (c) June 25, 1998, (d) July 1, 1998, (e) July 10, 1998, (f) July 16, 1998, (g) July 28, 1998, (h) August 7, 1998 (i) August 21, 1998, (j) November 19, 1998.

Reproduced with permission of the copyright owner. Further reproduction prohibited without permission.

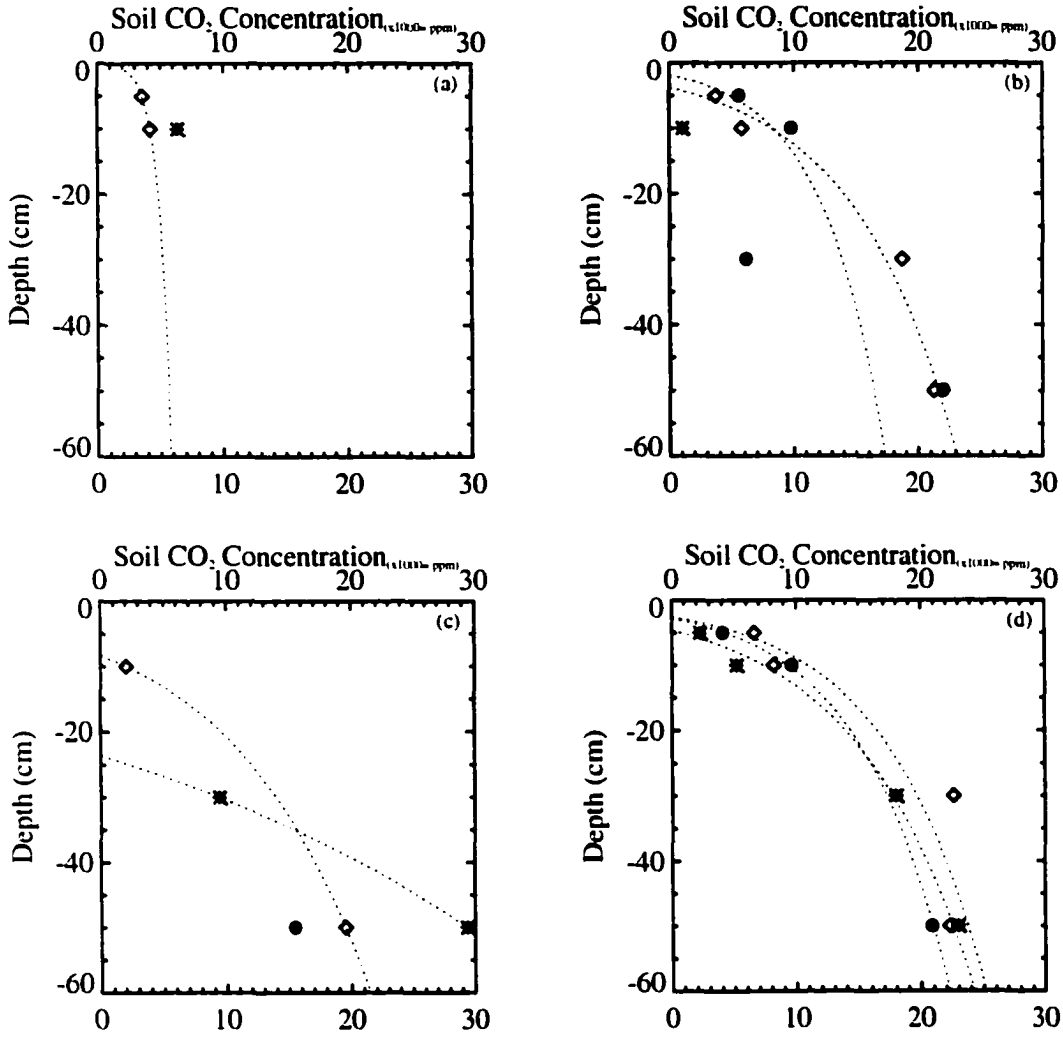

Figure III.4. Soil CO_2 concentration versus depth for the alpine tundra site on fine-textured soil. Different symbols represent different sampling tubes (placed 1-m apart). The smoothed curve is a log linear regression of the data (IDL program, RSI, Inc.). Samples taken (a) June 9, 1998, (b) July 2, 1998, (c) July 21, 1998, (d) August 5, 1998.

Reproduced with permission of the copyright owner. Further reproduction prohibited without permission.

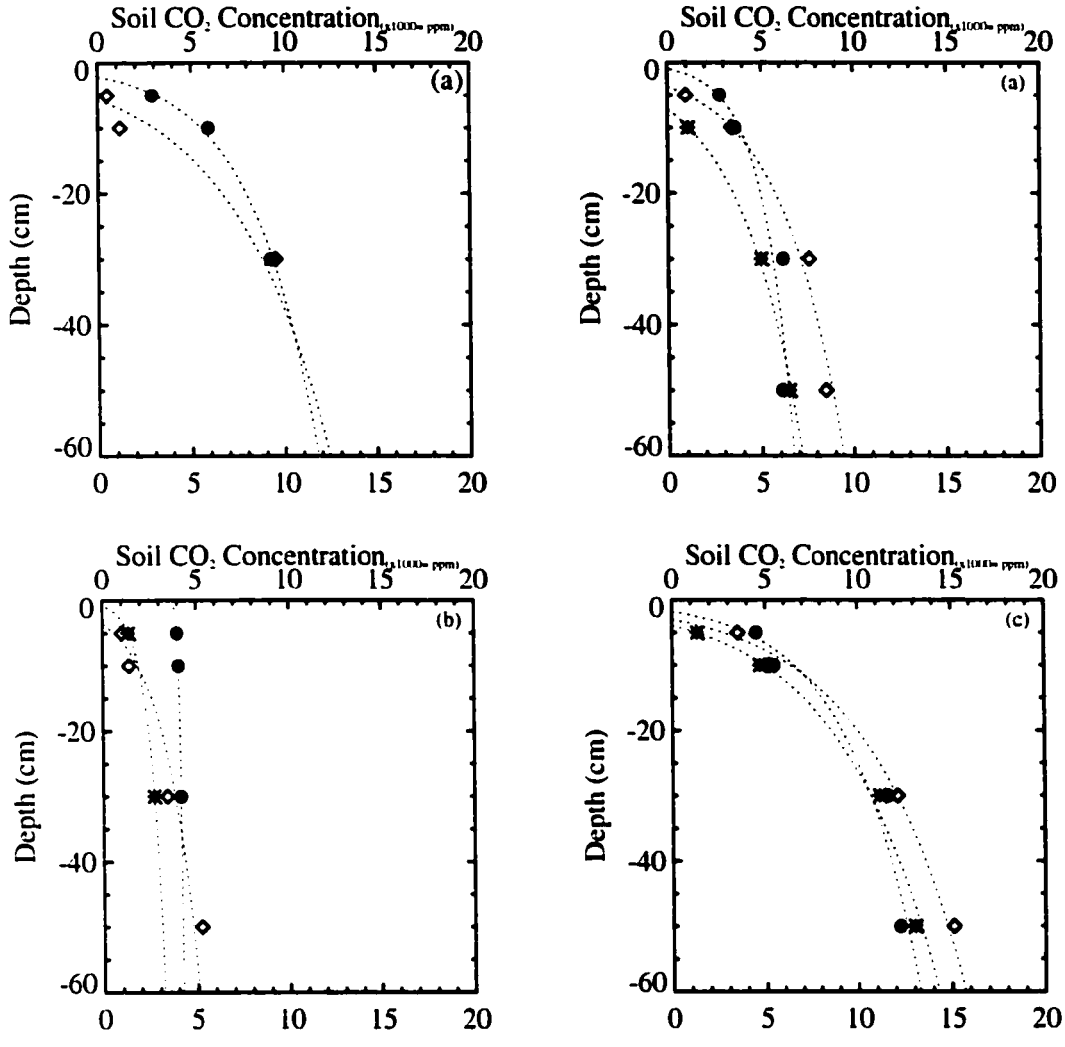

Figure III.5. Soil CO_2 concentration versus depth for the alpine tundra site on coarse-textured soil. Different symbols represent different sampling tubes (placed 1-m apart). The smoothed curve is a log linear regression of the data (IDL program, RSI, Inc.). Samples taken (a) June 9, 1998, (b) July 2, 1998, (c) July 21, 1998, (d) August 5, 1998.

Reproduced with permission of the copyright owner. Further reproduction prohibited without permission.

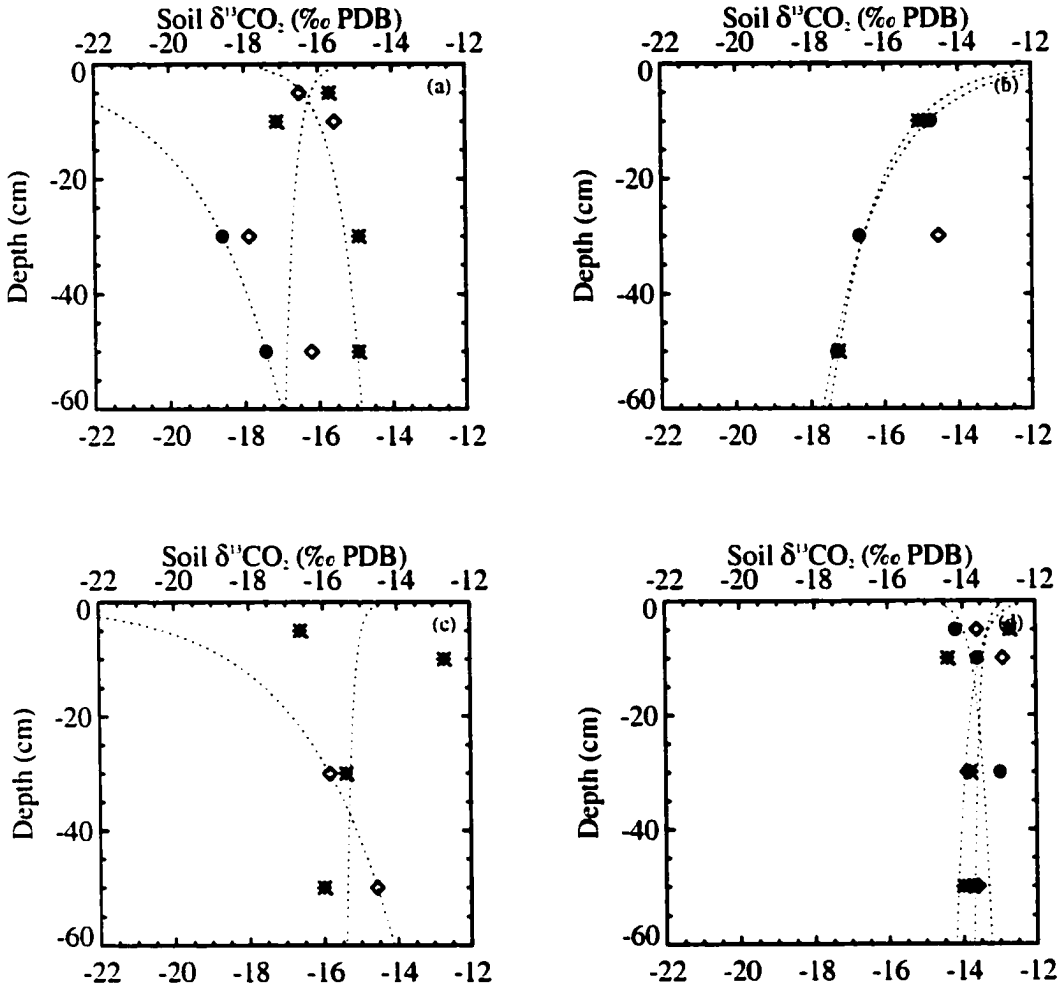

Figure III.6. Soil CO_2 $\delta^{13}C$ value versus depth for the shortgrass steppe site on coarse-textured soil. Different symbols represent different sampling tubes (placed 1-m apart). The smoothed curve is a log linear regression of the data (IDL program, RSI, Inc.). Samples taken (a) June 23, 1998, (b) July 14, 1998, (c) August 11, 1998, and (d) October 26, 1998.

Reproduced with permission of the copyright owner. Further reproduction prohibited without permission.

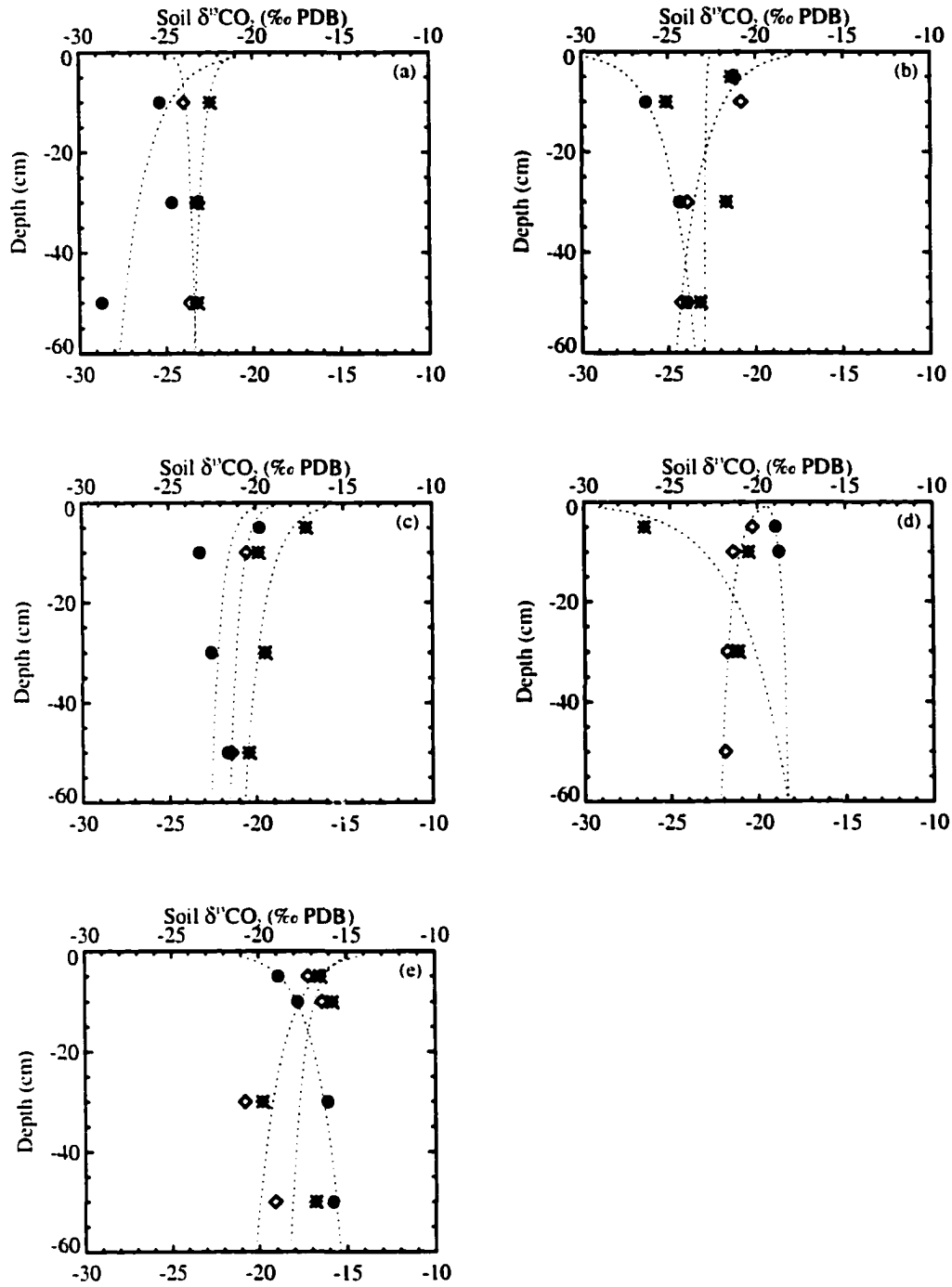

Figure III.7. Soil CO_2 $\delta^{13}C$ value versus depth for the lodgpole pine site on fine-textured soil. Different symbols represent different sampling tubes (placed 1-m apart). The smoothed curve is a log linear regression of the data (IDL program, RSI, Inc.). Samples taken (a) June 16, 1998, (b) July 7, 1998, (c) July 28, 1998, (d) August 21, 1998, (e) November 5, 1998.

Reproduced with permission of the copyright owner. Further reproduction prohibited without permission.

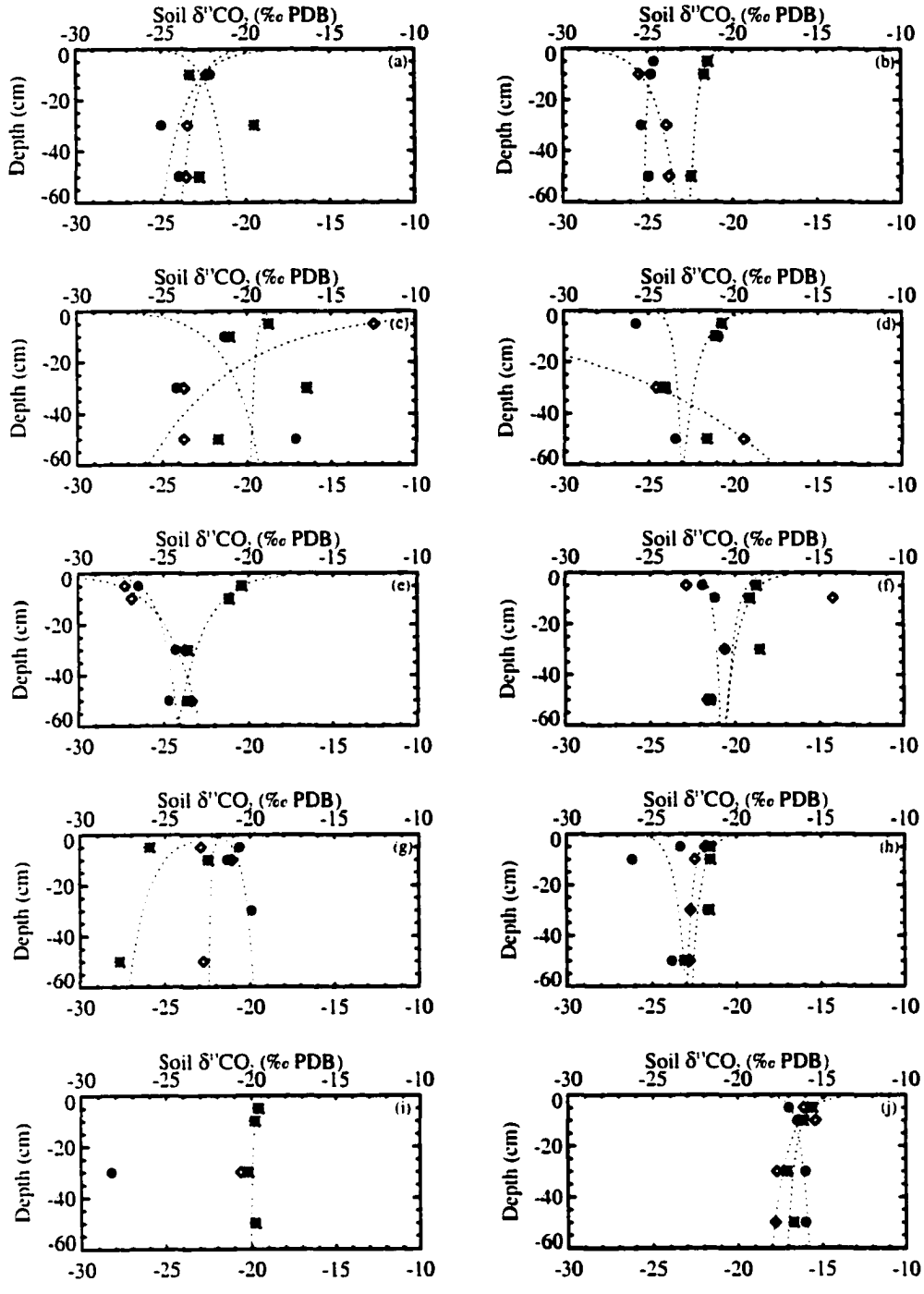

Figure III.8. Soil CO_2 $\delta^{13}C$ value versus depth for the lodgpole pine site on coarse-textured soil. Different symbols represent different sampling tubes (placed 1-m apart). The smoothed curve is a log linear regression of the data (IDL program, RSI, Inc.). Samples taken (a) June 11, 1998, (b) June 19, 1998, (c) June 25, 1998, (d) July 1, 1998, (e) July 10, 1998, (f) July 16, 1998, (g) July 28, 1998, (h) August 7, 1998 (i) August 21, 1998, (j) November 19, 1998.

Reproduced with permission of the copyright owner. Further reproduction prohibited without permission.

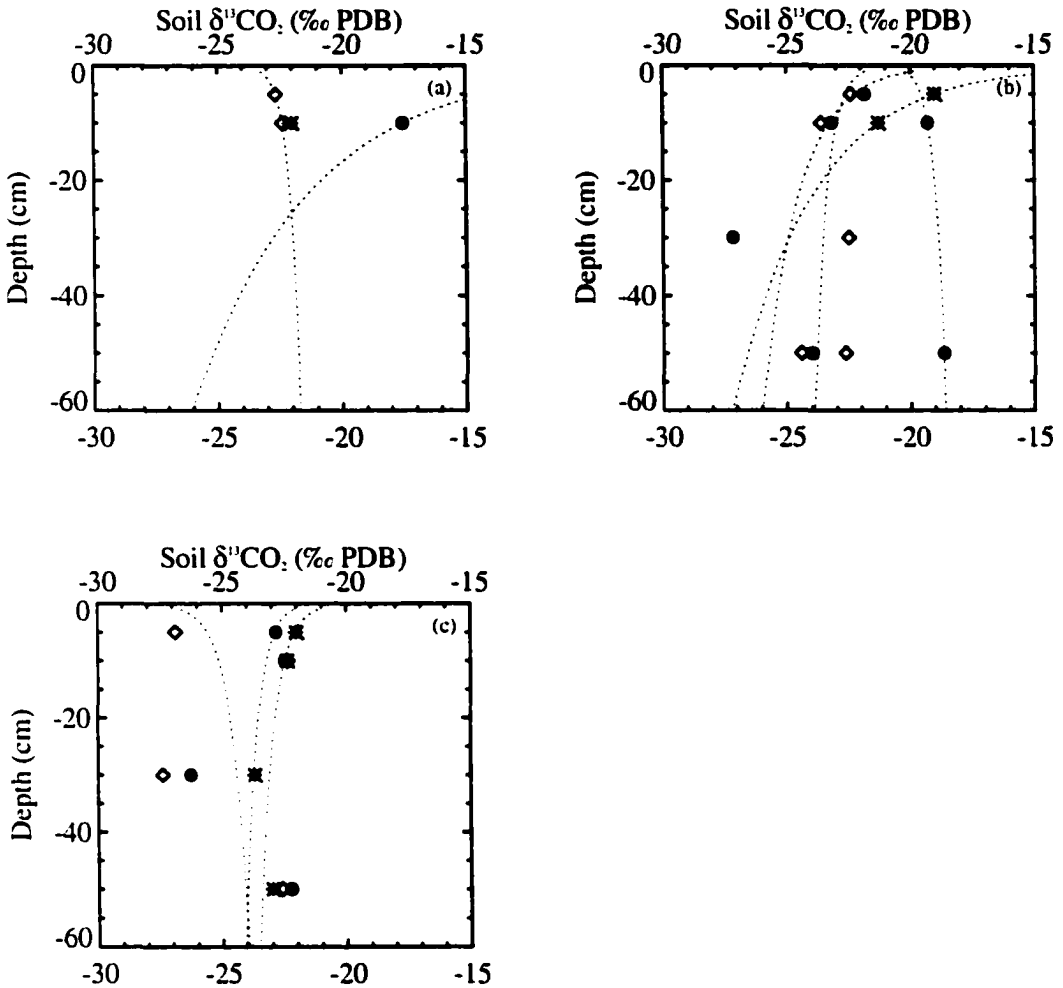

Figure III.9. Soil CO_2 $\delta^{13}C$ value versus depth for the alpine tundra site on fine-textured soil. Different symbols represent different sampling tubes (placed 1-m apart). The smoothed curve is a log linear regression of the data (IDL program, RSI, Inc.). Samples taken (a) June 9, 1998, (b) July 2, 1998, (c) July 21, 1998, (d) August 5, 1998.

Reproduced with permission of the copyright owner. Further reproduction prohibited without permission.

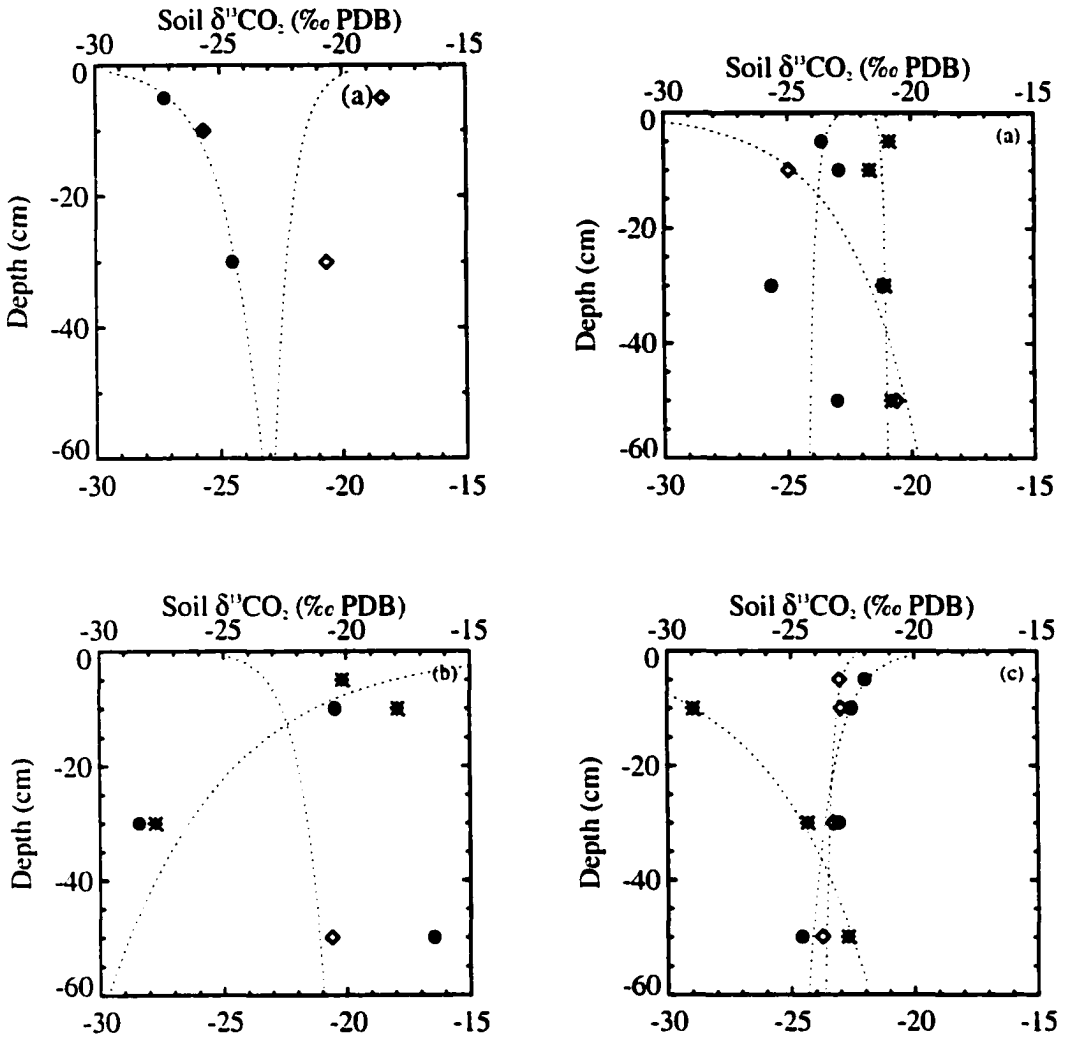

Figure III.10. Soil CO_2 $\delta^{13}C$ value versus depth for the alpine tundra site on coarse-textured soil. Different symbols represent different sampling tubes (placed 1-m apart). The smoothed curve is a log linear regression of the data (IDL program, RSI, Inc.). Samples taken (a) June 9, 1998, (b) July 2, 1998, (c) July 21, 1998, (d) August 5, 1998.

Reproduced with permission of the copyright owner. Further reproduction prohibited without permission.

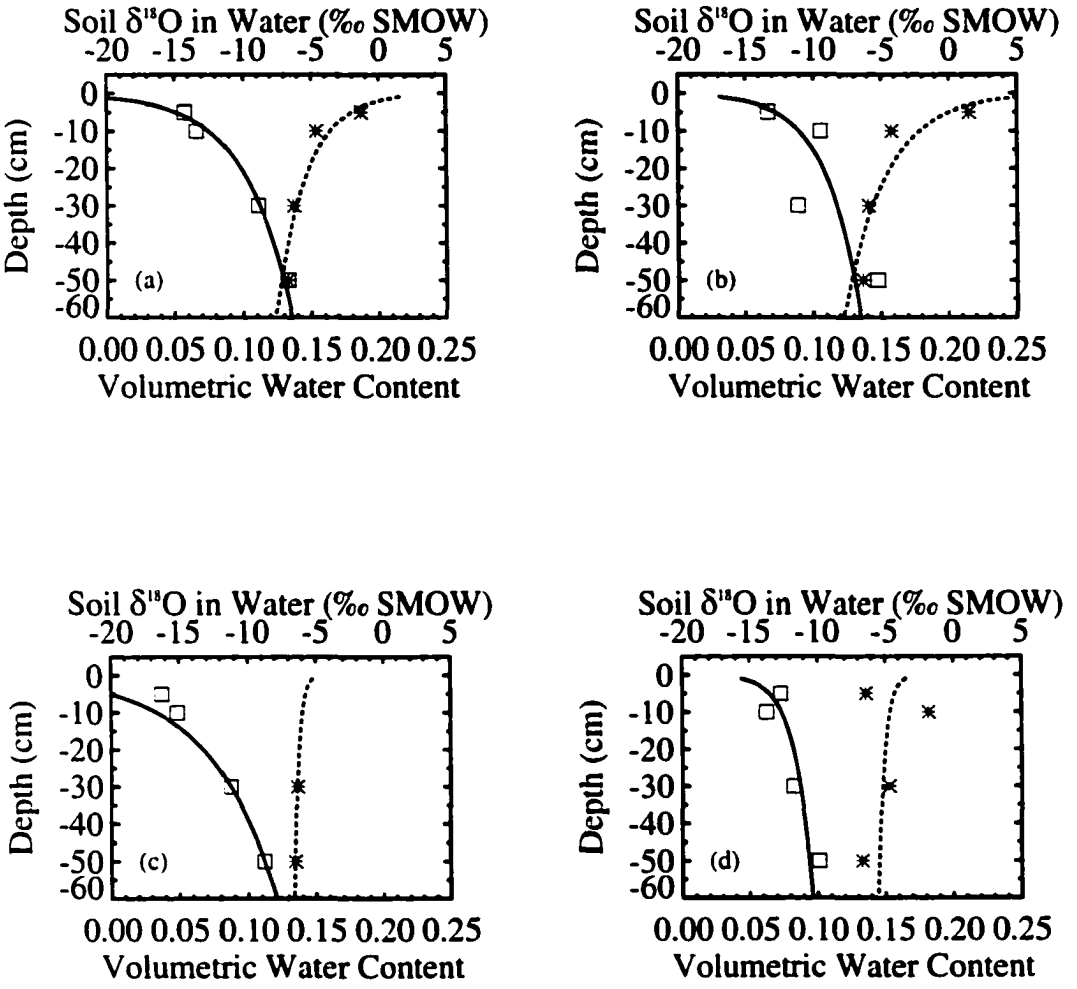

Figure III.11. Oxygen isotopic composition of soil water (asterix) and rainfall (solid diamond), as well as soil water content (open square, expressed as g H_2O/g soil) versus depth for each sampling date. Smoothed curves are a log linear regression of the data (IDL software, RSI, Inc.). These graphs are for the shortgrass steppe site on coarse soil. (a) June 23, 1998, (b) July 14, 1998, (c) August 11, 1998, (d) October 26, 1998.

Reproduced with permission of the copyright owner. Further reproduction prohibited without permission.

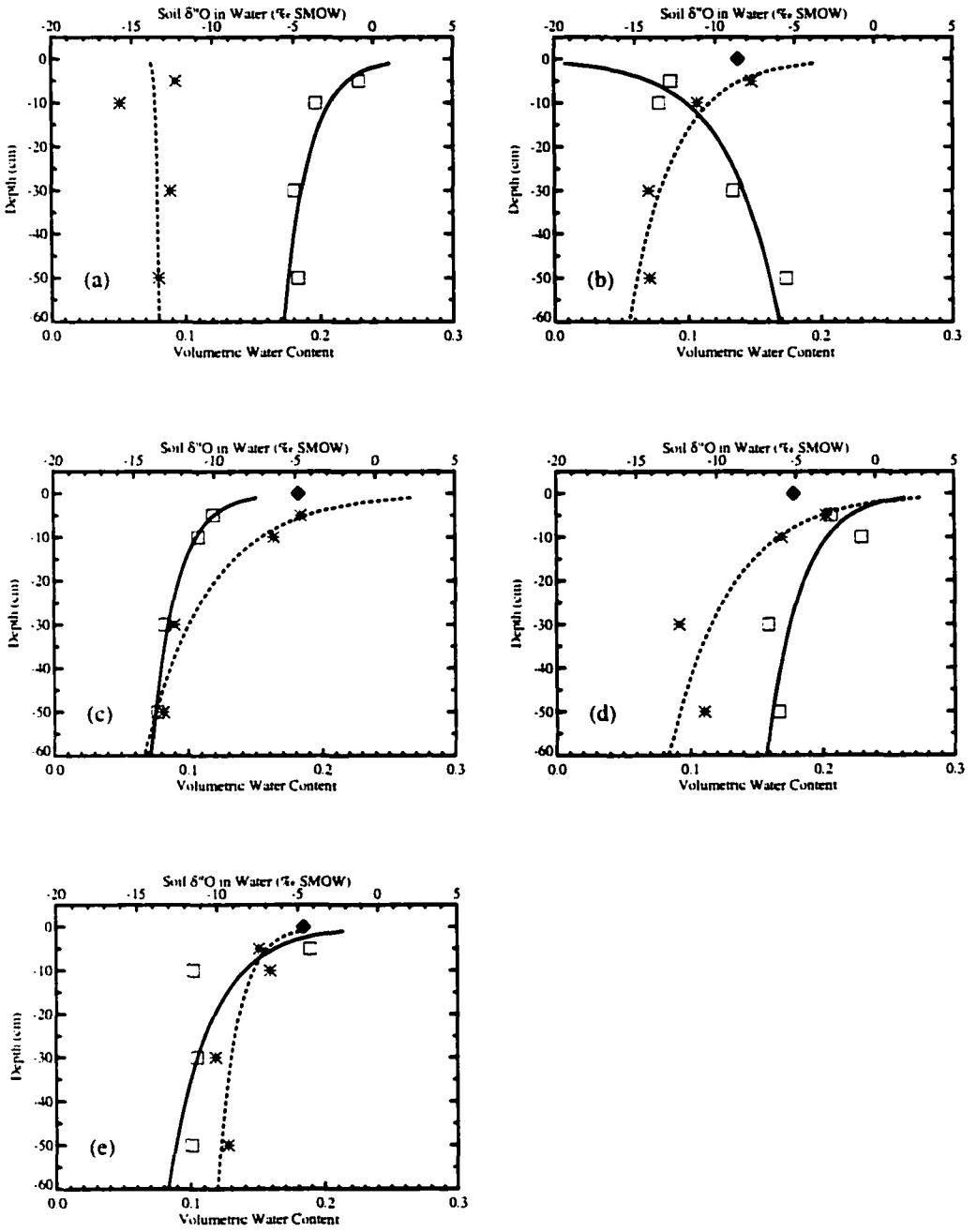

Figure III.12. Oxygen isotopic composition of soil water (asterix) and rainfall (solid diamond), as well as soil water content (open square, expressed as g H_2O/g soil) versus depth for each sampling date. Smoothed curves are a log linear regression of the data (IDL software, RSI, Inc.). These graphs are for the lodgepole pine site on fine soil. (a) June 16, 1998, (b) July 7, 1998, (c) July 28, 1998, (d) August 21, 1998, (e) November 5, 1998.

Reproduced with permission of the copyright owner. Further reproduction prohibited without permission.

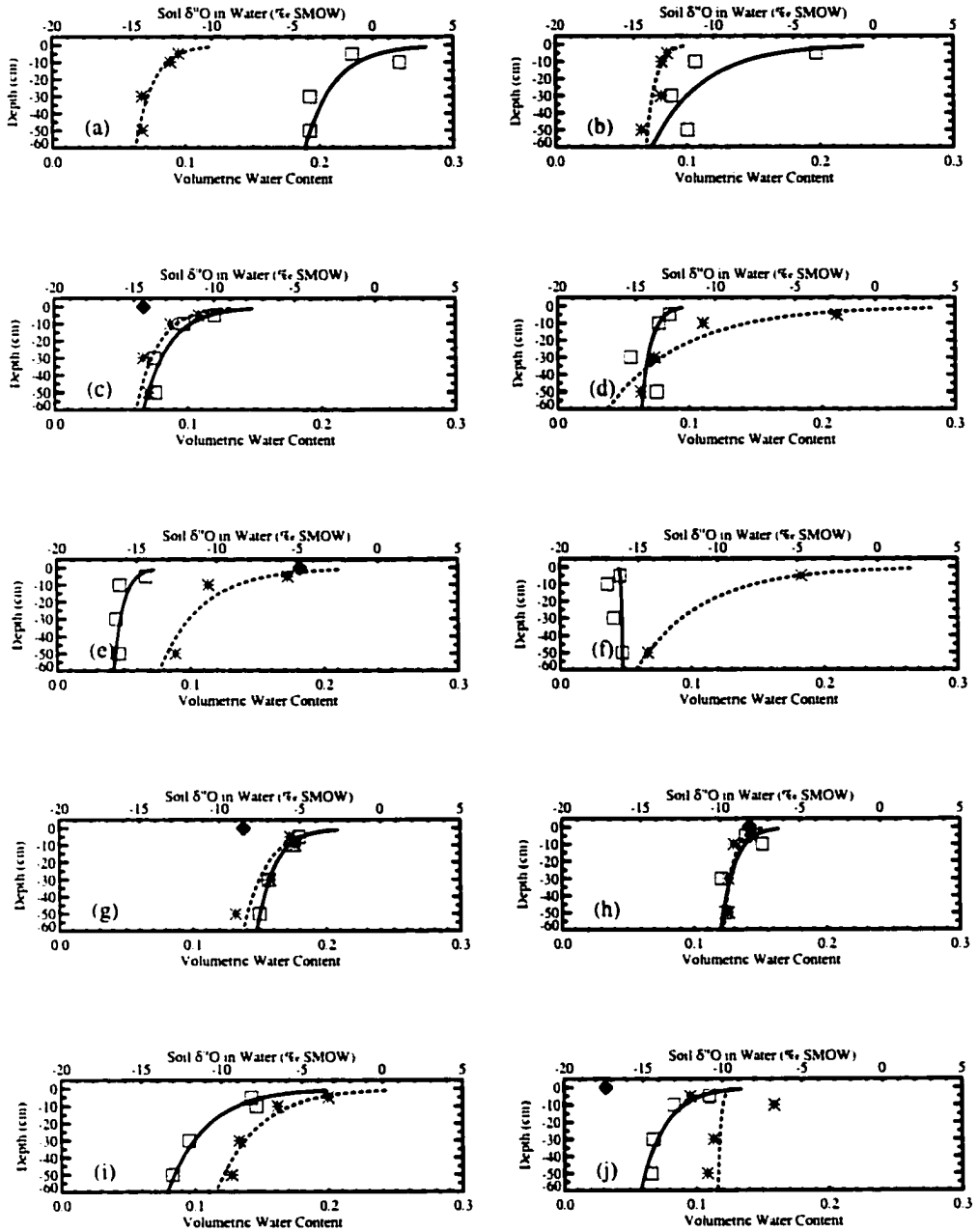

Figure III.13. Oxygen isotopic composition of soil water (asterix) and rainfall (solid diamond), as well as soil water content (open square, expressed as g H_2O/g soil) versus depth for each sampling date. Smoothed curves are a log linear regression of the data (IDL software, RSI, Inc.). These graphs are for the lodgepole pine site on coarse soil. (a) June 11, 1998, (b) June 19, 1998, (c) June 25, 1998, (d) July 1, 1998, (e) July 10, 1998, (f) July 16, 1998, (g) July 28, 1998, (h) August 7, 1998 (i) August 21, 1998, (j) November 19, 1998.

Reproduced with permission of the copyright owner. Further reproduction prohibited without permission.

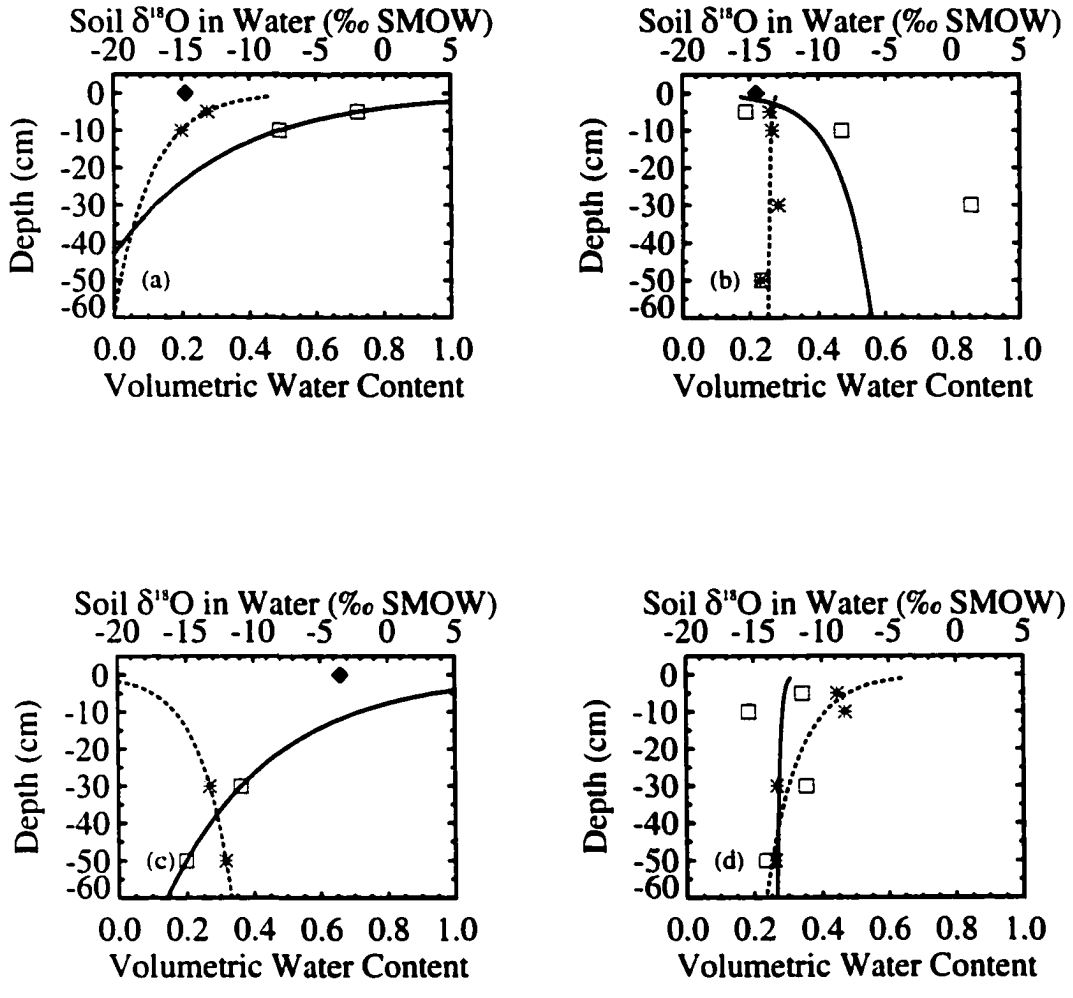

Figure III.14. Oxygen isotopic composition of soil water (asterix) and rainfall (solid diamond), as well as soil water content (open square, expressed as g H_2O/g soil) versus depth for each sampling date. Smoothed curves are a log linear regression of the data (IDL software, RSI, Inc.). These graphs are for the alpine tundra site on fine soil. (a) June 9, 1998, (b) July 2, 1998, (c) July 21, 1998, (d) August 5, 1998.

Reproduced with permission of the copyright owner. Further reproduction prohibited without permission.

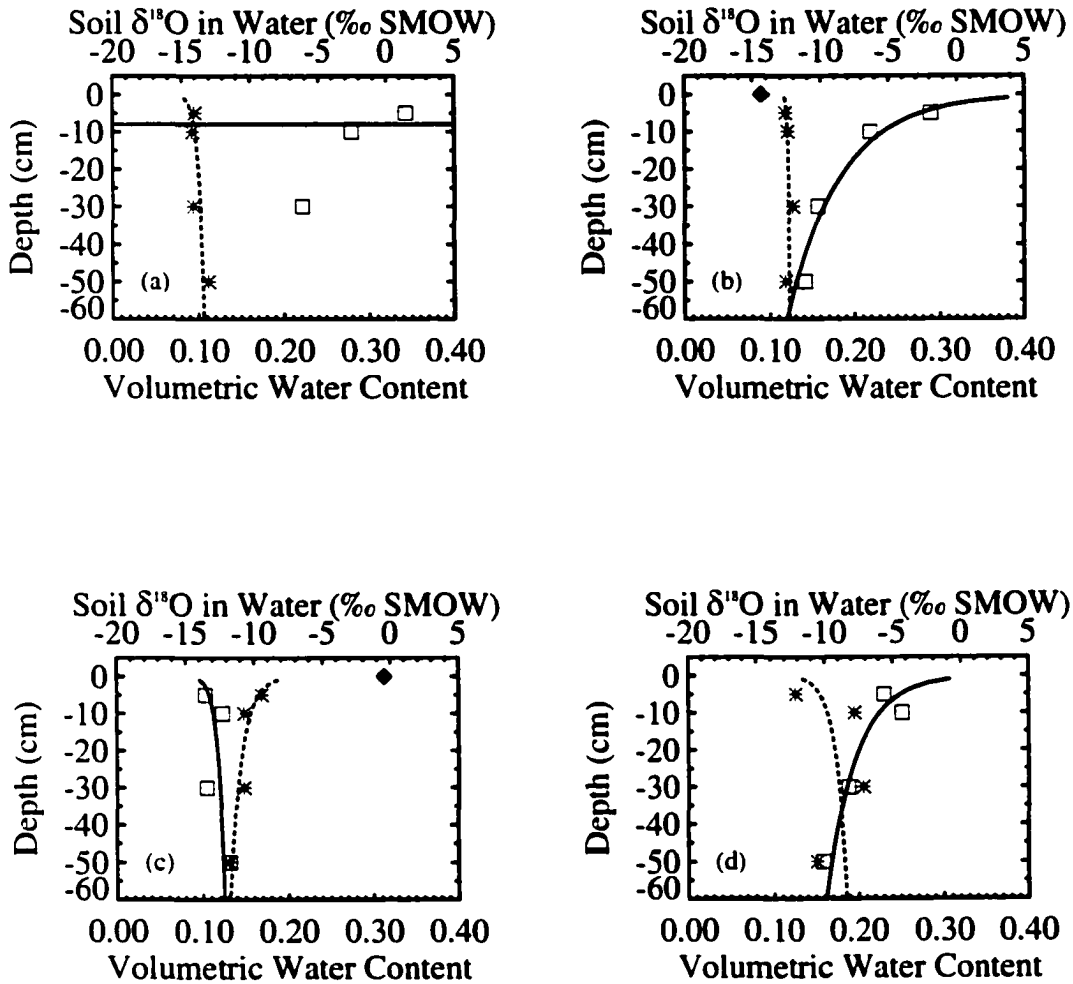

Figure III.15. Oxygen isotopic composition of soil water (asterix) and rainfall (solid diamond), as well as soil water content (open square, expressed as g H_2O/g soil) versus depth for each sampling date. Smoothed curves are a log linear regression of the data (IDL software, RSI, Inc.). These graphs are for the alpine tundra site on coarse soil. (a) June 9, 1998, (b) July 2, 1998, (c) July 21, 1998, (d) August 5, 1998.

Reproduced with permission of the copyright owner. Further reproduction prohibited without permission.

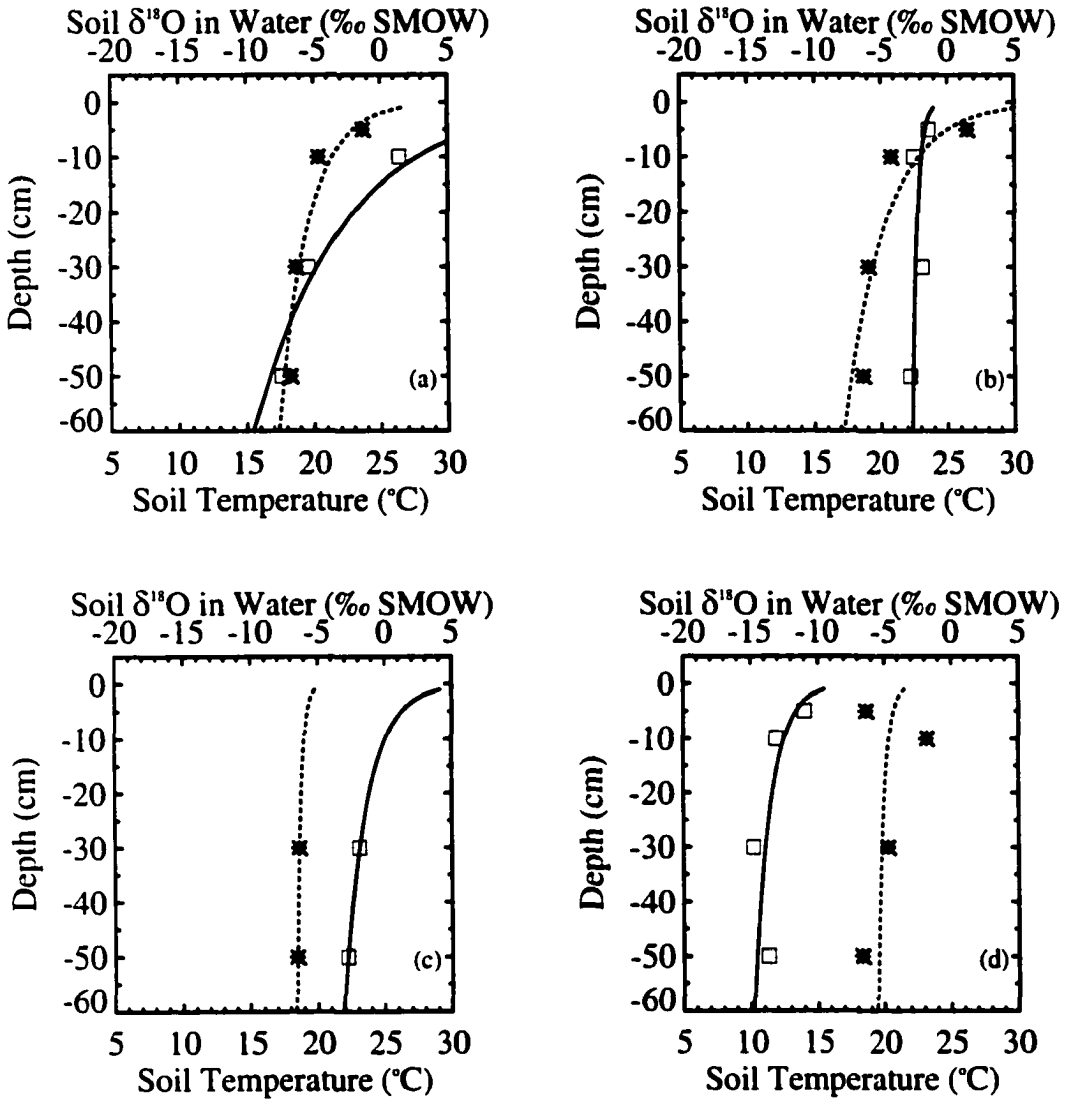

Figure III.16. Oxygen isotopic composition of soil water (asterix) and rainfall (solid diamond), as well as soil temperature (open square) versus depth for each sampling date. These graphs are for the shortgrass steppe site on coarse soil. Smoothed curves are a log linear regression of the data (IDL software, RSI, Inc.). (a) June 23, 1998, (b) July 14, 1998, (c) August 11, 1998, (d) October 26, 1998.

Reproduced with permission of the copyright owner. Further reproduction prohibited without permission.

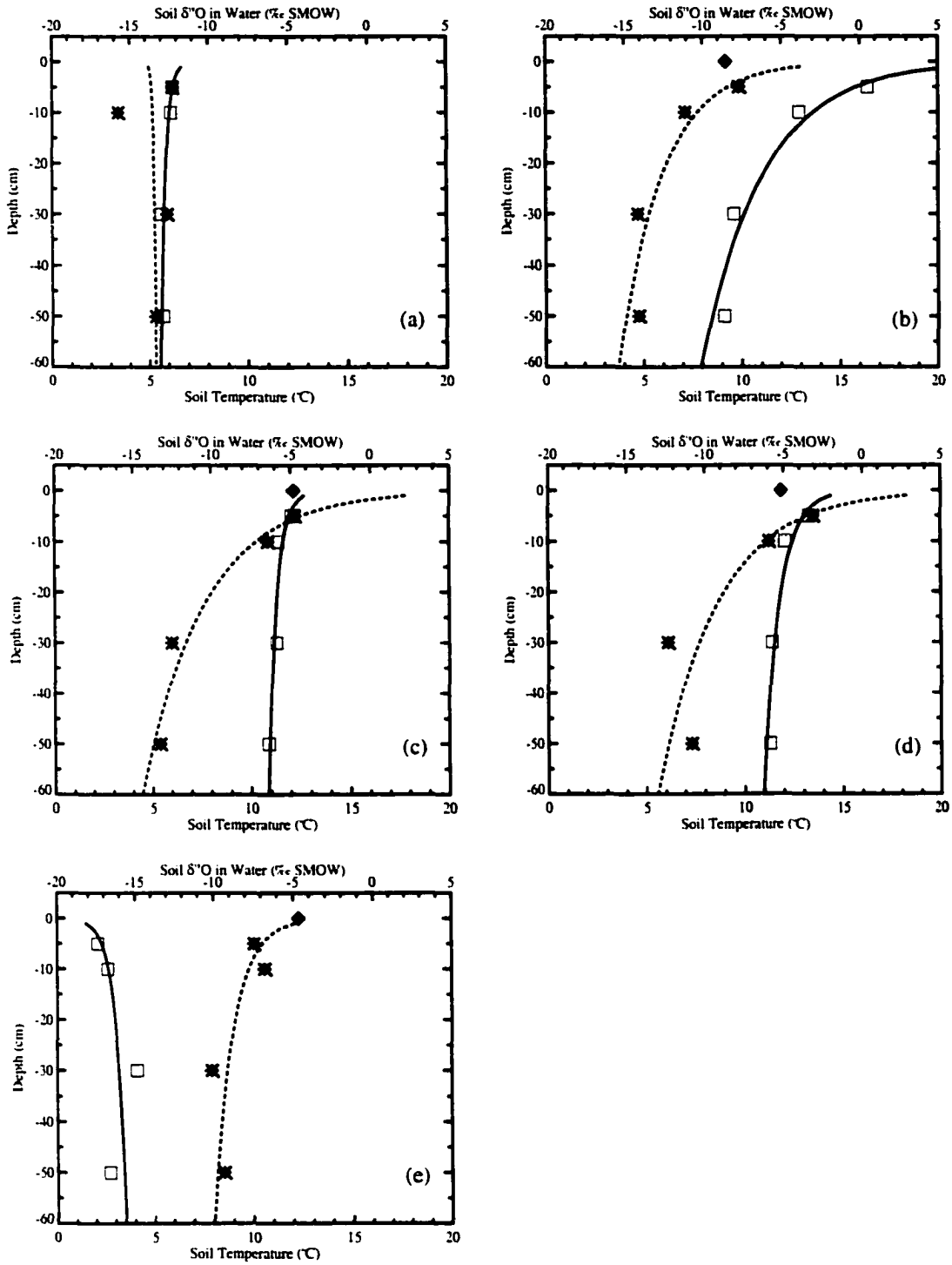

Figure III.17. Oxygen isotopic composition of soil water (asterix) and rainfall (solid diamond), as well as soil temperature (open square) versus depth for each sampling date. These graphs are for the lodgepole pine site on fine soil. Smoothed curves are a log linear regression of the data (IDL software, RSI, Inc.). (a) June 16, 1998, (b) July 7, 1998, (c) July 28, 1998, (d) August 21, 1998, (e) November 5, 1998.

Reproduced with permission of the copyright owner. Further reproduction prohibited without permission.

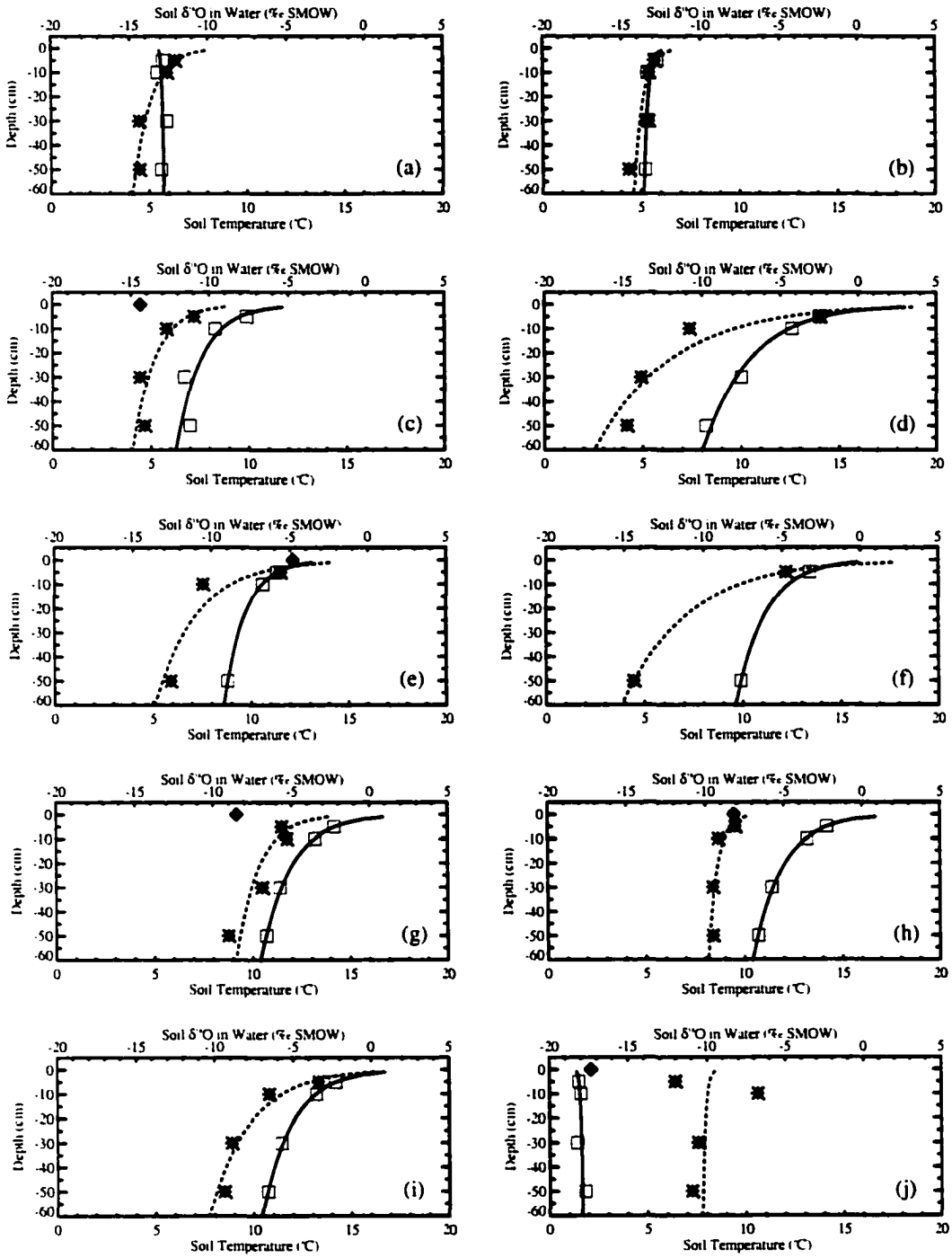

Figure III.18. Oxygen isotopic composition of soil water (asterix) and rainfall (solid diamond), as well as soil temperature (open square) versus depth for each sampling date. These graphs are for the lodgepole pine site on coarse soil. Smoothed curves are a log linear regression of the data (IDL software, RSI, Inc.). (a) June 11, 1998, (b) June 19, 1998, (c) June 25, 1998, (d) July 1, 1998, (e) July 10, 1998, (f) July 16, 1998, (g) July 28, 1998, (h) August 7, 1998 (i) August 21, 1998, (j) November 19, 1998.

Reproduced with permission of the copyright owner. Further reproduction prohibited without permission.

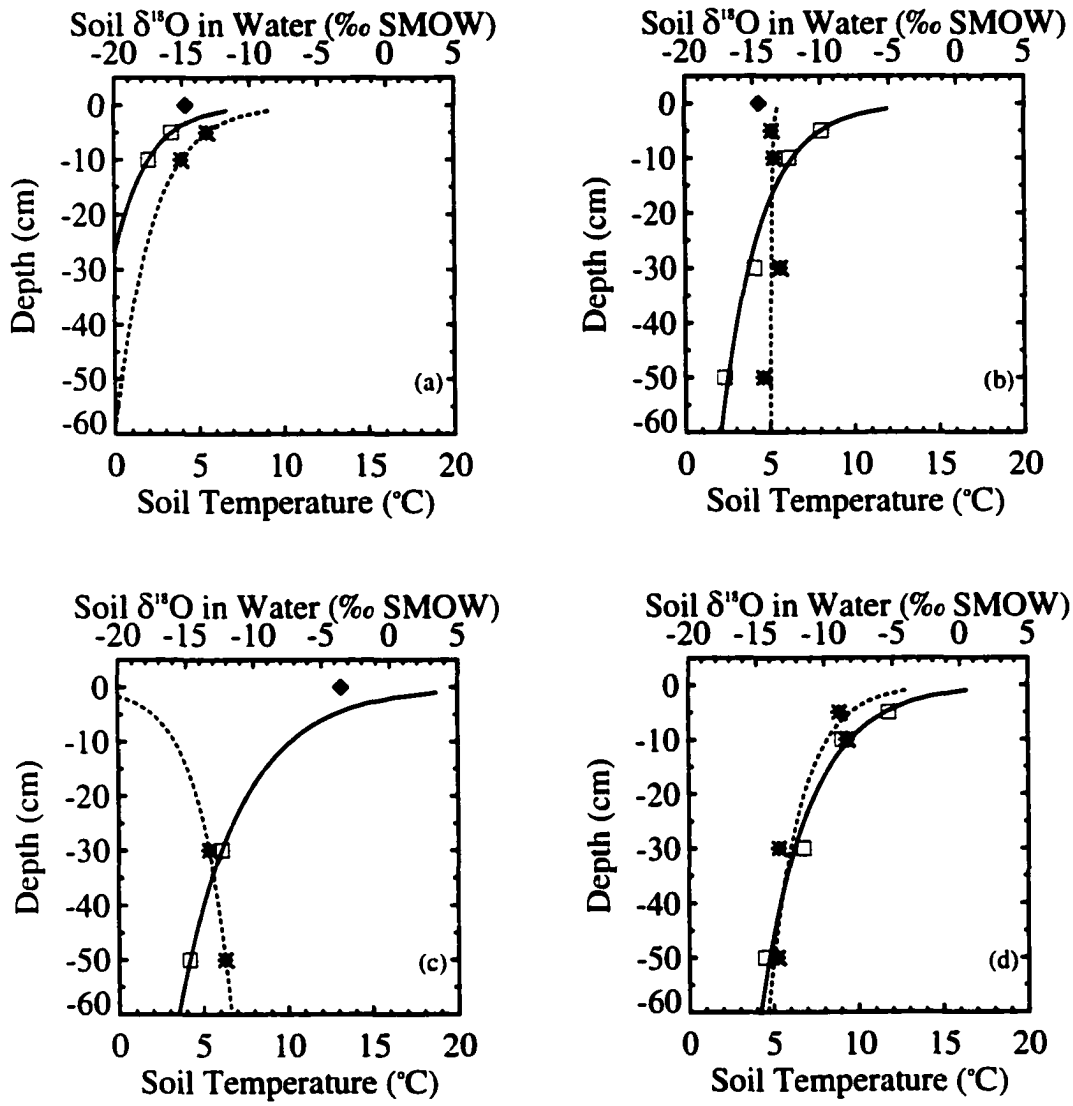

Figure III.19. Oxygen isotopic composition of soil water (asterix) and rainfall (solid diamond), as well as soil temperature (open square) versus depth for each sampling date. These graphs are for the alpine tundra site on fine soil. Smoothed curves are a log linear regression of the data (IDL software, RSI, Inc.). (a) June 9, 1998, (b) July 2, 1998, (c) July 21, 1998, (d) August 5, 1998.

Reproduced with permission of the copyright owner. Further reproduction prohibited without permission.

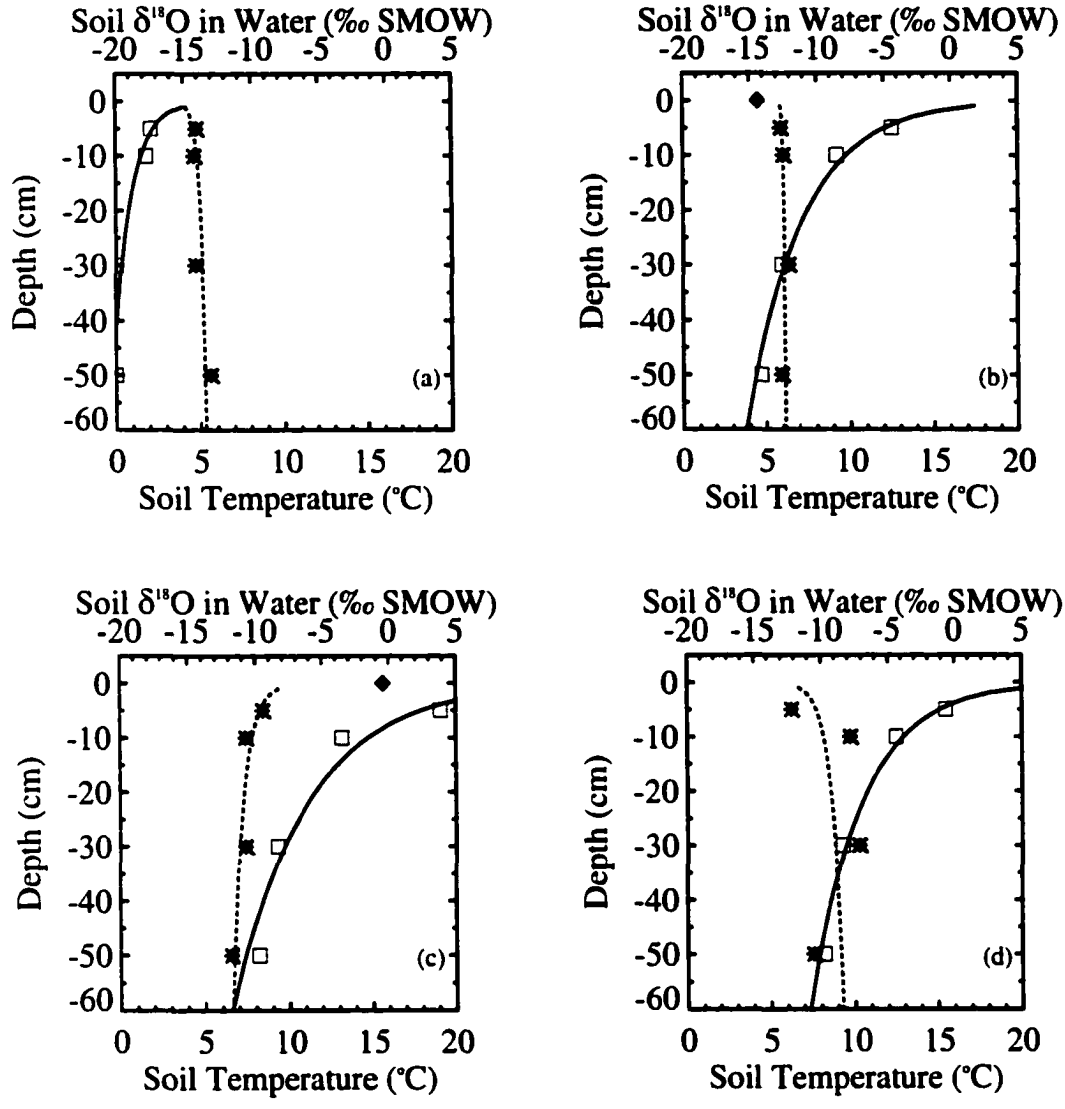

Figure III.20. Oxygen isotopic composition of soil water (asterix) and rainfall (solid diamond), as well as soil temperature (open square) versus depth for each sampling date. These graphs are for the alpine tundra site on coarse soil. Smoothed curves are a log linear regression of the data (IDL software, RSI, Inc.). (a) June 9, 1998, (b) July 2, 1998, (c) July 21, 1998, (d) August 5, 1998.

Reproduced with permission of the copyright owner. Further reproduction prohibited without permission.

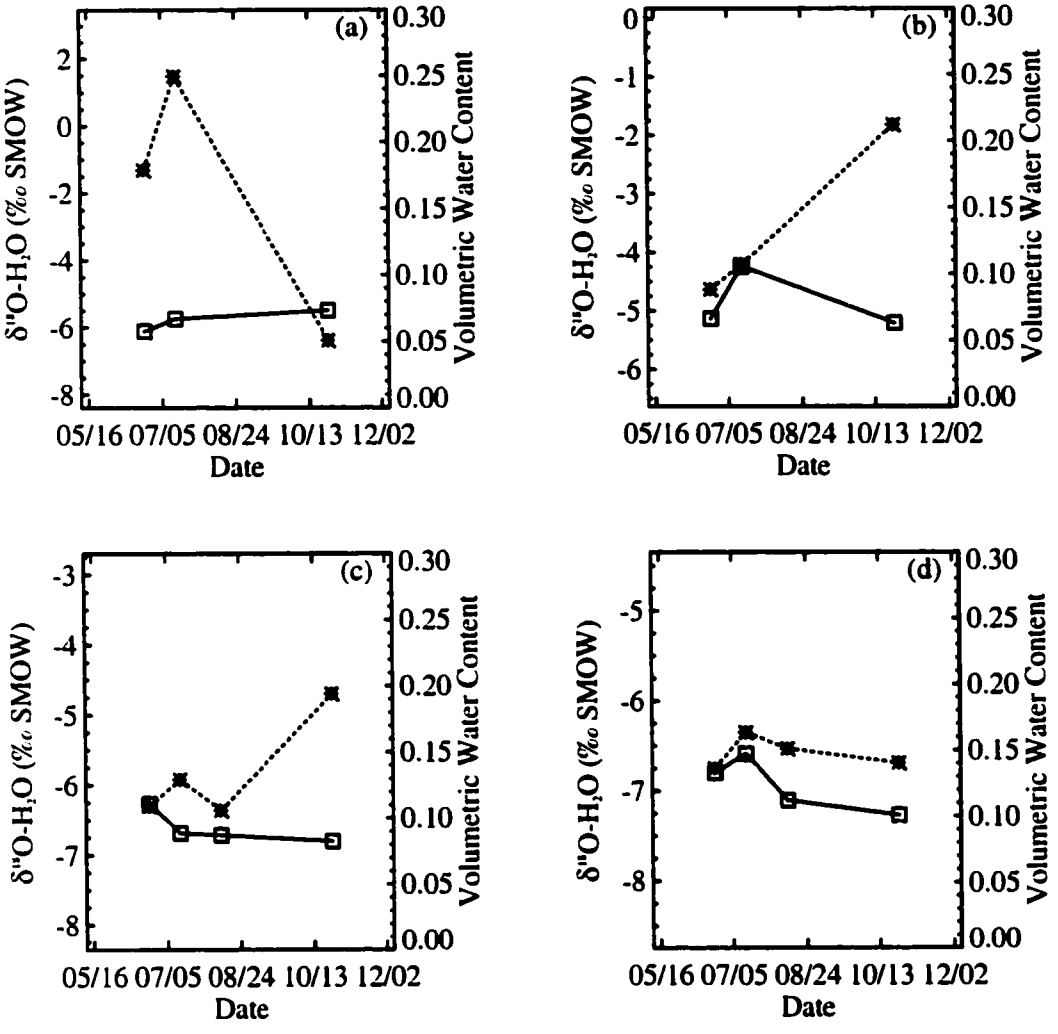

Figure III.21. Patterns of soil water content (open square) and soil water $\delta^{18}O$ values (asterix) over the sampling period in 1998 for the shortgrass steppe site on coarse soil. Data are for the following depths: (a) 5 cm, (b) 10 cm, (c) 30 cm, (d) 50 cm. Data are not continuous in time; points are connected merely for visualization.

Reproduced with permission of the copyright owner. Further reproduction prohibited without permission.

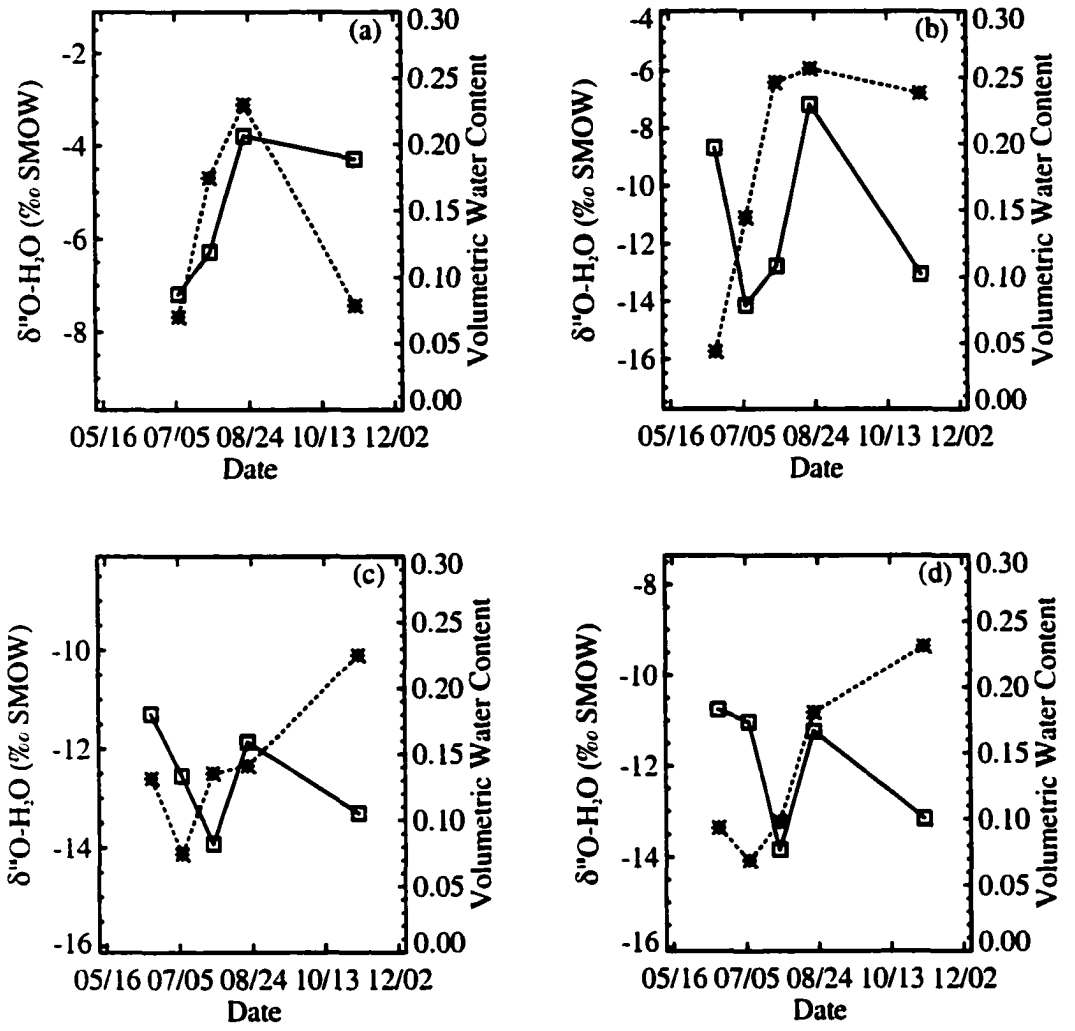

Figure III.22. Patterns of soil water content (open square) and soil water $\delta^{18}O$ values (asterix) over the sampling period in 1998 for the lodgepole pine site on fine soil. Data are for the following depths: (a) 5 cm, (b) 10 cm, (c) 30 cm, (d) 50 cm. Data are not continuous in time; points are connected merely for visualization.

Reproduced with permission of the copyright owner. Further reproduction prohibited without permission.

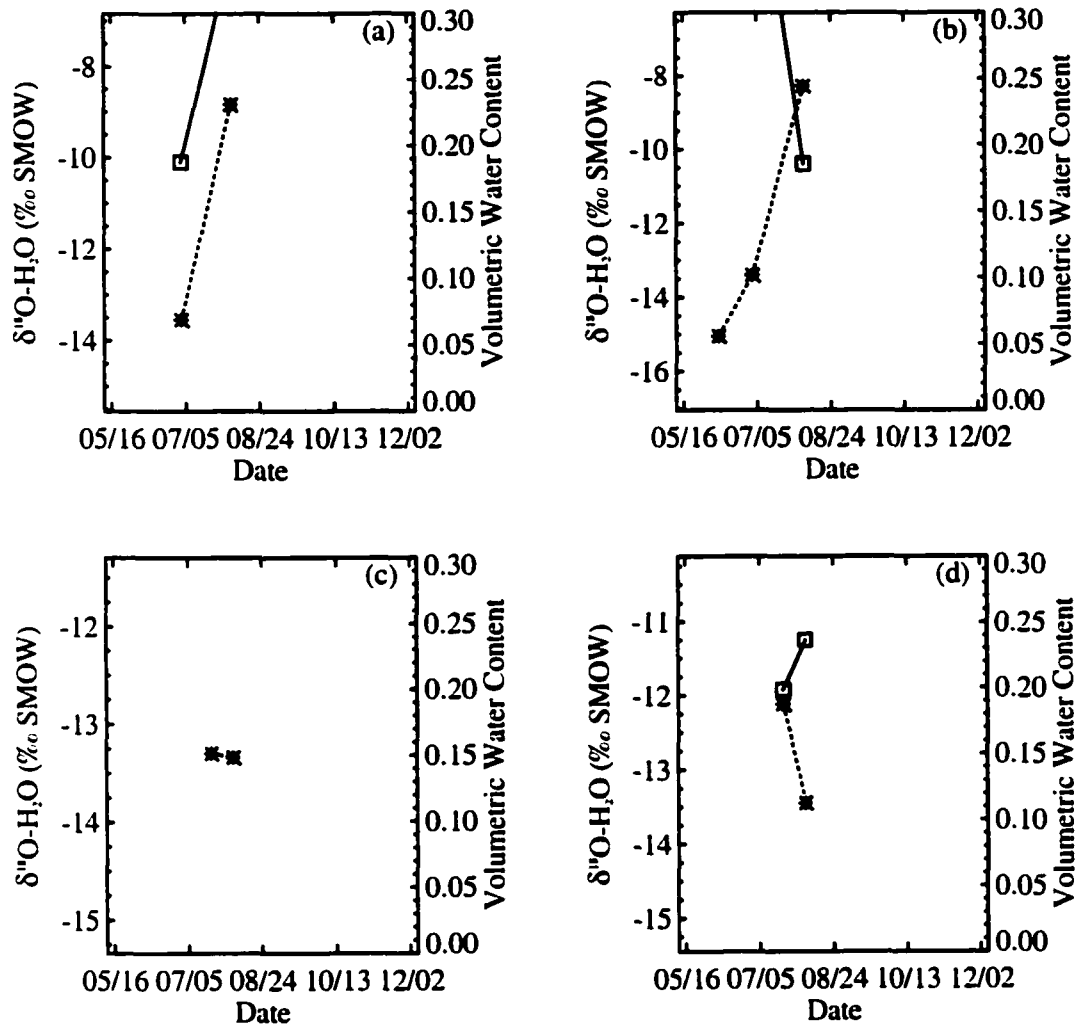

Figure III.23. Patterns of soil water content (open square) and soil water $\delta^{18}O$ values (asterix) over the sampling period in 1998 for the alpine tundra site on fine soil. Data are for the following depths: (a) 5 cm, (b) 10 cm, (c) 30 cm, (d) 50 cm. Data are not continuous in time; points are connected merely for visualization.

Reproduced with permission of the copyright owner. Further reproduction prohibited without permission.

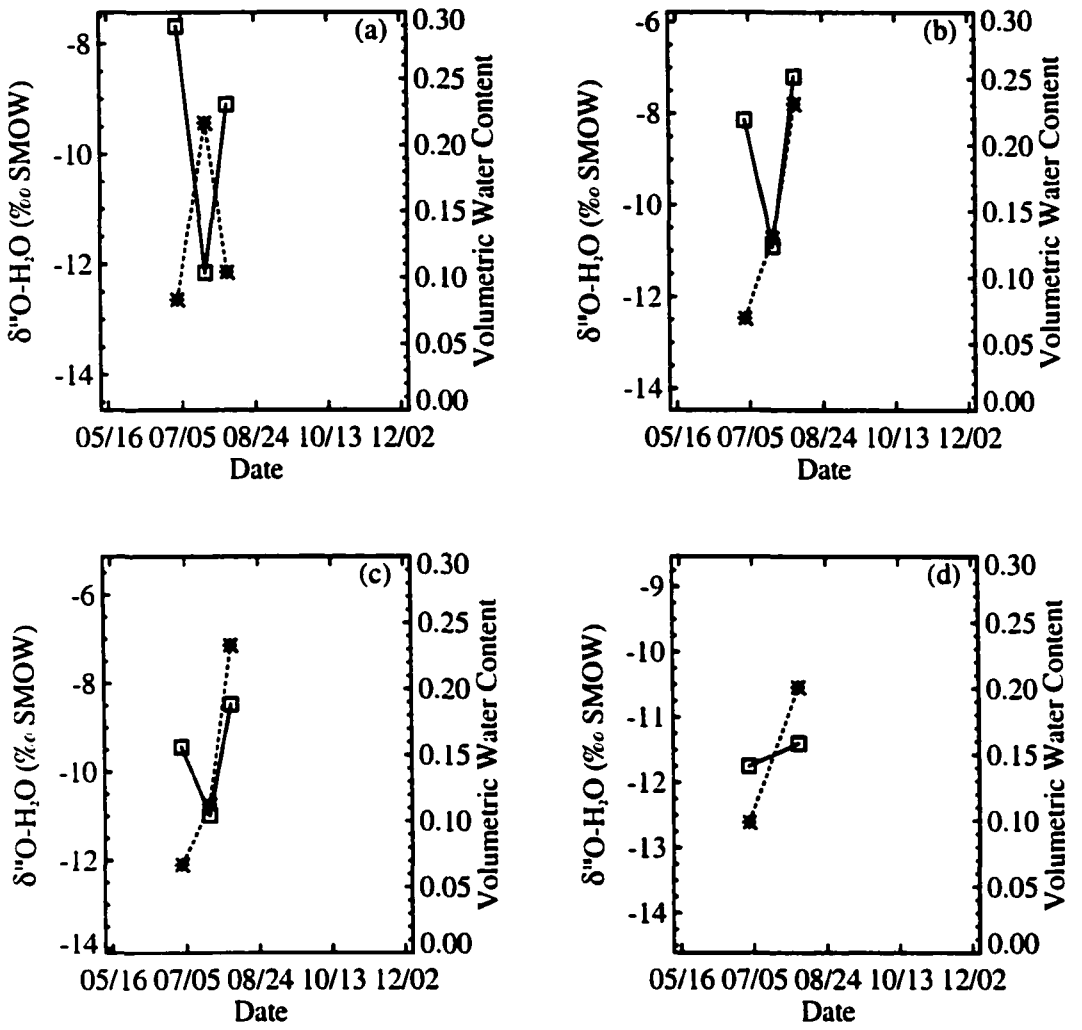

Figure III.24. Patterns of soil water content (open square) and soil water $\delta^{18}O$ values (asterix) over the sampling period in 1998 for the alpine tundra site on coarse soil. Data are for the following depths: (a) 5 cm, (b) 10 cm, (c) 30 cm, (d) 50 cm. Data are not continuous in time; points are connected merely for visualization.

Reproduced with permission of the copyright owner. Further reproduction prohibited without permission.

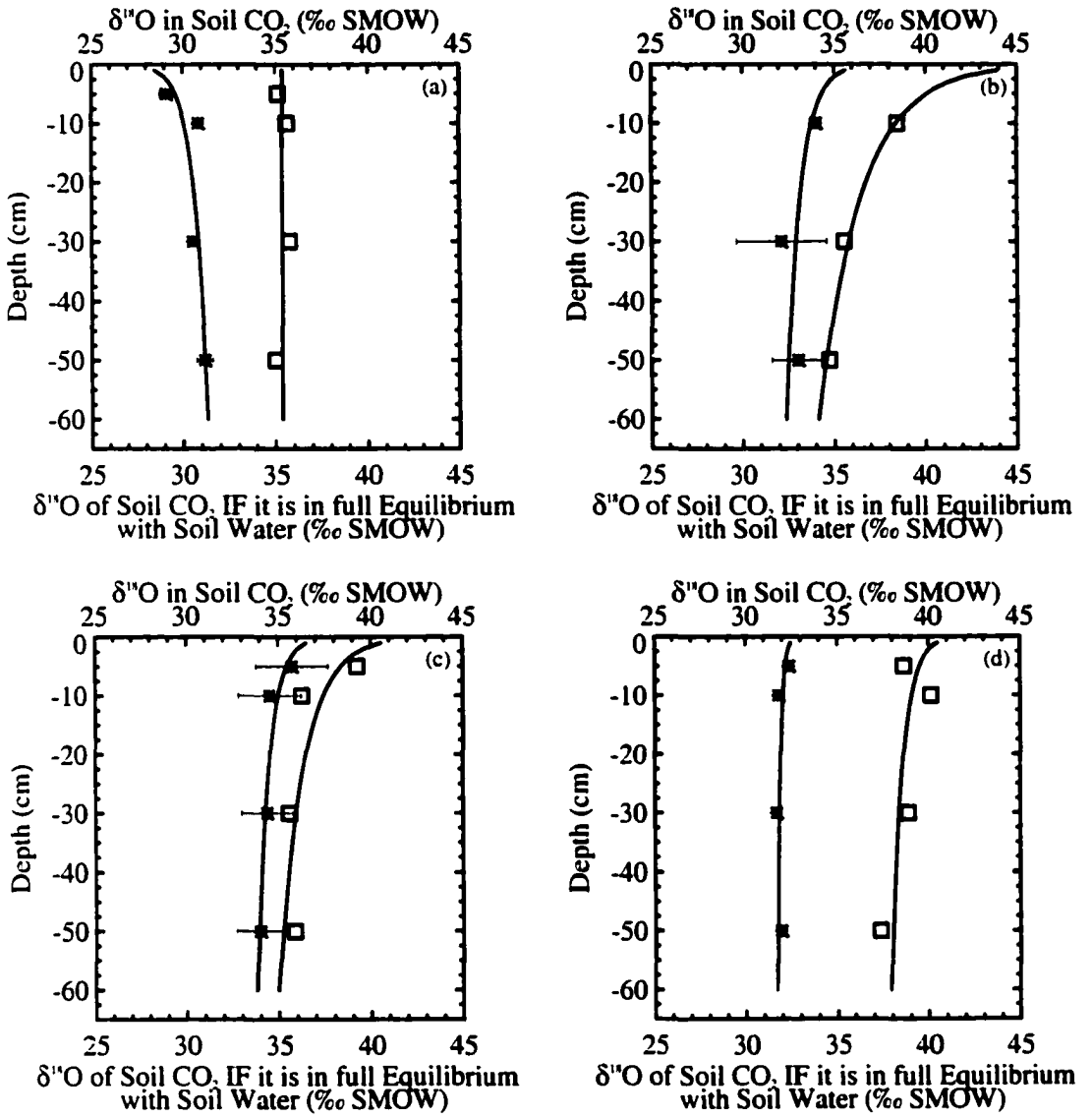

Figure III.25. Comparison of $\delta^{18}O$ values measured in soil CO_2 (asterix, mean ± standard error, three sample tubes) with those calculated (open square) based on the assumption of full isotopic equilibrium with soil water measured at the same depths (accounting for temperature-dependent fractionation [*Brenninkmeijer et al.*, 1983]). Smoothed lines are log linear regressions of the data. Plots are for the shortgrass steppe site on fine soil. Each panel represents an individual sampling date: (a) June 23, 1998, (b) July 14, 1998, (c) August 11, 1998, and (d) October 26, 1998.

Reproduced with permission of the copyright owner. Further reproduction prohibited without permission.

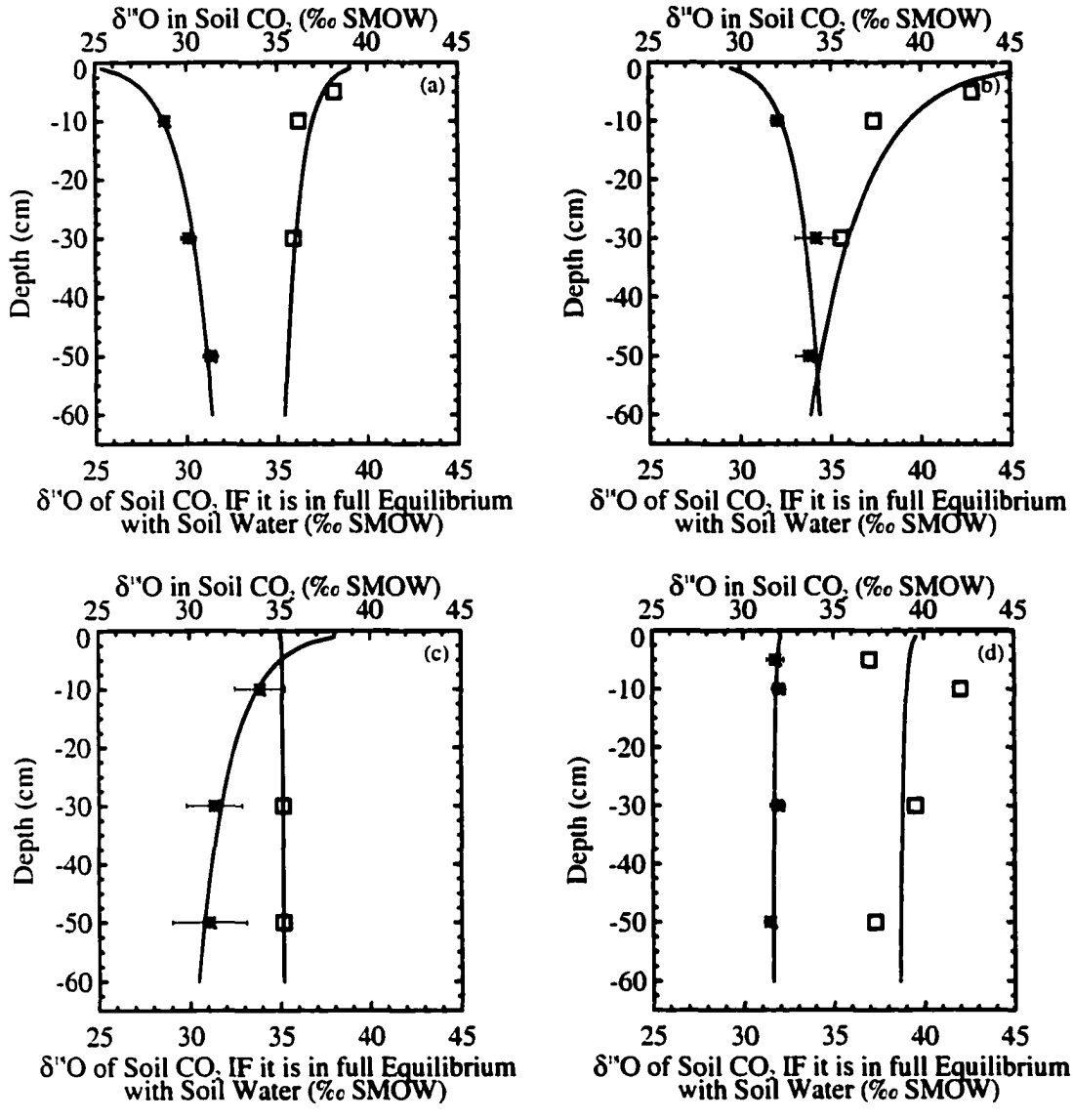

Figure III.26. Comparison of $\delta^{18}O$ values measured in soil CO_2 (asterix, mean ± standard error, three sample tubes) with those calculated (open square) based on the assumption of full isotopic equilibrium with soil water measured at the same depths (accounting for temperature-dependent fractionation [*Brenninkmeijer et al.*, 1983]). Smoothed lines are log linear regressions of the data. Plots are for the shortgrass steppe site on coarse soil. Each panel represents an individual sampling date: (a) June 23, 1998, (b) July 14, 1998, (c) August 11, 1998, and (d) October 26, 1998.

Reproduced with permission of the copyright owner. Further reproduction prohibited without permission.

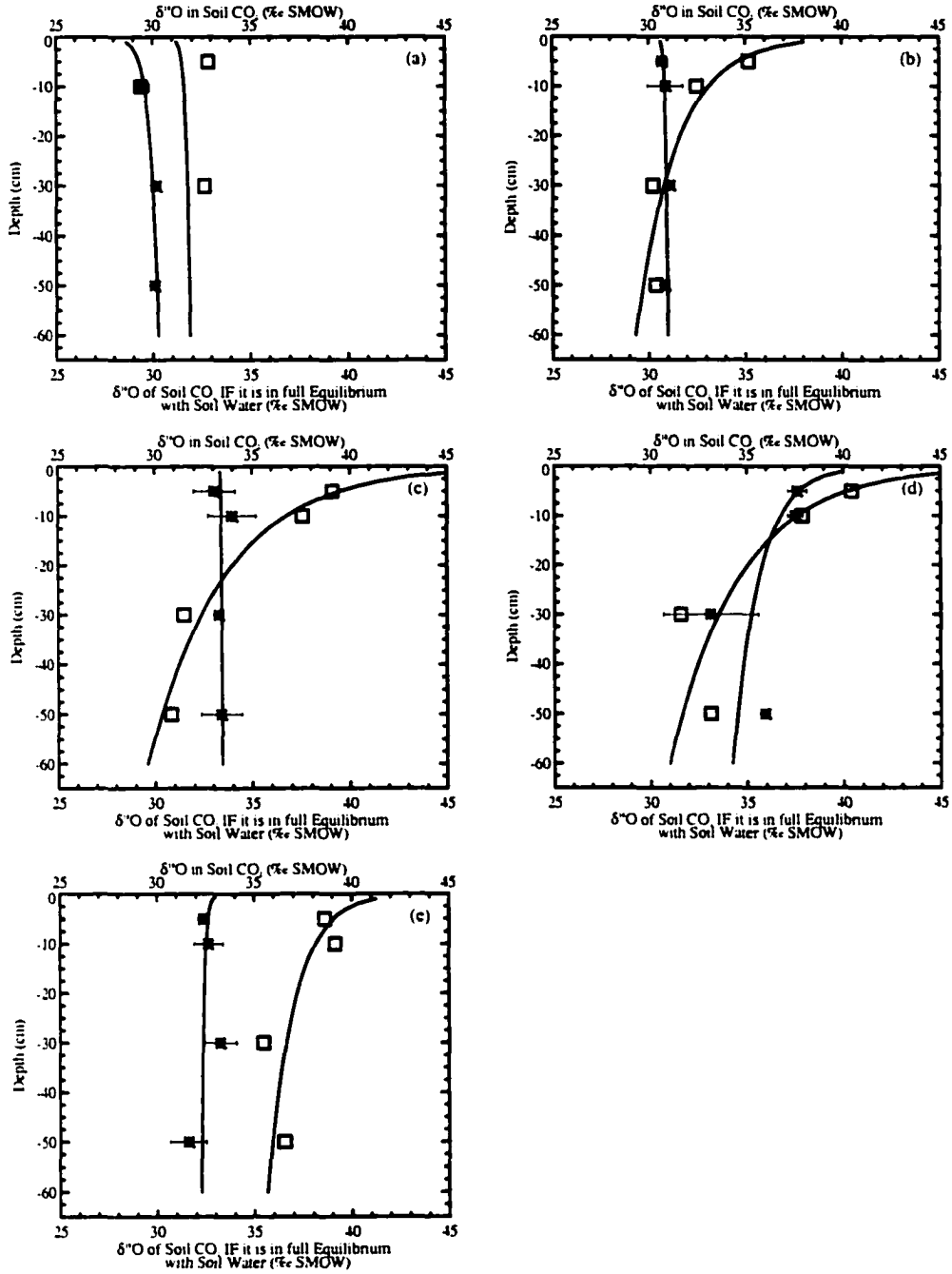

Figure III.27. Comparison of $\delta^{18}O$ values measured in soil CO_2 (asterix, mean ± standard error, three sample tubes) with those calculated (open square) based on the assumption of full isotopic equilibrium with soil water measured at the same depths (accounting for temperature-dependent fractionation [*Brenninkmeijer et al.*, 1983]). Smoothed lines are log linear regressions of the data. Plots are for the lodgepole pine site on fine soil. Each panel represents an individual sampling date: (a) June 16, 1998, (b) July 7, 1998, (c) July 28, 1998, (d) August 21, 1998, (e) November 5, 1998.

Reproduced with permission of the copyright owner. Further reproduction prohibited without permission.

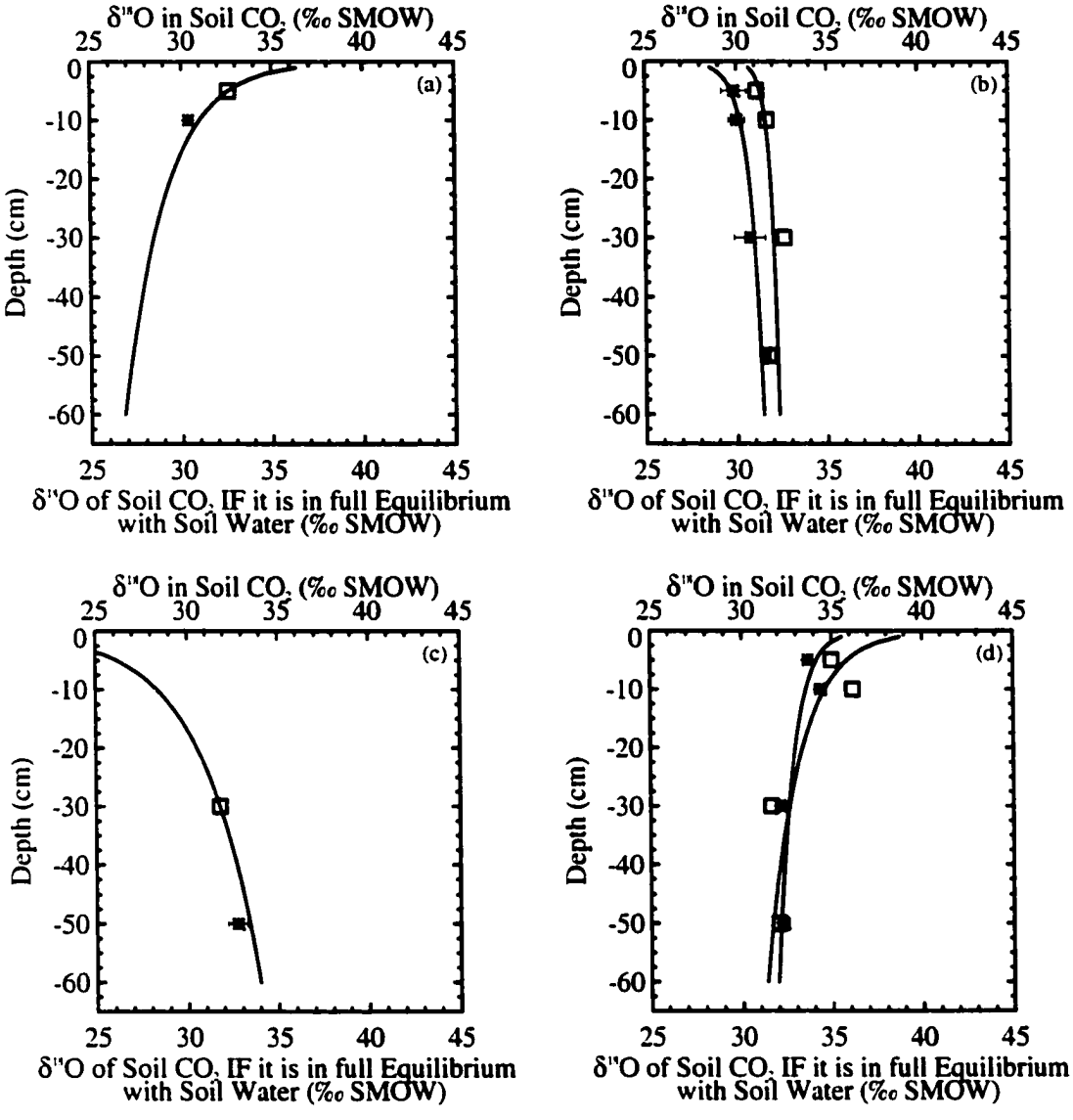

Figure III.28. Comparison of $\delta^{18}O$ values measured in soil CO_2 (asterix, mean ± standard error, three sample tubes) with those calculated (open square) based on the assumption of full isotopic equilibrium with soil water measured at the same depths (accounting for temperature-dependent fractionation [*Brenninkmeijer et al.*, 1983]). Smoothed lines are log linear regressions of the data. Plots are for the alpine tundra site on fine soil. Each panel represents an individual sampling date: (a) June 9, 1998, (b) July 2, 1998, (c) July 21, 1998, (d) August 5, 1998.

Reproduced with permission of the copyright owner. Further reproduction prohibited without permission.

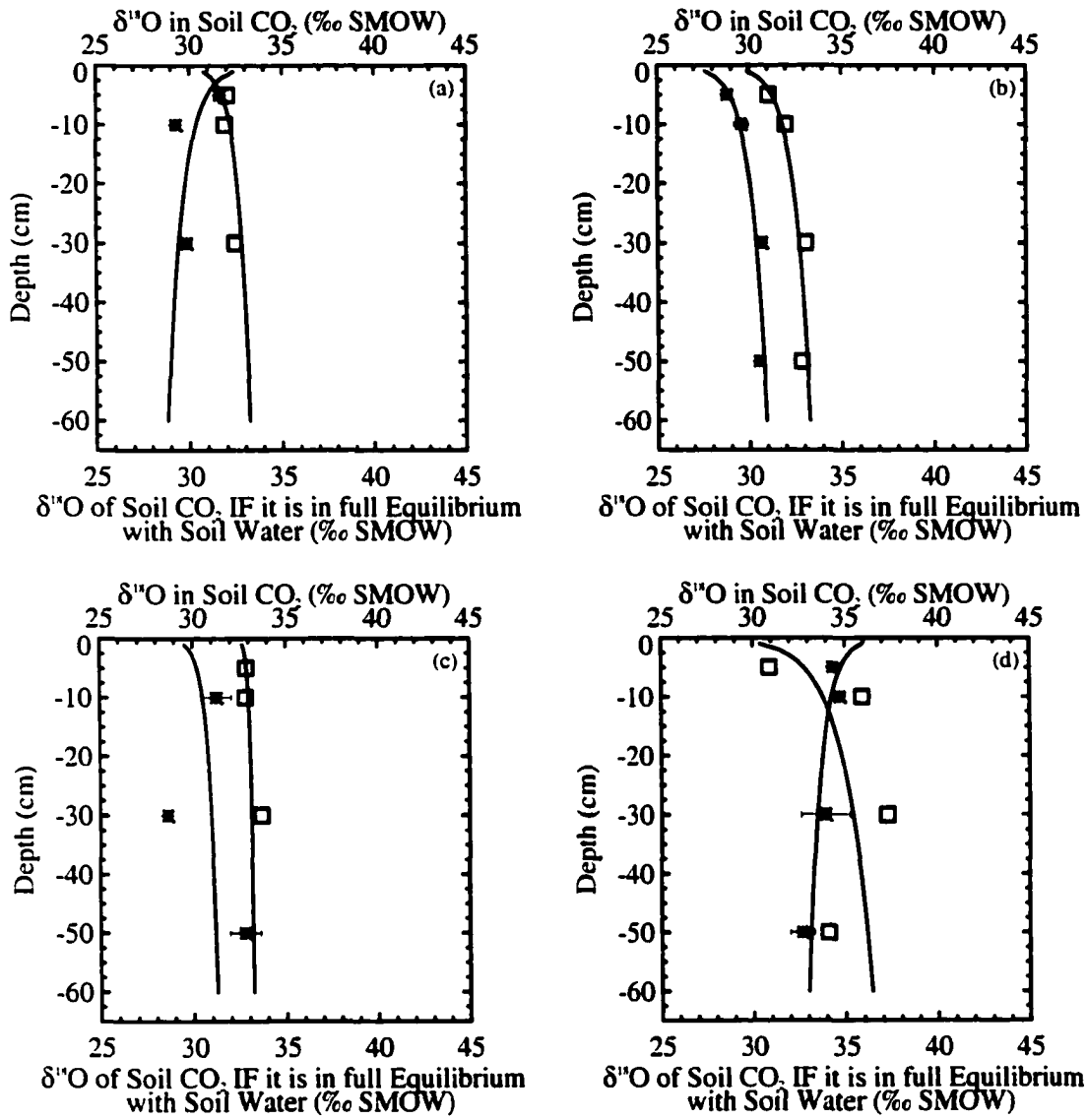

Figure III.29. Comparison of $\delta^{18}O$ values measured in soil CO_2 (asterix, mean ± standard error, three sample tubes) with those calculated (open square) based on the assumption of full isotopic equilibrium with soil water measured at the same depths (accounting for temperature-dependent fractionation [*Brenninkmeijer et al.*, 1983]). Smoothed lines are log linear regressions of the data. Plots are for the alpine tundra site on coarse soil. Each panel represents an individual sampling date: (a) June 9, 1998, (b) July 2, 1998, (c) July 21, 1998, (d) August 5, 1998.

Reproduced with permission of the copyright owner. Further reproduction prohibited without permission.

Table III.1. Calculation of the difference between the $\delta^{18}O$ measured in soil CO_2 and that in equilibrium with soil water (last column, Modeled-Observed) for each sampling date.

Shortgrass Steppe, Fine Soil 6/23/98						
Site	Depth	Soil CO2	Soil Water	Soil temp	Eq@stemp	Mod-Obs
1	5	29.110	-5.920	25.300	41.055	6.025
1	10	30.858	-6.030	22.200	41.674	4.785
1	30	30.539	-6.400	19.800	42.162	5.223
1	50	31.178	-7.470	18.200	42.492	3.844
Shortgrass Steppe, Fine Soil 7/14/98						
Site	Depth	Soil CO2	Soil Water	Soil temp	Eq@stemp	Mod-Obs
1	5	-99.000	-0.890	29.300	40.275	na
1	10	34.034	-3.060	22.900	41.533	4.439
1	30	32.125	-6.110	22.300	41.654	3.419
1	50	33.065	-7.010	21.900	41.734	1.660
Shortgrass Steppe, Fine Soil 8/11/98						
Site	Depth	Soil CO2	Soil Water	Soil temp	Eq@stemp	Mod-Obs
1	5	35.747	-1.030	29.300	40.275	3.498
1	10	34.520	-5.260	22.900	41.533	1.753
1	30	34.384	-6.070	22.300	41.654	1.200
1	50	33.985	-5.880	21.900	41.734	1.869
Shortgrass Steppe, Fine Soil 10/26/98						
Site	Depth	Soil CO2	Soil Water	Soil temp	Eq@stemp	Mod-Obs
1	5	32.393	-5.340	11.200	43.980	6.246
1	10	31.803	-4.120	10.000	44.242	8.319
1	30	31.700	-5.320	10.300	44.176	7.156
1	50	31.943	-6.630	11.200	43.980	5.406

Reproduced with permission of the copyright owner. Further reproduction prohibited without permission.

Table III.2. Calculation of the difference between the $\delta^{18}O$ measured in soil CO_2 and that in equilibrium with soil water (last column, Modeled-Observed) for each sampling date.

Shortgrass Steppe, Coarse Soil 6/23/98						
Site	Depth	Soil CO2	Soil Water	Soil temp	Eq@stemp	Mod-Obs
2	5	-99.000	-1.310	33.500	39.477	na
2	10	28.830	-4.635	26.400	40.838	7.373
2	30	30.112	-6.300	19.600	42.203	5.791
2	50	31.288	-6.750	17.600	42.617	4.579
Shortgrass Steppe, Coarse Soil 7/14/98						
Site	Depth	Soil CO2	Soil Water	Soil temp	Eq@stemp	Mod-Obs
2	5	-99.000	1.480	23.600	41.393	na
2	10	32.042	-4.210	22.500	41.613	5.362
2	30	34.204	-5.920	23.100	41.493	1.369
2	50	33.719	-6.350	22.200	41.674	1.605
Shortgrass Steppe, Coarse Soil 8/11/98						
Site	Depth	Soil CO2	Soil Water	Soil temp	Eq@stemp	Mod-Obs
2	5	-99.000	-99.000	23.600	41.393	na
2	10	33.875	-99.000	22.500	41.613	na
2	30	31.345	-6.360	23.100	41.493	3.788
2	50	31.058	-6.530	22.200	41.674	4.086
Shortgrass Steppe, Coarse Soil 10/26/98						
Site	Depth	Soil CO2	Soil Water	Soil temp	Eq@stemp	Mod-Obs
2	5	31.737	-6.390	14.000	43.376	5.249
2	10	31.910	-1.820	11.900	43.828	10.098
2	30	31.837	-4.700	10.200	44.198	7.661
2	50	31.420	-6.690	11.300	43.958	5.848

Reproduced with permission of the copyright owner. Further reproduction prohibited without permission.

Table III.3. Calculation of the difference between the $\delta^{18}O$ measured in soil CO_2 and that in equilibrium with soil water (last column, Modeled-Observed) for each sampling date.

Lodgepole pine, Fine Soil 6/16/98

Site	Depth	Soil CO2	Soil Water	Soil temp	Eq@stemp	Mod-Obs
3	5	-99.000	-12.260	6.200	45.088	na
3	10	29.513	-15.740	6.100	45.110	-0.143
3	30	30.161	-12.600	5.600	45.223	2.462
3	50	30.090	-13.360	5.700	45.201	1.750

Lodgepole pine, Fine Soil 7/798

Site	Depth	Soil CO2	Soil Water	Soil temp	Eq@stemp	Mod-Obs
3	5	30.695	-7.680	16.400	42.868	4.493
3	10	30.869	-11.100	12.900	43.612	1.643
3	30	31.096	-14.130	9.600	44.330	-0.896
3	50	30.817	-14.080	9.100	44.440	-0.457

Lodgepole pine, Fine Soil 7/28/98

Site	Depth	Soil CO2	Soil Water	Soil temp	Eq@stemp	Mod-Obs
3	5	33.051	-4.690	12.100	43.78	6.040
3	10	33.960	-6.400	11.400	43.936	3.576
3	30	33.291	-12.500	11.300	43.958	-1.834
3	50	33.408	-13.230	10.900	44.045	-2.593

Lodgepole pine, Fine Soil 8/21/98

Site	Depth	Soil CO2	Soil Water	Soil temp	Eq@stemp	Mod-Obs
3	5	37.632	-3.110	13.300	43.526	2.784
3	10	37.525	-5.920	12.100	43.784	0.339
3	30	33.132	-12.350	11.400	43.936	-1.546
3	50	35.920	-10.820	11.300	43.958	-2.782

Lodgepole pine, Fine Soil 11/5/98

Site	Depth	Soil CO2	Soil Water	Soil temp	Eq@stemp	Mod-Obs
3	5	32.393	-7.430	2.100	46.026	6.203
3	10	32.640	-6.770	2.600	45.910	6.500
3	30	33.263	-10.100	4.100	45.565	2.202
3	50	31.597	-9.360	2.700	45.887	4.931

Reproduced with permission of the copyright owner. Further reproduction prohibited without permission.

Table III.4. Calculation of the difference between the $\delta^{18}O$ measured in soil CO_2 and that in equilibrium with soil water (last column, Modeled-Observed) for each sampling date.

Lodgepole pine, Coarse Soil 6/11/98						
Site	Depth	Soil CO2	Soil Water	Soil temp	Eq@stemp	Mod-Obs
4	5	-99.000	-12.080	5.700	45.201	na
4	10	29.858	-12.590	5.400	45.269	2.820
4	30	30.694	-14.400	5.900	45.155	0.062
4	50	31.704	-14.390	5.600	45.223	-0.870
Lodgepole pine, Coarse Soil 6/19/98						
Site	Depth	Soil CO2	Soil Water	Soil temp	Eq@stemp	Mod-Obs
4	5	30.127	-12.910	5.800	45.178	2.142
4	10	29.101	-13.250	5.300	45.291	2.941
4	30	30.642	-13.290	5.300	45.291	1.359
4	50	29.883	-14.540	5.200	45.314	0.892
Lodgepole pine, Coarse Soil 6/25/98						
Site	Depth	Soil CO2	Soil Water	Soil temp	Eq@stemp	Mod-Obs
4	5	-99.000	-10.970	9.900	44.264	na
4	10	-99.000	-12.740	8.300	44.618	na
4	30	29.735	-14.460	6.700	44.975	0.780
4	50	29.340	-14.140	7.000	44.908	1.428
Lodgepole pine, Coarse Soil 7/1/98						
Site	Depth	Soil CO2	Soil Water	Soil temp	Eq@stemp	Mod-Obs
4	5	29.652	-2.440	14.000	43.376	11.284
4	10	29.529	-10.790	12.600	43.676	3.358
4	30	29.480	-13.860	10.000	44.242	0.902
4	50	29.781	-14.730	8.200	44.640	0.129
Lodgepole pine, Coarse Soil 7/10/98						
Site	Depth	Soil CO2	Soil Water	Soil temp	Eq@stemp	Mod-Obs
4	5	30.884	-5.620	11.300	43.958	7.453
4	10	31.212	-10.540	10.600	44.111	2.359
4	30	31.876	-99.000	9.300	44.396	na
4	50	31.604	-12.610	8.800	44.507	0.292
Lodgepole pine, Coarse Soil 7/16/98						
Site	Depth	Soil CO2	Soil Water	Soil temp	Eq@stemp	Mod-Obs
4	5	32.804	-4.750	13.400	43.504	5.950
4	10	31.085	-99.000	12.200	43.763	na
4	30	33.192	-99.000	10.800	44.067	na
4	50	32.405	-14.420	9.900	44.264	-2.561
Lodgepole pine, Coarse Soil 7/28/98						
Site	Depth	Soil CO2	Soil Water	Soil temp	Eq@stemp	Mod-Obs
4	5	35.642	-5.620	14.200	43.333	2.071
4	10	39.229	-5.290	13.200	43.547	-0.972
4	30	37.168	-6.890	11.400	43.936	-0.122
4	50	31.972	-9.030	10.700	44.089	3.087
Lodgepole pine, Coarse Soil 8/21/98						
Site	Depth	Soil CO2	Soil Water	Soil temp	Eq@stemp	Mod-Obs
4	5	32.300	-3.350	14.200	43.333	7.683
4	10	36.157	-6.530	13.200	43.547	0.860
4	30	35.554	-8.910	11.400	43.936	-0.528
4	50	35.528	-9.390	10.700	44.089	-0.830
Lodgepole pine, Coarse Soil 11/19/98						
Site	Depth	Soil CO2	Soil Water	Soil temp	Eq@stemp	Mod-Obs
4	5	31.180	-12.010	1.500	46.166	2.976
4	10	30.207	-6.750	1.600	46.143	9.186
4	30	31.180	-10.570	1.400	46.189	4.439
4	50	31.213	-10.970	1.800	46.096	3.913

Reproduced with permission of the copyright owner. Further reproduction prohibited without permission.

Table III.5. Calculation of the difference between the $\delta^{18}O$ measured in soil CO_2 and that in equilibrium with soil water (last column, Modeled-Observed) for each sampling date.

Alpine tundra, Fine Soil 6/9/98

Site	Depth	Soil CO2	Soil Water	Soil temp	Eq@stemp	Mod-Obs
5	5	-99.000	-13.120	3.400	45.726	na
5	10	30.395	-15.050	2.000	46.050	0.605
5	30	-99.000	-99.000	0.700	46.353	na
5	50	-99.000	-99.000	-99.000	83.155	na

Alpine tundra, Fine Soil 7/2/98

Site	Depth	Soil CO2	Soil Water	Soil temp	Eq@stemp	Mod-Obs
5	5	29.871	-13.550	8.100	44.662	1.241
5	10	30.014	-13.400	6.200	45.088	1.674
5	30	30.724	-12.970	4.100	45.565	1.871
5	50	31.539	-14.220	2.300	45.980	0.221

Alpine tundra, Fine Soil 7/21/98

Site	Depth	Soil CO2	Soil Water	Soil temp	Eq@stemp	Mod-Obs
5	5	-99.000	-99.000	11.500	43.914	na
5	10	-99.000	-11.900	8.600	44.551	na
5	30	-99.000	-13.300	6.100	45.110	na
5	50	32.760	-12.120	4.200	45.542	0.662

Alpine tundra, Fine Soil 8/5/98

Site	Depth	Soil CO2	Soil Water	Soil temp	Eq@stemp	Mod-Obs
5	5	33.683	-8.850	11.800	43.849	1.316
5	10	34.374	-8.280	9.100	44.440	1.786
5	30	32.137	-13.340	6.800	44.953	-0.524
5	50	32.254	-13.450	4.500	45.474	-0.230

Reproduced with permission of the copyright owner. Further reproduction prohibited without permission.

Table III.6. Calculation of the difference between the $\delta^{18}O$ measured in soil CO_2 and that in equilibrium with soil water (last column, Modeled-Observed) for each sampling date.

Alpine tundra, Coarse Soil 6/9/98

Site	Depth	Soil CO2	Soil Water	Soil temp	Eq@stemp	Mod-Obs
6	5	31.642	-14.010	2.100	46.026	0.374
6	10	29.271	-14.190	1.800	46.096	2.635
6	30	29.848	-14.110	0.000	46.518	2.560
6	50	-99.000	-13.010	0.000	46.518	na

Alpine tundra, Coarse Soil 7/2/98

Site	Depth	Soil CO2	Soil Water	Soil temp	Eq@stemp	Mod-Obs
6	5	28.796	-12.640	12.500	43.698	2.261
6	10	29.554	-12.470	9.200	44.418	2.394
6	30	30.694	-12.100	5.900	45.155	2.362
6	50	30.515	-12.610	4.700	45.428	2.303

Alpine tundra, Coarse Soil 7/21/98

Site	Depth	Soil CO2	Soil Water	Soil temp	Eq@stemp	Mod-Obs
6	5	-99.000	-9.430	19.100	42.306	na
6	10	31.252	-10.720	13.200	43.547	1.575
6	30	28.621	-10.740	9.300	44.396	5.035
6	50	32.781	-11.810	8.200	44.640	0.049

Alpine tundra, Coarse Soil 8/5/98

Site	Depth	Soil CO2	Soil Water	Soil temp	Eq@stemp	Mod-Obs
6	5	34.364	-12.140	15.500	43.057	-3.446
6	10	34.740	-7.790	12.500	43.698	1.168
6	30	33.958	-7.140	9.300	44.396	3.298
6	50	32.683	-10.540	8.200	44.640	1.417

Reproduced with permission of the copyright owner. Further reproduction prohibited without permission.

APPENDIX IV

LABORATORY INTERCOMPARISON

A formal laboratory inter-comparison between the CSU and Utah isotope facilities has never been carried out. To assess whether data analyzed at each facility could be compared to that from the other facility, the same working standard was run at both facilities every time samples were processed (prior to any analysis and after every 10 samples). The working standard was a commercial tank gas of 0.5% CO_2 in nitrogen. A teflon syringe with stopcock was used to load standard gas into evacuated sample vials. The pressure difference drew the standard gas from the syringe (after an initial amount was purged through the needle). The needle was left open in the sample vial septa for at least 30 seconds to allow equilibration in the event that not all of the gas from the syringe was drawn into the vial. The standard was shipped with the real samples to assure that shipping and storage did not affect the results. For analysis, the standard gas was drawn from the vials with a gas tight syringe in the same manner as the samples. A second standard of lower CO_2 concentration (1020 ppm) was also run at the both facilities. The repeatability of injections at the SIRFER facility was 0.9‰ for ^{13}C and 1.5‰ for ^{18}O. The poor precision appears to be related to differences from one sample vial to the next, as the standard deviation across injections from a single vial was 0.2‰ for both ^{13}C and ^{18}O using the Finnigan PreCon. It is possible that the method used to transfer the working standard to the sample vials caused fractionation, especially as the entire contents of the

Reproduced with permission of the copyright owner. Further reproduction prohibited without permission.

syringe might not have been transferred in every case. However, the precision of the method tested at the CSU facility appeared reliable even among vials (±0.5‰, n=28). Futher, plots of $\delta^{18}O$ versus $\delta^{13}C$ for the tank gas samples indicated that only one of the vials was fractionated (slope about 2‰, suggesting kinetic fractionation, J.White, personal communication). This vial was not used for the inter-laboratory comparison. The comparison of the two methods used to analyze the working standard (Microgas at CSU versus PreCon at UT) revealed an offset of about 3‰ in the ^{18}O data, but a good match for ^{13}C data (Table IV.1). Thus, a correction factor was applied to all field data to account for this offset.

Table IV.1. Comparison of $\delta^{13}C$ and $\delta^{18}O$ values for soil gas samples analyzed at two isotope facilities (Colorado State University, and University of Utah).

CARBON SAMPLES

Grassland data

Utah_mean	n	UTserr[1]	Utsdev[2]	Colo_mean	n	COserr	COsdev
-12.858	14	0.623	2.33	-11.371	19	0.646	2.817

Pine & Tundra data

Utah_mean	n	UTserr	UTsdev	Colo_mean	n	COserr	COsdev
-22.7	3	2.022	3.503	-22.463	46	0.273	1.85

OXYGEN SAMPLES

All ecosystems

Utah_mean	n	UTserr	UTsdev	Colo_mean	n	COserr	COsdev
-9.437	12	0.355	1.228	-0.754	67	0.507	4.151

Grassland data

Utah_mean	n	UTserr	UTsdev	Colo_mean	n	COserr	COsdev
-7.645	15	1.032	3.997	-1.439	21	1.166	5.344

Pine & Tundra data

Utah_mean	n	UTserr	UTsdev	Colo_mean	n	COserr	COsdev
-8.757	1	0	0	-1.06	49	0.6	4.197

[1] standard error about the mean for UT samples; same notation for CO samples
[2] standard deviation about the mean for UT samples; same notation for CO samples

Reproduced with permission of the copyright owner. Further reproduction prohibited without permission.

Tests for potential fractionation by either laboratory method were also carried out for the field samples. None of the field data appear to have been affected by fractionation (Figure IV.1). However, when data for field samples are compared (this is indirect, as samples were only analyzed at one lab), there appears to be some inconsistency between labs, even after the offset correction. Just as there was no offset for ^{13}C in the working standard, the $\delta^{13}C$ of field samples measured at either lab are not significantly different (Figure IV.2). However, the ^{18}O of samples analyzed at CSU were significantly heavier than samples analyzed at the SIRFER facility (Figure IV.3), even after the correction to the same working standard. Although the samples were dried prior to collection, it is possible that water adsorbed to surfaces within the Microgas system may be the reason for the differences between labs. The SIRFER lab manager found that keeping all surfaces about 10°C above ambient was necessary for good precision at their facility (C.Cook, personal communication). Another difference between the systems is the column temperature, which is 40°C higher at CSU. However, this difference should be accounted for in the cross-comparison of the working standard. Unfortunately, the poor precision for working standards analyzed after storage in the serum vials at the SIRFER facility does not lend confidence that samples analyzed at this facility are "right," even if the problem lies in the means that the method was tested. Although the SIRFER facility has undergone more rigorous testing than has the CSU facility, the available data do not necessarily indicate that samples processed at the CSU facility are "wrong."

The problems outlined here are presented merely to alert future students to two serious issues. First, the isotope facility used must be properly calibrated against other facilities. This is true even if all samples will be processed in only one facility!

Reproduced with permission of the copyright owner. Further reproduction prohibited without permission.

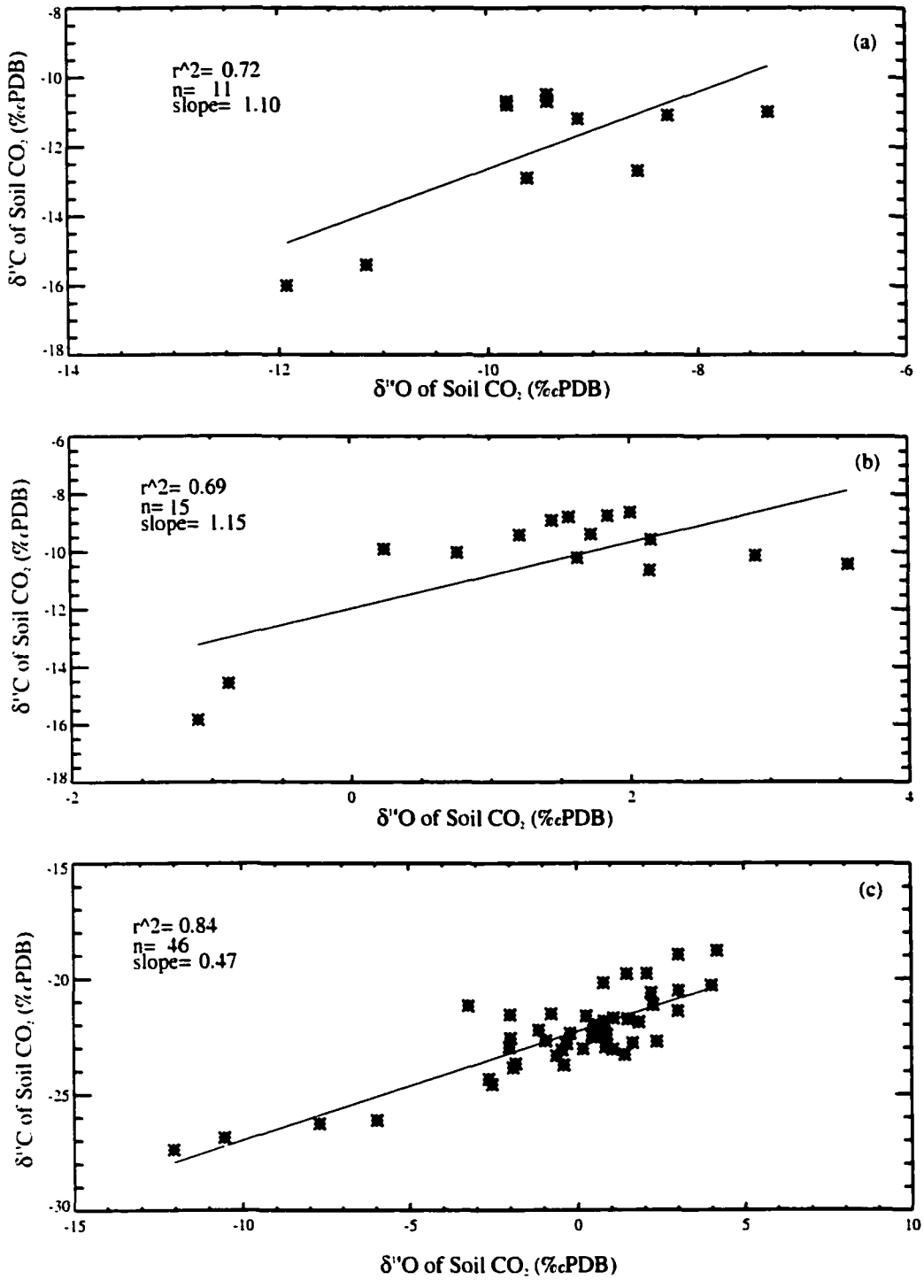

Figure IV.1. Plots of $\delta^{13}C$ versus $\delta^{18}O$ in soil CO_2 samples. (a) August samples from the shortgrass steppe sites processed in Utah, (b) August samples from the shortgrass steppe sites processed in Colorado, (c) August samples from the pine and tundra sites, processed in Colorado. Slopes greater than 2 indicate fractionation likely during sample analysis.

Reproduced with permission of the copyright owner. Further reproduction prohibited without permission.

There are few labs currently able to process a small number of moles of CO_2 in a mixture of gases as was analyzed for this study. The method used was relatively new to both facilities, and thus it is even more crucial that the methodology be cross-checked. Second, comparison of working standards to an international standard can be less straightforward than one might think. In this case, one facility was calibrated to PDB gas, whereas the other was calibrated to PDB-calcite (which was converted to gas). Analysis of the working reference at both facilities did not highlight this discrepancy because the standard itself had a signature between that of the two international standards. It was only after dissection of the data in multiple ways (Figures IV.4-IV.7) and the input of one of the most knowledgeable people in the field of mass spectrometry (W.A. Brand), that the problem was discovered.

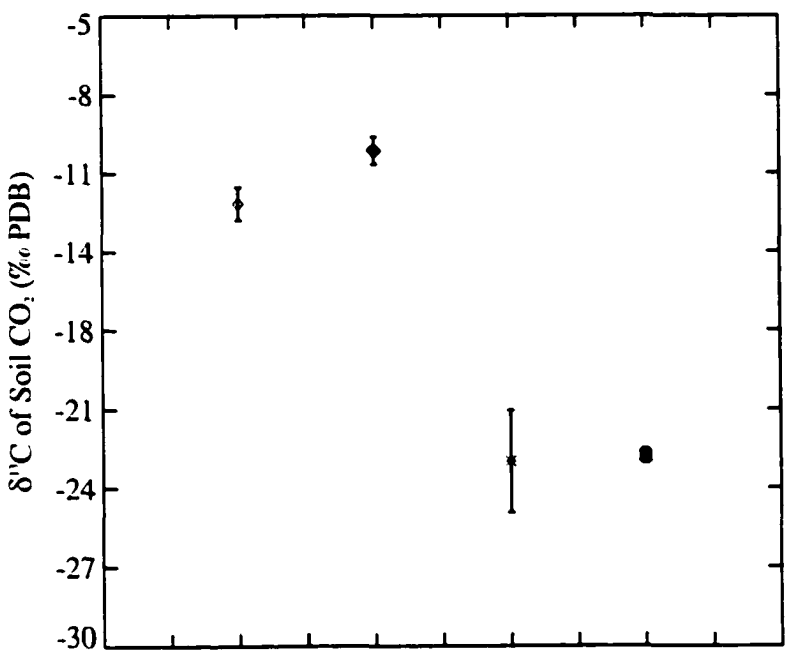

Figure IV.2. Comparison of $\delta^{13}C$ in soil CO_2 analyzed in two facilities. Open diamond is mean of shortgrass steppe data analyzed at the UT facility (n=12), closed diamond is mean of shortgrass steppe data analyzed at the CO facility (n=15). Asterix is mean of pine and tundra data analyzed at the UT facility (n=3), and bold asterix is mean of pine and tundra data analyzed at the CO facility (n=46). Bars indicate standard error.

Reproduced with permission of the copyright owner. Further reproduction prohibited without permission.

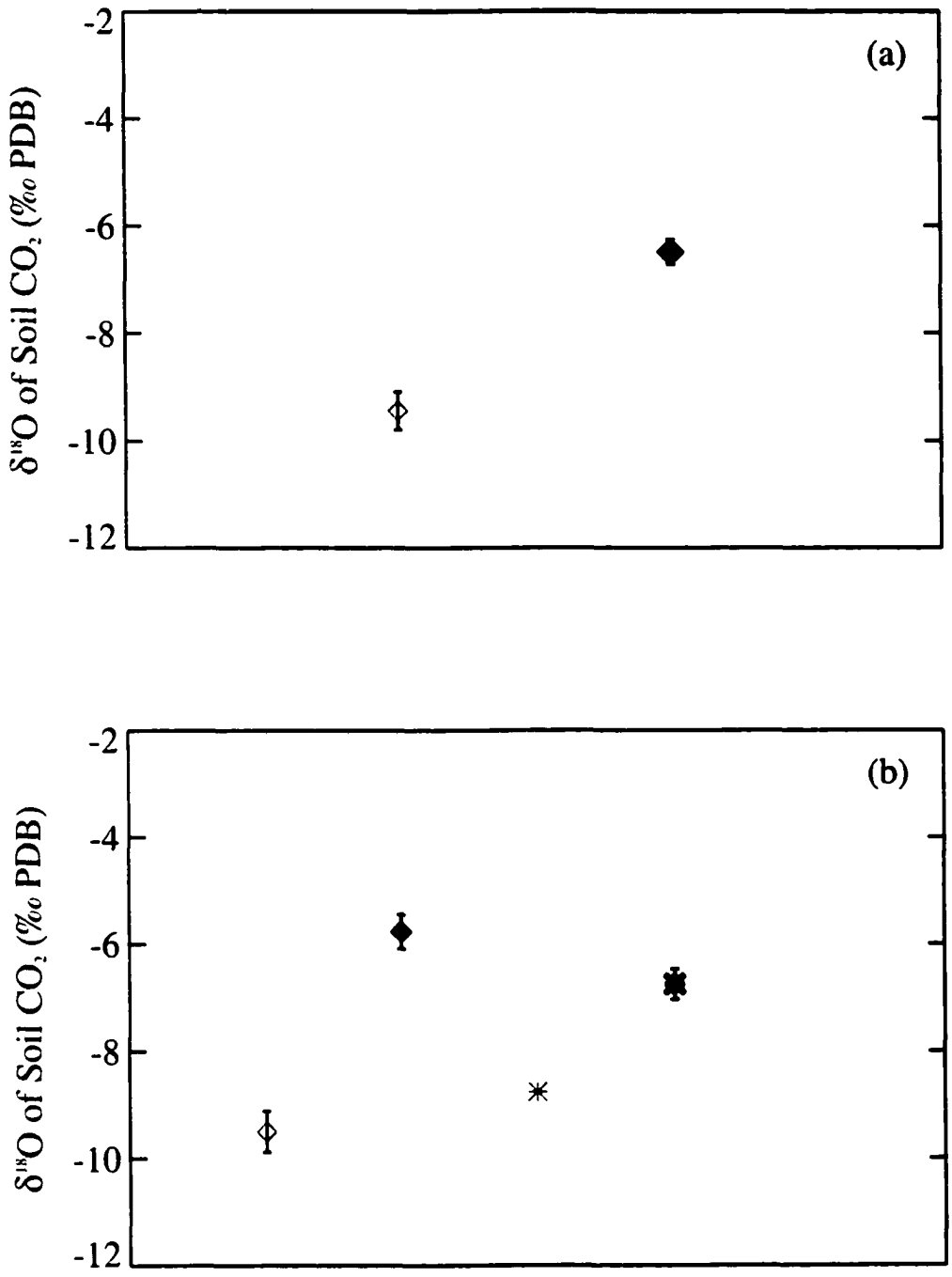

Figure IV.3. Comparison of $\delta^{18}O$ in soil CO_2 analyzed at the two isotope facilities (CO and UT) after correction to the same international standard (PBD-gas). (a) all sites combined, open diamond for samples analyzed at the UT facility, closed diamond for samples analyzed at the CO facility. (b) Shortgrass steppe sites shown separated from other ecosystems. Open diamond for shortgrass steppe samples analyzed at the UT facility, closed diamond for shortgrass steppe samples analyzed at the CO facility. Asterix for pine and tundra samples analyzed at the UT facility, bold asterix for pine and tundra samples analyzed at the CO facility.

Reproduced with permission of the copyright owner. Further reproduction prohibited without permission.

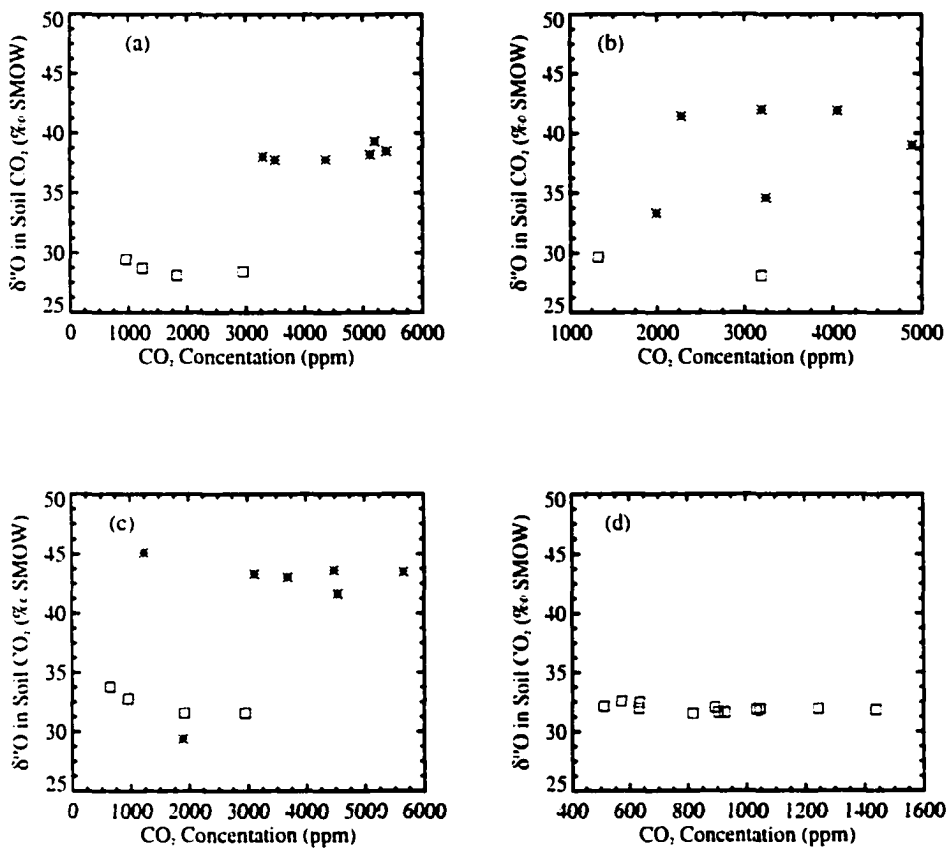

Figure IV.4. Analysis of $\delta^{18}O$ in soil CO_2 *prior* to discovery of the use of different international standards. These plots show data from the shortgrass steppe site on fine-textured soil. The same analysis was performed on data for each of the other field sites. Open squares are data analyzed at the UT facility, asterix are data analyzed at the CO facility. (a) Samples collected June 23, 1998, (b) samples collected July 14, 1998, (c) samples collected August 11, 1998, (d) samples collected October 26, 1998.

Reproduced with permission of the copyright owner. Further reproduction prohibited without permission.

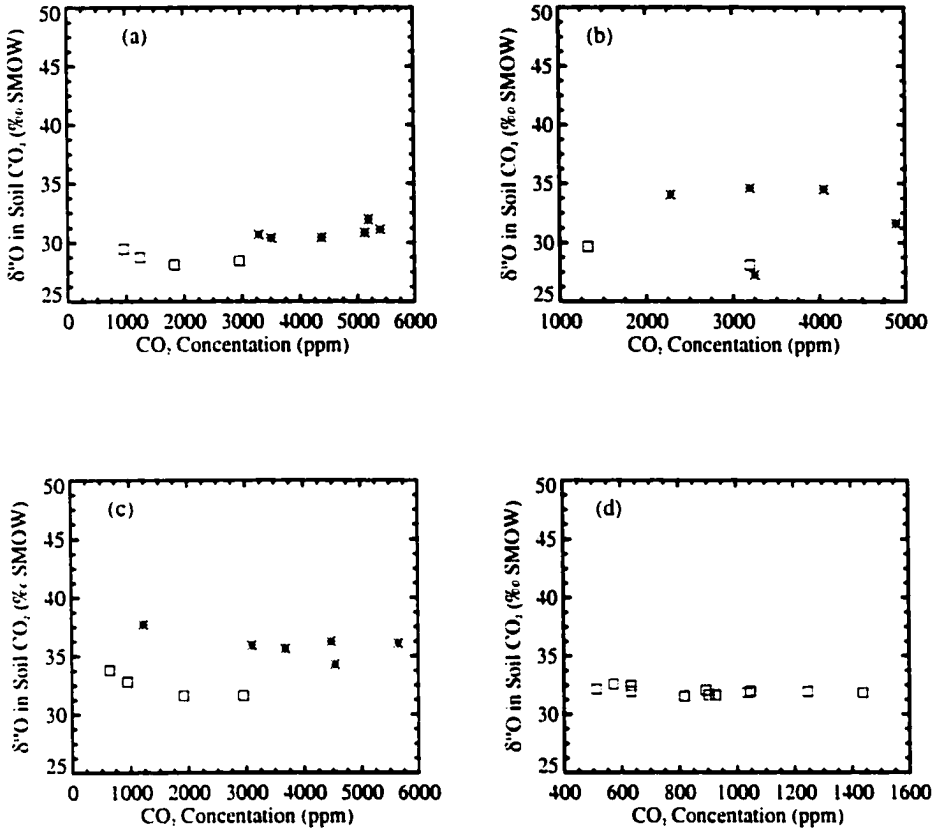

Figure IV.5. Analysis of $\delta^{18}O$ in soil CO_2 *after correction* to the same international standard (PDB-gas). These plots show data from the shortgrass steppe site on fine-textured soil. The same analysis was performed on data for each of the other field sites. Open squares are data analyzed at the UT facility, asterix are data analyzed at the CO facility. (a) Samples collected June 23, 1998, (b) samples collected July 14, 1998, (c) samples collected August 11, 1998, (d) samples collected October 26, 1998.

Reproduced with permission of the copyright owner. Further reproduction prohibited without permission.

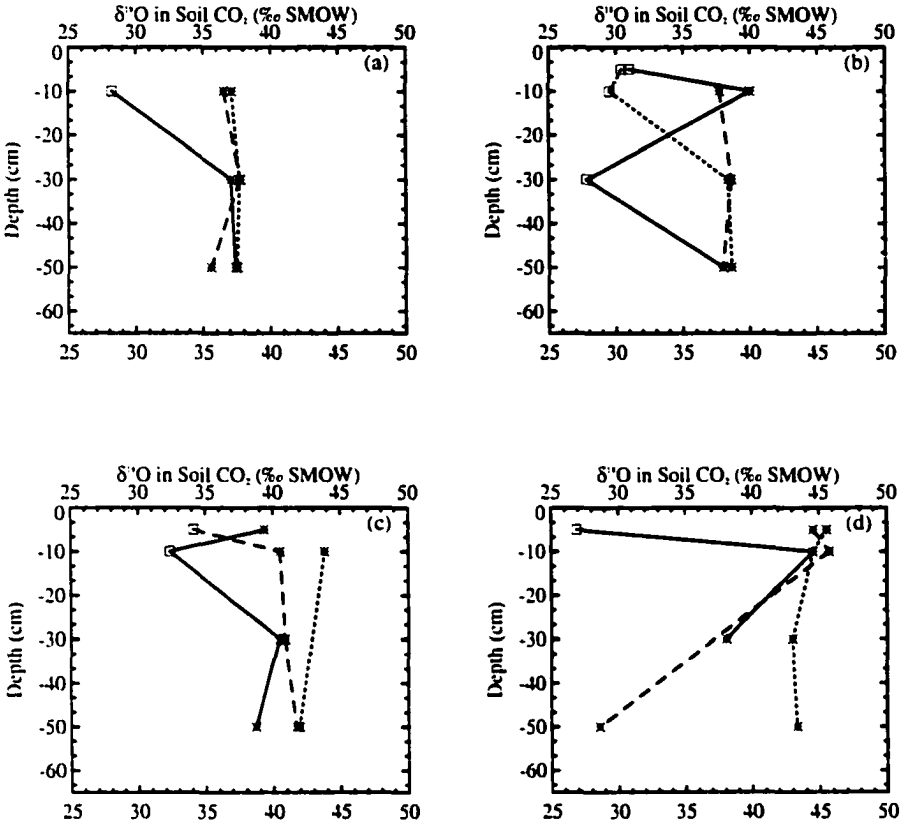

Figure IV.6. Analysis of $\delta^{18}O$ in soil CO_2 *prior* to discovery of the use of different international standards. These plots show data from the lodgepole pine site on fine-textured soil. The same analysis was performed on data for each of the other field sites. Open squares are data analyzed at the UT facility, asterix are data analyzed at the CO facility. Different line styles represent unique sampling tubes. Samples from the same tube (but different depths) were sometimes analyzed at different facilities. (a) Samples collected June 6, 1998, (b) samples collected July 7, 1998, (c) samples collected July 28, 1998, (d) samples collected August 21, 1998.

Reproduced with permission of the copyright owner. Further reproduction prohibited without permission.

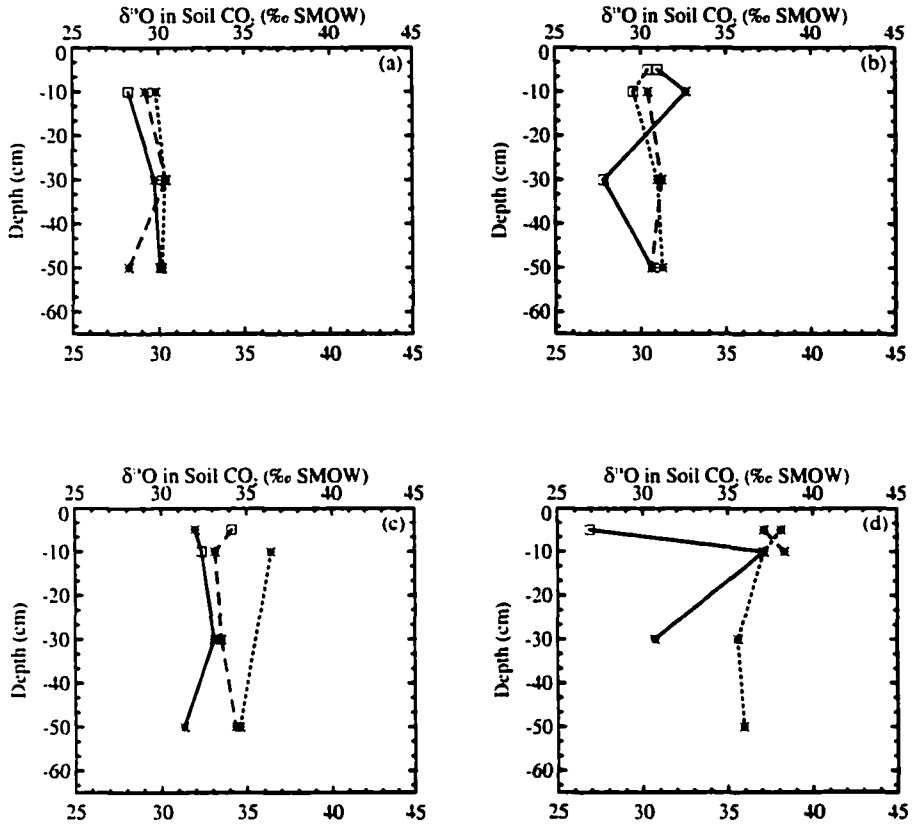

Figure IV.7. Analysis of $\delta^{18}O$ in soil CO_2 *after correction* to the same international standard (PDB-gas). These plots show data from the lodgepole pine site on fine-textured soil. The same analysis was performed on data for each of the other field sites. Open squares are data analyzed at the UT facility, asterix are data analyzed at the CO facility. Different line styles represent unique sampling tubes. Samples from the same tube (but different depths) were sometimes analyzed at different facilities. (a) Samples collected June 6, 1998, (b) samples collected July 7, 1998, (c) samples collected July 28, 1998, (d) samples collected August 21, 1998.

Reproduced with permission of the copyright owner. Further reproduction prohibited without permission.